Dissertations - ALL   SURFACE

December 2018

Regulation of in vivo excitatory/inhibitory balance by the cystine/glutamate exchanger system xc-

Sheila Marie Shahidzadeh Sears
Syracuse University

Follow this and additional works at: https://surface.syr.edu/etd

Part of the Life Sciences Commons

Abstract

System x_c^- (Sx_c^-) is a cellular antiporter that links the import of L-cystine with the export of L-glutamate. In the central nervous system (CNS), this export contributes to the ambient glutamate levels found in the synaptic cleft. To wit, a 50% reduction in extracellular glutamate has been demonstrated in animals null for the substrate-specific light chain, xCT. Moreover, in most tissues, including the CNS, cystine import through Sx_c^- is necessary for the synthesis and maintenance of glutathione (GSH) levels. Given that either a reduction in ambient glutamate levels and/or a redox imbalance involving GSH have been reported to affect synaptic strength and intrinsic neuronal excitability, the main focus of this dissertation was to elucidate whether Sx_c^- signaling contributes to brain excitatory/inhibitory (E/I) balance *in vivo*. Using chemoconvulsants to uncover excitability changes in *SLC7A11*$^{sut/sut}$ mice — mice that are null for Sx_c^- because of a spontaneous mutation in exon 12 of *SLC7A11* — we uncovered a sex-independent alteration in neuronal excitability. Specifically, we found that both female and male *SLC7A11*$^{sut/sut}$ mice had lower convulsive seizure thresholds than their wild-type (*SLC7A11*$^{+/+}$) littermates after acute challenge with two pharmacologically distinct chemoconvulsants: the glutamate receptor agonist, kainic acid (KA), or the GABA$_A$ receptor antagonist, pentylenetetrazole (PTZ). Paradoxically, after repeated repeated/chronic administration of the same chemoconvulsants, *SLC7A11*$^{sut/sut}$ mice exhibit signs of hypo-excitability, a response polar opposite to that which occurs in *SLC7A11*$^{+/+}$ littermate controls. Whether the aberrant neuronal excitability in *SLC7A11*$^{sut/sut}$ mice occurred in association with alterations in brain morphology – at the gross, cellular, and sub-cellular level – or with alterations in redox balance or plasma

membrane protein expression levels, was also investigated. Overall, our data demonstrate that neuronal excitability in $SLC7A11^{sut/sut}$ mice provoked by chemoconvulsant challenge deviates from that of $SLC7A11^{+/+}$ littermates in a complex manner that differs in sign depending on the chemoconvulsant dosing paradigm employed. Moreover, mutations in Sx_c^- trigger sex-dependent changes in redox status, brain morphology, and plasma membrane protein expression, any or all of which could contribute to the observed E/I imbalance in $SLC7A11^{sut/sut}$ mice.

Regulation of *in vivo* excitatory/inhibitory balance by the

cystine/glutamate exchanger system x_c^-

by

Sheila Marie Shahidzadeh Sears

B.S., Biopsychology, University of California, Santa Barbara 2012

Dissertation

Submitted in partial fulfillment of the requirement for the degree of

Doctor of Philosophy in Biology

Neuroscience Concentration

Syracuse University

December 2018

Acknowledgements

First and foremost, I want to thank my PhD advisor Dr. Sandra Hewett. With her support and guidance, I was able to pursue a novel line of inquiry that I found interesting for my dissertation research. Her rigorous training in experimental design, scientific writing, and oral presentations will serve me throughout my career, and I am grateful for the many hours that she has spent mentoring me in these important skills. Having pursued a doctorate under Dr. Hewett, I have been and will continue to be well-prepared to present my work to the broader neuroscience community and to have rewarding discussions with colleagues. I am excited for what lies ahead in my career - in large part because Dr. Hewett's contagious enthusiasm for science has inspired my own.

I would like to thank my committee members, including my informal co-advisor, Dr. Jim Hewett, whose insight and expertise of the seizure models used in this dissertation have been an invaluable resource. Drs. Frank Middleton and Melissa Pepling were instrumental members of my research committee, whose thought-provoking questions drove my scientific thoughts in novel directions. My sincere thanks also goes to Dr. Jessica MacDonald, who allowed me to access her laboratory facilities in order to pursue my neuronal morphological analyses and who, as a member of my defense committee, provided thoughtful feedback on my dissertation.

My colleagues in the Hewett[2] labs have provided a supportive environment over the years – and I would like to especially thank Dr. Yan He, Trista Thorn, Dr. Jingxue Shi, Yifan Gong, Twinkle Chowdury, Megan Leblanc, Valarie Vought, Matthew Allen, and Spandita Dutta for their assistance, expertise, and friendship inside and outside of

the lab. I will miss our coffee trips dearly, as well as coming into work each day to a lab full of colleagues that truly cared for and looked out for one another. Moreover, the departmental grad students – many of whom were roommates, friends, and confidants – were important in keeping me well-balanced. Our support of one another in our shared endeavor towards a graduate degree has been integral in my success.

Finally, I would like to thank my family – especially my parents, Laura and Shahram, and brother – for their support in my pursuit of a PhD – even though it was on the opposite side of the country. My parents have always taught us to pursue knowledge, and my work ethic – which was learned by watching their examples growing up – has allowed for me to successfully reach the PhD finish line. Last but certainly not least, I thank my husband Will. Though often times he was 3,445 miles away, his unwavering love and support (as my #1 fan), as well has his daily words of encouragement for five years, have meant the world to me.

Table of Contents

List of Figures

List of Tables

List of Abbreviated Terms

AMPA	alpha-amino-3-hydroxy-5-methyl-4-isoxazole propionic acid
CA1	Cornu Ammonis 1
CA3	Cornu Ammonis 3
cDNA	Complementary DNA
CNS	Central nervous system
Cys	Cysteine
CySS	Cystine
DG	Dentate Gyrus
EAAT	Excitatory amino acid transporter
E/I	Excitatory/inhibitory
EPSC	Excitatory postsynaptic current
EPSP	Excitatory postsynaptic potential
GABA	gamma-aminobutyric acid
GSH	Glutathione
GSSG	Glutathione disulfide
i.p.	Intraperitoneal
iGluRs	Ionotropic glutamate receptors
IPSC	Inhibitory postsynaptic current
IPSP	Inhibitory postsynaptic potential
KA	Kainic acid
KARs	Kainic acid receptors
KCC2	Potassium/chloride (K^+/Cl^-) cotransporter
Km	Substrate concentration at which velocity is $^1/_2$ of V_{max}
LTP	Long term potentiation
Mg^{2+}	Magnesium
mGluRs	Metabotropic glutamate receptors
MMSS	Median maximal seizure score
NAC	N-acetylcysteine
NMDA	*N*-methyl-D-aspartate receptors
PTZ	Pentylenetetrazole
qPCR	Quantitative real-time polymerase chain reaction
SE	Status epilepticus
SLC7A11	Solute carrier family 7 member 11
Sx_c^-	System x_c^-
VGATs	Vesicular GABA transporters
xCT	Light chain subunit of Sx_c^- transporter
4f2hc	Heavy chain of the surface antigen 4f2

Chapter 1: Introduction

1.1   Overview

In several brain disorders including autism, stroke, and epilepsy an imbalance between the excitatory and inhibitory (E/I) neurotransmitter systems exists. Understanding fully the cellular and molecular processes that underlie normal, physiological synaptic transmission is the first step in determining how such aberrations might be countered to provide affected individuals with E/I imbalance symptomatic relief. This dissertation focuses on the role of the cystine/glutamate antiporter System x_c^- (Sx_c^-) — which exports glutamate and imports cystine, the latter of which is the rate-limiting substrate for the synthesis of the thiol antioxidant glutathione — in maintenance of E/I balance.

1.2   The cystine/glutamate antiporter System x_c^- (Sx_c^-)

Sx_c^- was first described in 1980 by Bannai and Kitamura who demonstrated that the Na^+-independent uptake of cystine into cultured human diploid fibroblasts was inhibited by glutamate (and *vice versa*) (Bannai & Kitamura 1980). Sx_c^- is an amino acid antiporter that imports L-cystine and exports L-glutamate in a Na^+-independent, Cl^--dependent, 1:1 stoichiometric ratio (Bannai 1986, Bannai & Kitamura 1980). Cystine/glutamate exchange is electroneutral, with transport limited to the anionic form of these amino acids. The direction of exchange is determined by the substrate concentration gradient and is independent of membrane potential (Bannai 1986). Though Sx_c^- is capable of transporting either amino acid in either direction, rapid kinetics of excitatory amino acid transport (EAAT) systems and intracellular reductases maintain relatively low levels of extracellular glutamate and intracellular cystine, respectively, whereas intracellular glutamate levels are typically in the millimolar range,

conferring the aforementioned directionality of transport (Bannai & Kitamura 1980, Hertz et al 1988).

1.2.1 Sx$_c^-$ structure

Identification of Sx$_c^-$ by expression cloning revealed it is a heteromeric amino acid transporter (HAT) and therefore composed of a light chain and a heavy chain covalently linked through a disulfide bridge (Sato et al 1999). The light (catalytic) chains of HATs, also known as glycoprotein-associated amino acid transporters (gpaATs), are members of the solute carrier 7 (SLC7) family and confer their substrate specificity (Verrey et al 2004). HAT light chains must associate with a glycoprotein heavy chain of the SLC3 family in order to allow for surface expression (Verrey et al 2004). With respect to Sx$_c^-$ the gpaAT light chain is xCT, encoded by the solute carrier gene *SLC7A11*, and the heavy chain is 4f2hc (4f2 cell-surface antigen heavy chain, also known as cluster of differentiation 98 [CD98]), encoded by *SLC3A2* (Bassi et al 2001, Sato et al 1999). While xCT is specific to Sx$_c^-$, 4f2hc forms a heterodimer with at least five other gpaAT light chains within the HAT family (Verrey et al 2004).

In humans, the *SLC7A11* gene is located on chromosome 4q28-31, producing a 40 kDa protein of a predicted 501 amino acids (Bassi et al 2001). The encoded xCT protein shares 93-96% similarity and 89% identity to mouse xCT protein, which is a predicted 502 amino acids (Bassi et al 2001, Sato et al 1999). The mouse *SL7A11* gene maps on chromosome 3 (Lane 1988). As with other proteins of the HAT family, xCT has 12 putative transmembrane domains and is thus highly hydrophobic (Gasol et al 2004). Both the N- and C-termini are intracellularly localized, and there is a reentrant loop

between transmembrane domains 2 and 3 (Gasol et al 2004). This reentrant loop is believed to be a site of substrate binding, as biotinylation of His[110] at the apex of loops 2 and 3 does not occur in the presence of cystine, glutamate, or the non-transportable Sx$_c^-$ inhibitor, (s)-4-carboxyphenylglycine (4-CPG) (Gasol et al 2004). Another potential substrate binding site is near Cys[327] in the middle of the eighth transmembrane domain; in a study by Jimenez-Vidal and colleagues, the authors proposed a scenario whereby small side-chains at this position are permissive to substrate binding and translocation whereas bulky amino acids inflict steric hindrance to transporter activity (Jiménez-Vidal et al 2004). More recently, precrystallization screening of xCT bacterial orthologs and subsequent identification of a representative amino acid, polyamine, and organocation (APC) transporter revealed greater insight into HAT structure (Shaffer et al 2009). Further substrate permeation residues were identified including human xCT residue Arg[135], suggested to be a binding-site of the substrate's γ-carboxylate entity (Shaffer et al 2009). Using the crystal structure of this APC transporter, Bridges et al proposed a novel three-dimensional representation of xCT protein structure using protein threading of human xCT (Fig. 1.1) (Bridges et al 2012b).

The *SLC3A2* gene encoding the type II membrane glycoprotein 4f2hc is located on chromosome 11q12-13 in humans (chromosome 19 in mouse) and produces a ≈94 kDa glycosylated protein (72 kDa unglycosylated) of approximately 526-529 amino acids in humans (Francke et al 1983, Lumadue et al 1987, Quackenbush et al 1987). This protein shares 75% amino acid identity with mouse 4f2hc, which has a predicted 526 amino acids (Parmacek et al 1989). Mouse 4f2hc consists of a 428 amino acid

4
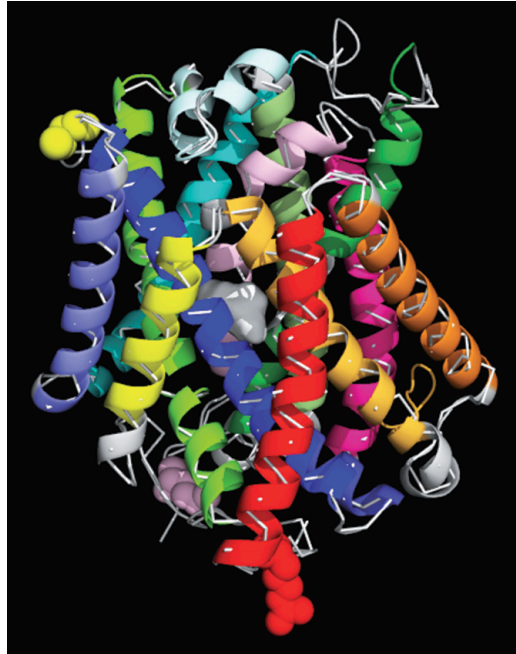
Figure 1.1 xCT homology model

xCT homology model depicting xCT protein in its inwardly-facing Apo form as proposed by Bridges et al 2012. The human xCT protein sequence was threaded over the crystal structure of a bacterial xCT homolog, ApcT (Shaffer et al 2009). Each helical ribbon represents a transmembrane domain of xCT, while the white thread demonstrates the ApcT structure. The truncated N and C termini are depicted by light pink and red spheres, respectively. Yellow spheres depict the conserved cysteine residue (Cys[158]), located between pore loops three and four of the xCT protein, that forms a bond with 4f2hc. Adapted from (Bridges et al 2012b).

extracellular C-terminal domain, a 23 amino acid transmembrane domain, and a 75

amino acid N-terminal cytoplasmic domain (Parmacek et al 1989). The bulky C-terminus

is heavily glycosylated, with nine potential N-linked glycosylation sites in mouse and

four such sites in human (Parmacek et al 1989). Northern blot analysis has revealed

that 4f2hc is ubiquitously expressed in mouse, with highest levels of expression found in

kidney, lung, spleen, testis, and brain (Parmacek et al 1989). It is involved in a diverse

array of biological processes including integrin signaling, cell adhesion, and cell

activation and proliferation (Bron et al 1986, Fenczik et al 1997, Nguyen et al 2008).

The latter role is supported by evidence that its expression is induced upon fibroblast

activation and maintained at high expression levels throughout the cell cycle (Parmacek

et al 1989). Given that 4f2hc is abundantly expressed throughout the body, Sx_c^-

transport activity is tied to the expression and availability of the light-chain subunit xCT

(Verrey et al 2004).

Multiple studies have confirmed that xCT forms a disulfide bridge with 4f2hc at a

single, conserved cysteine residue (Cys^{158}) located between pore loops three and four

of the xCT protein (Bassi et al 2001, Bridges et al 2012b, Sato et al 1999). Experiments

using cysteine-to-serine mutagenesis or reducing agents with 4f2hc/HAT dimers

suggest that this light-chain residue interacts with Cys^{109} of 4f2hc (Estévez et al 1998,

Torrents et al 1998). Intriguingly, the functional role of this covalent linkage remains

elusive. This cys-cys interaction is not required to induce transporter activity in at least

one other HAT; cysteine-to-serine mutagenesis at the disulfide bridge in LAT1, an

aromatic and branched-chain amino acid HAT, results in functional transport activity in

both *Xenopus* oocytes and mammalian cells (Nakamura et al 1999, Wagner et al 2000).

Whether the same is true for the xCT/4f2hc disulfide bridge remains to be investigated. Furthermore, exactly how 4f2hc interacts with xCT is unknown, though it too may share similar characteristics with other HATs. In the case of LAT2, a neutral amino acid transporter, the 4f2hc ectodomain interacts with its extracellular loops, covering the extracellular surface of the light chain protein and increasing transporter stability (Rosell et al 2014).

As mentioned previously, 4f2hc can interact with five other gpaAT light-chains at Cys[109] besides xCT; LAT1 (*SLC7A5*) (Kanai et al 1998, Mastroberardino et al 1998), LAT2 (*SLC7A8*) (Pineda et al 1999, Rossier et al 1999, Segawa et al 1999), system asc1 (small neutral amino acid transporter, *SLC7A10*) (Fukasawa et al 2000), and the cationic amino acid transporters y+LAT1 (*SLC7A7*) and y+LAT2 (*SLC7A6*) (Pfeiffer et al 1999, Torrents et al 1998) [for detailed reviews see (Palacín et al 2005, Verrey et al 2004)]. All 4f2hc-associated light-chains require the heavy chain to translocate to the plasma cell membrane and induce transporter activity. With respect to Sx_c^-, this was demonstrated in *Xenopus* oocytes whereby co-injection of xCT and 4f2hc cRNA induced transport of L-glutamate and L-cystine and resulted in expression of xCT at the oocyte plasma membrane (Bassi et al 2001, Sato et al 1999). In contrast, injection of xCT or 4f2hc alone did not induce transport activity, with the former scenario resulting in intracellular retention of xCT (Bassi et al 2001, Sato et al 1999). Induction of cystine/glutamate exchange can also be induced by co-injection of mouse, but not human, cRNA for xCT and rBAT, a heavy chain with significant homology to 4f2hc (Bassi et al 2001, Wang et al 2003). Whether xCT associates with rBAT *in vivo* has yet to be ascertained.

1.2.2 Sx$_c^-$ expression

Expression of xCT mRNA and protein have been detected throughout the body suggesting that Sx$_c^-$ plays a role in maintaining cellular health in a variety of biological processes. Northern blot and quantitative polymerase chain reaction (PCR) analyses have revealed widespread xCT mRNA expression in the pancreas, intestine, ovary, spleen, and stomach (Bassi et al 2001, Dave et al 2004). Using an xCT specific antibody confirmed by xCT siRNA knockdown in HT22 cells, Burdo and colleagues also demonstrated xCT protein expression in kidney (Burdo et al 2006).

Within the mouse central nervous system (CNS), *in situ* hybridization studies have revealed xCT mRNA expression at the brain/cerebral spinal fluid (CSF) borders including the cerebral ventricles, meninges, and circumventricular organs such as the area postrema and subfornical organ (Sato et al 2002). Furthermore, robust expression of xCT mRNA was found in most major brain regions including in the cerebral cortex, putamen, and medulla, with xCT protein detected in cortex, hippocampus, and striatum (Sato et al 2002, Shih et al 2006). Weak xCT mRNA expression was found in the choroid plexus, thalamus, cerebellum, brainstem, and nucleus of the solitary tract, with no expression detected in mouse brain vasculature (Sato et al 2002). Interestingly, xCT protein is present in human brain vasculature, suggesting that cystine/glutamate exchange across the blood brain barrier may be species specific (Burdo et al 2006).

Despite the scarcity of reliable antibodies against xCT protein – largely owing to its hydrophobicity bestowed by its 12 transmembrane domains – the cell-type specificity of xCT expression in the CNS is becoming increasingly better understood. While Sx$_c^-$ is expressed in cultured microglia (Jackman et al 2010, Piani & Fontana 1994), neurons

(Burdo et al 2006, Dun et al 2006, Jackman et al 2010, Murphy et al 1990), and the

HT22 neuronal cell line (Lewerenz et al 2003), there is a growing consensus that

astrocytes are the primary cell types expressing Sx_c^- in the mature brain *in vivo* (Fig.

1.2). Nearly 20 years ago, Pow and colleagues elucidated the cell-type specificity of Sx_c^-

activity using an antibody against the xCT substrate inhibitor, α-aminoadipate, in rat

brain slice (Pow 2001). Substrate accumulation occurred in glia – specifically Bergmann

glia, radial glia, and astrocytes – and was conspicuously absent from neurons and

oligodendrocytes (Pow 2001). Furthermore, rodent astrocytes in cell culture express

xCT, as do human glioma cell lines (Bender et al 2000, Burdo et al 2006, Cho & Bannai

1990, Gochenauer & Robinson 2001, Pow 2001, Ye & Sontheimer 1999), and

transcriptome data from both human and mouse cortex indicates that xCT is enriched in

astrocytes as compared to other parenchymal cells (Zhang et al 2014, Zhang et al

2016b). More recently, Ottestad-Hansen and colleagues engineered an xCT specific

antibody and determined that Sx_c^- is expressed throughout the adult mouse brain

parenchyma in a subpopulation of astrocytes – but not any other cell type investigated

including neurons, microglia, and oligodendrocytes (Ottestad-Hansen et al 2018).

Confirming *in situ* studies, xCT labeling was found concentrated at the

brain/blood/cerebral spinal fluid periphery, as well as in most major brain regions

including cortex, thalamus, hypothalamus, striatum, and hippocampus – where labeling

intensity was greatest in the molecular layer of the dentate gyrus and the *stratum*

lacunosum moleculare (Ottestad-Hansen et al 2018). Finally, the concentration of xCT

protein was estimated to be comparable to that of EAAT3 (0.013 mg/g hippocampal
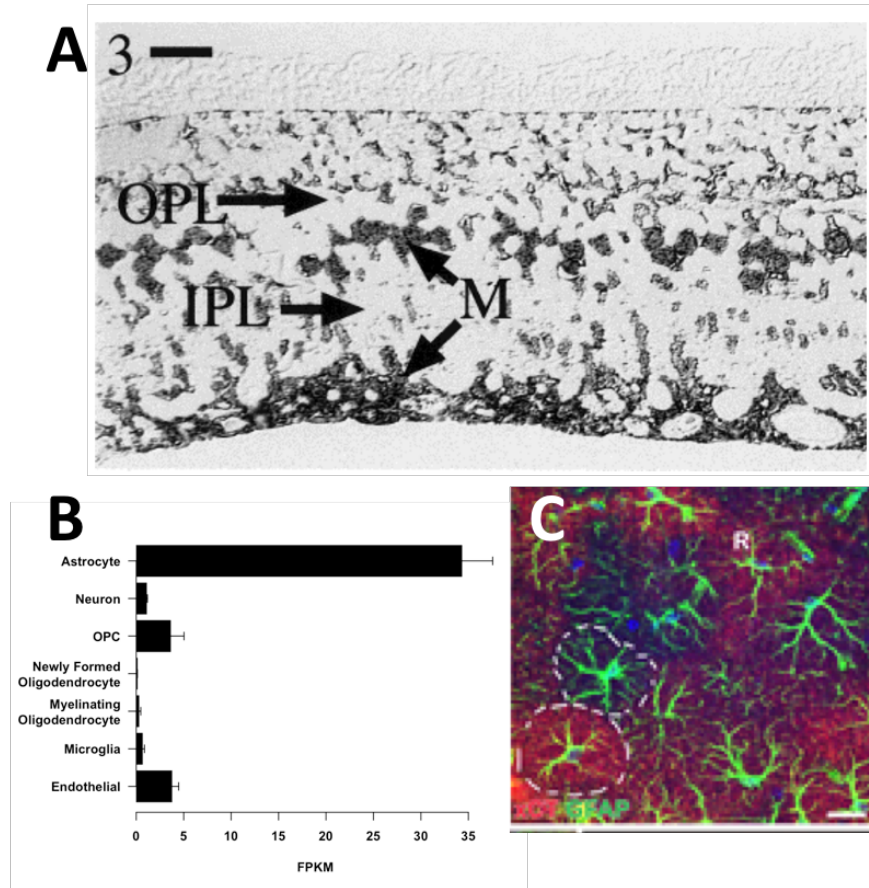
Figure 1.2 Sx$_c$⁻ is predominantly localized to CNS astrocytes

(A) An antibody against the xCT substrate inhibitor, α-aminoadipate, demonstrated that α-aminoadipate uptake occurred mainly in Muller glia cells (M) and was excluded from synaptic terminals in the outer (OPL) and inner (IPL) plexiform layers of rat retina. (B) Mouse cortical transcriptome data from the Barres lab indicates that astrocytes are the predominant cell types expressing *SLC7A11* in mouse cortex (OPC: oligodendrocyte precursor cell; FPKM: Fragments Per Kilobase of transcript per Million mapped reads). (C) Ottestad-Hansen and colleagues observed that xCT expression (red) exclusively co-localized with a subset of GFAP (green) expressing astrocytes in CA1 hippocampus (shown) and throughout the CNS (not shown). Figures adapted from [A (Pow 2001), B (Zhang et al 2014), and C (Ottestad-Hansen et al 2018)].

tissue), suggesting that xCT abundance is sufficient to contribute to brain function

(Holmseth et al 2012, Ottestad-Hansen et al 2018).

1.2.3. Sx$_c^-$ function

1.2.3.1 Use of xCT null mice to characterize Sx$_c^-$ function in vivo

Insight into the *in vivo* contribution of Sx$_c^-$ signaling has been possible due to the

use of genetic xCT loss of function mouse models. Sato and colleagues genetically

engineered the first global xCT knock-out (xCT$^{-/-}$) mouse on the C57BL/6 background by

removing the ATG start codon in exon 1 of *SLC7A11* (Sato et al 2005). These mice lack

glutamate-sensitive cystine uptake as well as xCT transcript and protein in all tissues

examined, including in brain and thymus where constitutive expression is normally

observed (McCullagh & Featherstone 2014, Sato et al 2005). xCT$^{-/-}$ mice, however,

were healthy in appearance, fertile, and all of the major organs examined – including

the kidney, pancreas, lung, liver, and brain – had no apparent abnormalities (Sato et al

2005). A second xCT loss of function mouse was engineered by inducing an in-frame

TGA stop codon in exon 10 of *SLC7A11* in C57BL/6 mice using *N*-ethyl-*N*-nitrosourea

(ENU) mutagenesis (Nabeyama et al 2010). Finally, a spontaneous mutation in

SLC7A11 gave rise to the subtle gray (sut) mutant mice on the C3H/HeSnJ background,

henceforth referred to as the *SLC7A11$^{sut/sut}$* mice (Chintala et al 2005). The

SLC7A11$^{sut/sut}$ mice have a large deletion (481,280 base pairs) that extends from intron

11 to exon 12 and into the *SLC7A11* intergenic region neighboring the *Pcdh18* gene,

resulting in a new stop codon in exon 12' (Chintala et al 2005). Important for this

dissertation, no xCT protein or transcript have been detected in the brains of

SLC7A11$^{sut/sut}$ mice (Chintala et al 2005, McCullagh & Featherstone 2014). These mice are fertile and healthy in appearance (Hewett lab unpublished observations). *SLC7A11$^{sut/sut}$* mice have a subtle gray coat color, which is a result of decreased pheomelanin (red/yellow) pigment production due to reduced Sx_c^--mediated cystine import into melanocytes (Chintala et al 2005). Interestingly, Shih et al found that *SLC7A11$^{sut/sut}$* mice exhibit gross brain atrophy by 13 weeks of age compared to wild-type C3H/HeSnJ mice maintained on a separate, homozygous background as demonstrated by a reduction in hemisphere and striatal area, cortical thinning, and ventricular enlargement (Shih et al 2006). However, the observed neurodegeneration in this particular *SLC7A11$^{sut/sut}$* sub-strain may be attributable to genetic drift from the authors wild-type colony as a result of maintaining homozygous colonies (Henderson 1997, Masel 2011). Indeed, *SLC7A11$^{sut/sut}$* mice derived from heterozygous breeding units do not exhibit gross brain atrophy when compared to wild-type littermate controls (Chapter 2), suggesting the phenotype reported by Shih et al is not exclusively due to loss of the *SLC7A11* gene.

1.2.3.2 Cellular cystine supplier

Sx_c^--mediated cystine import is fundamental in maintaining the extracellular and intracellular redox balance as it provides the rate-limiting substrate (cysteine) for the biosynthesis of the thiol antioxidant glutathione (GSH; γ-glutamylcysteinylglycine) (Sato et al 1998) and it facilitates the cysteine/cystine redox coupling across the cell plasma membrane (Banjac et al 2008). Once transported intracellularly, cystine is rapidly reduced into two cysteine molecules that can be incorporated in proteins, GSH, or

exported via the neutral alanine-serine-cysteine transporters (system ASC) in maintenance of the cystine/cysteine redox couple (Banjac et al 2008, Sato et al 1998).

It should be noted that cells throughout the body can accumulate cyst(e)ine via several alternative mechanisms. *De novo* cysteine synthesis from methionine via the transsulfuration pathway represents a mechanism by which cells can obtain cysteine, and evidence suggests this pathway may be particularly active in supplying cysteine for GSH synthesis under conditions of oxidative stress or when Sx_c^- transport is limited (McBean 2012). In addition, several cystine transporters are expressed throughout the body, including system $b^{0,+}$ and the aspartate/glutamate transporter 1 (AGT1), responsible for cystine reabsorption in the renal proximal tubules (Fernández et al 2002, Nagamori et al 2016). In the CNS, other known cysteine transporters include system X_{AG}^- transporters EAAT2 and EAAT3, expressed in astrocytes and/or neurons (Chen & Swanson 2003, Watts et al 2014), the ASC transporters 1 and 2, predominantly expressed in astrocytes (Fernández et al 2005, Fotiadis et al 2013, Nagamori et al 2016), the aromatic preferring amino acid transporter (ArpAT) (Fernández et al 2005), the system A Na^+-coupled neutral amino acid transporters 1 and 2 (SNAT1 and SNAT2) (Mackenzie & Erickson 2004), and the neurotransmitter transporter 4 (NTT4) (Zaia & Reimer 2009).

Despite the prevalence of cyst(e)ine transporters, GSH synthesis in CNS astrocytes is tightly linked to Sx_c^--mediated cystine import. In fact, in their seminal characterization of Sx_c^--mediated cystine/glutamate exchange, Bannai and Kitamura demonstrated that approximately 15% of Sx_c^--mediated cystine import is incorporated into GSH within five minutes of transport (Bannai & Kitamura 1980). This is further

exemplified by evidence demonstrating enhanced Sx_c^- activity occurs in association with

increases in GSH (Hosoya et al 2002, Sasaki et al 2002), and that inhibition of Sx_c^-

diminishes intracellular GSH stores (Kato et al 1992, Sagara et al 1996).

GSH synthesis takes places intracellularly in the cytosol in a two-step reaction

(Fig. 1.3) (Meister 1974). In the first step, glutamate and the rate-limiting substrate

cysteine are used to form the dipeptide γ-glutamylcysteinyl in a reaction catalyzed by γ-

glutamylcysteinyl synthetase (glutamate-cysteine ligase). In the second step,

glutathione synthetase catalyzes the formation of γ-glutamylcysteinylglycine (GSH) from

γ-glutamylcysteinyl and glycine; with the final product (GSH) capable of feedback

inhibiting γ-glutamylcysteinyl synthetase (step one) (Meister 1974, Richman & Meister

1975). In fulfillment of its role as an antioxidant, GSH either directly detoxifies radicals

or serves as a cofactor for the antioxidant enzyme glutathione peroxidase in the

reduction of peroxides (Chance et al 1979, Saez et al 1990, Winterbourn & Metodiewa

1994). In either case, GSH oxidation results in a glutathione disulfide (GSSG) product,

which itself is a substrate for glutathione reductase in a reaction that regenerates GSH

[reviewed in (Dringen et al 2000)]. In this way, GSH molecules synthesized

intracellularly and used for detoxification are recycled. Conversely, GSH molecules

used as a substrate for intracellular glutathione-S-transferases (GST) lower the

intracellular GSH concentration, as does GSH export [reviewed in (Dringen et al 2000)].

In the CNS, increased astrocyte GSH production is intimately linked to decreased

oxidative stress susceptibility in neurons (Gegg et al 2005). Interestingly, astrocytes

export 10% of their GSH per hour (Minich et al 2006). Once extracellular, GSH may

serve as a substrate for the ectoenzyme γ-glutamyl transpeptidase (γGT) and its
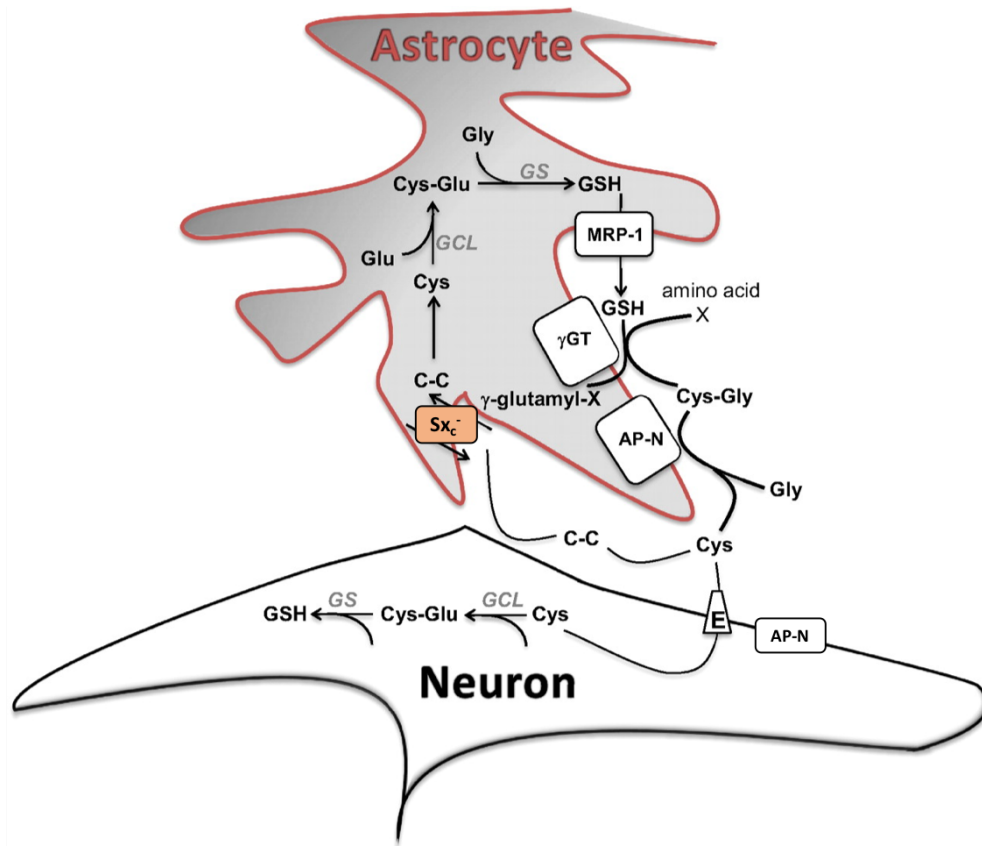
Figure 1.3 GSH metabolism and transport

Astrocyte Sx_c^- imports cystine (C-C) which, once intracellular, is rapidly reduced to cysteine (Cys). Glutamate-cysteine ligase (GCL; also known as γ-glutamylcysteinyl synthetase) catalyzes the formation of glutamate (Glu) and Cys to γ-glutamylcysteine (Cys-Glu). Glycine (Gly) is added to the dipeptide by GSH synthetase (GS) to form the tripeptide glutathione (GSH). Astrocytic export of GSH is facilitated through the multidrug resistance protein 1 (MRP-1) transporter. Once extracellular, GSH is cleaved by γ-glutamyltransferase (γ-GT) into cysteinylglycine (Cys-Gly). Aminopeptidase N (AP-N) promotes further breakdown of cysteinylglycine into glycine and cysteine. Cysteine is taken up into neurons via EAATs (E), where it is metabolized into GSH. Alternatively, the extracellular oxidation of cysteine into cystine promotes Sx_c^--mediated uptake into astrocytes. Adapted from (Bridges et al 2012a).

product, cysteinylglycine (CysGly), can serve as a GSH precursor (Taniguchi & Ikeda 1998). Neurons express an ectopeptidase of their own (aminopeptidase N) which allows them to utilize CysGly by taking up its constituent amino acids (cysteine and glycine) to be used for GSH synthesis intracellularly (Dringen et al 2001). Thus, astrocytic GSH production is not only used as a cell-autonomous thiol antioxidant, but its export confers protection to neurons as well. Apart from its role as an antioxidant, GSH is perhaps the most important cellular thiol that participates in signal transduction and regulates cellular metabolism and proliferation, gene expression, cytokine and growth factor production, and the function of proteins with redox-modification residues (Dringen 2000, Klatt & Lamas 2000, Poot et al 1995, Shih et al 2006, Stamler & Hausladen 1998).

Since astrocytes derive the majority of their cystine from Sx_c^- transport, and cyst(e)ine is the rate-limiting substrate in the synthesis of GSH and forms a redox couple (cysteine/cystine) on its own, it follows that Sx_c^- is involved in maintaining redox balance *in vivo*. Indeed, male xCT-deficient mice on a C57BL/6 background have a plasma redox imbalance characterized by elevated CySS and decreased GSH levels as compared to wild-type control animals (Sato et al 2005). Intriguingly, male xCT null mice on this same background do not have a hippocampal or striatal redox imbalance as evidenced by lack of oxidative stress markers and similar GSH levels as compared to wild-type controls (De Bundel et al 2011, Massie et al 2011b). Furthermore, the striatum of male xCT null mice have similar expression levels of oxidative stress-related markers HO-1, HNE, and NT as compared to wild-type controls following a 6-hydroxydopamine (6-OHDA) injection (Massie et al 2011b). Whether a compensatory

expression of other cysteine transporters in xCT null mice explains their lack of brain redox imbalance is not known.

1.2.3.3 Regulation of ambient extracellular glutamate levels

Evidence from xCT null animals has demonstrated that Sx_c^--derived glutamate contributes to the extracellular glutamate pool that bathes the CNS *in vivo*. In male $xCT^{-/-}$ mice, extracellular glutamate levels are decreased by $\approx$40% in the hippocampus and $\approx$70% in the striatum as compared to wild-type C57BL/6 controls (De Bundel et al 2011, Massie et al 2011b). Similarly, in male *SLC7A11*$^{sut/sut}$ mice, extracellular glutamate levels are decreased in the striatum by $\approx$50% as compared to wild-type C3H/HeSnJ mice (McCullagh & Featherstone 2014). Interestingly, extracellular glutamate levels in male *SLC7A11*$^{sut/sut}$ cerebellum are comparable to wild-type controls, suggesting that the contribution of Sx_c^- to ambient glutamate occurs in a brain region-dependent manner (McCullagh & Featherstone 2014). These findings are in line with results from the Danbolt lab showing relatively weak cerebellar xCT expression levels as compared to forebrain (Ottestad-Hansen et al 2018). Of note, the one study that investigated extracellular glutamate levels in both male and female Sx_c^- null mice found that male, but not female, *SLC7A11*$^{sut/sut}$ mice have decreased extracellular glutamate levels in the striatum as compared to wild-type sex-matched controls (Borra et al 2014). Interestingly, the authors did find a $\approx$70% decrease in striatal extracellular glutamate levels in wild-type females versus males, giving rise to the idea that there are sex-differences in glutamate physiology and perhaps, Sx_c^--mediated glutamate release (Borra et al 2014).

Regulation of ambient extracellular glutamate levels by Sx_c^- is conserved across species. In *Drosophila*, genetic disruption of the xCT homolog, *genderblind*, results in a ≈50% reduction in hemolymph glutamate levels (Augustin et al 2007, Piyankarage et al 2008). Furthermore, reverse dialysis of the xCT pharmacological inhibitors homocysteic acid or (*S*)-4-carboxyphenylglycine (CPG) leads to a 60% decrease in extracellular glutamate levels in rat striatum (Baker et al 2002).

The role of ambient glutamate appears to be multifaceted (section 1.3.3.2), and several mechanistic studies have shed light on whether Sx_c^--derived glutamate contributes to physiological neural transmission. In *genderblind* mutants, Augustin and colleagues demonstrated that a reduction in glutamate levels occurs in association with increased ionotropic glutamate receptor immunoreactivity and enhanced spontaneous excitatory junction current amplitudes at the neuromuscular junction (NMJ) (Augustin et al 2007). Moreover, bathing wild-type larval NMJs in abnormally low levels of glutamate was sufficient to phenocopy glutamate receptor expression levels in *genderblind* mutants (Augustin et al 2007). More recently, this same group confirmed Sx_c^--derived glutamate controls synaptic strength at the mouse hippocampal CA3-CA1 synapse by demonstrating that slices derived from male $xCT^{-/-}$ mice have enhanced AMPA receptor immunoreactivity and spontaneous and evoked excitatory postsynaptic currents (EPSCs) in CA1 as compared to wild-type control slices (Williams & Featherstone 2014). Similar to their studies in *Drosophila*, the authors phenocopied their $xCT^{-/-}$ electrophysiology findings by incubating wild-type slices in Glu-free artificial cerebrospinal fluid or by using the Sx_c^- inhibitor (*S*)-4-carboxyphenylglycine (4-CPG), providing evidence that glutamate released via Sx_c^- modulates synaptic strength

(Williams & Featherstone 2014). Finally, Sx_c^--derived glutamate negatively modulates release of synaptic glutamate and dopamine in the nucleus accumbens and striatum, respectively, by exerting glutamatergic tone on group II metabotropic glutamate receptors in male rats (Baker et al 2002, Moran et al 2005). Thus, evidence across multiple species suggests that Sx_c^--derived ambient glutamate contributes to the delicate balance between excitatory and inhibitory neurotransmission (E/I balance) that exists in the CNS.

1.2.4 Role of Sx_c^- in CNS function

While Sx_c^- signaling has been implicated in a number of disorders and disease states associated with a primary or secondary excitatory/inhibitory (E/I) imbalance including multiple sclerosis (Domercq et al 2007, Evonuk et al 2015, Pampliega et al 2011), amyotrophic lateral sclerosis (Albano et al 2013, Mesci et al 2014), Huntington's disease (Frederick et al 2014), Alzheimer's disease (Barger & Basile 2001, Qin et al 2006, Zhang et al 2016a), Parkinson's disease (Bentea et al 2015b, Massie et al 2011b, Massie et al 2008), cerebral ischemia (Fogal et al 2007, Soria et al 2014), addiction (Baker et al 2003, Knackstedt et al 2010, Moran et al 2005), epilepsy (Lewerenz et al 2014, Takaki et al 2008), and glioblastoma multiforme (Chung et al 2005, Takeuchi et al 2012, Ye et al 1999, Ye & Sontheimer 1999) and its associated epileptiform activity (Buckingham et al 2011, Robert et al 2015), a growing body of evidence suggests that Sx_c^- may also contribute to physiological brain E/I balance. Behaviorally, male xCT$^{-/-}$ mice demonstrate decreased spatial working memory as determined by reduced alternations in the three-arm spontaneous alternation task compared to wild-type

controls, and similar deficits were found in male and female *SLC7A11[sut/sut]* mice (De

Bundel et al 2011, McCullagh & Featherstone 2014). Furthermore, male *SLC7A11[sut/sut]*

mice have impaired long-term memory in a hippocampal and amygdala-dependent fear

conditioning task as well as in a hippocampal-dependent passive avoidance task (Li et

al 2012). Given the memory deficits across several distinct tasks, it is perhaps

unsurprising that long-term potentiation at the CA1-Schaeffer collateral synapse is also

reduced in male *SLC7A11[sut/sut]* mice (Li et al 2012).

In assays of anxiety, male xCT^{-/-} mice have a decreased latency to eat in a

novelty suppressed eating paradigm and spend an increased amount of time in an open

field or in the lighted portion of a light/dark box as compared to wild-type littermates

(Bentea et al 2015a). These results suggest that Sx_c^- increases behavioral anxiety. In

addition, xCT^{-/-} mice demonstrate increased climbing behavior and decreased

immobility in the forced swim and tail suspension tests as compared to wild-type

littermate controls, suggesting that xCT^{-/-} mice have less behavioral despair as

compared to wild-type controls (Bentea et al 2015a). Of note, motor activity and visual

acuity is normal in xCT^{-/-} and *SLC7A11[sut/sut]* mutants, suggesting that these are unlikely

confounds in any of the aforementioned behavioral paradigms (Bentea et al 2015a,

McCullagh & Featherstone 2014).

Despite xCT^{-/-} mice demonstrating enhanced spontaneous and evoked EPSCs at

the hippocampal CA3-CA1 synapse (discussed above), De Bundel and colleagues have

demonstrated that male xCT^{-/-} mice have an apparent increase in seizure threshold

upon acute stimulation with the chemoconvulsants kainic acid, NMDA, or pilocarpine

(De Bundel et al 2011, Williams & Featherstone 2014). Specifically, male xCT^{-/-} mice

require a higher dose of kainic acid or pilocarpine, delivered via intravenous infusion, to induce seizure activity as compared to wild-type controls (De Bundel et al 2011). Furthermore, xCT$^{-/-}$ mice have a decreased incidence of mortality and increased latency to convulsive seizure upon administration of a single intraperitoneal dose of NMDA as compared to wild-type mice (De Bundel et al 2011). The increase in seizure threshold in xCT$^{-/-}$ mice *in vivo* is in stark contrast to their enhanced excitability in *ex vivo* slice (Williams & Featherstone 2014), suggesting a complex regulation of E/I balance by Sx$_c^-$ *in vivo*. Moreover, these results are also in contrast to findings reported in this dissertation demonstrating a sex-independent decrease in seizure threshold in *SLC7A11$^{sut/sut}$* mice as compared to *SLC7A11$^{+/+}$* sex-matched littermate controls in response to an acute dose of two pharmacologically distinct chemoconvulsants, pentylenetetrazole (Chapter 2, Fig. 2.9) or kainic acid (Chapter 4, Fig. 4.1).

1.3   Excitatory/inhibitory (E/I) balance in the brain

Effective communication between cells in the CNS requires a balance between excitatory and inhibitory neural transmission. This balance is established during development and maintained throughout adulthood (Turrigiano & Nelson 2004). At the network level, the E/I balance refers to the innumerable inhibitory and excitatory neurons that together, maintain a stable circuit [reviewed in (Gao & Penzes 2015, Nelson & Valakh 2015)]. At the cellular level, E/I balance is influenced by the intrinsic membrane excitability and synaptic strength controlling the overall output – or firing probability – of a given neuron (Beck & Yaari 2008, Megías et al 2001, Pratt & Aizenman 2007, Turrigiano et al 1998). Importantly, the physiological E/I balance

21

provides a stable substrate upon which the information transfer underlying learning and memory formation can occur (Cannon 1932, Zhou & Yu 2018).

Of particular interest to this dissertation is the balance between excitatory glutamatergic and inhibitory GABAergic neural transmission – including the synthesis, release, and uptake of these neurotransmitters, as well as the myriad receptors upon which they exert their influence. Functional alterations at excitatory or inhibitory synapses have been implicated in numerous neurodevelopmental disorders (Gao & Penzes 2015, Nelson & Valakh 2015) and disease states (Foerster et al 2013, Fritschy 2008, Lai et al 2014, Ren et al 2018, Snyder et al 2005), and as such, understanding all factors that contribute to maintenance of E/I balance is integral in developing novel therapeutic targets to provide symptomatic relief. In this section, factors driving normal glutamatergic or GABAergic neural transmission, as well as modulators of E/I balance, including those influenced by Sx_c^- transport, are discussed.

1.3.1 Inhibitory GABAergic neural transmission

GABA (γ-aminobutyric acid) is the major inhibitory neurotransmitter in the CNS. Originally classified as a glutamatergic neuromodulator, evidence demonstrating that it is present in large concentrations in the mammalian brain and that ionotophoretic application to cortex is sufficient to inhibit cell firing paved the way for its classification as an inhibitory neurotransmitter (Awapara et al 1950, Elliott 1965, Krnjević & Phillis 1963, Krnjević & Whittaker 1965). Additionally, GABA signaling regulates proliferation of neural progenitors and neuronal development (Ge et al 2007, Platel et al 2010).

GABA synthesis and packaging: GABA is predominantly synthesized from glutamate via one of two molecularly distinct enzymes – glutamate decarboxylase 65 (GAD65) or GAD67 – using pyridoxal 5'-phosphate as a cofactor. The subcellular distribution of the two GAD enzymes differs. GAD65 is primarily located in nerve terminals and thus produces GABA for neurotransmission (Martin & Rimvall 1993, Waagepetersen et al 1999). GAD67 is distributed uniformly throughout neurons and provides GABA to fulfill non-neurotransmitter roles such as redox regulation and developmental synaptogenesis (Lamigeon et al 2001, Martin & Rimvall 1993, Waagepetersen et al 1999). Approximately 50% of GAD exists in its inactive, apoenzyme form; this is thought to function as a reserve for when enhanced GABA synthesis is required (Itoh & Uchimura 1981, Miller et al 1980). Alternatively, GABA can be synthesized directly from glutamine derived from the Kreb's cycle via 2-oxoglutarate and glutamate (Waagepetersen et al 1998, Westergaard et al 1995). Following its synthesis, GABA is transported into synaptic vesicles via vesicular GABA transporters (VGATs) in a process dependent on both the membrane potential and the proton gradient (Chaudhry et al 1998, McIntire et al 1997). Interestingly, glycine is a shared substrate for VGATs, and as such, glycine is co-released at certain GABAergic synapses (Wojcik et al 2006).

GABA signaling: Upon depolarization of the GABAergic nerve terminal, a rise in intracellular calcium levels stimulates exocytosis of GABA-containing vesicles (Chen et al 2017). In the synaptic cleft, GABA can activate one of three major GABA receptors (GABARs): the ionotropic $GABA_AR$ and $GABA_CR$ as well as the G-protein coupled metabotropic $GABA_BR$ [for review see (Bormann 2000)].

The GABA$_A$R and GABA$_C$R are pentameric ligand-gated ion channels that mediate the majority of fast synaptic inhibition [for review see (Bormann 2000)]. As the potassium/chloride (K$^+$/Cl$^-$) cotransporter (KCC2) maintains relatively low intracellular Cl$^-$ levels in mature neurons, GABA binding to either ionotropic receptor facilitates a Cl$^-$ influx and bicarbonate (HCO$_3^-$) efflux leading to a net hyperpolarization (Rivera et al 1999). Each receptor is composed of five subunits: there are 18 GABA$_A$R subunits (α1-6, β1-4, γ1-4, δ, ε, π, and θ) and three GABA$_C$R subunits (ρ1-3) [(Bonnert et al 1999, Hedblom & Kirkness 1997) and reviewed in (Macdonald & Olsen 1994, Zhang et al 2001)]. While GABA$_A$Rs must contain at least three subunits (including an obligatory α and β subunit) and are expressed throughout the brain, GABA$_C$Rs are only composed of ρ subunits and are predominantly expressed in the vertebrate retina (Bormann 2000, Bormann & Feigenspan 1995). Despite structural dissimilarities, both GABA$_A$ and GABA$_C$ receptors allow for Cl$^-$ influx upon ligand binding. However, GABA$_C$Rs are more sensitive to GABA and have a smaller single channel conductance compared to GABA$_A$Rs (major conductance state of 1–5 pS versus $\approx$30 pS) (Chang & Weiss 1999, Karim et al 2013, Wotring et al 1999, Zhang et al 2001). Pharmacologically, GABA$_A$Rs are positively modulated by benzodiazepines and barbiturates via binding sites at their subunit interfaces (Chiara et al 2013, Macdonald & Olsen 1994, Pritchett et al 1989). Moreover, GABA$_A$Rs are selectively inhibited by the competitive antagonist bicuculline (Andrews & Johnston 1979). In contrast, GABA$_C$Rs are benzodiazepine, barbiturate, and bicuculline insensitive (Bormann & Feigenspan 1995).

The GABA$_B$R is a G-protein coupled metabotropic receptor capable of modulating synaptic transmission through its intracellular effector systems (Padgett &

Slesinger 2010). Each receptor is a heterodimer consisting of a $GABA_{B1}$ subunit – of which there are A and B isoforms – and a $GABA_{B2}$ subunit [reviewed in (Heaney & Kinney 2016)]. $GABA_BR$ activation results in a bicuculline-insensitive GABAergic current that is modulated by the $GABA_BR$ selective agonist baclofen (Bowery et al 1979). Moreover, $GABA_BR$ activation is negatively coupled to adenylate cyclase and therefore has an overall inhibitory effect, with presynaptic activation inhibiting neurotransmitter release and postsynaptic activation increasing the K^+ conductance responsible for long-lasting inhibitory postsynaptic potentials (IPSPs) (Kabashima et al 1997, Pérez-Garci et al 2006, Sakaba & Neher 2003).

GABA uptake: GABA released into the synaptic cleft is cleared by GABA transporters expressed on both neurons and astrocytes. There are four known high-affinity GABA transporters, all of which belong to the SLC6 family: GABA transporter 1-3 (GAT1-3), and the betaine-GABA transporter (BGT1) (Guastella et al 1990, Liu et al 1993, Lopez-Corcuera et al 1992, Radian et al 1986, Yamauchi et al 1992). All transporters are Na^+ and Cl^- coupled, with reported Km values of 8 μM (GAT1), 18 μM (GAT2), 0.8 μM (GAT3), and 80 μM (BGT1) (Liu et al 1993, Liu et al 1992, Lopez-Corcuera et al 1992). In the CNS, GAT1 is localized to both neurons and astrocytes whereas GAT3 is selectively expressed in astrocytes (Minelli et al 1995, Minelli et al 1996). In contrast, GAT2 and BGT1 are largely excluded from the brain, except for the encompassing leptomeninges and blood vessels, but are predominantly expressed in the kidney and liver (Zhou et al 2012, Zhou et al 2011). In the brain, GABA taken up by neurons can be directly packaged into vesicles for neurotransmission (Coulter & Eid 2012, Eulenburg & Gomeza 2010). Alternatively, in a process known as the GABA

shunt, GABA taken up by neurons or astrocytes can replenish TCA cycle intermediates via its catabolism into succinate by GABA-transaminase (GABA-T) and succinic semialdehyde dehydrogenase (SSADH) (Bak et al 2006, Fonnum & Fyske 2000).

1.3.2 Excitatory glutamatergic neural transmission

Glutamate is the most abundant excitatory amino acid neurotransmitter in the vertebrate nervous system (Fonnum 1984, Ottersen & Storm-Mathisen 1984). The first evidence of its role as an excitatory neurotransmitter came from the seminal discovery that direct application of glutamate to neural tissue resulted in epileptic seizure activity (Hayashi 1952, Hayashi 1954, Okamoto 1951). Its presence in concentrations three- to four-fold greater than aspartate, glutamine, or taurine – the next three most abundant amino acids in brain – also provided suggestion that it had specialized functions apart from serving as an amino acid building block (McGeer et al 1978). Later work established that glutamate fulfills the criteria for classification as a neurotransmitter: it is localized to nerve terminals, it is released from a neuron upon stimulation, it is capable of activating its cognate receptors, direct application of glutamate mimics neuronal stimulation, and mechanisms exist to rapidly terminate its action (Fonnum 1984, Watkins & Evans 1981). In addition to its role as the major excitatory neurotransmitter in the brain, glutamate is a precursor for GABA and other various Krebs cycle intermediates and it is involved in the regulation of ammonia levels and osmotic balance (McGeer et al 1978, Roberts & Frankel 1950, Weil-Malherbe 1950). Furthermore, glutamate is involved in the synthesis of fatty acids, proteins, and peptides, including glutathione (Meister 1979).

Approximately 80-90% of neurons, and the same proportion of central synapses, are glutamatergic (Braitenberg & Schüz 2013, Ottersen & Storm-Mathisen 1984). Given its ubiquitous CNS localization, it is unsurprising that glutamate signaling is involved in a diverse array of brain functions including sensory transduction, motor coordination, and cognitive processes such as learning and memory [for review see (Hassel & Dingledine 2012)]. However, high fidelity glutamatergic transmission requires a stable substrate – efficient glutamate release and uptake, as well as low ambient extracellular glutamate concentrations – and it follows that alterations in such are associated with neurological disorders and disease states. For example, hypo-glutamatergic signaling is implicated in the cognitive deficits associated with schizophrenia (Moghaddam & Javitt 2012). Moreover, excessive glutamate release and prolonged activation of its receptors can lead to seizures and neuronal cell death via excitotoxicity (Choi 1992, Nadler et al 1978, Olney 1969). Thus, it is essential that the release and uptake of glutamate be tightly regulated.

Glutamate synthesis and packaging: Neurons synthesize glutamate via the hydrolysis of glutamine to glutamate and ammonia, catalyzed by the phosphate-dependent mitochondrial enzyme glutaminase (Errera & Greenstein 1949baker, Laake et al 1999). Alternatively, glutamate can be rapidly transaminated from α-ketoglutarate, a key intermediate in the Kreb's cycle, via the enzyme glutamate dehydrogenase (Peng et al 1993). Finally, glutamate can be directly transported from the extracellular space into neurons through Na^+-dependent EAATs (Danbolt et al 2016). In its final form, glutamate is transported into synaptic vesicles via vesicular glutamate transporters, of which there are three mammalian isoforms (VGLUT1-3 encoded by the genes

SLC17A6-8), to a maximum glutamate concentration of approximately 70-210 mM per vesicle (Burger et al 1989, Omote et al 2011, Riveros et al 1986). Accumulation of glutamate via VGLUTs is chloride-dependent and driven by both the membrane potential and an electrochemical gradient of H^+ ions established by the V-ATPase (Naito & Ueda 1985, Omote et al 2011).

Glutamate release: Upon depolarization of nerve terminals, increasing intracellular calcium levels stimulate vesicular fusion with the presynaptic membrane, allowing for glutamate molecules to be released into the synaptic cleft (Fernandez-Chacon et al 2001, Geppert et al 1994). Though vesicular-mediated neuronal glutamate release mediates the majority of fast excitatory neurotransmission, glutamate can also be released by neurons and/or astrocytes via several other mechanisms. In both cell types, calcium-independent glutamate release can occur via EAAT reversal, especially under pathological conditions such as cerebral ischemia wherein the Na^+ and K^+ gradients across the plasma cell membrane are reduced (Longuemare & Swanson 1995, Nicholls & Attwell 1990, Szatkowski et al 1990). In an attempt to achieve volume homeostasis under hypo-osmotic conditions, neurons and astrocytes may release anions, including glutamate, through volume-regulation anion channels (VRACs) (Kimelberg et al 1990, Mongin & Orlov 2001). Additionally, astrocytic hemichannels – when left unopposed versus aligned with a hemichannel on a neighboring astrocyte to allow for intercellular gap junction-mediated transport – are independently functional and can efflux glutamate and other amino acids (Ye et al 2003). This mechanism of glutamate release may be functional under conditions of metabolic inhibition when hemichannels appear to open (Contreras et al 2002, John et al 1999), though some

evidence also indicates hemichannels are open physiologically (Bruzzone et al 2001, Kamermans et al 2001, Plotkin & Bellido 2001, Quist et al 2000). Furthermore, $P2X_7$ receptor-associated ion channels are capable of glutamate efflux upon ligand binding (Duan et al 2003). Moreover, calcium-dependent vesicular glutamate release from astrocytes has been demonstrated, and is supported by evidence that G-protein coupled receptor activation, and the ensuing rise in intracellular calcium levels, culminate in glutamate release (Bezzi et al 1998, Parpura et al 1994). This release mechanism is further substantiated by astrocytic expression of exocytotic machinery including cellubrevin, synaptobrevin II, syntaxin, vesicular soluble N-ethylmaleimide-sensitive factor attachment protein receptors (SNAREs), and VGLUTs (Bezzi et al 2004, Parpura et al 1995, Schwarz et al 2017). However, opposing evidence indicates lack of metabotropic glutamate receptors in adult astrocytes suggesting that vesicular-mediated glutamate release may be a developmental phenomenon (Sun et al 2013). Moreover, astrocyte transcriptome analyses and more recent immunohistochemical data demonstrate a paucity of VGLUT expression (Barres 2008, Cahoy et al 2008, Li et al 2013, Zhang et al 2014) and as such, whether this route of glutamate release exists *in vivo* is hotly debated (for dual perspective reviews see (Fiacco & McCarthy 2018, Savtchouk & Volterra 2018)). Finally, of particular interest to this dissertation, glutamate release occurs via Sx_c^--mediated cystine/glutamate exchange (Bannai & Kitamura 1980). Route of release notwithstanding, once released into the synaptic cleft or extracellular space, glutamate binds to its cognate receptors and/or is taken up by EAATs.

Glutamate receptors: Two distinct classes of glutamate receptors exist within the CNS, ionotropic (iGluR) and metabotropic (mGluR) [for reviews see (Niswender & Conn 2010, Traynelis et al 2010)]. Canonical iGluRs are integral membrane cation channels capable of mediating rapid synaptic transmission and can be further classified into three subtypes based upon structure and agonist pharmacology: α-amino-3-hydroxy-5-methyl-4-isoxazole propionic acid receptors (AMPARs), kainic acid receptors (kainate, KARs), and N-methyl-D-aspartate receptors (NMDARs) [for review see (Traynelis et al 2010)]. Glutamate delta receptors (δ1 and δ2) are a fourth iGluR subtype, which have been classified as such solely upon sequence homology as they are not gated by glutamate (Lomeli et al 1993, Yamazaki et al 1992). Instead, endogenous ligands for these receptors include D-serine and glycine (Naur et al 2007). The eight mGluR subtypes function as G-protein coupled receptors and can be broadly classified into three subcategories based upon sequence homology, pharmacology, and second messenger systems (Pin & Acher 2002).

Tetrameric AMPARs are assembled using combinations of subunits GluA1-4, with forebrain receptors containing predominantly GluA1/GluA2 and GluA2/GluA3 subunits (Craig et al 1993). Upon glutamate binding, the opening of the ion-channel pore allows for Na^+ influx and K^+ efflux, facilitating postsynaptic membrane depolarization with rapid onset and desensitization kinetics (Jones & Westbrook 1996). RNA editing of the GluA2 subunit (Q/R edit) is prevalent in the adult brain, and this feature bestows calcium-impermeability to the pore channel (Greger et al 2003). However, the presence of unedited GluA2 subunits and/or GluA2-lacking AMPARs allow for AMPA-mediated calcium influx; the latter receptors have been demonstrated to

play a role in plasticity, including in the stabilization of long-term potentiation (Plant et al 2006, Yang et al 2010). AMPARs are enriched at glutamatergic synapses, and dendritic spine morphology correlates with the number of synaptic AMPARs (Kasai et al 2003, Matsuzaki et al 2001). Their dynamic trafficking to and from the postsynaptic membrane, often via lateral diffusion from extrasynaptic sites, are key determinants of synaptic strength (Lüscher et al 1999).

KARs are tetrameric receptors composed of a combination of the subunits GluK1-5. These subunits have heterogeneous expression patterns and, although expressed throughout the CNS, predominant localization has been demonstrated in the hippocampus (GluK2, GluK3, GluK4, GluK5) and cerebellum (GluK1, GluK2, GluK5) (Porter et al 1997). In addition to agonist binding, KARs require external monovalent cations and anions at binding sites on the GluK1-5 subunits to allow for pore opening (Bowie 2002, Paternain et al 2003). Similar to AMPARs, Q/R editing within subunits GluK5-6 bestows calcium-impermeability (Köhler et al 1993, Sommer et al 1991). At the postsynaptic membrane, KAR activation enhances excitation, albeit via a slower and smaller excitatory postsynaptic current than AMPAR activation (Castillo et al 1997, Frerking et al 1998). Presynaptically, KAR activation induces depression of inhibition (Rodríguez-Moreno et al 1997, Sloviter & Damiano 1981), thought to occur via a noncanonical metabotropic route of KAR signaling (Rodríguez-Moreno & Lerma 1998). Moreover, presynaptic KAR activation can modulate glutamate release, with facilitation or depression of release at the mossy fiber-CA3 and CA3-CA1 hippocampal synapses dependent upon agonist concentration (Chittajallu et al 1996, Frerking et al 2001, Schmitz et al 2000).

NMDARs are distinct from the aforementioned iGluRs in that they exhibit high calcium permeability (in addition to fluxing Na^+ and K^+) and mediate the slow component of excitatory synaptic currents, thus allowing for temporal summation (Schiller & Schiller 2001). NMDARs function as coincidence detectors: channel opening is dependent upon the binding of glutamate and glycine along with membrane depolarization to relieve a voltage-dependent magnesium (Mg^{2+}) block (Mayer et al 1984). Much like AMPARs and KARs, the tetrameric assembly of GluN1, GluN2A-D, and/or GluN3A-B subunits dictates their physiology [reviewed in (Sanz-Clemente et al 2013)]. GluN1 and GluN2 subunits are required for receptor function as they contain the glutamate and glycine binding sites, respectively, while receptors containing a GluN3 subunit are calcium impermeable (Kew et al 2000, Laube et al 1997, Matsuda et al 2002, Nishi et al 2001). Given their calcium conductance, NMDARs play a role in the expression of activity-dependent plasticity and multiple lines of evidence suggests that NMDAR trafficking contributes to both Hebbian (long-term potentiation and depression) and homeostatic forms of plasticity as well (Hunt & Castillo 2012, Pérez-Otaño & Ehlers 2005).

G-protein coupled mGluRs are classified into three groups based on agonist pharmacology and intracellular second messenger cascades [for reviews see (Niswender & Conn 2010, Pin & Acher 2002)]. Group I (mGluR 1 and mGluR5) receptors are coupled to phospholipase C and generally lead to increases in protein phosphorylation and activation of calcium binding proteins. Group II (mGluR2 and mGluR3) and III (mGluR4 and mGluR6-8) receptors are negatively coupled to adenylate cyclase, decreasing cAMP production and protein phosphorylation. In the CNS, the

physiological role of mGluR signaling is varied, ranging from positive and negative

facilitation of presynaptic neurotransmitter release to inhibition of postsynaptic calcium

channels (Pin & Acher 2002).

Glutamate uptake: Extracellular glutamate is taken up by EAATs in an

electrogenic process driven by the import of $3Na^+$ and $1H^+$ coupled to the export of $1K^+$

(Barbour et al 1991, Kanner & Schuldiner 1987, Levy et al 1998, Nicholls & Attwell

1990, Zerangue & Kavanaugh 1996). Transport also occurs with an uncoupled Cl^-

gradient (Bergles et al 2002, Wadiche et al 1995). Rapid glutamate uptake by the

EAATs is necessary to prevent overactivation of glutamate receptors and excitotoxic

cell death. There are five mammalian EAAT transporters that differ in their cellular and

regional distribution, all of which belong to the SLC1 (high affinity glutamate and neutral

amino acid) family of transporters (Hediger et al 2013). Found throughout the brain are

EAAT1 (GLAST) (Storck et al 1992, Tanaka 1993), localized exclusively on astrocytes

(Lehre et al 1995), EAAT2 (GLT-1) (Danbolt et al 1990), localized predominately to

astrocytes but also located on some neuronal axon terminals (Chen et al 2004, Furness

et al 2008, Zhou et al 2018), and EAAT3 (EAAC1) (Bjørjås et al 1996, Kanai & Hediger

1992), localized to neuronal somata and dendrites (Holmseth et al 2012, Rothstein et al

1994). EAAT4 is found primarily in cerebellar Purkinje cells (Fairman et al 1995, Itoh et

al 1997), but also astrocytes (Hu et al 2003), whereas EAAT5 is restricted to retinal

bipolar and photoreceptor neurons (Arriza et al 1997). Despite redundant functional

activity among the EAATs, the vast majority ($\approx$95%) of extracellular glutamate uptake is

performed by EAAT2 (Danbolt et al 1992, Haugeto et al 1996, Otis & Kavanaugh 2000).

Indeed, genetic deletion of EAAT2 in mice results in spontaneous epileptiform activity

by three weeks of age (Tanaka et al 1997), and spontaneous electrographic seizures and increased mortality have been reported in astrocytic (but not neuronal) EAAT2 conditional knock-out mice (Petr et al 2015). Once taken up into astrocytes, glutamate can be released via one of the aforementioned mechanisms, including Sx_c^-, or it can be incorporated into proteins, metabolized via the Kreb's cycle, or converted to glutamine via the enzyme glutamine synthetase (Erecińska & Silver 1990, Krebs 1935). The transport of glutamine from astrocytes into neurons via sodium-coupled neutral amino acid transporters (SNATs) or other glutamine transporters is thought to provide the majority of glutamate precursor to neuronal terminals (Jenstad et al 2008, Mackenzie & Erickson 2004, Solbu et al 2010). Together, neuronal glutamate release, its astrocytic uptake and conversion to glutamine, and its subsequent transport to neurons for glutamate or GABA synthesis is referred to as the glutamine-glutamate (GABA) shuttle (Hertz 2013).

1.3.3 Modulators of E/I Balance

Other than fast inhibitory or excitatory synaptic transmission, a comprehensive understanding of mechanisms underlying brain E/I balance includes the effects exerted by neuromodulators. These include substances such as brain derived neurotrophic factor (BDNF) and adenosine, as well as a cell type of particular interest to this dissertation, astrocytes. Interestingly, astrocytes can release soluble factors, such as glypicans, tumor necrosis factor-α (TNFα), and secreted protein acidic and rich in cysteine (SPARC), that influence synaptogenesis and synaptic activity (Allen et al 2012, Jones et al 2011, Stellwagen & Malenka 2006). Moreover, the glutamate-glutamine

cycle, maintained by astrocytes, controls synaptic strength during period of intense neuronal activity (Tani et al 2014). Of interest to this dissertation is how the intracellular/extracellular redox environment and ambient extracellular glutamate levels – two parameters maintained in part by astrocytes and influenced by Sx_c^- signaling – contribute to E/I balance.

1.3.3.1 Redox status

Numerous lines of evidence suggest that redox status influences the E/I balance. For instance, a redox imbalance is associated with impaired neuronal synaptic plasticity (Almaguer-Melian et al 2000, Robillard et al 2011), with effects of such on seizure activity reported (Jiang et al 2000, Liang & Patel 2004). However, the exact mechanism by which redox signaling influences E/I balance is unclear, with reports of increased (Liang & Patel 2004) or decreased (Jiang et al 2000) seizure activity in mice under oxidative stress. Moreover, compounds with antioxidant properties (vitamin C, superoxide dismutase [SOD], melatonin, and N-acetylcysteine) have been demonstrated to reduce seizures and seizure-induced cell death in several animal models of epilepsy (MacGregor et al 1996, Rong et al 1999, Tan et al 1998, Zaeri 2015). Interestingly, both glutamate transporters and the NMDAR possess redox-sensing properties that regulate their activity (Aizenman et al 1989, Köhr et al 1994, Sullivan et al 1994, Trotti et al 1997), suggesting that a redox imbalance can modulate E/I balance through influencing glutamatergic neural transmission.

1.3.3.2 Ambient extracellular glutamate

Despite the efficient glutamate uptake mechanisms described earlier, there is a pool of ambient extracellular glutamate that bathes the CNS *in vivo*. Estimates of the ambient extracellular glutamate concentration range from 25-90 nM as determined by electrophysiological measurement of tonic NMDAR activity in acute brain slices (Benveniste et al 1984, Cavelier & Attwell 2005, Herman & Jahr 2007, Meur et al 2007) to 0.2-35 μM as measured by *in vivo* microdialysis (Baker et al 2003, Dash et al 2009, De Bundel et al 2011, Massie et al 2011b). Some reports postulate that the discrepancy in ambient glutamate concentrations could reflect compartmentalization within distinct synaptic (nM) and extrasynaptic (μM) glutamate compartments (Baker et al 2002, Moussawi et al 2011). Another possibility for the discordant measurements in ambient glutamate is that *in vivo* microdialysis studies are typically performed in adult mice whereas acute slice experiments are performed using young rodents (postnatal day 11-19), a point in development when glutamate transporters, including Sx_c^-, are not yet fully expressed (Kugler & Schleyer 2004, La Bella et al 2007). However, the two aforementioned theories were recently refuted by work demonstrating that ambient glutamate levels in acute brain slices are $\approx$25 nM *throughout* the brain in both young (postnatal day 15-22) and old (8-12 week old) rats, indicating a distinct lack of compartmentalization and age-related differences in rat (Chiu & Jahr 2017). Finally, micromolar glutamate levels as measured by *in vivo* microdialysis could be an artifact of tissue damage inflicted by the sampling probe, thus rendering the adjacent neuropil metabolically impaired (Sun et al 2014).

Despite conflicting reports over the precise concentration of extracellular

glutamate, evidence suggests that ambient levels are sufficient to influence E/I balance.

For instance, tonic activation of NMDARs by glutamate of non-vesicular origin (Ca^{2+}-

independent, tetrodotoxin-insensitive) regulates the intrinsic excitability and

synchronization of hippocampal pyramidal and granule cells (Angulo et al 2004,

Cavelier & Attwell 2005, Dalby & Mody 2003, Jabaudon et al 1999, Meur et al 2007,

Sah et al 1989). Moreover, tonic exposure to micromolar levels of glutamate has been

demonstrated to cause steady-state glutamate receptor desensitization and

suppression of synaptic strength (Augustin et al 2007, Williams & Featherstone 2014,

Zorumski et al 1996). Other evidence points to a role for ambient glutamate in

depolarization induced suppression of inhibition (DSI) of inhibitory interneurons through

its activation of pyramidal cell mGluRs in the hippocampus (Varma et al 2001). Finally, a

developmental role for ambient glutamate in E/I circuit formation has been suggested,

with reports indicating it can regulate cellular differentiation and migration (LoTurco et al

1991, LoTurco et al 1995, Manent et al 2005, Nguyen et al 2001).

1.3.4 Use of chemoconvulsants to investigate E/I balance in vivo

Experimentally, baseline E/I balance can be measured using brain slice or *in vivo*

electrophysiological recordings. Alternatively, the use of pharmacological agents to

stimulate or inhibit excitatory and/or inhibitory signaling can be used to uncover an E/I

imbalance that may not be apparent physiologically. Pertinent to the studies performed

in this dissertation, the chemoconvulsants pentylenetetrazole (PTZ) and kainic acid (KA)

will be discussed. As potent chemoconvulsants, PTZ and KA are capable of eliciting

seizures, which is a brain state characterized by abnormally excessive or synchronous neuronal activity (Fisher et al 2005). The aberrant electrical activity induced by a seizure can be recorded via electroencephalography; it also manifests as behavioral motor changes ranging from immobility to generalized convulsive seizures involving clonic limb movements. Thus, by using frank motor seizures as a behavioral readout, chemoconvulsant-induced brain excitation is readily observable.

1.3.4.1 Pentylenetetrazole (PTZ)

PTZ was first characterized as an inhibitor of GABARs in 1978 (Macdonald & Barker 1978). Several years later, radioligand studies determined its site of action to be at the picrotoxin binding site within the $GABA_AR$ channel pore (Ramanjaneyulu & Ticku 1984, Squires et al 1984). A more recent report by Huang and colleagues indicated that PTZ and picrotoxin share common but not identical domains of action, as the PTZ antagonized-$GABA_AR$ current occurs exclusively through competitive inhibition whereas picrotoxin displays both non-competitive and competitive inhibition of $GABA_ARs$ (Huang et al 2001). Following its synthesis in 1924, PTZ was initially used as a cardiovascular and respiratory stimulant (Haury 1939). In a line of investigation stemming from his postmortem neuropathological observations of decreased gliosis in schizophrenic tissue versus enhanced gliosis in epileptic tissue, Meduna began using PTZ in 1934 as a therapeutic treatment to induce epileptic activity in schizophrenic individuals in an attempt to stimulate gliosis (Meduna 1932, Meduna 1935). Eventually, PTZ was replaced with electroconvulsive therapy as the therapeutic stimulant of choice in mood disorders and schizophrenia (Bini 1938).

PTZ administration in laboratory animals is traditionally used to experimentally test the efficacy of anti-seizure drugs in response to seizure activity (Swinyard 1949). Alternatively, it can be used in rodents to explore their seizure threshold, or the innate balance between excitation and inhibition that influences seizure susceptibility (Steppuhn & Turski 1993). Finally, PTZ can be used as a chemical kindling agent to model epileptogenesis – which is the process by which a normal brain network develops spontaneous recurrent seizures (i.e. epilepsy) over time. The kindling phenomenon occurs via a gradual sensitization of neuronal circuitry to repeated application of a low intensity stimulus (Goddard 1967). A similar period of sensitization is thought to occur during the latent period of acquired epilepsies, which are a group of diseases characterized by spontaneous seizures resulting from an antecedent CNS injury and ensuing latent, seizure-free period (Braunwald et al 2001, Victor & Ropper 2002). Thus, kindling serves as a model of acquired epilepsies, and understanding the cellular and molecular mechanisms facilitating this period of sensitization is integral in developing therapeutic targets to thwart their progression (Jensen 2009). Moreover, given that kindling induces synaptic changes over time it is, at its core, a plasticity model. In fact, kindling shares common mechanisms with long-term potentiation (LTP) (Cain 1989, Goddard & Douglas 1975) and as such, it can be used to study how E/I balance evolves during plastic sensitization of neuronal circuitry.

Though strain differences exist with regards to seizure presentation, in general, within tens of seconds of receiving a systemic dose of PTZ rodents will socially isolate themselves, becoming distinctly hypomobile and unresponsive (Kosobud et al 1992). These seizures can evolve into myoclonic muscle jerks, indicative of increased

synchronous neuronal activity in the motor cortex. Depending on the dose of PTZ (sub-convulsive vs. convulsive), seizure severity can further progress into a generalized convulsive episode involving forelimb and/or hindlimb clonus. This progression of seizure activity – from behavioral immobility and facial automatisms, to forelimb clonic movements and generalized convulsions – was first characterized by Ronald Racine (Racine 1972).

In the seminal kindling studies performed by Goddard, the stimulus was a sub-convulsive threshold electrical current, delivered daily via depth electrodes implanted in rat amygdala (Goddard 1967). Several years later, several studies pioneered the use of PTZ as a chemical kindling agent (Ito et al 1977, Mason & Cooper 1972). In this model, a low dose of PTZ is administered daily via systemic injections. Over time, an initially sub-convulsant dose will evoke behavioral convulsions, at which point an animal is considered to be "kindled" (Dennison et al 1995, Wada et al 1974), an effect generally viewed as being permanent. It should be noted that the kindling phenomenon is not specific to rodents, rather, it has been demonstrated in every species tested, from frog to humans, where a similar seizure progression was observed in response to brain tumors (McNamara 1986, Morrell 1985).

1.3.4.2 Kainic Acid (KA)

The excitatory agent KA was first isolated by Murakami and colleagues from the red seaweed *Digenea simplex* (Murakami et al 1953). Soon after, it was found that microiontophoretic administration to cortical neurons resulted in prolonged spike discharges (Shinozaki 1978, Shinozaki & Konishi 1970), followed next by the

observation that parenteral KA delivery resulted in excitotoxic, depolarization-induced cell death (Olney et al 1974). In its seminal use as a chemoconvulsant, Lagowska and Ben-Ari discovered that KA administration in the amygdala produced prolonged, recurrent convulsive seizures (status epilepticus), heralding its use in epilepsy research (Ben-Ari & Lagowska 1978). Indeed, KA induces excitatory activity as it exhibits affinity for both AMPARs as well as its own cognate receptors, bindings to KARs containing the GluK1-2 and GluK5-7 subunits with high-affinity (Vincent & Mulle 2009). Within minutes of systemic KA administration, animals become immobile and/or hypermobile – including unilateral rotations and/or pacing – which can further progress to displays of myoclonic twitching, kyphotic rearing, and paw clonus associated with rearing [personal observations and (Ben-Ari 2012, McKhann II et al 2003)]. Depending on the dose, these seizures can evolve into generalized convulsions and "popcorn" like violent jumping that in some instances culminates in death [personal observations and (Ben-Ari 2012, McKhann II et al 2003)]. Following KA administration, early activation of the hippocampus and amygdala, two brain regions with a particularly low seizure threshold, is observed via EEG recording (Ben-Ari 2012). Postmortem analysis of KA-treated animals reveals extensive cell loss in hippocampal CA3, a region particularly vulnerable to KA-induced excitation, in part, due to a high density of KARs and excitatory recurrent collaterals that, once synchronous, propagate to other structures within the limbic system and brain (Ben-Ari 2012, Ben-Ari & Cossart 2000, Miles & Wong 1983, Robinson & Deadwyler 1981, Vincent & Mulle 2009, Westbrook & Lothman 1983). Finally, the KA-induced model of status epilepticus represents a model of acquired

epilepsy as animals can develop spontaneous seizures several weeks to months following the initiation of seizure activity (Ben-Ari 2012).

1.3.5 Current need for understanding E/I balance

An E/I imbalance has been implicated in numerous neurological disorders and disease states. For instance, dysfunction of GABAergic signaling, glutamatergic signaling, or both has been implicated in the etiology of autism spectrum disorders (ASD), anxiety, depression, intellectual disability, cerebral ischemia, traumatic brain injury, schizophrenia, and epilepsy (Coghlan et al 2012, Luscher & Fuchs 2015, Meldrum 1994, Moghaddam & Javitt 2012, Olsen & Avoli 1997). This is exemplified by ASDs and schizophrenia which, despite varied genetic etiologies, both present with similar E/I deficits including NMDAR hypofunction (Akbarian et al 1996, Blundell et al 2010, Duffney et al 2013, Gao & Penzes 2015, Maliszewska-Cyna et al 2010, Morris et al 2005). In fact, an emerging hypothesis is that a shared pathophysiological E/I imbalance underlies similar social and cognitive behavioral phenotypes in ASD and schizophrenia (Gao & Penzes 2015). Furthermore, while dozens of disease associated genes have been implicated in epilepsy (Poduri & Lowenstein 2011), behavioral presentation of spontaneous seizures – the hallmark of epilepsy diseases – are thought to be a result of commonalities in GABAergic hypofunction and/or glutamatergic hyperfunction (Bradford 1995). Given the prevalence of disorders and disease states associated with an E/I imbalance, it is necessary to fully understand all cellular and molecular processes that underlie normal, physiological E/I transmission in order to

develop novel therapeutic options to provide individuals with an E/I imbalance

symptomatic relief.

1.4   Specific Aims

Numerous studies demonstrate that Sx_c^- is an important contributor to the ambient extracellular glutamate levels that bathe the central nervous system *in vivo* (Augustin et al 2007, Baker et al 2002, Bannai 1986, De Bundel et al 2011, Massie et al 2011a, Melendez et al 2005). Moreover, Sx_c^--mediated cystine import provides cells with the rate-limiting substrate (cysteine) of the major cellular antioxidant glutathione; it also forms a redox couple on its own (Banjac et al 2008, Dringen 2000). Given that glutamate signaling and cellular redox status both influence neuronal excitability, the objective of this dissertation was to determine whether endogenous Sx_c^- signaling contributes to E/I balance *in vivo* and if so, to investigate the mechanism(s) underlying its contribution.

1.4.1 Specific Aim 1

Experiments were designed to determine whether Sx_c^- contributes to the E/I balance *in vivo* using the acute-PTZ seizure threshold test (Chapter 2). Female and male mice that harbor a spontaneous mutation in Sx_c^- (*SLC7A11$^{sut/sut}$* mice) were used to assess the contribution of endogenous Sx_c^- signaling in acute seizures induced indirectly by disinhibition achieved via administration of the $GABA_A$ receptor antagonist PTZ. Moreover, experiments in this aim characterized naïve *SLC7A11$^{sut/sut}$* mice by exploring the extent to which loss of Sx_c^- affected brain morphometry at the gross and cellular level.

1.4.2 Specific Aim 2

Experiments were designed to determine whether Sx$_c^-$ signaling affects synaptic plasticity assessed using the PTZ-kindling model of epileptogenesis (Chapter 3). Whether endogenous Sx$_c^-$ signaling contributed to epileptogenesis was assessed by comparing PTZ-kindling acquisition between male *SLC7A11$^{sut/sut}$* and *SLC7A11$^{+/+}$* littermates. Furthermore, experiments in this aim addressed whether observed changes in PTZ-kindling were associated with morphological changes implicated in epileptogenesis, with changes in brain redox status, and/or with changes in plasma membrane protein expression.

1.4.3 Specific Aim 3

Experiments were designed to determine whether Sx$_c^-$ signaling regulates E/I balance using both the acute-KA seizure threshold test and the elevated KA dosing model of status epilepticus (Chapter 4). To explore whether results found in chapters two and/or three were model-dependent, this specific aim used a pharmacologically distinct chemoconvulsant, KA, to directly elicit excitation *in vivo* in two different dosing paradigms.

> **Aim 3.1:** Female and male *SLC7A11$^{sut/sut}$* and *SLC7A11$^{+/+}$* littermates were used to assess the contribution of endogenous Sx$_c^-$ signaling to acute seizures induced by KA.
>
> **Aim 3.2:** Whether endogenous Sx$_c^-$ signaling contributed to the incidence of status epilepticus elicited using an elevated KA dosing paradigm was assessed using female and male *SLC7A11$^{sut/sut}$* and *SLC7A11$^{+/+}$* littermates. Furthermore,

the contribution of endogenous Sx_c^- signaling to repeated KA dosing-induced cell death and KA-mediated changes in glutamate or GABA receptor plasma membrane protein expression levels was investigated.

1.5   Significance

A variety of neurological disorders and disease states are afflicted by an E/I imbalance (Section 1.3.5). In order to develop therapeutic targets for disease states resulting from an E/I imbalance, including epilepsy, we must first fully understand the cellular and molecular processes that underlie normal, physiological transmission. Towards this end, the results presented herein provide the first evidence that physiological Sx_c^- function maintains E/I balance *in vivo* in both female and male mice. Additionally, evidence is presented implicating Sx_c^- in epileptogenesis. As such, the work presented in this thesis may pave the way for the development of therapeutic targets to combat an E/I imbalance.

Chapter 2: Sex-dependent alterations in neuronal morphometry occur in association with altered E/I balance in system x_c^- null mice

2.1   Summary

Despite evidence that the cystine/glutamate antiporter Sx_c^- contributes to ambient extracellular glutamate levels and redox status, its contribution to physiological brain function *in vivo* remains incompletely defined. As such, the present study investigated whether and how Sx_c^- contributes to morphological parameters implicated in E/I balance, as well as, whether it contributes to acute seizure activity elicited by the chemoconvulsant PTZ. Gross brain and cellular morphology were explored using thionin or Golgi-Cox staining, respectively, in female and male *SLC7A11$^{+/+}$* and *SLC7A11$^{sut/sut}$* mice. Furthermore, littermate mice were administered an acute dose of PTZ (i.p.) and seizure severity was scored using a five-point behavioral scale. Our results demonstrate that loss of Sx_c^- signaling results in sex-dependent brain morphological alterations at the gross, cellular, and sub-cellular level. Specifically, female *SLC7A11$^{sut/sut}$* mice have decreased corpus callosum thickness, soma size, and dendritic spine head widths as compared to *SLC7A11$^{+/+}$* sex-matched littermate controls. Conversely, male *SLC7A11$^{sut/sut}$* mice have enhanced dendritic complexity and dendritic spine head widths as compared to *SLC7A11$^{+/+}$* sex-matched littermate controls. Interestingly, these sex-dependent morphological alterations occur in association with a sex-independent enhancement of neuronal excitability, exemplified by a decreased convulsive seizure threshold upon administration of an acute dose of PTZ. This study provides the first evidence that Sx_c^- signaling regulates brain morphology in a sex-dependent manner, and that loss of Sx_c^- disrupts E/I balance in the acute PTZ seizure threshold test.

2.2   Introduction

System x_c^- (Sx_c^-) is an amino acid antiporter that couples the import of L-cystine

(CySS) with the export of L-glutamate (Glu) with 1:1 stoichiometry (Bannai 1986, Bannai

& Kitamura 1980). Sx_c^- is a heterodimer composed of a light chain (xCT, encoded by

SLC7A11) that confers substrate specificity linked via a disulfide bridge to a heavy chain

(4f2hc or CD98, encoded by *SLC3A2*) that traffics xCT to the plasma membrane (Bassi

et al 2001, Sato et al 1999, Verrey et al 2004). Within the central nervous system

(CNS), transcriptome and immunohistochemical analyses conclude that Sx_c^- is

predominantly localized to astrocytes (Ottestad-Hansen et al 2018, Pow 2001, Zhang et

al 2014).

Evidence from xCT mutants indicates that Sx_c^--mediated glutamate release

accounts for >50% of the ambient extracellular glutamate pool that bathes the CNS *in*

vivo (Augustin et al 2007, De Bundel et al 2011). This pool of glutamate is largely

regulated by glial transporters, and multiple studies suggest it plays a role in maintaining

physiological excitatory/inhibitory (E/I) balance. For example, glial-derived ambient

glutamate can modulate neuronal Kv2.1 channels, whose somatodendritic location and

delayed-rectifier K^+ current exert a strong influence on action potential initiation

(Mulholland et al 2008, Murakoshi & Trimmer 1999). Moreover, tonic activation of

NMDA receptors by ambient glutamate regulates the intrinsic excitability and

synchronization of hippocampal pyramidal and granule cells (Angulo et al 2004,

Cavelier et al 2005, Dalby & Mody 2003, Meur et al 2007, Sah et al 1989). Other

evidence points to a role for ambient glutamate in depolarization induced suppression of

inhibition (DSI) of inhibitory interneurons through its activation of pyramidal cell

metabotropic glutamate receptors (mGluRs) in the hippocampus (Varma et al 2001).

Pertinently, studies performed in xCT mutants have demonstrated that genetic deletion

of xCT results in increased (200-300%) postsynaptic glutamate receptors in *Drosophila*,

and male transgenic xCT null mice have enhanced AMPA receptor surface expression

and larger evoked and spontaneous EPSCs in *ex vivo* slice (Augustin et al 2007,

Williams & Featherstone 2014). Although the magnitude of EPSCs is positively

correlated with morphological parameters, such as dendritic complexity (Klenowski et al

2016) and dendritic spine geometry (Matsuzaki et al 2001), whether mice null for Sx_c^-

have cellular morphological alterations is not known.

Sx_c^- also contributes to the intracellular/extracellular redox homeostasis; CySS

import through Sx_c^- is necessary for the synthesis and maintenance of the cellular

antioxidant glutathione (GSH) and contributes to the cysteine/cystine (Cys/CySS) redox

cycle across the cell plasma membrane (Banjac et al 2008, Sato et al 2005).

Interestingly, cellular redox status influences the E/I balance in part because glutamate

receptors (NMDA) and transporters are susceptible to redox modification; disulfide

reduction potentiates NMDA mediated currents and increases glutamate uptake

whereas thiol oxidation does the opposite (Aizenman et al 1989, Köhr et al 1994,

Sullivan et al 1994, Trotti et al 1997). Additionally, GSH participates in signal

transduction and regulates gene expression, cellular metabolism, and cell proliferation

(Lu 2009, Wu et al 2004). Moreover, GSH deficiency in excitatory amino acid

transporter 3 (EAAT3/EAAC1) null mice (Aoyama et al 2006), as well as

pharmacologically induced GSH deficiency in rats (Jain et al 1991), occurs in

association with brain tissue atrophy, suggesting that decreased GSH levels induces

neurodegeneration. However, exactly how redox balance influences excitability *in vivo* appears to be complex; mice deficient in glutathione peroxidase, with elevated brain oxidative stress levels, display less seizure activity following KA administration whereas manganese superoxide dismutase ($SOD^{+/-}$) mice with chronic mitochondrial oxidative stress have increased seizure severity (Jiang et al 2000, Liang & Patel 2004). Pertinently, male and female transgenic xCT null mice have elevated levels of plasma CySS (Sato et al 2005). However, male transgenic xCT null mice have normal levels of hippocampal GSH and are resistant to seizures elicited by intravenous infusion of three pharmacologically distinct chemoconvulsant – pilocarpine, NMDA, or KA (De Bundel et al 2011).

Taking an *in vivo* approach, we investigated whether female and male Sx_c^- null (*SLC7A11^{sut/sut}*; *sut/sut*) mice have alterations in brain excitability as compared to wild-type littermate control mice. Given that changes in synaptic efficacy and redox balance are associated with changes in brain morphology, we investigated whether alterations in such occurred in *SLC7A11^{sut/sut}* mice. Herein, we demonstrate that sex-dependent changes in neuronal morphology occur in association with a sex-independent increase in susceptibility to PTZ-evoked convulsive seizures in *SLC7A11^{sut/sut}* mice. These results indicate that Sx_c^- signaling contributes to the endogenous network activity that maintains E/I balance *in vivo*.

2.3   Materials and Methods

2.3.1 Animals

Mice were bred and maintained in the AALAC accredited Laboratory Animal Resource facility of Syracuse University on a 12 hr light/dark schedule (7am/7pm). Standard mouse chow and water were provided *ad libitum*. Wild-type (*SLC7A11*$^{+/+}$) and xCT mutant (*SLC7A11*$^{sut/sut}$) littermates for studies were derived from heterozygous (*SLC7A11*$^{+/sut}$) breeding units (F1) that were obtained by crossing *SLC7A11*$^{sut/sut}$ male mice [Jackson Laboratories (JAX) Stock #001310] with *SLC7A11*$^{+/+}$ female C3H/HeSnJ mice (JAX, Stock #000661). F2 *SLC7A11*$^{+/sut}$ progeny were also used as breeding units for studies. Genotyping was performed via PCR analysis of tail genomic DNA samples: *+/+* primers, 5'- GAA GTG CTC CGT GAA GAA GG -3' (forward), 5'- ATC TCA ATC CTG GGC AGA TG -3' (reverse); *sut/sut* primers, 5'- CCA CTG TTG TAG GTC AGC TTA GG -3' (forward), 5'- CAG GAC CTG TGA ATA TGA TAG GG -3' (reverse). Mice were segregated by sex at weaning and *SLC7A11*$^{+/+}$ and *SLC7A11*$^{sut/sut}$ housed two to four per cage. Experiments were carried out on female and male mice 8-12 weeks of age in accordance with the National Institutes of Health guidelines for the use of experimental animals as approved by the Institutional Animal Care and Use Committee of Syracuse University. These breeding and housing strategies were employed to control for environmental differences, genetic background influences, and genetic drift (Barnwell et al 2009, Pick & Little 1965).

2.3.2 Gross Brain Morphology Measurements

Brains were harvested from naïve 12 week old $SLC7A11^{+/+}$ and $SLC7A11^{sut/sut}$ littermates and snap-frozen on dry ice in Optimal Cutting Temperature (O.C.T) compound (Tissue-Tek, Torrance, CA). Frozen sections (coronal, 40 µm) were cut on a cryostat at 80 µm intervals, mounted on SuperFrost Plus slides (Fisher Scientific, Houston, TX), and thionin-stained as we previously describe (Chowdhury et al 2018). ImageJ Software (version 1.47v or 1.51n; National Institutes of Health, Bethesda, MD, RRID: SCR_003070) was used to make gross brain morphological measurements on scanned images (Epson 3170; 720 dpi) of slices at +1.1, -0.1, -0.94, -1.46, and -2.54 mm relative to bregma by three individuals blind to genotype. Mean cortical width was obtained by averaging six non-overlapping, straight tool measurements taken from the apex of the corpus callosum to the pial layer in the somatosensory cortex (3 each bilaterally). Mean corpus callosum width was obtained by averaging three non-overlapping, straight tool measurements taken from the base to the apex of the corpus callosum at the midline. Mean ventricular, striatal, hemispheric, and corpus callosum areas were determined by averaging user-defined pixel volumes using the free hand tool taken of the respective regions measured three times bilaterally (six in total) or three times total for structures decussating the midline (corpus callosum). In all cases, data are expressed as the mean ± SEM of measurements obtained from animals in the respective genotype derived from the mean calculated from three individual raters blind to experimental conditions.

2.3.3 Cellular Morphological Measurements

2.3.3.1. Golgi-Cox Staining

Brains from naïve *SLC7A11*^{+/+} and *SLC7A11*[sut/sut] littermates were Golgi-Cox

stained using the FD Rapid Golgi Stain Kit (FD Neuro Technologies, Inc., Baltimore,

MD) as per manufacturer's instructions. Following removal from the cranium, brains

were immediately rinsed in deionized (DI) water, placed in a proprietary impregnation

solution (Solution A plus B) containing potassium dichromate, potassium chromate, and

mercuric chloride, and stored at room temperature for 14 days in the dark. Brains were

then transferred to a sucrose solution (Solution C) for 3 days followed by rapid freezing

on dry ice. Frozen brain were cut serially ($\approx$ +2.46 – -2.30 mm posterior to bregma) into

140 μm coronal sections, mounted on gelatin-coated slides (FD Neuro Technologies,

Inc., Baltimore, MD), air dried at room temperature for 2 days in the dark. Sections were

Golgi-Cox stained as per manufacturer's instructions (FD Rapid Golgi Stain Kit). Briefly,

sections were initially rinsed 2x with DI water (4 min each) then placed in a solution

containing silver nitrate (Solution D plus E) for 10 min. Slides were rinsed in DI water 2x

for 4 min each followed by serial dehydration in absolute ethanol (50%, 75%, 95%,

100%, 100%, 100%, 100%; 4 min each). Ethanol was cleared with xylene (3x for 4 min

each), after which coverslips were mounted using Permount mounting media.

2.3.3.2 Dendritic Morphology and Soma Area Analysis

Photomicrographs of Golgi-Cox stained layer V pyramidal cells in the primary

motor cortex (PM1) were obtained with a Nikon eclipse Ni-U upright microscope with

motorized stage at 20x magnification. Neurons whose cell body and dendrites were

completely impregnated and visible within the plane(s) of focus were selected for

analysis. Neurons were reconstructed with Adobe Illustrator. The complexity of dendritic arborization in reconstructed neuronal drawings was quantified (Image J) using Sholl analysis as described (Sholl 1953). Briefly, the number of dendrites intersecting concentric circles of a gradually increasing radius from the centroid of the soma were calculated. The soma cross-sectional area was quantified using the polygon tool in Image J. The number and length of primary, secondary, tertiary, apical, and basal dendrites were also determined using Neuron J. Experimenters blind to genotype performed the image acquisition and analyses. Six to 11 neurons from 3-5 mice/genotype/sex were analyzed; data are expressed as the mean ± SEM of all measurements obtained.

2.3.3.3 Spine Morphometric and Density Analysis:

Photomicrographs of Golgi-Cox stained secondary apical dendrites on layer V pyramidal cells in the PM1 were obtained with a Nikon eclipse Ni-U upright microscope with motorized stage at 60x magnification. Neurons whose cell body and dendrites were completely impregnated and were visible within the plane(s) of focus were selected for analysis. Spine morphometric analysis was carried out as described (Risher et al 2014). In brief, Z-stack sections were analyzed using RECONSTRUCT software by measuring the length and head width of all protrusions (spines) along the dendritic segment of interest. The spine density was determined by calculating the number of protrusions/µm of dendrite. The length-to-width ratios (LWR) of individual spines were calculated in Microsoft Excel and used for hierarchical classification into the following categories: branched (entered manually by experimenter), filopodia (length > 2µm), mushroom (width > 0.6 µm), long thin (length > 1µm), thin (LWR > 1), and stubby (LWR ≤ 1). All

image acquisition and analyses were performed by experimenters blinded to genotype. Eight-nine neurons from three mice/genotype/sex were analyzed; data are expressed as the mean ± SEM of all measurements obtained.

2.3.4 PTZ dosing paradigm

Five days prior to each study, *SLC7A11*$^{+/+}$ or *SLC7A11*$^{sut/sut}$ mice were acclimated to handling by performing mock daily intraperitoneal (i.p.) injections which consisted of inverting the mouse and rubbing its abdomen. Prior to each experiment, mice were brought into the procedure room, weighed, and allowed to acclimatize for at least one hour. PTZ (Sigma Chemical Co., St. Louis, MO) was dissolved in saline, filter sterilized, and administered i.p. in a volume of 10 ml/kg body weight. Mice were injected with a single dose of PTZ. Doses were chosen following initial dose ranging studies in female and male *SLC7A11*$^{+/+}$ or *SLC7A11*$^{sut/sut}$ mice to determine the PTZ seizure threshold for each strain (Supplementary Fig. S1) (Kosobud et al 1992). Following each injection, mice were observed for acute behavioral seizures over the next 30 min. The time and severity of behavioral seizures (see Table 2.1 below) were scored and recorded for each mouse by an observer blinded to genotype to ensure unbiased scoring. The percentage of animals exhibiting convulsive seizures was determined by dividing the number of animals with a maximum seizure score of 3 or 4 by the total number of animals injected.

2.3.5 Statistical analysis

All statistical analyses were performed using GraphPad Prism (Version 6.0.1, Graphpad Software, Inc., La Jolla, CA). Brain morphological parameters, including areas, lengths, and widths, were compared using two-way ANOVA. Prior to parametric analysis, count or percentage data were log (y = log(y)) or arcsine (y = arcsine[sqrt(y/100)] transformed, respectively. Seizure severity was compared using a Mann-Whitney U test, whereas proportions indicating the percent of mice convulsing were compared using a Fisher's exact test. In all cases, significance was set at $p < 0.05$.

Table 2.1: *Descriptive PTZ-induced Seizure Scoring System*

Seizure Score	Abbreviated Description	Detailed Description
0	Normal behavior	Frequent ambulation/exploration, sniffing, rearing, peer interactions, grooming, eating, digging, climbing are common.
1	Hypomobility and hypoactivity	Mice will socially isolate self and disregard peers; body will be positioned close to bottom of cage. The overall behavioral picture will be dominated by bouts (>10 sec in duration) of staring and motionlessness that may be interrupted by brief sniffing or ambulation.
2	Repeated myoclonus	Animal exhibits at least two isolated myoclonic seizures typically involving axial muscles, commonly seen as neck flexion. Straub tail (dorsiflexion) is also common, as is an increase in locomotor activity (compared to score 1).
3	Convulsive seizure with intact righting reflex	Clonic seizures involve forelimbs and neck while the animal assumes an upright posture using hind limbs to support body weight.
4	Convulsive seizure with loss of righting reflex	Clonic seizures involve both forelimbs and hind limbs preventing the maintenance of upright posture. Infrequently, these seizures can be associated with violent running and jumping episodes and tonic hind limb extension.

Table adapted from descriptions in (Ferraro et al 1999, Pitkanen 2006, Racine 1972).

2.4   Results

Gross morphometric analysis of SLC7A11$^{+/+}$ and SLC7A11$^{sut/sut}$ mice

Mice null for the neuronal cysteine uptake transporter EAAT3 (EAAC1) exhibit gross brain atrophy in association with decreased GSH levels (Aoyama et al 2006). Whether loss of the predominant cyst(e)ine supplier in astrocytes, Sx_c^-, similarly influences brain morphology was explored. Though quantification of female brain hemisphere area using coronal sections spanning +1.1 to -2.54 bregma revealed a slight decrease in overall brain size in *SLC7A11$^{sut/sut}$* mice as compared *SLC7A11$^{+/+}$* sex-matched littermate controls, this effect was not statistically significant (Fig. 2.1B; *p* = 0.2520; repeated measures two-way ANOVA). Similarly, *SLC7A11$^{sut/sut}$* females showed a slight, but not significant, decrease in cortical area (Fig. 2.1C; *p* = 0.2472), striatal area (Fig. 2.1D; *p* = 0.5675), and corpus callosum area (Fig. 2.1F; *p* = 0.0739), while their lateral ventricle area was indistinguishable from *SLC7A11$^{+/+}$* littermates (Fig. 2.1E; *p* = 0.2941; repeated measures two-way ANOVA). However, a significant reduction in corpus callosum thickness was detected in *SLC7A11$^{sut/sut}$* female as compared to *SLC7A11$^{+/+}$* littermates (Fig. 2.1G; *p* = 0.0399; repeated measures two-way ANOVA). Interestingly, these findings were sex-dependent, as male *SLC7A11$^{sut/sut}$* mouse brains were virtually indistinguishable from their *SLC7A11$^{+/+}$* sex-matched littermate controls with respect to not only corpus callosum thickness, but also hemisphere area, cortical thickness, striatal area, lateral ventricle area, and corpus callosum area (Fig. 2.2).
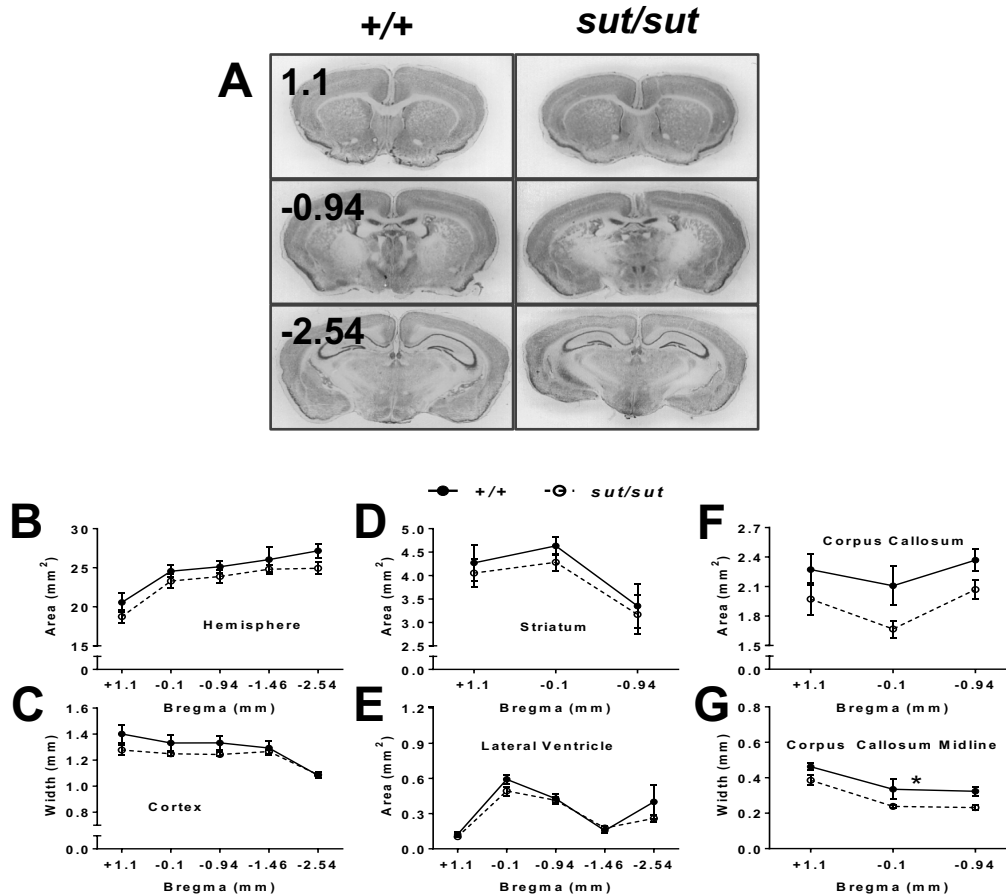
Figure 2.1 Comparison of gross brain morphology between female SLC7A11+/+ and SLC7A11sut/sut mice

Gross brain morphological measurements were made on thionin-stained coronal brain sections from 12 week old naïve female *SLC7A11+/+* (+/+) (n = 4) and *SLC7A11sut/sut* (*sut/sut*) (n = 4) littermates. Sections of 40 µm thickness were imaged using an Epson Digital Scanner at 720 dpi. Digitized images were processed and quantified using NIH Image J software.

A) Representative thionin-stained coronal sections spanning +1.1 to -2.54 anterior to posterior from bregma from +/+ and *sut/sut* mice derived from *sut*/+ breeders.

B-E) Quantification of (B) hemispheric area, (C) cortical width, (D) striatal area, (E) lateral ventricle area, (F) corpus callosum area, and (G) corpus callosum width from +/+ and *sut/sut* mice was performed over 3-5 coronal sections as described in Materials and Methods. Data are expressed as the mean ± SEM width (mm) or area (mm^2). No significant difference between +/+ and *sut/sut* mice was observed in hemispheric area (B; p = 0.2520), cortical thickness (C; p = 0.2472), striatal area (D; p = 0.5675), lateral ventricle area (E; p = 0.2941), or corpus callosum area (F; p = 0.0739) as determined by repeated measures two-way ANOVA. *Corpus callosum width is significantly decreased in *sut/sut* as compared to +/+ littermates (G; p = 0.0399, repeated measures two-way ANOVA).
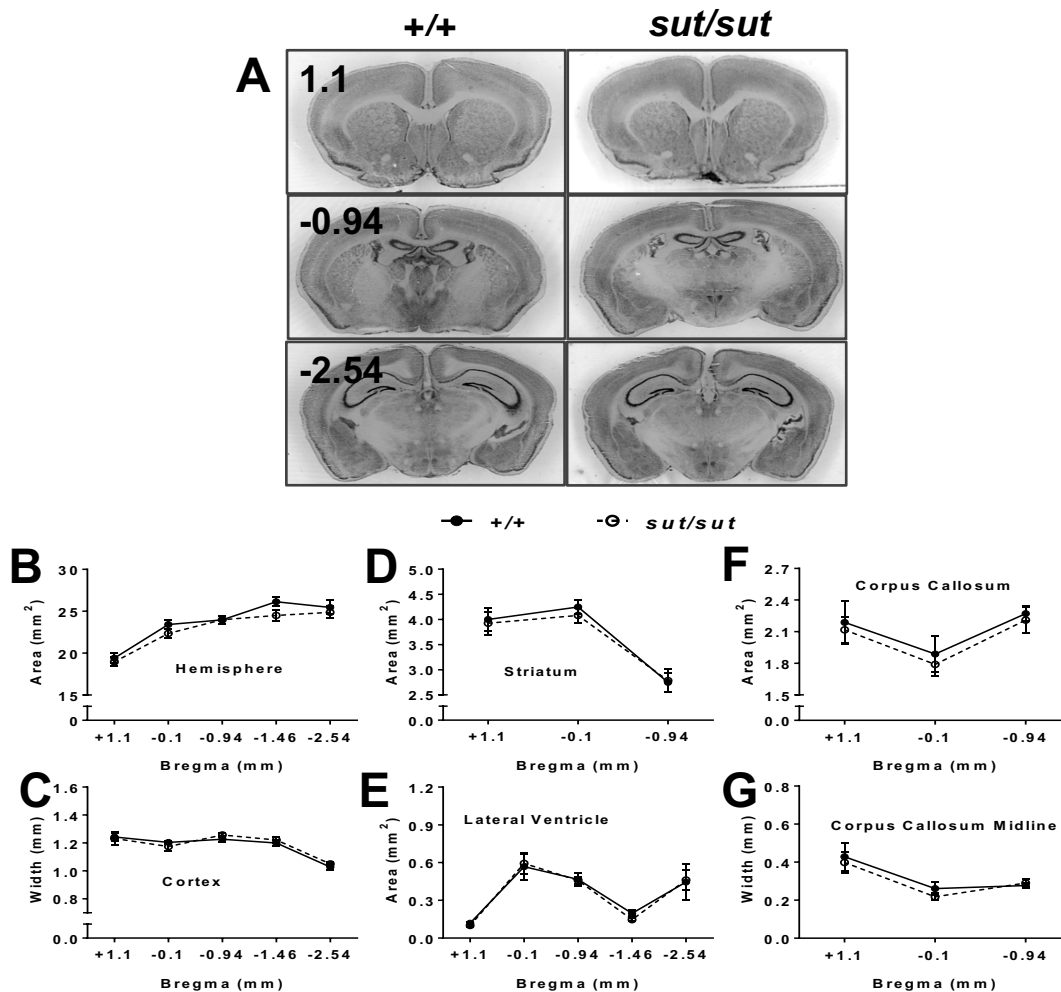
Figure 2.2 Comparison of gross brain morphology between male SLC7A11^{+/+} and SLC7A11[sut/sut] mice

Gross brain morphological measurements were made on thionin-stained coronal brain sections from 12 week old naïve male *SLC7A11^{+/+}* (+/+) (n = 7) and *SLC7A11[sut/sut]* (*sut/sut*) (n = 8) littermates. Sections of 40 μm thickness were imaged using an Epson Digital Scanner at 720 dpi. Digitized images were processed and quantified using NIH Image J software.

A) Representative thionin-stained coronal sections spanning +1.1 to -2.54 anterior to posterior from bregma from +/+ and *sut/sut* mice derived from *sut*/+ breeders.

B-E) Quantification of (B) hemispheric area, (C) cortical width, (D) striatal area, (E) lateral ventricle area, (F) corpus callosum area, and (G) corpus callosum width from +/+ and *sut/sut* mice was performed over 3-5 coronal sections as described in Materials and Methods. Data are expressed as the mean ± SEM width (mm) or area (mm^2). No significant difference between +/+ and *sut/sut* mice was observed in hemispheric area (B; p = 0.3061), cortical thickness (C; p = 0.6010), striatal area (D; p = 0.7010), lateral ventricle area (E; p = 0.7990), corpus callosum area (F; p = 0.6587), or corpus callosum width (G; p = 0.6321) as determined using repeated measures two-way ANOVA.

Quantification of primary motor cortex layer V pyramidal cells in SLC7A11$^{+/+}$ and

SLC7A11$^{sut/sut}$ mice

The dendritic tree complexity of cortical layer V excitatory pyramidal cells can influence their stereotypical repetitive spike bursting train firing pattern and thus E/I balance (Mainen & Sejnowski 1996). At the cellular level, the dendritic complexity of layer V neurons derived from the primary motor cortex of female *SLC7A11$^{sut/sut}$* mice was indistinguishable from sex-matched *SLC7A11$^{+/+}$* controls (Fig. 2.3C; p = 0.8603; two-way ANOVA). Conversely, neurons derived from male *SLC7A11$^{sut/sut}$* mice had enhanced dendritic complexity as compared to *SLC7A11$^{+/+}$* sex-matched littermates (Fig. 2.3C; p < 0.0001) and in fact, were indistinguishable from *SLC7A11$^{sut/sut}$* female mice (Fig. 2.3C; p = 0.4185). Interestingly, a sex-difference was uncovered in that *SLC7A11$^{+/+}$* males had decreased dendritic complexity as compared to *SLC7A11$^{+/+}$* females (Fig. 2.3C; p < 0.0001) (two-way ANOVA). While this data indicates a clear sex difference with respect to dendritic complexity in female and male *SLC7A11$^{+/+}$* mice on the C3H/HeSnJ background, it also indicates that loss of Sx$_c^-$ in male mice rendered dendritic complexity more "female-like" overall.

Quantification of primary, secondary, and tertiary neurite numbers and length revealed further sex differences: while no within-sex genotype differences were observed, the number of tertiary neurites in *SLC7A11$^{sut/sut}$* male mice was enhanced as compared to *SLC7A11$^{sut/sut}$* females (Fig. 2.4A; p < 0.05; two-way ANOVA with Bonferroni's multiple comparisons). Moreover, the length of both primary (Fig. 2.4C; p = 0.0210) and secondary (Fig. 2.4C; p = 0.0014) neurites was enhanced in females versus males (two-way ANOVA), and further classification of primary, secondary, and
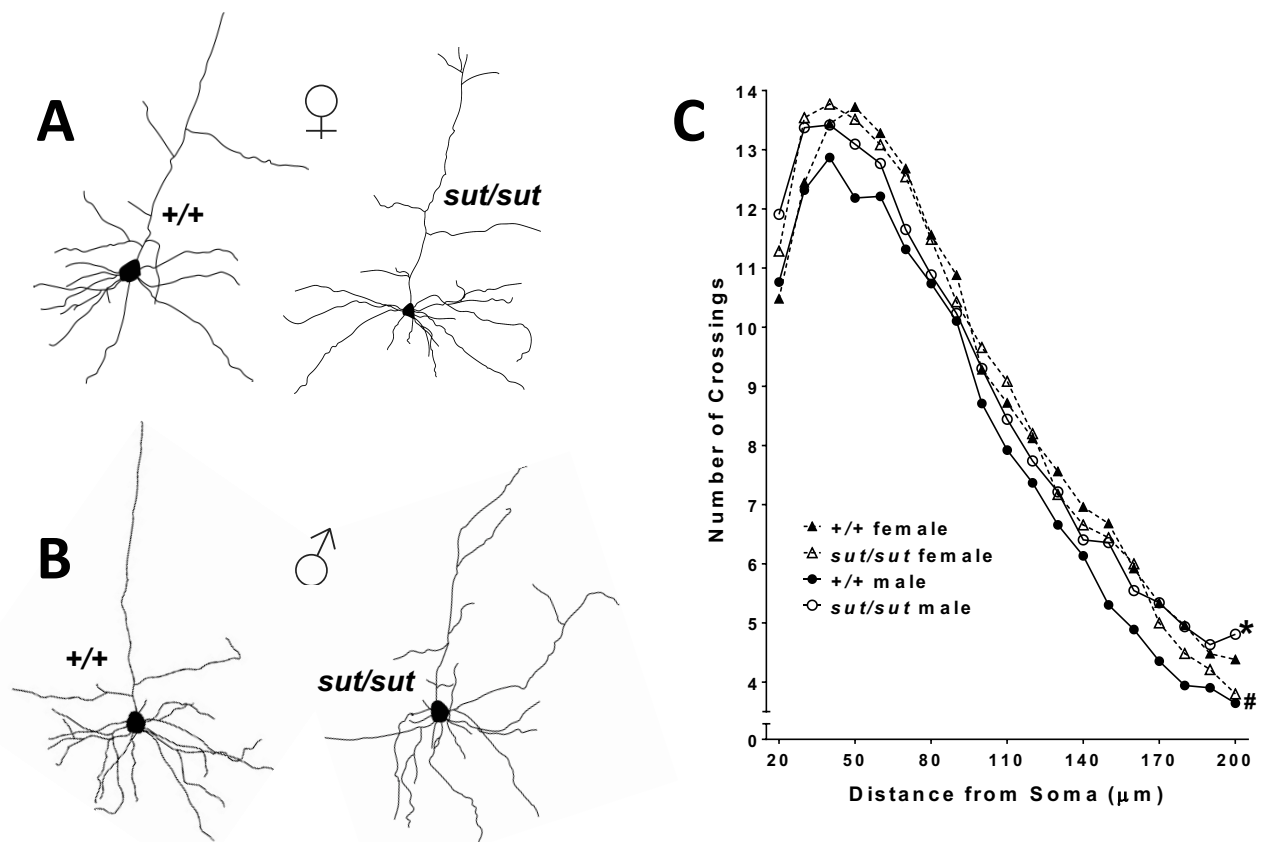
Figure 2.3 Comparison of dendritic complexity between SLC7A11$^{+/+}$ and SLC7A11$^{sut/sut}$ mice

Photomicrographs of Golgi-Cox stained primary motor cortex (PM1) layer V pyramidal cells from naïve *SLC7A11$^{+/+}$* [+/+, n = 64 neurons (39M, 25F) from 7 mice (4M, 3F)] and *SLC7A11$^{sut/sut}$* [*sut/sut*, n = 82 neurons (43M, 39F) from 9 mice (5M, 4F)] littermates from eight separate litters were reconstructed using Adobe Illustrator as depicted by representative tracings from **(A)** females or **(B)** males.

C) The complexity of dendritic arborization in these neurons was explored by Sholl analysis in females and males. Each data point represents the mean number of crossings ± SEM. *Neurons derived from *sut/sut* male mice have enhanced dendritic complexity compared to +/+ littermate controls ($p < 0.0001$; two-way ANOVA with Bonferroni's multiple comparisons). #Male +/+ neuronal complexity is also significantly decreased as compared to +/+ females as denoted by the # sign ($p < 0.0001$).
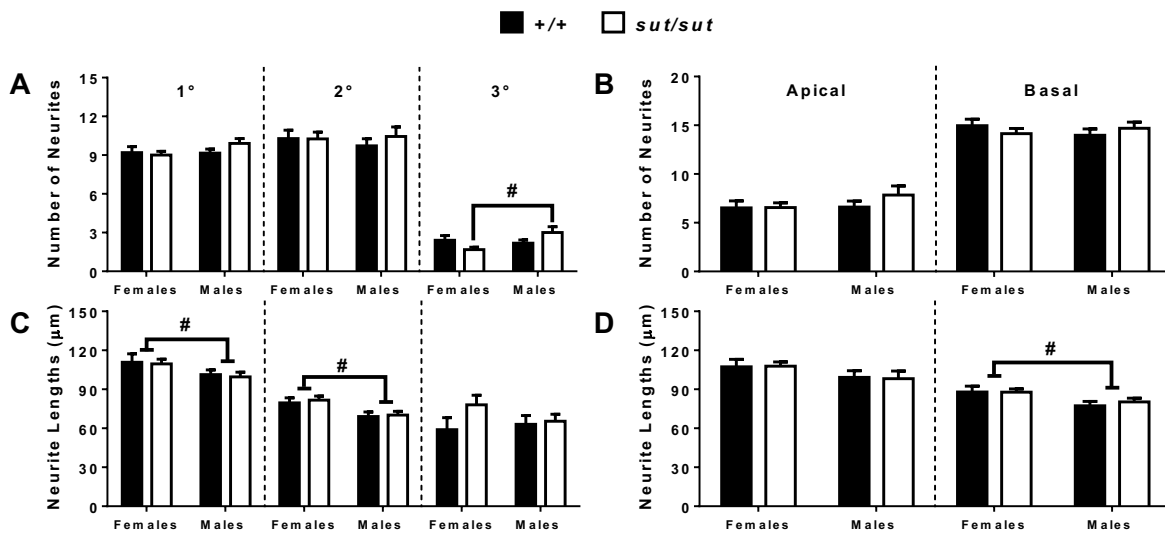
Figure 2.4 Neurite number and length analysis in female and male SLC7A11^{+/+} and SLC7A11^{sut/sut} mice

Figure 2.4 Neurite number and length analysis in female and male SLC7A11$^{+/+}$ and SLC7A11$^{sut/sut}$ mice

Neurite processes on reconstructed neurons from Figure 2.3 were quantified by NIH Image J analysis.

A-B) Bars [black bar (*SLC7A11$^{+/+}$*; +/+) and open bar (*SLC7A11$^{sut/sut}$*; *sut/sut*)] represent the mean ± SEM number of (A) primary, secondary, or tertiary or (B) apical or basal neurites. No significant within-sex genotype differences were observed in the number of neurites at any order (1°, 2°, or 3°) or polarity (apical or basal) quantified (two-way ANOVA). However, *sut/sut* males have an increased number of 3° neurites as compared to female *sut/sut* mice as denoted by the asterisk ($p < 0.05$, Two-way ANOVA with Bonferroni's multiple comparisons on log transformed data).

C-D) Bars [black bar (+/+) and open bar (*sut/sut*)] represent the mean ± SEM length of (C) primary, secondary, or tertiary or (D) apical or basal neurites. No significant within-sex genotype differences were observed in the length of neurites at any order (1°, 2°, or 3°) or polarity (apical or basal) quantified (two-way ANOVA). #Females have increased 1° ($p = 0.0210$) and 2° ($p = 0.0014$) order as well as basal ($p = 0.0067$) neurite lengths as compared to males (two-way ANOVA with Bonferroni's multiple comparisons).

tertiary neurite polarity into apical or basal revealed enhanced basal neurite length in females as compared to males (Fig. 2.4D; p = 0.0067; two-way ANOVA).

Evaluation of the neuronal cell body revealed that the cross-sectional soma area was similar in neurons derived from male $SLC7A11^{+/+}$ and $SLC7A11^{sut/sut}$ littermates. However, an 18% reduction in cross-sectional soma area was revealed in female $SLC7A11^{sut/sut}$ as compared to $SLC7A11^{+/+}$ sex-matched littermate controls (Fig. 2.5; 335.6 ± 14.18 μm^2 for $SLC7A11^{+/+}$ and 273.7 ± 10.98 μm^2 for $SLC7A11^{sut/sut}$ mice, mean ± SEM; $p < 0.01$; two-way ANOVA with Bonferroni's multiple comparisons). Once more, sex-differences between $SLC7A11^{+/+}$ male and $SLC7A11^{+/+}$ female mice were observed (Fig. 2.5; $p < 0.01$; two-way ANOVA with Bonferroni's multiple comparisons), and loss of Sx_c^- in female mice rendered their cross-sectional soma area more "male-like" given that they were indistinguishable from $SLC7A11^{sut/sut}$ male mice (Fig. 2.5; two-way ANOVA with Bonferroni's multiple comparisons).

Cortical layer V pyramidal cell dendritic spine analysis

The majority of fast excitatory synaptic activity occurs at ionotropic glutamate receptors residing on dendritic spines. Moreover, the spine structure-function relationship has been well-characterized, with increases and decreases in spine head width correlating with increases and decreases in glutamate receptors and thus, strengthening and weakening of synaptic efficacy, respectively (Matsuzaki et al 2001, Noguchi et al 2005). Herein, the head width and length of spines were used for categorical classification to determine the proportion of nascent (filopodia, long thin), immature (thin), or mature (stubby, mushroom, branched) dendritic spines
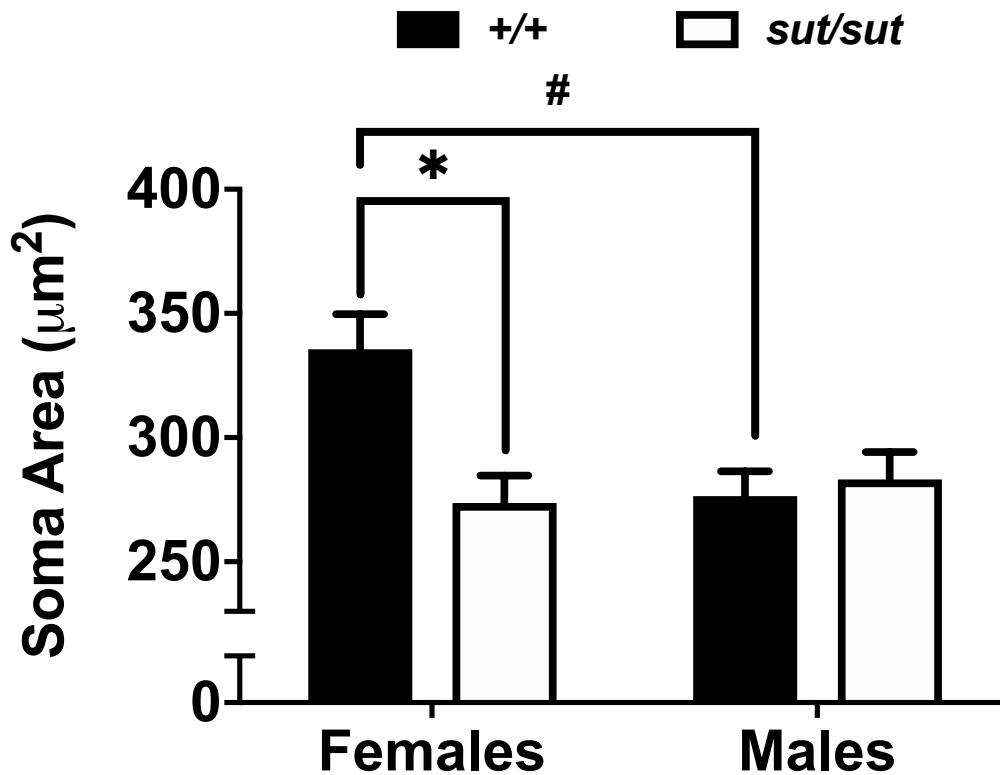
Figure 2.5 Soma analysis in female and male SLC7A11$^{+/+}$ and SLC7A11$^{sut/sut}$ mice

The cross sectional soma area of reconstructed neurons from Figure 2.3 were quantified by NIH Image J analysis. Bars [black bar (+/+) and open bar (*sut/sut*)] represent the mean soma area ± SEM in females (left) or males (right). *Neurons derived from female *sut/sut* mice have a decreased soma area compared to +/+ sex-matched littermate controls as denoted by the asterisk ($p < 0.01$); two-way ANOVA with Bonferroni's multiple comparisons). #Female +/+ neurons are also significantly different from male +/+ neurons ($^{#}p < 0.01$).
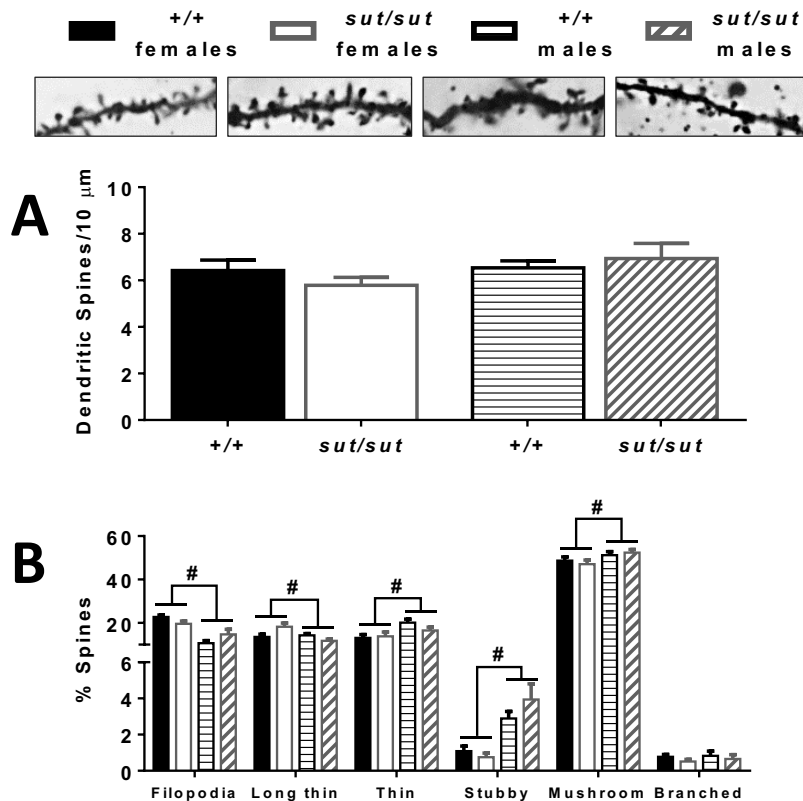
Figure 2.6 Comparison of dendritic spine density and morphology between SLC7A11^+/+ and SLC7A11^sut/sut mice

Golgi-Cox stained dendritic spines located on secondary apical dendrites of primary motor cortex layer V pyramidal cells from naïve *SLC7A11*$^{+/+}$ [+/+, n = 18 neurons (9M, 9F) from 6 mice (3M, 3F)] and *SLC7A11*$^{sut/sut}$ [*sut/sut*, n = 17 neurons (8M, 9F) from 6 mice (3M, 3F)] littermates from seven separate litters were analyzed using the *Risher et al*. method as described in materials and methods. The spine density was determined by calculating the number of protrusions/μm of dendrite.

A) Bars represent the mean number of spines/10 μm dendritic length ± SEM in +/+ or *sut/sut* female or male mice. No significant difference between female or male +/+ and *sut/sut* mice was observed in dendritic spine density in layer V pyramidal cells (two-way ANOVA on log-transformed data). *Inset*: Representative photomicrographs (60x) of secondary apical dendritic spines from Golgi-Cox stained +/+ and *sut/sut* female or male mice.

B) Bars represent the mean percentage of spines ± SEM in female or male +/+ or *sut/sut* mice categorized as either mushroom, filopodia, stubby, branched, thin, or long thin. No significant within-sex genotype differences in spine typology were observed between +/+ and *sut/sut* mice (two-way ANOVA on arcsine transformed data). $^{#}$Males have increased mushroom (p = 0.0261), stubby (p < 0.0001), and thin (p = 0.0060) spines as compared to females whereas females have increased filopodia (p < 0.0001) and long thin (p = 0.0242) spines as compared to males (two-way ANOVA on arcsine transformed data).

(Risher et al 2014). Assessment of secondary apical dendritic spines on cortical layer V

pyramidal cells indicated that spine density was similar in both *SLC7A11*^{+/+} and

SLC7A11[sut/sut] female and male mice (Fig. 2.6A, two-way ANOVA). Further categorical

classification of these spines – facilitated by calculating the spine length to head-width

ratios – revealed sex-differences, with male mice exhibiting an increased proportion of

mature mushroom ($p = 0.0261$) and stubby ($p < 0.0001$) spines, as well as thin spines

($p = 0.0060$), as compared to female littermates (Fig. 2.6B; two-way ANOVA).

Furthermore, female mice demonstrated an increased proportion of nascent filopodia (p

< 0.0001) and long thin ($p = 0.0242$) spines as compared to males (Fig. 2.6B; two-way

ANOVA). These genotype-independent sex-differences demonstrated that a greater

proportion of male spines are classified into mature (versus nascent) categories as

compared to females, suggesting that male spines may be strengthened overall as

compared to females.

Further analysis of the spine length and head width parameters used to derive

the aforementioned classifications revealed that spine head widths were significantly

decreased in female *SLC7A11*[sut/sut] mice as compared to *SLC7A11*^{+/+} sex-matched

littermates (Fig. 2.7A-B; $p < 0.0001$; two-way ANOVA). The opposite occurred in males,

wherein *SLC7A11*[sut/sut] male mice had increased spine head widths as compared to

sex-matched *SLC7A11*^{+/+} controls (Fig. 2.7A-B; $p < 0.0001$; two-way ANOVA). Analysis

of sex-differences revealed that spine head widths of *SLC7A11*^{+/+} females were

enhanced as compared to *SLC7A11*^{+/+} males whereas *SLC7A11*[sut/sut] females were

decreased as compared to *SLC7A11*[sut/sut] males (Fig. 2.7A-B; two-way ANOVA
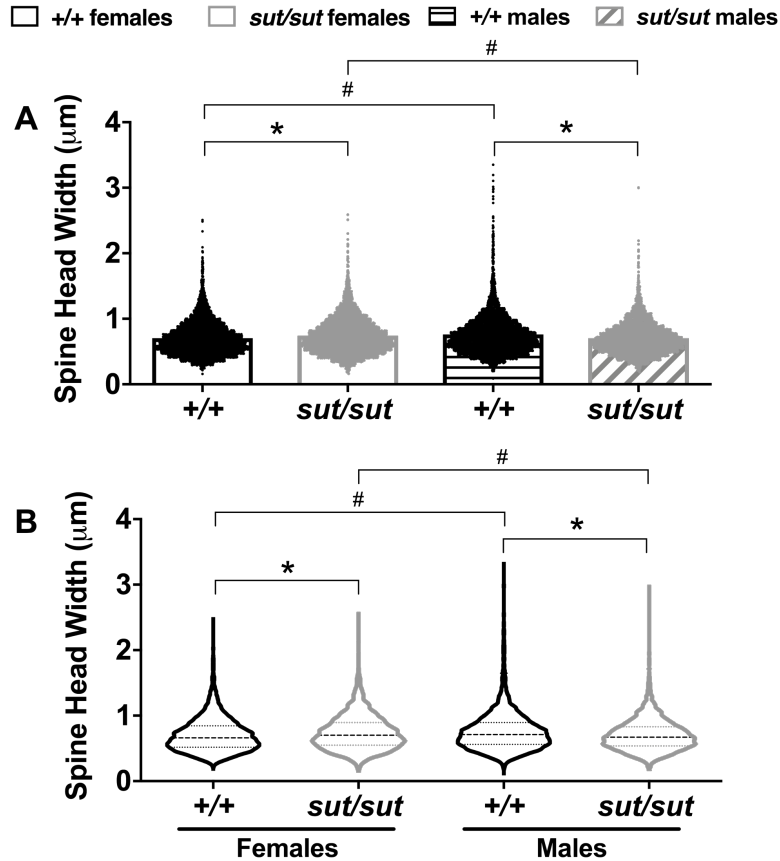
Figure 2.7 Comparison of spine head width between SLC7A11$^{+/+}$ and SLC7A11$^{sut/sut}$ mice

The distribution of head width variables from *SLC7A11*$^{+/+}$ [+/+; females, n = 4763; males, n = 5056) on 18 neurons (9F, 9M) from 6 mice (3M, 3F)] and *SLC7A11*$^{sut/sut}$ [*sut/sut*; females, n = 4430; males, n = 5355) on 17 neurons (9F, 8M) from 6 mice (3F, 3M)] littermates used to derive length-to-width ratios in Figure 2.6 were compared.

A and B) *Top:* Each data point [black circles (+/+) or gray circles (*sut/sut*)] represents the head width of a spine in female (open bars) or male (hatched bars) mice. Bars represent the mean spine head width for each genotype. *Bottom:* the distribution of variables in the above scatterplot were fit to a violin plot. *Sut/sut* female mice have significantly decreased mushroom spine head widths as compared to +/+ littermate controls (p < 0.0001; two-way ANOVA performed on head widths [n = 9 neurons/genotype]); the opposite effect was observed in males (p < 0.0001; two-way ANOVA [n = 8-9 neurons /genotype]). Within-genotype sex-differences are indicated by the $^{\#}$ signs.
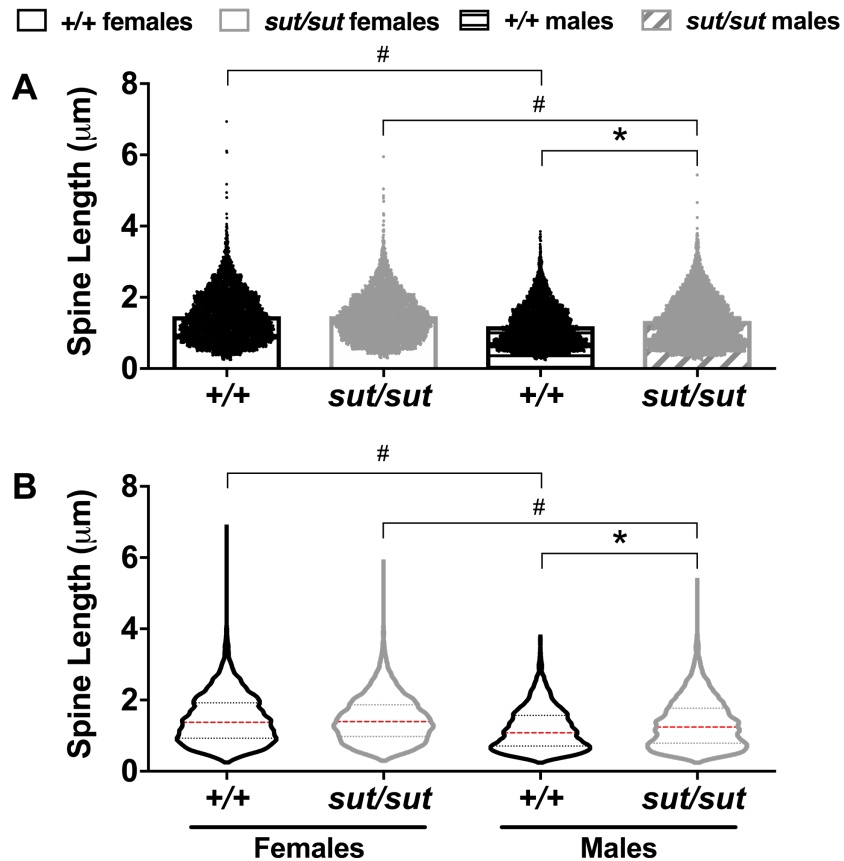
Figure 2.8 Comparison of spine length between SLC7A11$^{+/+}$ and SLC7A11$^{sut/sut}$ mice

The distribution of spine length variables from *SLC7A11$^{+/+}$* [+/+; females, n = 4763; males, n = 5056) on 18 neurons (9F, 9M) from 6 mice (3M, 3F)] and *SLC7A11$^{sut/sut}$* [*sut/sut*; females, n = 4430; males, n = 5355) on 17 neurons (9F, 8M) from 6 mice (3F, 3M)] littermates used to derive length-to-width ratios in Figure 2.6 were compared.

A and B) *Top:* Each data point [black circles (+/+) or gray circles (*sut/sut*)] represents the spine length of spine in female (open bars) or male (hatched bars) mice. Bars represent the mean spine length for each genotype. *Bottom:* the distribution of variables in the above scatterplot were fit to a violin plot. *Sut/sut* male mice have significantly increased mushroom spine length as compared to +/+ littermate controls (males, $p < 0.0001$; two-way ANOVA performed on head widths [n = 8-9 neurons/genotype/sex]). Within-genotype sex-differences are indicated by the # signs.

with Bonferroni's multiple comparisons). With respect to spine lengths, *SLC7A11*^{+/+} and

SLC7A11[sut/sut] female mice were identical whereas *SLC7A11*[sut/sut] males had increased

spine lengths as compared to *SLC7A11*^{+/+} sex-matched littermate controls (Fig. 2.8A-B;

$p < 0.0001$; two-way ANOVA with Bonferroni's multiple comparisons). Moreover,

analysis of sex-differences indicated that male spine head lengths were decreased as

compared to females (Fig. 2.8A-B; *p* < 0.0001; two-way ANOVA). Taken together, these

results demonstrate that loss of Sx_c^- signaling results in a sex-dependent change in

layer V cortical pyramidal cell spine head width, with decreases or increases occurring

in *SLC7A11*[sut/sut] females or males, respectively, as compared to sex-matched littermate

controls.

Functional assessment of E/I balance in SLC7A11*^{+/+} *and SLC7A11*[sut/sut] *mice

Increases in excitability have been associated with cellular morphological

alterations including enhanced dendritic complexity (Klenowski et al 2016, Mainen &

Sejnowski 1996), decreased soma size (Hsu et al 2012, Ye et al 2015), and increased

spine head width (Zito et al 2009),. To determine whether the aforementioned

morphological phenotypes affect E/I balance in *SLC7A11*[sut/sut] mice, the seizure

threshold of female and male *SLC7A11*^{+/+} and *SLC7A11*[sut/sut] littermates was assessed

using the $GABA_AR$ antagonist PTZ. Within minutes of an acute PTZ dose (42 mg/kg,

i.p.), a hypomobility phenotype (seizure score = 1) was evoked in the vast majority of

mice regardless of sex or genotype. Despite this initial similarity, the behavioral

response of *SLC7A11*[sut/sut] mice progressed such that by the end of the 30 minute
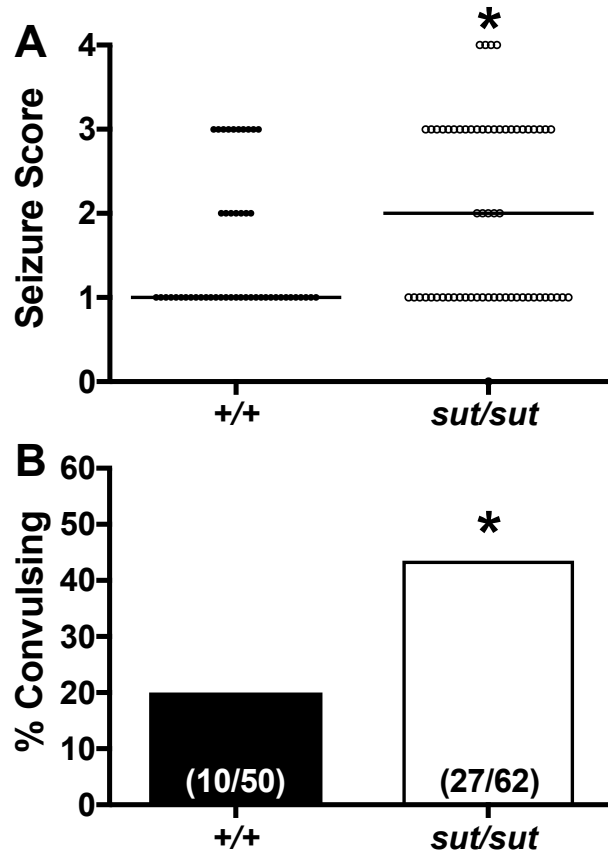
Figure 2.9 SLC7A11*sut/sut* mice are hyper-excitable

Naïve female (n = 21) and male (n = 29) *SLC7A11⁺/⁺* (+/+, total n = 50) and female (n = 25) and male (n = 37) *SLC7A11sut/sut* (*sut/sut,* total n = 62) littermates were treated with a single dose of 42 mg/kg PTZ (i.p.). Seizure behavior was scored using a 5 point scale. Data were pooled from 16 independent experiments performed over 9 months.

A) *Individual seizure scores*: Each data point [closed black circles (+/+) or open circles (*sut/sut*)] represents the maximal seizure score obtained by an individual mouse during a 30 min observation period. Horizontal lines represent the median seizure score for each genotype. *Sut/sut* mice have a significantly greater seizure score than +/+ littermate controls (p = 0.0237; Mann-Whitney U Test).

B) *Convulsive index:* Bars [black bar (+/+) and open bar (*sut/sut*)] represent the proportion (fraction within bars) of mice that experienced a convulsive seizure (seizure score ≥ 3) in A expressed as a % of total mice exposed to PTZ. *Sut/sut* mice have a higher convulsive index compared to +/+ littermate controls (p = 0.0093; Fisher's Exact Test).
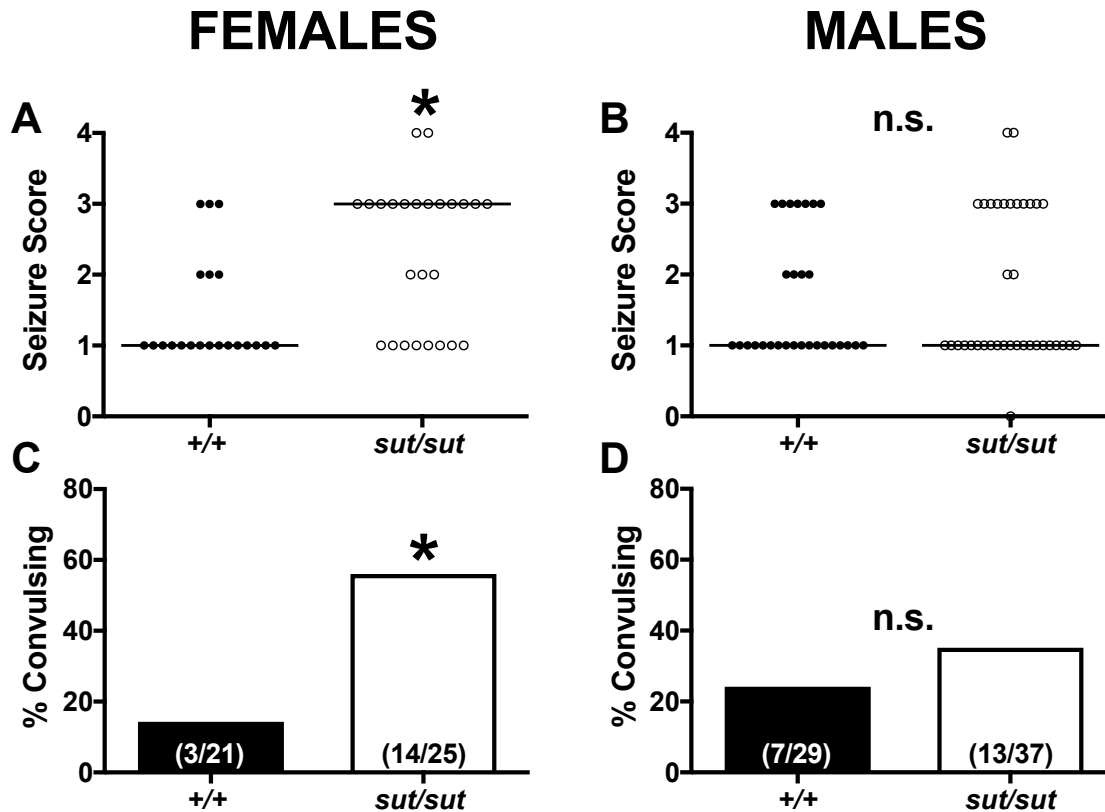
Figure 2.10 Enhancement of acute PTZ-induced seizure activity in SLC7A11$^{sut/sut}$ mice differs by sex

The distribution of variables from mice used to derive Figure 2.9 were grouped and analyzed separately by sex.

A-B) *Individual seizure scores*: Each data point [closed black circles (+/+) or open circles (*sut/sut*)] represents the maximal seizure score obtained by individual female (A) or male (B) mice during a 30 min observation period. Horizontal lines represent the median seizure score for each genotype. *Sut/sut* female (p = 0.0030) but not male (p = 0.6459) mice have a significantly greater seizure score than +/+ sex-matched littermate controls as denoted by the asterisk (Mann-Whitney U Test).

C-D) *Convulsive index*: Bars [black bar (+/+) and open bar (*sut/sut*)] represent the proportion (fraction within bars) of mice that experienced a convulsive seizure (seizure score ≥ 3) in A (C) or B (D) as a % of total mice exposed to PTZ. *Sut/sut* female (p = 0.0054) but not male (p = 0.4223) mice have a higher convulsive index compared to +/+ sex-matched littermate controls as denoted by the asterisk (Fisher's Exact Test). n.s. denotes not-significant (p > 0.05).
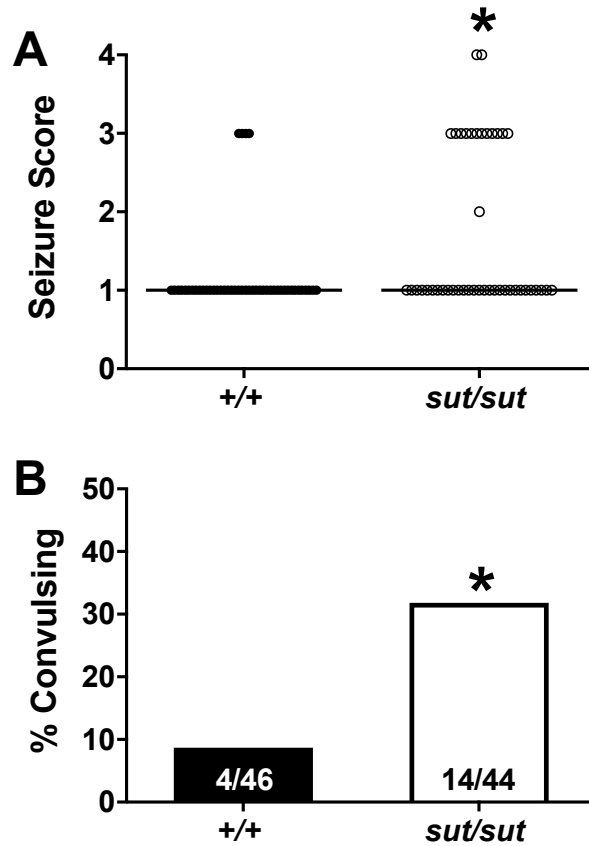
Figure 2.11 Enhancement of acute PTZ-induced seizure activity in male *SLC7A11^sut/sut* mice uncovered by using a lower dose

Naïve male *SLC7A11^+/+* (+/+, total n = 46) and *SLC7A11^sut/sut* (*sut/sut,* total n = 44) littermates were treated with a single dose of 35 mg/kg PTZ (i.p.). Seizure behavior was scored using a 5 point scale.

A) *Individual seizure scores*: Each data point [closed black circles (+/+) or open circles (*sut/sut*)] represents the maximal seizure score obtained by individual mice during a 30 min observation period. Horizontal lines represent the median seizure score for each genotype. *Sut/sut* male mice have a significantly greater seizure score than +/+ sex-matched littermate controls as denoted by the asterisk (p = 0.0031, Mann-Whitney U Test).

B) *Convulsive index*: Bars [black bar (+/+) and open bar (*sut/sut*)] represent the proportion (fraction within bars) of mice that experienced a convulsive seizure (seizure score ≥ 3) in A as a % of total mice exposed to PTZ. **Sut/sut* male mice have a higher convulsive index compared to +/+ sex-matched littermate controls as denoted by the asterisk (p = 0.0081, Fisher's Exact Test).

observation period their median seizure score was significantly enhanced compared to *SLC7A11*^{+/+} littermates (Fig. 2.9A; p = 0.0237; Mann-Whitney U Test). Similarly, *SLC7A11*[sut/sut] mice demonstrated an enhanced convulsive seizure incidence with 43.5% (27/62) achieving a seizure stage ≥ 3, compared to 20% (10/50) of *SLC7A11*^{+/+} mice (Fig. 2.9B; p = 0.0093; Fisher's Exact Test). The mean latency to convulsive seizure, however, did not differ between genotypes (342.8 ± 59 and 387.5 ± 55 sec, mean ± SEM, for *SLC7A11*^{+/+} and *SLC7A11*[sut/sut] mice, respectively; p = 0.6500; unpaired *t* test).

Stratification of the variables in Figure 2.9 by sex revealed that female (Fig. 2.10A; p = 0.0030), but not male (Fig. 2.10B; p = 0.6459), *SLC7A11*[sut/sut] mice significantly contribute to this observed hyperexcitability (Mann-Whitney U Test). While female *SLC7A11*[sut/sut] mice had an elevated convulsive seizure incidence, with 14/25 (56%) of mice achieving a seizure stage ≥ 3, compared to just 3/21 (14.3%) of *SLC7A11*^{+/+} mice (Fig. 2.10C; p = 0.0054; Fisher's Exact Test), male *SLC7A11*^{+/+} and *SLC7A11*[sut/sut] mice had a similar convulsive seizure incidence (Fig. 2.10D; p = 0.4223; Fisher's Exact Test). However, given that a greater proportion of male (7/29; 24.1%) versus female (3/21; 14.3%) *SLC7A11*^{+/+} mice had a convulsive seizure, we reasoned that males could have a lower seizure threshold overall that could mask our ability to detect a difference in excitability. To test this, male *SLC7A11*^{+/+} and *SLC7A11*[sut/sut] mice were administered a lower dose of PTZ (35 mg/kg, i.p.) and observed for behavioral seizure activity. Indeed, hyper-excitability in male *SLC7A11*[sut/sut] mice was uncovered at this dose, reflected by their enhanced seizure severity (Fig. 2.11A; p = 0.0031; Mann-Whitney U Test) and convulsive seizure incidence (Fig. 2.11B; p = 0.0081; Fisher's

Exact Test) as compared to *SLC7A11*^{+/+} sex-matched littermate controls. Taken together, the sex-independent decrease in *SLC7A11*[sut/sut] convulsive seizure threshold, unmasked by chemoconvulsant challenge, suggests that *SLC7A11*[sut/sut] mice have a shift in their E/I balance towards excitation as compared to *SLC7A11*^{+/+} sex-matched littermate controls.

2.5   Discussion

Glutamate transporters, such as the excitatory amino acid transporters (EAATs), have been demonstrated to be important in maintaining E/I balance [reviewed in (Danbolt 2001)]. Despite the well-characterized significance of EAAT signaling, whether and how Sx_c^--mediated cystine/glutamate exchange contributes to E/I balance has not, until now, been fully investigated *in vivo*. In this study, we provide the first evidence that sex-dependent morphological differences occur in both female and male Sx_c^- null mice in comparison to their wild-type littermate controls. These morphological changes occur in association with a sex-independent behavioral hyper-excitability phenotype in *SLC7A11*[sut/sut] mice manifest by a decrease in their acute PTZ convulsive seizure threshold. The latter observation demonstrates that Sx_c^- signaling contributes to the endogenous network activity that maintains brain E/I balance *in vivo* in both female and male mice.

Two parameters maintained by Sx_c^- – redox balance and glutamate signaling – could influence brain structure and, in turn, E/I balance. For example, mice null for the neuronal EAAT3 transporter have decreased brain GSH levels that occur in association with age-dependent brain atrophy (Aoyama et al 2006). Moreover, high frequency

stimulation at the hippocampal CA1 synapse results in dendritic spine growth (Engert & Bonhoeffer 1999), which is dependent on glutamate receptor (NMDA) activation (Maletic-Savatic et al 1999). Overall, there was no evidence of gross brain atrophy in most brain regions of female or male *SLC7A11^{sut/sut}* mice as compared to *SLC7A11^{+/+}* sex-matched littermates. One exception was the thickness of the corpus callosum in *SLC7A11^{sut/sut}* females – it was significantly decreased – as compared to *SLC7A11^{+/+}* littermates. As the largest inter-hemispheric connection in brain, the corpus callosum is important for integrating information through its primarily excitatory connections (Bloom & Hynd 2005). In fact, transection of the corpus callosum is a therapeutic option to thwart generalization of seizure activity in epileptic individuals (Bogen & Vogel 1962, Van Wagenen & Herren 1940). While callosal thinning could be a result of decreased myelination, and electroencephalographic and behavioral seizures have been reported in animal models of demyelination (Hoffmann et al 2008), it could also result from aberrant development and/or connectivity of callosal projection neurons (Fame et al 2016). With respect to temporal lobe epilepsy, decreased thickness in the posterior and anterior callosal regions have been demonstrated, with anterior corpus callosum thickness positively correlating with epilepsy age of onset (Hermann et al 2003, Weber et al 2007). However, increased corpus callosum thickness at the midline has also been reported in epileptic individuals (Conlon & Trimble 1988). Furthermore, it remains uncertain as to whether changes in callosal thickness are cause or consequence of seizure activity, especially given that diffuse white matter changes are not restricted to the corpus callosum and have been reported to occur throughout the epileptic brain (Arfanakis et al 2002, Gross et al 2006, Scanlon et al 2013).

While gross structural abnormalities of entire brain regions – including the corpus callosum – can perturb E/I balance, so too can morphological changes occurring at the cellular level. For example, the complexity of dendritic arborization increases with neural activity (Redmond et al 2002, Sin et al 2002, Yu & Malenka 2003). Moreover, enhanced dendritic complexity occurs in association with increases in spontaneous excitatory postsynaptic current (EPSC) frequency (Klenowski et al 2016). While we saw no difference in dendritic complexity between female *SLC7A11*^{+/+} and *SLC7A11*[sut/sut] sex-matched littermates, male *SLC7A11*[sut/sut] dendritic complexity was significantly enhanced as compared to *SLC7A11*^{+/+} sex-matched controls. Moreover, male *SLC7A11*[sut/sut] dendritic complexity was indistinguishable from that of female *SLC7A11*[sut/sut] mice, whereas *SLC7A11*^{+/+} male dendritic complexity was significantly reduced as compared to *SLC7A11*^{+/+} females. These sex-differences were further exemplified in examining primary, secondary, and basal neurite lengths, which were enhanced in females versus males. Together, these findings suggest that the enhanced complexity in *SLC7A11*[sut/sut] versus *SLC7A11*^{+/+} males may be a result of aberrant, tortuous morphometry versus increases in neurite length. These observed genotype-dependent differences in male mice could plausibly underlie an E/I imbalance manifest by enhanced excitation in *SLC7A11*[sut/sut] as compared to *SLC7A11*^{+/+} sex-matched controls.

E/I balance is integrally related to cellular soma size as evidenced by results demonstrating increases in soma area enhance inhibitory input from perisomatic parvalbumin-positive interneurons (Ye et al 2015). Moreover, reductions in soma size occur in association with decreased inhibitory postsynaptic current (IPSC) frequency

(Hsu et al 2012) and increased seizure susceptibility (Hsu et al 2012, McLeod et al 2013). Our results indicate that soma size in female *SLC7A11^(sut/sut)* mice is significantly decreased as compared to *SLC7A11^(+/+)* sex-matched controls. However, this effect was sex-dependent, as the soma size of male *SLC7A11^(sut/sut)* mice was indistinguishable from that of sex-matched *SLC7A11^(+/+)* controls. Interestingly, a sex-difference was uncovered in that *SLC7A11^(+/+)* males had soma sizes that were significantly smaller than *SLC7A11^(+/+)* female mice. Taken together, changes in *SLC7A11^(sut/sut)* neuronal morphometry at the cellular level, including enhanced dendritic complexity in males and a reduction in soma area in females, could plausibly facilitate a physiological E/I imbalance, characterized by enhanced excitation, in *SLC7A11^(sut/sut)* mice.

The vast majority of fast synaptic neurotransmission occurs at spine heads (Colonnier 1968), and increases or decreases in head width are associated with increases or decreases in glutamate receptor abundance, respectively (Matsuzaki et al 2001). While the overall density of spines/µm was not altered between female or male mice of either genotype, male mice had an increased proportion of mature spines classified as mushroom or stubby and a concomitant decreased proportion of immature spines, classified as filopodia or long thin, as compared to female mice of either genotype, suggesting that, independent of genotype, male spines may be strengthened as compared to female spines. However, when comparing spine head widths of all dendritic protrusions, we found that head widths of spines measured in male *SLC7A11^(+/+)* mice were ≈7% smaller than female *SLC7A11^(+/+)* mice. Upon examination of within-sex genotype differences, we found that both spine head widths (≈4%) and spine lengths (≈11%) were enhanced in male *SLC7A11^(sut/sut)* as compared to *SLC7A11^(+/+)* sex-

matched mice. The former observation suggests that their spines have increased

glutamate receptors (Matsuzaki et al 2001). However, an increase in spine lengths is

associated with enhanced filtering of the signal received at the post synaptic density

and thus, synaptic weakening (Araya et al 2006), and it is unclear what the overall

functional effect of both increased spine head widths and spine lengths would be with

regards to synaptic strength. Conversely, female $SLC7A11^{sut/sut}$ spine head widths were

decreased by ≈8% as compared to $SLC7A11^{+/+}$ littermates, and no changes in spine

lengths were observed. While an increase in spine head widths in $SLC7A11^{sut/sut}$ male

mice as compared to $SLC7A11^{+/+}$ sex-matched littermates is consistent with their

hyperexcitable phenotype, a decrease in spine head widths in $SLC7A11^{sut/sut}$ females is

somewhat surprising, given that they too have a decreased convulsive seizure

threshold. However, it is possible that a reduction in synaptic strength at excitatory

pyramidal cell synapses in female $SLC7A11^{sut/sut}$ mice could be a compensatory

response to a hyper-excitable circuit elicited by other changes – such as a reduction in

soma size and inhibitory drive (Hsu et al 2012, McLeod et al 2013, Ye et al 2015).

Any of the aforementioned morphometric alterations could result in an E/I

imbalance. Indeed, both female and male $SLC7A11^{sut/sut}$ mice exhibited increased

seizure severity and convulsive seizure incidence as compared to $SLC7A11^{+/+}$ sex-

matched littermate controls in response to a single dose of the chemoconvulsant PTZ.

Thus, despite sex-dependent brain morphological differences, $SLC7A11^{sut/sut}$ mice

exhibit a sex-independent functional hyper-excitability. These findings raise the

intriguing possibility that morphological sex-differences serve to maintain E/I balance in

brains of female and male wild-type mice, and these sex-differences are, at least in part,

maintained by Sx_c^- signaling. For instance, the decreased dendritic complexity in male versus female *SLC7A11*$^{+/+}$ mice may be integral in dampening aberrant connectivity in males. In male mice, loss of Sx_c^- renders complexity more "female like", and this occurs in association with hyper-excitability. With respect to soma size, the increased soma area in female versus male *SLC7A11*$^{+/+}$ mice may be integral for females in maintaining an elevated level of somatic inhibitory input to thwart aberrant neural activity. In female mice, loss of Sx_c^- renders their soma area more "male like", and this too occurs in association with hyper-excitability. That a null mutation in Sx_c^- eliminates morphological sex differences – and decreases convulsive seizure threshold – is suggestive that morphological sex differences exist to prevent adverse behavioral outcomes, such as an E/I imbalance.

Taken together, our results are the first to detail a role for Sx_c^- in maintenance of cellular morphology. Specifically, we found that female *SLC7A11*$^{sut/sut}$ mice with a null mutation in the substrate specific light chain of Sx_c^- demonstrate decreased corpus callosum thickness, cross-sectional soma area, and dendritic spine head widths as compared to *SLC7A11*$^{+/+}$ sex-matched littermate controls. Conversely, male *SLC7A11*$^{sut/sut}$ mice exhibited enhanced dendritic complexity and spine head widths compared to *SLC7A11*$^{+/+}$ mice. These sex-dependent morphological alterations occur in association with an E/I imbalance manifest by a decreased convulsive seizure threshold when provoked with the $GABA_AR$ antagonist PTZ. More broadly, these findings raise the intriguing possibility that morphological sex-differences serve to maintain E/I balance in brain, and these sex-differences are, at least in part, maintained by Sx_c^- signaling.

Chapter 3: Decreased epileptogenesis in mice lacking the system x_c^- transporter occurs in association with a reduction in AMPA receptor subunit GluA1

This chapter is near duplicate of the submitted manuscript:

Sears, Sheila M.S., Hewett, James A., and Hewett, Sandra J. (2018) Decreased epileptogenesis in mice lacking the System x_c^- transporter occurs in association with a reduction in AMPA receptor subunit GluA1. *Submitted*.

3.1   Summary

Although the cystine/glutamate antiporter System x_c^- (Sx_c^-) plays a permissive role in glioma-associated seizures, its contribution to other acquired epilepsies has not been determined. As such, the present study investigates whether and how Sx_c^- contributes to the PTZ chemical kindling model of epileptogenesis. Male *SLC7A11^sut/sut* mice and their wild-type *SLC7A11^+/+* littermates were administered PTZ (i.p.) daily for up to 21 days (kindling paradigm). Seizure severity was scored on a five-point behavioral scale. Mossy fiber sprouting, cellular degeneration, and Sx_c^- light chain (xCT) messenger RNA (mRNA) was explored using Timm staining, thionin staining, or real-time quantitative polymerase chain reaction (qPCR), respectively. Levels of reduced and oxidized glutathione and cysteine were determined via high performance liquid chromatography (HPLC). Plasma membrane protein levels of glutamate and GABA receptor subunits as well as the K^+/Cl^- co-transporter KCC2 were quantified in brains of *SLC7A11^+/+* and *SLC7A11^sut/sut* mice via Western blot analysis. Our results demonstrate that repeated administration of PTZ produced chemical kindling in only 50% of *SLC7A11^sut/sut* mice as compared to 82% of *SLC7A11^+/+* littermate control mice. Kindling did not result in any changes in xCT mRNA levels assessed in *SLC7A11^+/+* mice. No cellular degeneration or mossy fiber sprouting was discernible in either genotype. Except for a small, but significant, decrease in oxidized cysteine in the hippocampus, no other change in measured redox couples were determined in *SLC7A11^sut/sut* mice. Cortical levels of the AMPA receptor subunit GluA1 were decreased in *SLC7A11^sut/sut* mice as compared to *SLC7A11^+/+* littermates, whereas all other proteins tested showed no difference between genotypes. This study provides the first evidence that Sx_c^- signaling contributes to epileptogenesis in the PTZ kindling model of acquired epilepsy.

Further data indicate a reduction in AMPA receptor signaling could underlie the

resistance to PTZ kindling uncovered in *SLC7A11^{sut/sut}* mice.

3.2   Introduction

System x_c^- (Sx_c^-) is a sodium-independent anionic amino acid antiporter

comprised of two protein components linked via a disulfide bridge: xCT (encoded by

SLC7A11), the light chain that confers substrate specificity, and 4f2hc (encoded by

SLC3A2), the associated glycoprotein heavy chain that traffics xCT to the plasma

membrane (Bassi et al 2001, Sato et al 1999). While xCT expression is inducible in a

number of tissues, its constitutive expression is limited to the central nervous system

(CNS) and lymphoid organs, including the thymus and spleen (Sato et al 2002, Taguchi

et al 2007). Within the CNS, xCT is detected in most major brain regions with studies

investigating its cellular source demonstrating it is predominantly of astrocytic origin

(Ottestad-Hansen et al 2018, Pow 2001).

Sx_c^- imports cystine (CySS) and exports glutamate (Glu) with 1:1 stoichiometry

across the cellular plasma membrane (Bannai 1986). Early functional characterization

of Sx_c^- established its fundamental physiological role as a cellular CySS supplier.

Following Sx_c^--mediated uptake, CySS is rapidly reduced to cysteine (Cys), a critical

component of many structural, catalytic, and regulatory domains of proteins and a

precursor for the essential thiol antioxidant, glutathione (GSH) (Sato et al 1998). Cys is

also directly exported from the cell via neutral amino acid transporters (Banjac et al

2008). Thus, Sx_c^- regulates intracellular and extracellular thiol redox systems (Banjac et

al 2008, Sato et al 1998). Additionally, several studies have determined that Sx_c^-

contributes significantly to the ambient extracellular glutamate pool that bathes the CNS

in vivo (De Bundel et al 2011, Massie et al 2011b, McCullagh & Featherstone 2014).

Alterations in redox homeostasis adversely affect neuronal synaptic plasticity (Almaguer-Melian et al 2000, Robillard et al 2011), stressing the importance of redox balance in the normal function of brain network activity. Additionally, glutamate released from astrocytes is known to modulate neuronal excitability and enhance synaptic strength [for review see (De Pitta et al 2016)]. Further, multiple studies demonstrate that changes in redox balance and/or extracellular glutamate levels could be permissive in generating ictal activity. For example, mice under chronic oxidative stress show increased incidence of spontaneous and handling-induced seizures, which occurs in association with decreased expression of the glial glutamate transporters (GLT-1 and GLAST) (Liang & Patel 2004). Diminished glutamate uptake in mice null for the glutamate transporters GLT-1 or GLAST occurs in association with spontaneous seizures or prolonged seizure duration in an amygdaloid kindling model, respectively (Tanaka et al 1997, Watanabe et al 1999). Moreover, increased Sx_c^--mediated cystine/glutamate exchange in glioma (Ye et al 1999) occurs in association with elevated glutamate levels (Ye & Sontheimer 1999), and pharmacological inhibition of Sx_c^- reduces peritumoral glutamate levels in human glioblastoma patients (Robert et al 2015) as well as seizure frequency in glioma-bearing mice (Buckingham et al 2011). Whether Sx_c^- is involved in non-tumor associated seizure generation is not known, although xCT levels are upregulated in resected hippocampi from temporal lobe epileptics (Lewerenz et al 2014). Finally, male transgenic xCT null mice require an elevated dose of pilocarpine or KA to elicit behavioral seizures – in addition to demonstrating decreased seizure severity and mortality in response to an acute dose of

NMDA – suggesting that Sx_c^- signaling is permissive in generating acute seizure activity (De Bundel et al 2011).

The dual regulation of redox systems and glutamate homeostasis by Sx_c^- and the potential for alterations in such to regulate brain ictal activity prompted our interest in the possibility that this antiporter may also contribute to the aberrant changes that predispose the CNS to develop epilepsy. Thus, the overall goal of this study was to explore the contribution of Sx_c^- to epileptogenesis by comparing PTZ kindling in mice wild-type or null for the *SLC7A11* gene.

3.3   Materials and Methods

3.3.1 Animals

Mice were maintained in the AALAC accredited Laboratory Animal Resource facility of Syracuse University on a 12 hr light/dark schedule (7am/7pm). Standard mouse chow and water were provided *ad libitum*. Experiments were carried out using male mice (8-12 weeks at start of experimentation) in accordance with the National Institutes of Health guidelines for the use of experimental animals as approved by the Institutional Animal Care and Use Committee of Syracuse University. Purchased C57BL/6J mice [Jackson Laboratories (JAX) Stock #000664] were allowed to acclimatize to the facility for at least one week prior to any manipulations. Wild-type (*SLC7A11*^{+/+}) and xCT mutant (*SLC7A11*^{sut/sut}) mice were bred in-house from heterozygous (*SLC7A11*^{+/sut}) breeding units (F1) that were obtained by crossing *SLC7A11*^{sut/sut} male mice (JAX, Stock #001310) with *SLC7A11*^{+/+} female C3H/HeSnJ mice (JAX, Stock #000661). F2 *SLC7A11*^{+/sut} progeny were also used as breeding units

for studies. Genotyping was performed via PCR analysis of tail genomic DNA samples: +/+ primers, 5'- GAA GTG CTC CGT GAA GAA GG -3' (forward), 5'- ATC TCA ATC CTG GGC AGA TG -3' (reverse); *sut/sut* primers, 5'- CCA CTG TTG TAG GTC AGC TTA GG -3' (forward), 5'- CAG GAC CTG TGA ATA TGA TAG GG -3' (reverse). Mice were segregated by sex at weaning and placed two to three per cage such that at least one mouse of each genotype was represented. These breeding and housing strategies were employed to control for environmental differences, genetic background influences, and genetic drift. Gross morphological analysis of $SLC7A11^{sut/sut}$ and $SLC7A11^{+/+}$ male mouse brains at 12 weeks of age revealed no significant differences (not shown).

3.3.2 PTZ Kindling

Five days prior to each study, mice were acclimated to handling by performing mock daily intraperitoneal (i.p.) injections, which consisted of inverting the mouse and rubbing its abdomen. They were also acclimatized to the procedure room for at least one hour on each day of injection. PTZ (Sigma Chemical Co., St. Louis, MO), made fresh daily, was dissolved in saline and filter sterilized. PTZ was administered i.p. in a volume of 10 ml/kg body weight. C3H/HeSnJ or C57BL/6J mice were dosed at 35 mg/kg or 39 mg/kg, respectively, once daily for up to 21 days. The dose for C3H/HeSnJ and C57BL/6J mice was chosen following initial dose ranging studies to determine the PTZ seizure threshold [Supplementary Fig. S1 and (Claycomb et al 2011), respectively]. Following each injection, mice were monitored for 30 min and the time and severity of behavioral seizures scored and recorded by an observer blinded to genotype using a five-point modified Racine scale (0 - 4: 0 = no behavioral change; 1 = hypoactivity; 2 =

myoclonus; 3 = generalized convulsion with righting reflex; 4 = generalized convulsion with loss of righting reflex) [For full description see Table 1 (Racine 1972)]. Mice were deemed kindled after exhibiting convulsive seizures (≥ stage 3) on three consecutive days, after which PTZ injections were stopped. Ten days later, the permanence of the kindled state was assessed by rechallenging with PTZ. The percentage of permanently kindled mice was determined by dividing the number of animals with a maximum seizure score ≥ 3 by the total number of animals injected. It should be noted that six *SLC7A11*$^{sut/sut}$ mice were *a priori* excluded from the study as they responded to the first injection with a convulsive seizure (behavioral score ≥ 3) making any further reduction in seizure threshold elicited by the kindling protocol (*vide supra*) indeterminable.

3.3.3 Real-Time Quantitative Polymerase Chain Reaction (q-PCR)

Total RNA, isolated using TRIzol reagent (Invitrogen, Carlsbad, CA) from cortical or hippocampal tissue of PTZ-kindled, PTZ-non-kindled, or saline-injected C57BL/6J mice one day following the final injection with PTZ or saline, was subjected to first-strand cDNA synthesis. cDNA was subjected to real-time quantitative polymerase chain reaction (qPCR) in a reaction containing mouse-specific primers for the system x_c^- light chain (xCT) (*SLC7A11*, Mm01292531_m1, Taqman Gene Expression Assays, Applied Biosystems, Foster City, CA) and the reference gene hypoxanthine guanine phosphoribosyl transferase (*HPRT*, Mm01545399_m1, Taqman Gene Expression Assays, Applied Biosystems, Foster City, CA) along with TaqMan Universal PCR MasterMix (Applied Biosystems, Foster City, CA). HPRT expression levels were stable under our experimental conditions. A serial dilution of cortical or hippocampal cDNA

demonstrated that the calculated slope of the line comparing ΔC_T (C_T value of xCT – C_T value of HPRT) versus input cDNA was -0.007606 or -0.000905, respectively, and that the efficiency of both primers was >90% in either tissue. Reactions were performed in duplicate or triplicate using an Eppendorf Realplex^2 under the following conditions: 50°C for 2 min and 95°C for 10 min followed by 40 amplification cycles (95°C for 15 sec and 60°C for 1 min). Data analysis was performed using the comparative cycle threshold method ($\Delta\Delta C_T$), where C_T values of xCT were normalized to HPRT C_T values from the same sample and compared to the calibrator C_T values (saline controls) to determine the relative fold increase in xCT mRNA.

3.3.4 Timm and Thionin Staining

Mossy fiber sprouting, elucidated by Timm staining, was quantified in the supragranular layer of the dentate gyrus (DG) by an observer blinded to the experimental condition. Brain slices from PTZ kindled *SLC7A11$^{+/+}$* and *SLC7A11$^{sut/sut}$* mice and saline-injected *SLC7A11$^{+/+}$* mice were sacrificed 16-17 days after kindling acquisition or cessation of saline injections by transcardial perfusion with a proprietary (FD Rapid TimmStain Kit; FD Neuro Technologies, Inc., Baltimore, MD) sodium sulfide-containing perfusate (Perfusate A plus B), followed by 4% paraformaldehyde (PFA) in 0.1 M phosphate buffer (PB). Following removal from the cranium, brains were post-fixed in 4% PFA for 24 hr (4°C), transferred to a 30% sucrose solution in 0.1 M PB for 72 hr (4°C), and then snap-frozen on dry ice in Optimal Cutting Temperature (O.C.T.) compound (Tissue-Tek, Torrance, CA) prior to storage at -80°C. Frozen brains were cut serially (≈-0.94 – -2.46 mm posterior to bregma) into 40 µm coronal sections, mounted

on gelatin-coated slides (FD Neuro Technologies, Inc., Baltimore, MD), air dried at room

temperature for 24 hours, then stored in a light-protected box at -20°C. Timm staining

was carried out per manufacturer's instructions (FD Rapid TimmStain Kit) with the

exception that the time in the silver nitrate developing solution (Solution A, B, C, and D)

was extended to 55-70 min. Mossy fiber sprouting was quantified using a six-point

rating scale (0-5) developed by Cavazos et al.(Cavazos et al 1991): 0 = no Timm

granules; 1 = patchy distribution of sparse granules in supragranular layer; 2 =

continuous distribution of granules in supragranular layer; 3 = continuous distribution of

granules with patches of confluency in supragranular layer; 4 = prominent granules that

form a dense, confluent laminar band in supragranular layer; 5 = prominent granules

that form a dense, confluent laminar band in the supragranular layer that extend into the

inner molecular layer. A Timm score for each mouse was determined by calculating the

median of the scores assigned to the left and right DG at ≈-1.94 mm posterior to

bregma. Tissue sections within 80 μm of those processed for Timm staining were

thionin-stained (Sigma Chemical Co., St. Louis, MO) as we previously describe to

assess for any neurodegeneration. All tissue analyses were performed on identically

processed photomicrographs acquired using a DP73 digital color camera (Olympus,

Tokyo, Japan) mounted on an Olympus IX50 inverted microscope (Olympus, Tokyo,

Japan).

3.3.5 Reduced/Oxidized Glutathione and Cysteine Measurements

Fully anesthetized naïve *SLC7A11*$^{+/+}$ or *SLC7A11*$^{sut/sut}$ mice were perfused

transcardially with ice-cold phosphate buffered saline (PBS, 1x). Hippocampal and

cortical tissue were rapidly dissected and snap-frozen separately in liquid nitrogen. The concentrations of reduced and oxidized glutathione (GSH and GSSG) and cysteine (Cys and CySS) were determined via high performance liquid chromatography (HPLC) by the Emory-Children's Pediatric Biomarkers Core facility.

3.3.6 Immunoblotting

3.3.6.1 Plasma membrane protein isolation:

Naïve *SLC7A11$^{+/+}$* or *SLC7A11$^{sut/sut}$* mice were perfused transcardially with ice-cold 1x PBS under full anesthesia. Bilateral hippocampi and cortices were dissected, snap frozen in liquid nitrogen separately, and stored at -80°C prior to use. Plasma membrane proteins were isolated from pooled hippocampi (2-5 mice/sample) or bilateral cortices (one mouse/sample) using an aqueous two-phase separation method as per manufacturer's instructions (Plasma Membrane Protein Extraction Kit, Abcam, Cambridge, U.K.). Isolated proteins were suspended in 0.5% Triton X-100 in PBS. Samples were stored at -80°C until immunoblotting. Protein concentrations were quantified using the BCA assay kit (Pierce, Rockford, IL).

3.3.6.2 Gel electrophoresis and protein detection

Protein samples (7.5 µg) were separated by 8% SDS-PAGE under reducing (10mM dithiothreitol) and chaotropic (8M urea) conditions followed by electrophoretic transfer to a PVDF membrane (Bio-Rad; Hercules, CA). Membranes were blocked for one hr at room temperature (Odyssey® blocking buffer, LI-COR Biosciences; Lincoln, NE) then probed overnight (4°C) with the following antibodies: anti-Na^{+}/K^{+} ATPase α1

mouse monoclonal antibody (1:750; Abcam; RRID: AB_306023); anti-GluA1 rabbit

polyclonal antibody (1:750; Abcam; RRID:AB_2113447); anti-GluA2 rabbit polyclonal

antibody (1:750; Abcam; RRID:AB_2232655); anti-GluN1 rabbit monoclonal antibody

(1:750; Cell Signaling; RRID: AB_1904067); anti-GluN2A rabbit polyclonal antibody

(1:750; Cell Signaling; RRID: AB_2112295); anti-GluN2B rabbit polyclonal antibody

(1:750; Cell Signaling; RRID: AB_1264223); anti-GABA$_A$Rα1 rabbit polyclonal antibody

(1:3000; Abcam; RRID: AB_732498); anti-K$^+$/Cl$^-$ co-transporter (KCC2) rabbit polyclonal

antibody (1:750; Abcam; RRID: AB_881571). Species-specific secondary antibodies

labeled with spectrally distinct IRDye® fluorescent dyes (LI-COR Biosciences, Lincoln,

NE) were used to detect primary antibodies (1 hr at 25°C) (1:10,000 dilution). Results

were recorded on a LI-COR ODYSSEY® Fc Imaging system (LI-COR Biosciences;

Lincoln, NE) and protein levels quantified using Image Studio 3.1 (LI-COR Biosciences;

Lincoln, NE). Each protein was normalized to the Na$^+$/K$^+$ ATPase levels contained in

each lane. The signal intensity pertaining to the amount of hippocampal or cortical

protein per lane (7.5 µg) was determined to be in the linear range for each antibody at

their respective dilution (data not shown).

3.3.7 Statistical Analysis

All statistical analyses were performed using GraphPad Prism (Version 6.0.1,

Graphpad Software, Inc., La Jolla, CA). Curves depicting kindling acquisition as a

function of time were compared using a log-rank test. Two-way ANOVA or unpaired *t*

test was used to compare seizure latencies, mouse weight, and the concentrations of

reductants/oxidants. Proportions indicating the percent of mice convulsing were

compared using a Fisher's exact test. The Mann-Whitney U test was used to compare

Timm scores. Prior to parametric analysis, qPCR data were transformed to the

geometric means whereas immunoblot data was log transformed ($y = \log(y+1)$) and

compared using one-way ANOVA or an unpaired t test, respectively. In all cases,

significance was set at $p < 0.05$.

3.4   Results

Kindling acquisition, maintenance and mortality

Irrespective of the mouse's genotype, the rate of kindling steadily increased over

the 21-day dosing paradigm (Fig. 3.1A) with the mean latency to kindle being 10.3 ± 1.1

and 11.4 ± 1.2 days for *SLC7A11$^{+/+}$* and *SLC7A11$^{sut/sut}$* mice, respectively ($p = 0.54$,

unpaired t test). Although the latency to convulsive seizure on each of the three

consecutive days leading up to and inclusive of the kindled state was similar between

SLC7A11$^{+/+}$ and *SLC7A11$^{sut/sut}$* littermates (Fig. 3.1B; $p = 0.40$, two-way ANOVA),

kindling acquisition was significantly reduced in *SLC7A11$^{sut/sut}$* (9/18; 50%) as compared

to *SLC7A11$^{+/+}$* (22/27; 81.5%) (Fig. 3.1A; $p = 0.02$, log-rank test).

Permanency of the kindled state, determined by rechallenge with PTZ ten days

after the third convulsion, was neither 100% for either genotype nor statistically

significant between genotypes with only 82% of the *SLC7A11$^{+/+}$* (18/22) and 78% of

SLC7A11$^{sut/sut}$ (7/9) responding to the PTZ challenge with a seizure score of ≥ 3 ($p = $

1.00, Fisher's exact test). The latency to convulsion upon rechallenge also did not differ
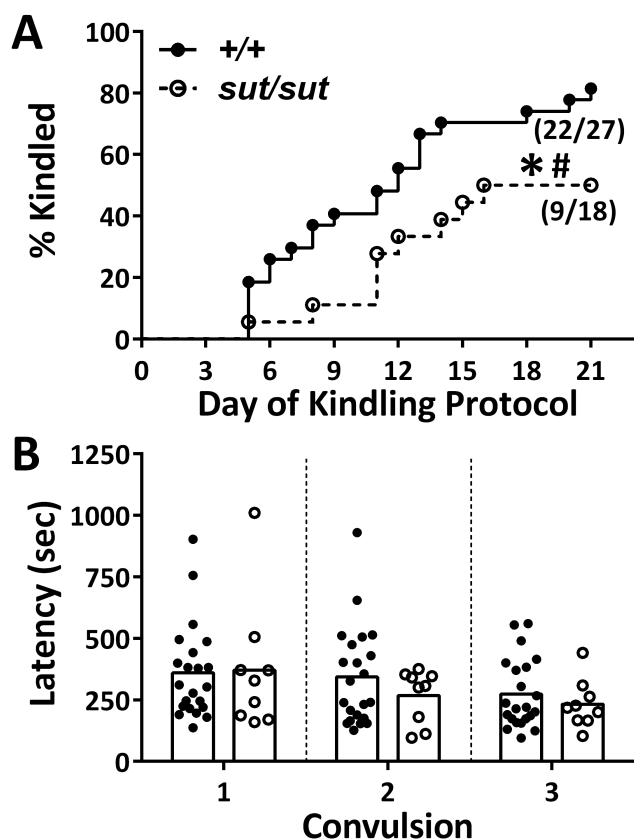
Figure 3.1 Comparison of PTZ kindling acquisition and convulsive seizure latency between SLC7A11⁺/⁺ and SLC7A11ˢᵘᵗ/ˢᵘᵗ mice

SLC7A11⁺/⁺ (+/+; closed circles, n = 27) and *SLC7A11ˢᵘᵗ/ˢᵘᵗ* (*sut/sut*; open circles, n = 18) mice were administered 35 mg/kg PTZ (i.p.) once daily for 21 days or until the mouse became kindled. Five separate experiments were performed over 24 months. **A)** *Kindling acquisition:* Each data point represents the percentage of mice kindled each day over the 21 day paradigm, which was determined by dividing the number of animals defined as kindled (see methods) by the total number of animals injected. Fractions represent the proportion of mice kindled at the end of the protocol. The rate and proportion of *SLC7A11ˢᵘᵗ/ˢᵘᵗ* mice that kindled is significantly decreased as compared to *SLC7A11⁺/⁺* littermate controls as denoted by the large and small asterisk, respectively (*p = 0.02, log-rank test; #p = 0.047, Fisher's exact test).
B) *Convulsive seizure latency:* Each data point [closed black circles (+/+) or open circles (*sut/sut*)] represents the latency to convulsion (behavioral score ≥ 3) of a single mouse for each of the three consecutive convulsions (depicted as Convulsion 1-3) that led to its kindled state. Bars represent the mean latency to convulsive seizure for each genotype. Kindled *SLC7A11⁺/⁺* and *SLC7A11ˢᵘᵗ/ˢᵘᵗ* mice have similar convulsive seizure latencies (p = 0.40, two-way ANOVA).

between the genotypes (431 ± 45 vs. 416 ± 51 s for $SLC7A11^{+/+}$ vs. $SLC7A11^{sut/sut}$,
respectively; p = 0.85, unpaired t test).

Of note, no mortality occurred in either group during the kindling paradigm. Mice
that completed the paradigm exhibited an average weight loss of 0.28 g. However, the
final weight of kindled mice did not differ between genotypes (25.2 ± 0.4 vs. 23.9 ± 0.5 g
for $SLC7A11^{+/+}$ and $SLC7A11^{sut/sut}$, respectively), nor did these differ from that of non-
kindled mice (23.2 ± 1.1 vs. 24.4 ± 0.5 g for $SLC7A11^{+/+}$ and $SLC7A11^{sut/sut}$,
respectively, two-way ANOVA).

xCT mRNA levels

To determine whether the kindling phenotype was associated with an increase in
xCT expression, we measured hippocampal and cortical xCT mRNA levels in kindled,
non-kindled, and saline-injected $SLC7A11^{+/+}$ mice via quantitative PCR one day
following the final PTZ or saline injection. Neither hippocampal nor cortical xCT mRNA
expression levels of kindled mice differed from non-kindled or saline-administered
control mice (Figure 3.2), suggesting that basal levels of Sx_c^- are sufficient to facilitate
kindling.

Histological analysis of injury and axonal sprouting

Sixteen to seventeen days following PTZ-kindling, brains were examined for
signs of overt cellular degeneration. Thionin-staining of brain slices revealed that the
cortex (not shown) and principal layers of the hippocampal formation (Fig. 3.3A, E, I),
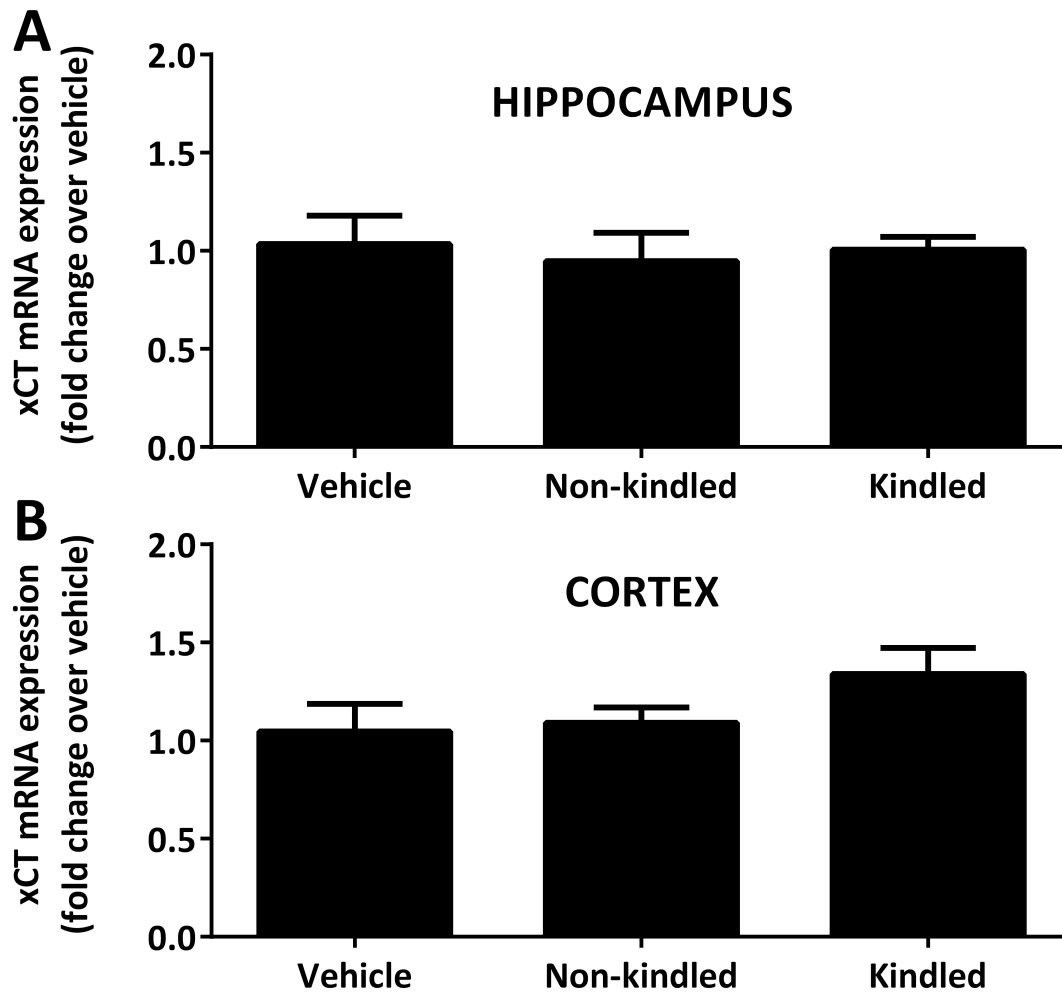
Figure 3.2 PTZ kindling phenotype is not associated with alterations in xCT mRNA

SLC7A11^{+/+} mice on a C57BL/6J background were administered 39 mg/kg PTZ once daily for 21 days or until kindled. Mice receiving vehicle (saline) were injected in parallel. A) The left hippocampus and (B) left cortex were harvested 24 hours following the final injection of PTZ or vehicle and xCT mRNA assessed via qPCR. Data are expressed as mean ± SEM fold change in xCT mRNA compared with vehicle-injected controls. No significant between-group differences in xCT mRNA expression in hippocampus (p = 0.84) or cortex (p = 0.26) was found as determined by one-way ANOVA. N = 4-5 each per treatment group.

Vehicle	PTZ-kindled	
+/+	+/+	*sut/sut*

A **E** **I** — 200 µm

B **F** **J**

C **G** **K**

D **H** **L** — 100 µm
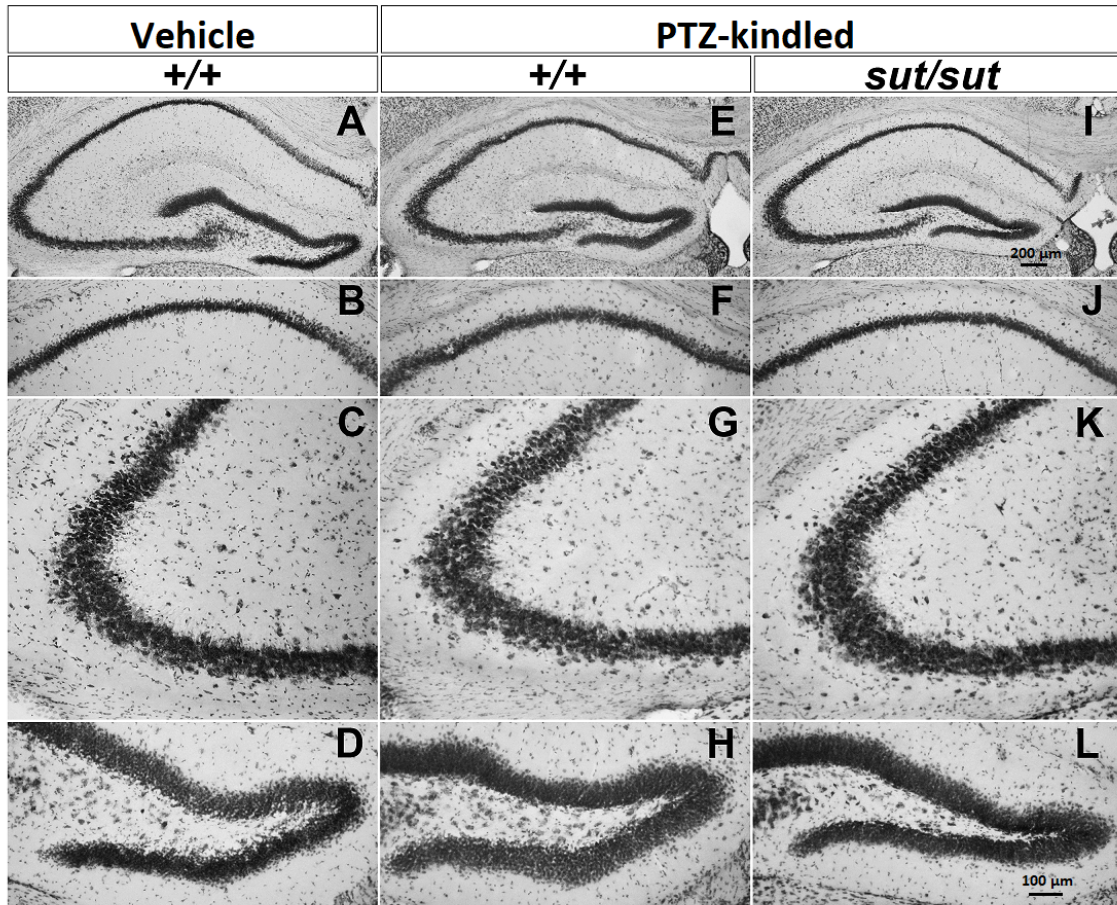
Figure 3.3 PTZ kindling phenotype is not associated with cellular degeneration

Representative photomicrographs of thionin-stained coronal brain sections ≈ -1.82 mm posterior to bregma: (A-D) vehicle (saline)-injected *SLC7A11*$^{+/+}$ (+/+; n = 3), (E-H) kindled *SLC7A11*$^{+/+}$ (+/+; n = 4), and (I-L) kindled *SLC7A11*$^{sut/sut}$ (*sut/sut*; n = 2) brain sections. Images represent the hippocampal formation (A, E, I; 8x), CA1 (B, F, J; 20x), CA3 (C, G, K; 20x), or the DG (D, H, L; 20x).
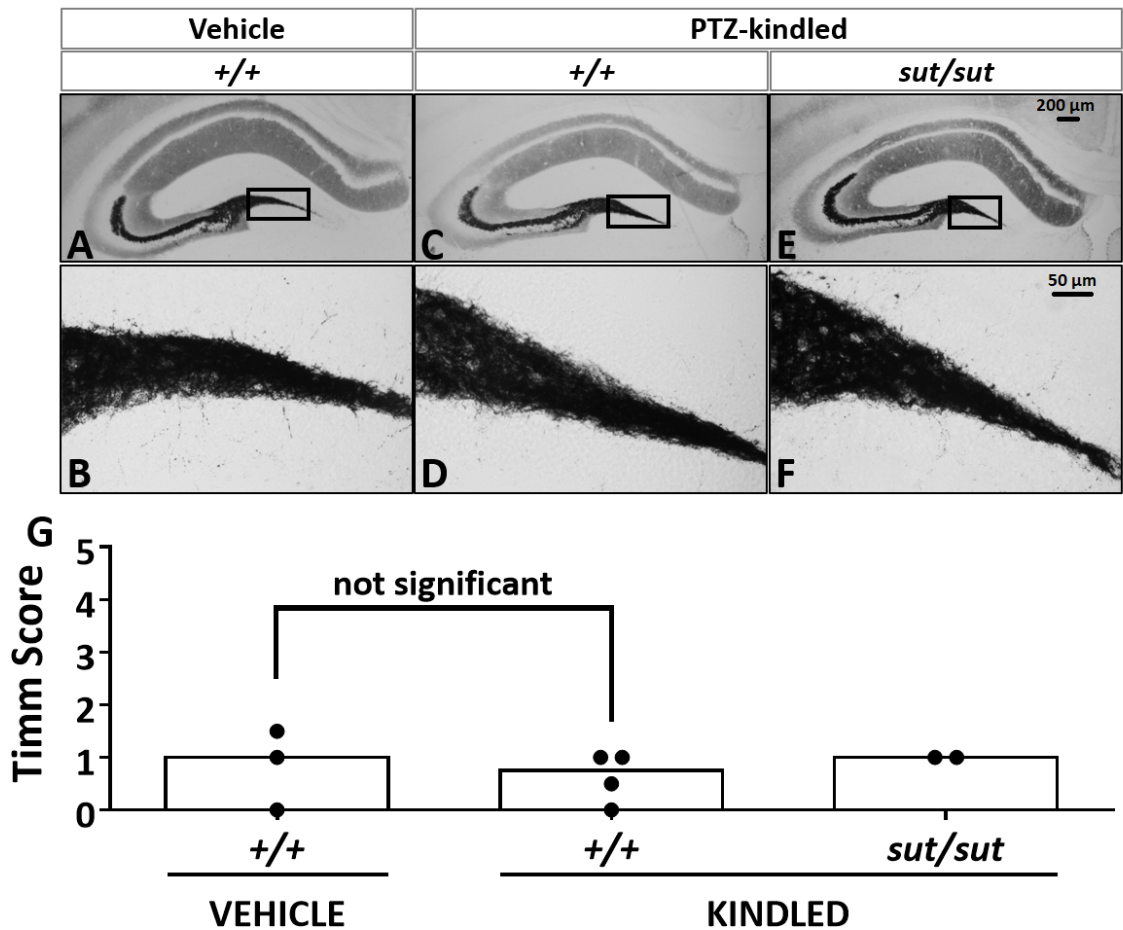
Figure 3.4 PTZ kindling phenotype is not associated with increased mossy fiber sprouting

A-F) Representative photomicrographs of Timm stained hippocampal formation ≈ -1.94 mm posterior to bregma: (A-B) vehicle (saline)-injected control $SLC7A11^{+/+}$ (+/+; n = 3), (C-D) kindled $SLC7A11^{+/+}$ (+/+; n = 4) (C-D), and (E-F) kindled $SLC7A11^{sut/sut}$ (*sut/sut*; n = 2). Images represent the hippocampal formation (A, C, E; 8X) and the DG (B, D, F; 40X). Boxes in A, C, and E depict the region of the DG assessed for mossy fiber sprouting.
G) Each closed circle represents the Timm score (see methods) of a single mouse determined by calculating the median of the scores assigned to the right and left DG (40x) at ≈ -1.94 mm bregma. Open bars represent the median Timm score for each group. There was no significant difference in mossy fiber sprouting between vehicle-injected $SLC7A11^{+/+}$ and kindled $SLC7A11^{+/+}$ mice as determined by the Mann-Whitney U test (p = 0.69).

including the CA1 (Fig. 3.3B, F, J), the CA3 (Fig. 3.3C, G, K), and the dentate gyrus

(DG; Fig. 3.3D, H, L) of kindled mice appeared grossly normal and intact irrespective of

genotype. The lack of degeneration was confirmed in adjacent sections using Fluoro

Jade C and a 4',6-Diamidino-2-Phenylindole, Dilactate (DAPI) counterstain (data not

shown). Aberrant sprouting of DG granule cell axons, known as mossy fiber sprouting,

is a common feature in temporal lobe epilepsy and is found in some, but not all, rodent

models of epileptogenesis. PTZ-kindled $SLC7A11^{+/+}$ mice, maintained on a C3H/HeSnJ

background, had few mossy fiber synaptic terminals as evidenced by little to no Timm

granules in the supragranular layer of the DG that were comparable in number to those

quantified in saline-treated control mice (Fig. 3.4; median Timm score = 0.75 vs. 1,

respectively; p = 0.69, Mann Whitney U test). $SLC7A11^{sut/sut}$ kindled mice also showed

little to no change in mossy fiber sprouting (Fig 3.4; median Timm score = 1). Thus,

alterations in mossy fiber sprouting cannot explain the reduction in kindling acquisition

in $SLC7A11^{sut/sut}$ as compared to $SLC7A11^{+/+}$ mice.

Redox signaling

Cys derived from Sx_c^- import of CySS is the rate-limiting substrate for the

production of the low molecular weight thiol GSH and contributes to the Cys/CySS

redox couple across the cell plasma membrane (Banjac et al 2008, Dringen 2000, Lu

2009). To determine whether loss of Sx_c^- resulted in a redox imbalance in $SLC7A11^{sut/sut}$

brains, the hippocampal and cortical levels of reduced and oxidized GSH (GSH and

GSSG) and Cys (Cys and CySS) were measured and compared to levels measured
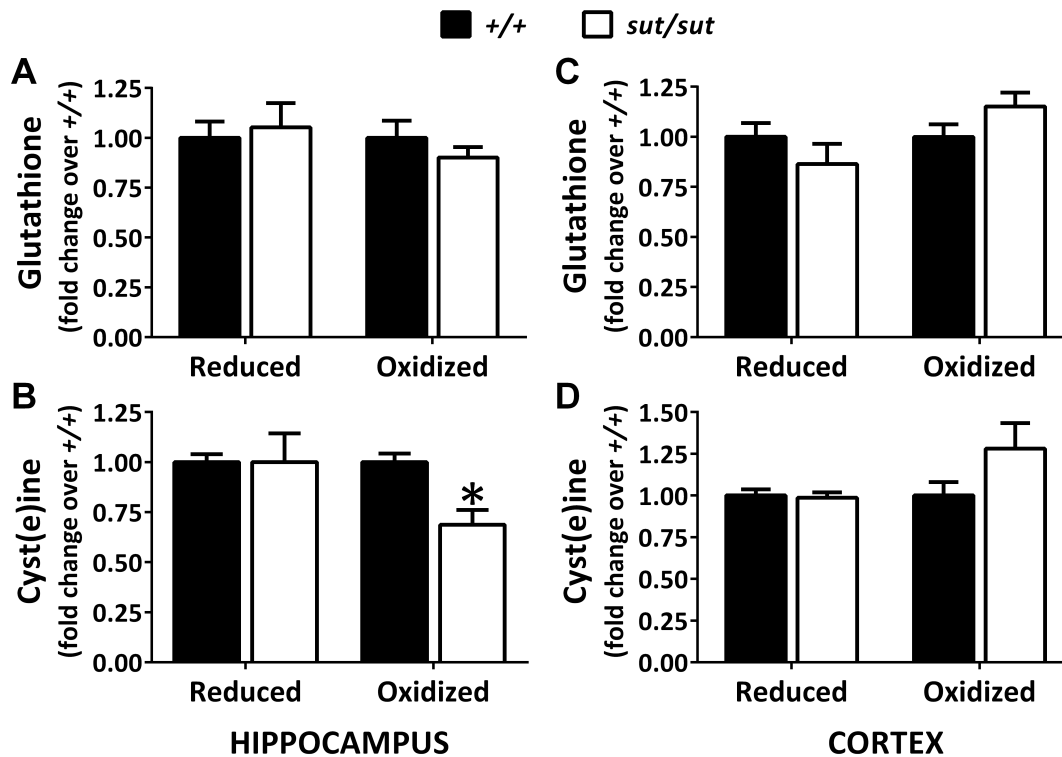
Figure 3.5 Comparison of redox couples in SLC7A11$^{+/+}$ and SLC7A11$^{sut/sut}$ mice

The concentration of reduced and oxidized glutathione (GSH and GSSG) or cysteine (Cys and CySS) was determined by high performance liquid chromatography (HPLC) in hippocampus (A-B) or cortex (C-D) of naïve SLC7A11$^{+/+}$ (+/+; n = 8-10) and SLC7A11$^{sut/sut}$ (sut/sut; n = 10) littermates. Bars represent the mean ± SEM fold-change over control (+/+, set to one) of the concentration of hippocampal or cortical GSH (A, C; left bars), GSSG (A, C; right bars), Cys (B, D; left bars), or CySS (B, D; right bars). Comparisons between individual levels of reduced or oxidized GSH or Cys were made using an unpaired t test on raw data. An asterisk (*) represents a significant between group difference (p = 0.002).
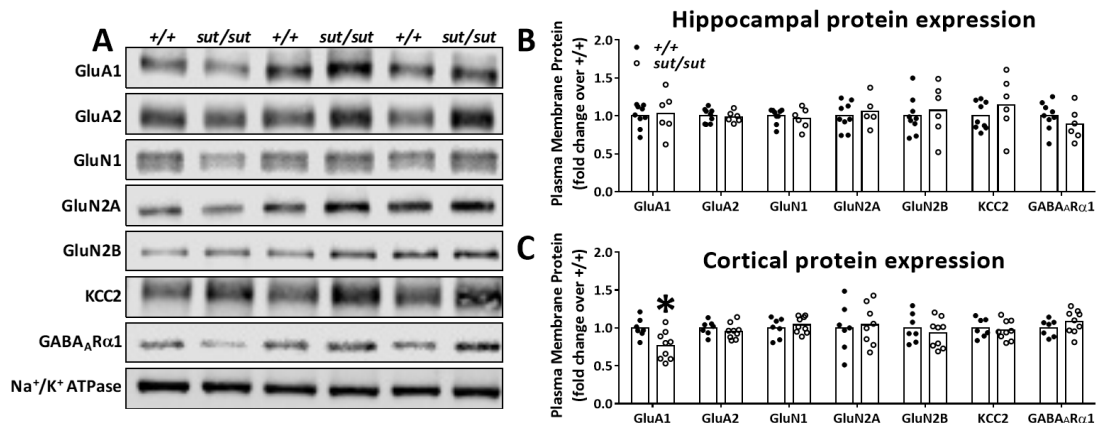
Figure 3.6 Comparison of plasma membrane protein expression in SLC7A11$^{+/+}$ and SLC7A11$^{sut/sut}$ mice

Plasma membrane protein levels in hippocampus or cortex derived from *SLC7A11$^{+/+}$* (+/+) or *SLC7A11$^{sut/sut}$* (*sut/sut*) littermates were compared using Western blot analysis (see methods). Representative Western blots of +/+ and *sut/sut* hippocampal plasma membrane proteins are shown in (A). Each data point [closed black circles (+/+; n = 7-9) or open circles (*sut/sut*; n = 5-9) represents the level of hippocampal (B) or cortical (C) protein following normalization to their respective loading control (i.e., Na$^+$/K$^+$ ATPase levels). Bars indicate the mean fold change over control (+/+), which was set to one. Hippocampal or cortical plasma membrane protein expression levels were compared using an unpaired *t* test on log-transformed data. An asterisk (*) represents a significant between group difference (*p* = 0.01).

102

from *SLC7A11*^{+/+} tissues. Neither hippocampal nor cortical GSH (Fig. 3.5A left; *p* = 0.74; Fig. 3.5C left; *p* = 0.28, unpaired *t* test) nor GSSG (Fig. 3.5A right; *p* = 0.34; Fig. 3.5C right; *p* = 0.12, unpaired *t* test) levels were different between *SLC7A11*^{+/+} and *SLC7A11*[sut/sut] mice. Cortical levels of Cys were also similar between the genotypes (Fig. 3.5D left; *p* = 0.80, unpaired *t* test), while there was a small, but non-significant, increase in CySS (Fig. 3.5D right; *p* = 0.12, unpaired *t* test). Notably, in the hippocampus, the level of CySS was significantly decreased in *SLC7A11*[sut/sut] mice as compared to *SLC7A11*^{+/+} littermate controls (Fig. 3.5B right; *p* = 0.002, unpaired *t* test), while Cys levels were unchanged (Fig. 3.5B left; *p* = 1.00, unpaired *t* test).

Plasma membrane protein expression levels

Finally, we assessed cortical and hippocampal surface expression of AMPA (GluA1, GluA2), NMDA (GluN1, GluN2A, and GluN2B), and GABA (GABA$_A$Rα1) receptor subunits, as well as, the K$^+$/Cl$^-$ co-transporter (KCC2) (Figure 3.6), as aberrations in plasma membrane levels of each has been associated with abnormal neuronal synchronization (Kelley et al 2016, Mathern et al 1998, Raol et al 2006). Western blot analysis of this suite of plasma membrane proteins revealed no change in expression levels between *SLC7A11*^{+/+} and *SLC7A11*[sut/sut] littermates in the hippocampus (Fig. 3.6A,B). Of note, cortical levels of the AMPA receptor subunit GluA1 were significantly decreased in *SLC7A11*[sut/sut] mice as compared to *SLC7A11*^{+/+} littermate controls (Fig. 3.6C; *p* = 0.01, unpaired *t* test on log transformed data). No other cortical plasma membrane proteins were altered in *SLC7A11*[sut/sut] as compared to *SLC7A11*^{+/+} littermate controls (Figure 3.6C).

3.5 Discussion

By virtue of its localization to astrocytes and its role in regulating thiol redox systems as well as ambient extracellular glutamate levels, Sx_c^- (cystine/glutamate antiporter) contributes importantly to CNS homeostasis. In fact, astrocytic transporters, in general, regulate brain excitatory/inhibitory (E/I) balance by providing neurons with energy substrates, by maintaining ion homeostasis, and by removing excess neurotransmitters from the extracellular space. Dysfunction in any one of these activities can facilitate epileptogenesis [reviewed in (Eid et al 2018)]. In this study, we now provide evidence that Sx_c^- signaling contributes to epileptogenesis in the PTZ-kindling model of acquired epilepsy (Figure 3.1). These findings complement studies demonstrating an incontrovertible role for Sx_c^- in glioma-associated epilepsy in both mice and man (Buckingham et al 2011, Robert et al 2015).

While Sx_c^- has been found to be upregulated in glioma(Yuen et al 2012), we do not find any changes in xCT mRNA expression in PTZ-kindled mice as compared to vehicle-injected controls (Figure 3.2), suggesting that basal levels of Sx_c^- are sufficient to facilitate PTZ-kindling. Given the lack of reliable commercial antibody for xCT (personal observations and (Van Liefferinge et al 2016)), we cannot rule out the possibility that enhanced transporter trafficking (as has been described in human glioma cells *in vitro* (Chase et al 2013)) or increased transporter kinetics (as demonstrated in rat striatum *in vivo*) occurs in wild-type mice (Baker et al 2002). However, present data suggests that *in vivo* glutamatergic tone — maintained in large part by non-vesicular release of glutamate by Sx_c^- (De Bundel et al 2011, Massie et al 2011b, McCullagh & Featherstone 2014) — may be enough to dysregulate excitatory signaling in wild-type

mice, as we previously documented in an *in vitro* paradigm of hypoglycemic neuronal cell death (Thorn et al 2015). Leading credence to this interpretation are the findings that a reduction in GABAergic inhibition (Kapur et al 1989a, Kapur et al 1989b) and an increase in extracellular glutamate and glutamate receptor levels (Li et al 2000, Schröder et al 1993) are associated with PTZ-kindling in rodents. Conversely, a decrease in ambient, extracellular glutamate levels has been reported in mice lacking Sx_c^- (De Bundel et al 2011, Massie et al 2011b, McCullagh & Featherstone 2014). This, together with the reduction in cortical GluA1 AMPA receptor subunit protein expression found herein (Figure 3.6), suggests that glutamatergic signaling may be hypo-functional in the *SLC7A11^{sut/sut}* mouse brain in a manner sufficient to reduce PTZ-kindling. In keeping with this idea, long-term potentiation (LTP), which is observed at glutamatergic excitatory synapses in hippocampus and cortex, is also reduced in *SLC7A11^{sut/sut}* mice (Li et al 2012). However, it should be noted that enhanced synaptic GluA1 expression has been reported in the CA1 region of the hippocampus of transgenic xCT null mice (Williams & Featherstone 2014), although we found no change in global hippocampal GluA1 levels in *SLC7A11^{sut/sut}* mice (Figure 3.6). It is difficult to compare these two studies as our plasma membrane measurements include all hippocampal subregions and would capture receptors of both synaptic and extrasynaptic origin. Nevertheless, a global plasma membrane reduction in cortical GluA1 is interesting given evidence from animal models that block of AMPA receptor signaling is anti-epileptogenic (Kodama et al 1999, Namba et al 1994).

Sx_c^--mediated CySS import has been demonstrated to be fundamental in maintaining the extracellular and intracellular redox balance (e.g., GSH/GSSG and

Cys/CySS) at least *in vitro* where growth of xCT deficient cells is dependent upon the addition of a reducing agent (Sato et al 2005). Interestingly, dysregulation of glutathione homeostasis is associated with impairment of synaptic strength (Almaguer-Melian et al 2000, Robillard et al 2011) and thus represents another possible explanation for the resistance of *SLC7A11*[sut/sut] mice to PTZ-kindling. However, *SLC7A11*[sut/sut] mice have normal Cys, GSH and GSSG levels in hippocampal and cortical tissue, although hippocampal CySS levels were found to be significantly decreased (Figure 3.4). Our data are in agreement with other studies in transgenic xCT nulls showing normal hippocampal GSH levels as compared to wild-type mice (De Bundel et al 2011). To our knowledge, this study is the first to measure the concentration of GSH in cortex as well as brain cyst(e)ine levels in a mouse null for Sx_c^-. Taken *in toto*, current and previous data in both transgenic xCT nulls and *SLC7A11*[sut/sut] mice suggest these animals must employ compensatory mechanisms (e.g., EAAT3 or the alanine-cysteine-serine transporter [ASCT1/2] as alternative Cys transporters) to sustain GSH levels *in vivo.*

Finally, epileptogenic network sensitization and its resultant E/I imbalance is associated with synaptic reorganization, particularly when hilar neurons in the dentate gyrus are lost (Buckmaster & Dudek 1997, Cavazos & Sutula 1990). This reorganization includes reactive synaptogenesis of granule cell mossy fibers, whose targets have been demonstrated to include both excitatory (Scharfman et al 2003) and inhibitory (Sloviter et al 2006) neurons. However, we found no cellular loss in the hippocampus or cortex of PTZ-kindled mice of either genotype (Figure 3.3). We also did not observe any significant hippocampal mossy fiber sprouting in any group tested, indicating that this structural alteration was not necessary for kindling development. These results are not

unprecedented as previous studies show that rats (Osawa et al 2001) and guinea pigs (Mohapel et al 2000) kindle in the absence of mossy fiber sprouting. Moreover, suppression of reactive sprouting in rats (Longo & Mello 1997) and mice (Buckmaster & Lew 2011) has been demonstrated to be ineffective in preventing epileptogenic neuronal sensitization following chemically-induced status epilepticus.

In sum, our results demonstrate that $SLC7A11^{sut/sut}$ mice have a reduction in PTZ-kindling acquisition that occurs in association with decreased GluA1 levels. Given the permissiveness of Sx_c^- signaling to epileptogenesis — both glioma- (Buckingham et al 2011, Robert et al 2015) and PTZ-induced (this study) — we postulate that inhibition of astrocyte Sx_c^- may represent an alternative therapeutic strategy to modulate excessive glutamatergic signaling in individuals predisposed to developing epilepsy.

Chapter 4: KA-mediated alterations in excitability in system x_c^- null mice differ according to dosing paradigm.

4.1   Summary

Sx_c^- null (*SLC7A11$^{sut/sut}$*) mice exhibited hyper-excitability (Chapter 2) or hypo-excitability (Chapter 3) following acute or chronic dosing with PTZ, respectively, which induces seizure activity indirectly via disinhibition. In this chapter, the model-dependency of these findings was explored using KA, a glutamate receptor agonist that directly elicits excitation. Female and male *SLC7A11$^{sut/sut}$* and *SLC7A11$^{+/+}$* littermates were injected with KA once (acute paradigm) or repeatedly (escalated dosing paradigm) and the resulting seizure severity scored on a nine-point behavioral scale. Following the elevated dosing paradigm, brains of *SLC7A11$^{+/+}$* and *SLC7A11$^{sut/sut}$* mice were evaluated for hippocampal cellular degeneration or for plasma membrane protein levels of glutamate and GABA receptor subunits using Fluoro jade C staining or Western blot analysis, respectively. Our results demonstrate that *SLC7A11$^{sut/sut}$* mice exhibit behavioral hyper-excitability following acute KA administration. In contrast, repeated administration of KA in the elevated dosing paradigm elicits behavioral hypo-excitability in *SLC7A11$^{sut/sut}$* mice, a response opposite to that observed in the vast majority of *SLC7A11$^{+/+}$* littermates who entered into a period of unremitting convulsive seizure activity (status epilepticus). The repeated KA dosing paradigm elicited neural degeneration in a subset of both *SLC7A11$^{+/+}$* and *SLC7A11$^{sut/sut}$* littermates. However, the hippocampal sub-region predominantly affected differed by genotype, with the CA3 or CA1 sub-region demonstrating degeneration in *SLC7A11$^{sut/sut}$* or *SLC7A11$^{+/+}$* littermates, respectively. Cortical levels of the GABA receptor subunit GABA$_A$Rα were increased in *SLC7A11$^{sut/sut}$* mice that became hypo-mobile by the end of the repeated dosing paradigm as compared to *SLC7A11$^{sut/sut}$* mice that entered into status epilepticus. No between-genotype differences were found in plasma membrane proteins tested following the repeated KA dosing protocol. These results extend findings in Chapters 2 and 3 and indicate that positive or negative excitability alterations elicited in

SLC7A11^{sut/sut} mice via acute or repeated/chronic chemoconvulsant administration, respectively, are not model dependent.

4.2   Introduction

System x_c^- (Sx_c^-) is a heteromeric amino acid antiporter that exports glutamate and imports cystine with 1:1 stoichiometry (Bannai & Kitamura 1980, Sato et al 1999). In most tissues, including the central nervous system (CNS), cystine import through Sx_c^- is necessary for the synthesis and maintenance of the cellular antioxidant, glutathione (GSH). This, along with the cysteine/cystine (Cys/CySS) redox cycle, also influenced by Sx_c^- activity, contributes to the intracellular/extracellular redox homeostasis (Banjac et al 2008, Sato et al 2005). Sx_c^- is also an important contributor to the ambient extracellular glutamate levels that bathe the CNS *in vivo* (Augustin et al 2007, Baker et al 2002, De Bundel et al 2011, Massie et al 2011b, Melendez et al 2005). Studies addressing the cellular source of this glutamate conclude that it is astrocyte-derived (Augustin et al 2007, Grosjean et al 2008, Warr et al 1999).

Data presented in Chapter 2 of this dissertation demonstrated that *SLC7A11^{sut/sut}* mice — who harbor a natural mutation in exon 12 of *SLC7A11*, rendering them null for the Sx_c^- substrate specific light chain xCT (Chintala et al 2005) — are more excitable (i.e., have lower convulsive seizure thresholds) than *SLC7A11^{+/+}* littermate control mice following acute challenge with the $GABA_A$ receptor antagonist PTZ (Fig 2.9). Despite this, *SLC7A11^{sut/sut}* mice show behavioral signs of hypoexcitability upon chronic administration of PTZ. Specifically, data presented in Chapter 3 established that repeated daily injections of a kindling dose of PTZ ultimately leads to a permanent decrease in the threshold of excitability in *SLC7A11^{+/+}* mice (i.e., mice become kindled), whereas the percent *SLC7A11^{sut/sut}* mice that kindle over the same 21 days is

significantly lower (Fig 3.1). These data suggest that Sx$_c^-$ activity modulates synaptic

strength *in vivo* in a context-dependent manner.

In contrast to our findings using PTZ – whereby excitation results from

endogenous glutamate signaling – transgenic xCT null mice on a C57BL/6 background

appear to have an elevated seizure threshold in response to three pharmacologically

distinct chemoconvulsants (De Bundel et al 2011). Specifically, xCT null mice require an

elevated dose of either the muscarinic acetylcholine agonist, pilocarpine, or the

glutamate receptor agonist, KA, to elicit the same behavioral seizure response as wild-

type controls (De Bundel et al 2011). Furthermore, this study demonstrated that xCT

null mice exhibit decreased seizure severity and mortality, as well as increased latency

to seize, in response to a systemic injection of the glutamate receptor agonist NMDA

(De Bundel et al 2011). Thus, contrary to our findings using the *SLC7A11$^{sut/sut}$* mice in

the acute PTZ paradigm (Chapter 2), these results suggest that xCT null mice on the

C57BL/6 background have an elevated seizure threshold.

The goal of this study was to determine if our findings using PTZ in the

SLC7A11$^{sut/sut}$ mice were model-dependent. As such, the susceptibility of *SLC7A11$^{+/+}$*

and *SLC7A11$^{sut/sut}$* littermates to seizures evoked by acute or repeated administration of

the glutamate receptor agonist KA was explored. Whether KA induced neural

degeneration or altered plasma membrane protein expression levels was also explored

given the association of these phenotypes with KA-mediated excitoxic cell death (Nadler

et al 1980) or neuronal synaptic strength, respectively (Mathern et al 1998, Raol et al

2006).

4.3   Materials and Methods

4.3.1 Animals

Mice were maintained in the AALAC accredited Laboratory Animal Resource facility of Syracuse University on a 12 hr light/dark schedule (7am/7pm). Standard mouse chow and water were provided *ad libitum*. Experiments were carried out using male and female mice (8-12 weeks old) in accordance with the National Institutes of Health guidelines for the use of experimental animals as approved by the Institutional Animal Care and Use Committee of Syracuse University. Wild-type ($SLC7A11^{+/+}$) and xCT mutant ($SLC7A11^{sut/sut}$) mice were bred in-house from heterozygous ($SLC7A11^{+/sut}$) breeding units (F1) that were obtained by crossing $SLC7A11^{sut/sut}$ male mice (JAX, Stock #001310) with $SLC7A11^{+/+}$ female C3H/HeSnJ mice (JAX, Stock #000661). F2 $SLC7A11^{+/sut}$ progeny were also used as breeding units for studies. Genotyping was performed via PCR analysis of tail genomic DNA samples: +/+ primers, 5'- GAA GTG CTC CGT GAA GAA GG -3' (forward), 5'- ATC TCA ATC CTG GGC AGA TG -3' (reverse); *sut/sut* primers, 5'- CCA CTG TTG TAG GTC AGC TTA GG -3' (forward), 5'- CAG GAC CTG TGA ATA TGA TAG GG -3' (reverse). Mice were segregated by sex at weaning and placed two to three per cage such that at least one mouse of each genotype was represented. These breeding and housing strategies were employed to control for environmental differences, genetic background influences, and genetic drift (Barnwell et al 2009, Pick & Little 1965).

4.3.2 KA dosing paradigms

Changes in *in vivo* network excitability were provoked in $SLC7A11^{+/+}$ and

$SLC7A11^{sut/sut}$ mice by injection of KA (Abcam, Cambridge, U.K.). Mice were acclimated

to handling by performing mock daily intraperitoneal (i.p.) injections five days prior to

each study, which consisted of inverting the mouse and rubbing its abdomen. They

were also acclimatized to the procedure room for at least one hour prior to

experimentation. The KA injection solution (1 – 1.5 mg/mL) was prepared fresh on day

of use in 0.05M phosphate buffered saline (PBS) and filter sterilized prior to i.p.

administration.

4.3.2.1 Acute Dose

$SLC7A11^{+/+}$ or $SLC7A11^{sut/sut}$ mice were injected once with KA (12 mg/kg, males;

15 mg/kg, females) in a volume of 10 ml/kg body weight. Following the injection, mice

were monitored for 30 min and the time and severity of behavioral seizures scored and

recorded by an observer blinded to genotype using a nine-point modified Racine scale

as described below. All mice received 5mg/kg diazepam (i.p., dissolved in 0.9% saline

containing 40% propylene glycol) 60 min after dosing to arrest any ongoing seizure

activity.

4.3.2.2 Escalating Dose

The escalating dosing paradigm was initiated by injecting $SLC7A11^{+/+}$ or

$SLC7A11^{sut/sut}$ mice with a loading dose of 10 mg/kg KA in a volume of 10 ml/kg body

weight. Booster doses of 2.5 mg/kg KA were administered 30, 60, 90, 120, and 150 min

later (see below) in a volume of 2.5 ml/kg body weight. Mice were continuously

monitored throughout the 240 min paradigm and the time and severity of behavioral

seizures scored and recorded by an observer blinded to genotype using a nine-point modified Racine scale as described in Section 4.3.2.3 (Table 4.1). All mice received 5mg/kg diazepam (i.p., dissolved in 0.9% saline containing 40% propylene glycol) 240 min after the initial dose of KA to arrest any on-going seizure activity.

TREATMENT (mg/kg)

KA
10   2.5   2.5   2.5   2.5   2.5   Diazepam 5

0   30   60   90   120   150   240

TIME (min)
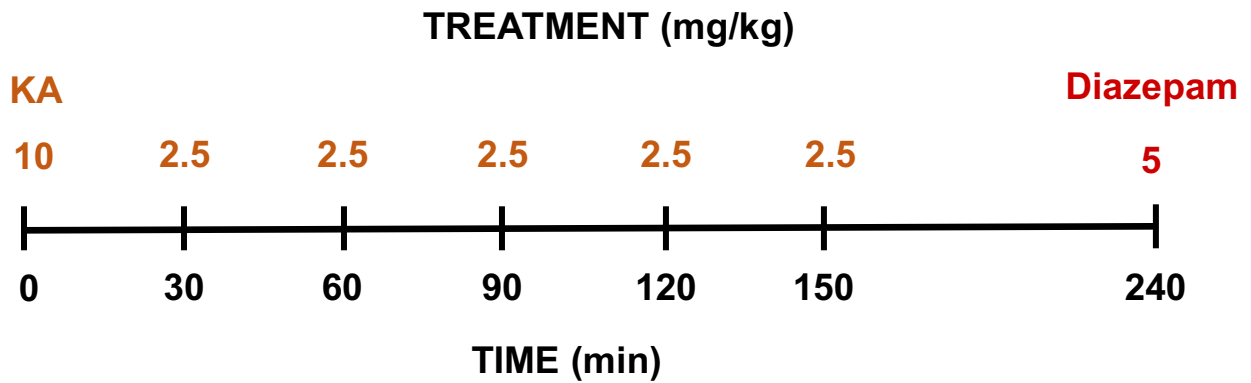
4.3.2.3 Quantification of KA-induced Seizure Behavior

Behavioral seizure scores were recorded for each mouse by an observer blinded to genotype to ensure unbiased scoring (see Table 4.1 below). Scores ≤ 4 = non-convulsive seizures; scores ≥ 5 = clonic/convulsive seizure.

Table 4.1: Descriptive KA-induced Seizure Scoring System

Seizure Score	Abbreviated Description	Detailed Description
0	Normal behavior	Normal ambulation/exploration: sniffing, rearing, grooming, eating, digging, and climbing are common. Unless sleeping, mice will rarely be motionless for more than a few seconds.
1	Hypomobility and hypoactivity	Overall behavior will be dominated by bouts (> 10 sec in duration) of staring and motionlessness that may be interrupted by brief sniffing or ambulation.
2	Hyperactivity	Hyperactivity includes excessive unidirectional rotations, escape-like behavior, and running with an abnormal gait. This generally follows periods of hypoactivity.
3	Repeated twitching or myoclonus	Animal with normal posture exhibiting two or more brief (≤ 2 sec) myoclonic twitches of head, tail or axial musculature. Twitching of whiskers and facial movements are apparent.
4	Rearing without clonus	Animal adopts a posture with prominent kyphosis. Head bobbing or nodding may occur, but movement is not clonic.
5	Rearing with clonus	Similar to score 4 with addition of clonic movement of one or both paws/forelimbs. Animal may transiently lose balance but never falls on side. Continuous clonic movements lasts ≤ 10 min.
6	Generalized seizure with righting reflex	Animals start showing generalized convulsive seizures but will not lose their righting reflex. Convulsive seizures rarely last longer than 1 min.
7	Generalized seizure with loss of righting or violent jumping	Similar to score 6, but animal will fall on side for ≥5 seconds due to hind and forelimb clonus. Animal may barrel roll or violently jump (popcorn) and run around cage.
8	Status Epilepticus, continuous generalized seizure activity	Sustained score 5-7 seizures for ≥ 20 min. Typically, score 5 seizures evolve to score 6-7 and resolve back to score 5 without any intervening periods of absent convulsive seizure activity or lesser seizure scores. Clonic seizures involving loss of posture may proceed uninterrupted for tens of minutes.

Table adapted from descriptions in (Ferraro et al 1999, Pitkanen 2006, Racine 1972).

4.3.3 Histology

SLC7A11$^{+/+}$ or SLC7A11$^{sut/sut}$ mice administered 22.5 mg/kg KA (escalated

dosing paradigm) were sacrificed 72 hr later by transcardial perfusion and fixation with

ice-cold 1x PBS and 4% paraformaldehyde (PFA) in PBS. Following removal from the

cranium, brains were post-fixed in 4% PFA in PBS for 24 hr (4°C), transferred to a 20%

sucrose solution for 24 hr (4°C), and then snap-frozen on dry ice in Optimal Cutting

Temperature (O.C.T.) compound (Tissue-Tek, Torrance, CA) prior to storage at -80°C.

Frozen brains were cut serially (≈-0.94 – -2.46 mm posterior to bregma) into 14 µm

coronal sections, mounted on SuperFrost Plus slides (Fisher Scientific, Houston, TX),

air dried at room temperature for 24 hours, and then stored at -20°C until processing.

4.3.3.1 Thionin staining

Frozen sections were removed from -20°C and initially incubated in a descending

ethanol series of 70% (five min) and 50% (one min) ethanol followed by a one min rinse

in deionized (DI) water prior to incubation in 0.5% thionin (Sigma Chemical Co., St

Louis, MO) for 10 min. Slides were rinsed in DI water 2x for one min each followed by

serial dehydration in absolute ethanol (70%, 95%, 100%, 100%; one min each). Ethanol

was cleared with xylenes (2x for one or three min each), after which coverslips were

mounted using Permount mounting media.

4.3.3.2 Fluoro Jade C staining

Tissue sections within 168 µm of those processed for thionin staining were

Fluoro Jade C stained (AAT Bioquest, Sunnyvale, CA). Frozen sections were removed

from -20°C and dried at 50-60°C for 25-30 min. Samples were initially incubated with

basic alcohol solution (1% NaOH in absolute ethanol) for 5 min followed by 70% ethanol

for 2 min and a 2 min rinse in deionized (DI) water. Sections were then placed in 0.06%

potassium permanganate for 10 min, rinsed in DI water for 2 min, and then placed in

0.0001% Fluoro Jade C in 0.1% acetic acid for 10 min. Samples were rinsed in DI water

3X for 1 min each, dried on a slide warmer at 50-60°C, and images captured with a

Zeiss Axio Imager A2 microscope equipped with epifluorescence and an AxioCam MRc

digital camera (Carl Zeiss, Germany). Following image acquisition, samples were

cleared with xylenes and mounted with DPX mounting media. All images were

processed identically using Zen Microscope and Imaging Software (Carl Zeiss,

Germany, RRID: SCR_013672) and Microsoft PowerPoint.

4.3.4 Immunoblotting

4.3.4.1 Plasma membrane protein isolation

A separate cohort of *SLC7A11*$^{+/+}$ or *SLC7A11*$^{sut/sut}$ mice having undergone the

escalating KA dosing paradigm were perfused transcardially with ice-cold 1x PBS under

full anesthesia within 5-25 min of diazepam injection. Cortices were dissected, snap

frozen in liquid nitrogen, and stored at -80°C prior to use. Plasma membrane proteins

were isolated from bilateral cortices (one mouse/sample) using an aqueous two-phase

separation method as per manufacturer's instructions (Plasma Membrane Protein

Extraction Kit, Abcam, Cambridge, U.K.). Isolated proteins were suspended in 0.5%

Triton X-100 in PBS. Samples were stored at -80°C until immunoblotting. Protein

concentrations were quantified using the BCA assay kit (Pierce, Rockford, IL).

4.3.4.2 Gel electrophoresis and protein detection

Protein samples (7.5 µg) were separated by 8% SDS-PAGE under reducing

(10mM dithiothreitol) and chaotropic (8M urea) conditions followed by electrophoretic

transfer to a PVDF membrane (Bio-Rad; Hercules, CA). Membranes were blocked for

one hr at room temperature (Odyssey® blocking buffer, LI-COR Biosciences; Lincoln,

NE) then probed overnight (4°C) with the following antibodies: anti-Na$^+$/K$^+$ ATPase α1

mouse monoclonal antibody (1:750; Abcam; RRID: AB_306023); anti-GluA1 rabbit

polyclonal antibody (1:750; Abcam; RRID:AB_2113447); anti-GluA2 rabbit polyclonal

antibody (1:750; Abcam; RRID:AB_2232655); anti-GluN1 rabbit monoclonal antibody

(1:750; Cell Signaling; RRID: AB_1904067); anti-GABA$_A$Rα1 rabbit polyclonal antibody

(1:3000; Abcam; RRID: AB_732498). Species-specific secondary antibodies labeled

with spectrally distinct IRDye® fluorescent dyes (LI-COR Biosciences, Lincoln, NE)

were used to detect primary antibodies (1 hr at 25°C) (1:10,000 dilution). Results were

recorded on a LI-COR ODYSSEY® Fc Imaging system (LI-COR Biosciences; Lincoln,

NE) and protein levels quantified using Image Studio 3.1 (LI-COR Biosciences; Lincoln,

NE). Each protein was normalized to the Na$^+$/K$^+$ ATPase (males) or total protein

(females) levels contained in each lane. The signal intensity pertaining to the amount of

cortical protein per lane (7.5 µg) was determined to be in the linear range for each

antibody at their respective dilution (data not shown).

4.3.5 Statistical analysis

All statistical analyses were performed using GraphPad Prism (Version 6.0.1,

Graphpad Software, Inc., La Jolla, CA). Acute seizure severity and proportions

indicating the percent of mice convulsing were compared using a Mann-Whitney U test and Fisher's exact test, respectively. An unpaired *t* test with Welch's correction was used to compare latency to seizure. Curves depicting the median seizure scores over time were compared using a comparison of fit test, while individual seizure scores over time were compared using the Kruskal-Wallis test. Kaplan Meier survival curves were compared using the Mantel-Cox log-rank test. Prior to parametric analysis, immunoblot data was log transformed (y = log(y+1)) and compared using two-way ANOVA. In all cases, significance was set at $p < 0.05$.

4.4   Results

Acute KA-induced seizure severity

The behavioral seizure severity in response to a single acute dose of KA (12-15 mg/kg) was compared in *SLC7A11^{+/+}* and *SLC7A11^{sut/sut}* mice. Irrespective of genotype or sex, within minutes of receiving the dose of KA, all mice exhibited a decrease in spontaneous locomotor activity (seizure score = 1). This behavior was often followed by hypermobility, manifest by excessive pacing, climbing, or unilateral rotations (seizure score = 2), or sporadic myoclonic twitches (seizure score = 3). In a subset of mice, behavioral seizures progressed to a kyphosis, or hunchback, posture (seizure score = 4). The majority of *SLC7A11^{sut/sut}* (19/20), and a subset of *SLC7A11^{+/+}* mice (4/17), progressed to behavioral clonic or convulsive seizures manifest by kyphosis with forelimb clonus (seizure score = 5), a generalized convulsion (seizure score = 6), or a generalized convulsion with loss of righting reflex and/or violent jumping (seizure score

120

Figure 4.1 Comparison of acute KA-induced seizure activity in SLC7A11*+/+* and SLC7A11*sut/sut* mice

Male (n = 6) and female (n = 11) *SLC7A11*+/+ (+/+, total = 17) and male (n = 7) and female (n = 13) *SLC7A11*sut/sut (*sut/sut*, n = 20) littermates were treated with a single dose of either 12 mg/kg (males) or 15 mg/kg (females) KA (i.p.). Seizure behavior was scored using a 9 point scale as described in the materials and methods. Data were pooled from 6 independent experiments performed over 2 months.

A-C) *Individual seizure scores*: Each data point [closed black circles (+/+) or open circles (*sut/sut*)] represents the maximal seizure score obtained by an individual mouse: (A) male and females combined, (B) females, or (C) males only during a 30 min observation period. Horizontal lines represent the median seizure score for each genotype. *SLC7A11*sut/sut mice have significantly greater seizure severity as compared to *SLC7A11*+/+ littermate controls (*p = 0.0002, **p < 0.0001; Mann-Whitney U Test).

B) *Convulsive index:* Bars [closed black bar (+/+) and open bar (*sut/sut*)] represent the proportion (fraction within bars) of mice that experienced a clonic seizure (seizure score ≥ 5) in A (D), B (E), or C (F) expressed as a % of total mice exposed to KA. *SLC7A11*sut/sut mice have a higher clonic index compared to *SLC7A11*+/+ littermate controls as denoted by the asterisk(s) (*p = 0.0210, **p = 0.0005, ***p < 0.0001; Fisher's Exact Test).

Figure 4.2 Comparison of convulsive seizure latency between SLC7A11+/+ and SLC7A11sut/sut mice

The latency to convulsion of *SLC7A11+/+* (+/+, n= 4; 2M, 2F) and *SLC7A11sut/sut* (*sut/sut,* n = 19; 7M, 12F) mice that achieved a score of ≥ 5 in Figure 4.1 is graphed.
A-C) Each data point [closed black circles (males) or open circles (females)] represents the latency to convulsion (behavioral score ≥ 5) of a single mouse during the 30 min observation period: (A) combined males plus females, (B) females, or (C) males only. Bars represent the median latency for each genotype. *SLC7A11sut/sut* mice have a decreased convulsive seizure latency as compared to *SLC7A11+/+* littermate controls as denoted by the asterisk (A only; *p = 0.0346, Unpaired *t* test with Welch's correction).

= 7). A fraction of $SLC7A11^{sut/sut}$ mice exhibited unremitting clonic/convulsive seizure activity as evidenced by a score of 5, 6, or 7 for ≥ 20 min and as such, these mice were assigned a score of 8 (status epilepticus).

The median seizure score in female and male $SLC7A11^{sut/sut}$ mice was significantly greater than that of $SLC7A11^{+/+}$ littermate controls (Fig. 4.1A $p < 0.0001$; Mann-Whitney U test). Stratification of this data by sex revealed that female (Fig. 4.1B; $p = 0.0002$) but not male (Fig. 4.1C; $p = 0.1142$) $SLC7A11^{sut/sut}$ mice have significantly enhanced seizure severity as compared to $SLC7A11^{+/+}$ sex-matched littermate controls at their respective KA doses (Mann Whitney U test). Furthermore, a decreased convulsive seizure threshold was evident in the $SLC7A11^{sut/sut}$ mice, with 95% (19/20) reaching a seizure stage ≥ 5, compared to 23.5% (4/17) of $SLC7A11^{+/+}$ mice (Fig. 4.1D; $p < 0.0001$; Fisher's exact test). This effect, however, was sex-independent, with 92.3% of female and 100% of male $SLC7A11^{sut/sut}$ mice experiencing a clonic seizure as compared to 18.2% of female and 33.3% of male $SLC7A11^{+/+}$ sex-matched littermate controls (Females, Fig. 4.1E, $p = 0.0005$; Males, Fig. 4.1F, $p = 0.0210$; Fisher's exact test). Finally, the mean latency to clonus was decreased in combined female and male $SLC7A11^{sut/sut}$ mice as compared to $SLC7A11^{+/+}$ littermate controls (Fig. 4.2A; 265 ± 57 and 302 ± 45 sec, mean ± SEM, for $SLC7A11^{+/+}$ and $SLC7A11^{sut/sut}$ mice, respectively, $p = 0.0346$, unpaired t-test with Welch's correction). It is also noteworthy that the latency to clonic seizure was reduced in $SLC7A11^{sut/sut}$ versus sex-matched $SLC7A11^{+/+}$ female (Fig. 4.2B; 1044 ± 148.5 s in $SLC7A11^{sut/sut}$ vs. 1493 ± 171 s in $SLC7A11^{+/+}$, mean ± SEM) and male (Fig. 4.2C; 1444 ± 122.6 s in $SLC7A11^{sut/sut}$ vs. 1711 ± 37.5 s in
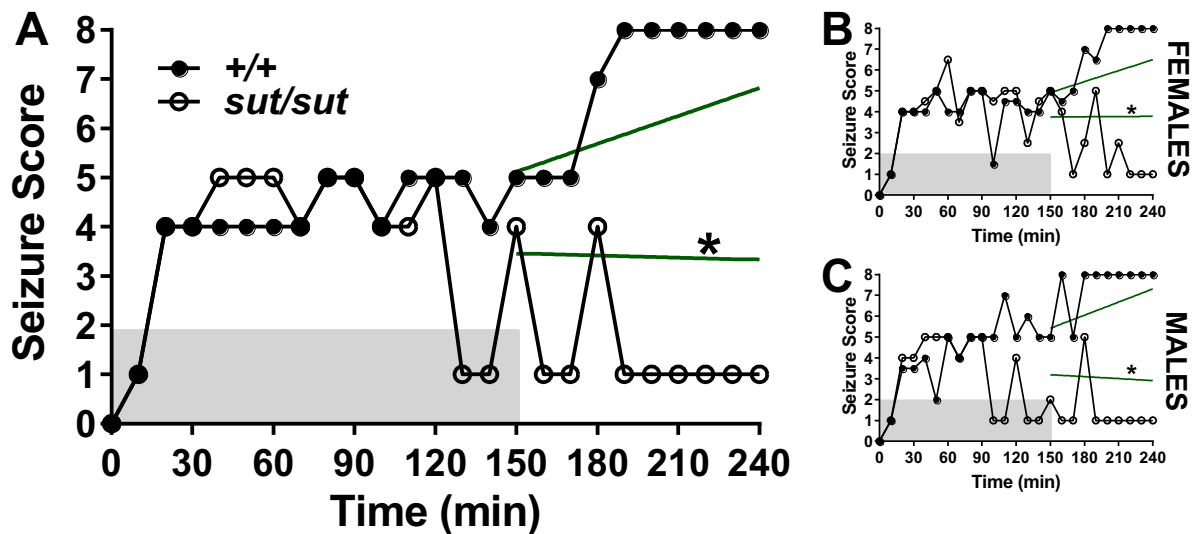
Figure 4.3 Comparison of SLC7A11$^{+/+}$ and SLC7A11$^{sut/sut}$ seizure severity in the escalating KA dosing paradigm

Male (n = 12) and female (n =16) *SLC7A11$^{+/+}$* (+/+, total n = 28) and male (n = 13) and female (n = 12) *SLC7A11$^{sut/sut}$* (*sut/sut*, total n = 25) littermates underwent the escalating KA dose treatment paradigm and behavioral responses were scored using a 9-point scale as described in the materials and methods. Data were pooled from 9 independent experiments performed over 4 months.

A-C) *Time Course*: The shaded area represents the 150 min interval in which KA was administered. Each data point [closed black circles (+/+) or open circles (*sut/sut*)] represents the median maximal seizure score obtained: (A) females and males combined, (B) females, or (C) males only for each 10 min interval of the 240 min treatment paradigm. Green linear regression lines are fitted from the last kainate dose (t = 150 min) to the end of the protocol (t = 240 min). Slope of the *SLC7A11$^{sut/sut}$* line is significantly different from slope of the *SLC7A11$^{+/+}$* line as denoted by the asterisk (*p* < 0.0001; Comparison of fit test).

124
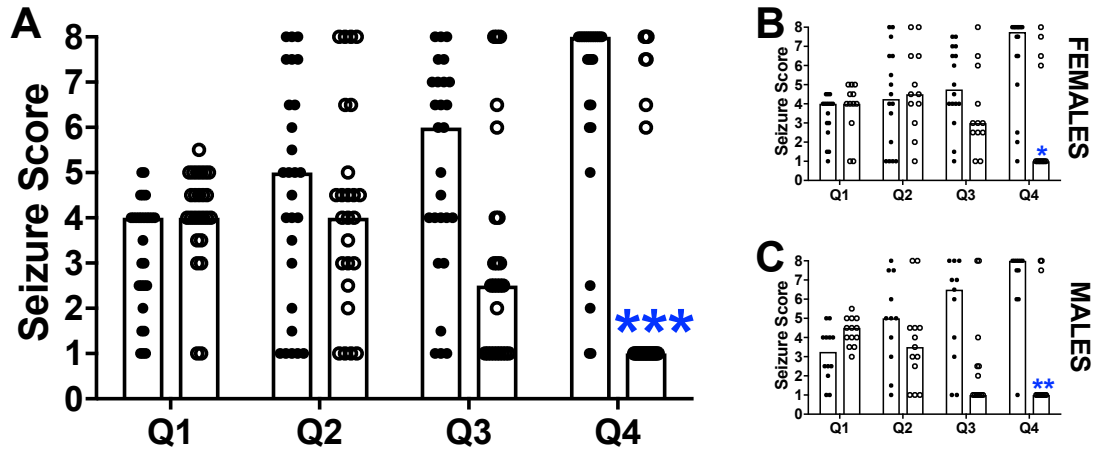
Figure 4.4 Comparison of individual SLC7A11+/+ and SLC7A11sut/sut mouse seizure severity in the escalating KA dosing paradigm

The individual seizure scores of mice administered KA in Figure 4.3 were compared. **A-C)** *Individual seizure scores*: Each data point [closed black circles (*+/+*) or open circles (*sut/sut*)] represents the median seizure score obtained by an individual mouse: (A) females and males combined, (B) females, or (C) males only calculated from the maximal seizure score obtained over the six 10 min intervals contained in each quartile (Q1-Q4). Bars represent the median seizure score for each genotype calculated using the median score from all animals. *SLC7A11sut/sut* mice have significantly lower seizure severity in the final 60 min quartile (Q4) of the four hour KA dosing paradigm as compared to *SLC7A11+/+* littermate controls as denoted by the asterisk(s) (*$p < 0.01$, **$p < 0.001$, ***$p < 0.0001$; Kruskal-Wallis test).

SLC7A11^{+/+}, mean ± SEM) littermates, although the sample sizes preclude a sufficiently powered statistical comparison.

Seizure severity in mice administered an escalating dose of KA

To further explore changes in excitability, mice were administered an escalating dose of KA (22.5 mg/kg over 150 min) (Claycomb et al 2012). Similar to behavioral seizure activity elicited in the acute paradigm, a profound hypomobility was observed in in all mice regardless of genotype or sex within minutes of the initial 10 mg/kg dose of KA. As the dosing protocol progressed over the first hour, the median maximal seizure score (MMSS) in the *SLC7A11*[sut/sut] mice reached a score of 5 (kyphosis with forelimb clonus) compared to a score of 4 (kyphosis) in *SLC7A11*^{+/+} littermate controls (Fig. 4.3A). However, by the second hour of the protocol (t = 120 min), the behavior of *SLC7A11*[sut/sut] mice was indistinguishable from their *SLC7A11*^{+/+} littermate controls (Fig. 4.3A). Interestingly, in the 90 min following the final KA dose (t = 150-240 min), the MMSS trend lines fit to seizure scores in *SLC7A11*^{+/+} and *SLC7A11*[sut/sut] mice began to diverge (green lines on Fig. 4.3A, $p < 0.0001$, comparison of fit test). Upon receiving the final dose of KA at t = 150 min, seizure activity in *SLC7A11*^{+/+} mice escalated such that the MMSS reached status epilepticus (seizure score = 8) by the final hour of the protocol. Unexpectedly, *SLC7A11*[sut/sut] mice exhibited a striking decrease in behavioral seizure severity within the final hour of the protocol dominated by immobility (seizure score = 1) in the majority of mice. Of note, the aforementioned seizure behaviors occurred independent of sex, with both female (Fig. 4.3B) and male (Fig. 4.3C) *SLC7A11*[sut/sut] mice exhibiting hypomobility in the final quartile of the paradigm as

compared to *SLC7A11*$^{+/+}$ sex-matched littermate controls, which were consistently in status epilepticus.

A comparison of the MMSS of individual mice in each quartile of the paradigm further demonstrated the divergence in seizure activity between *SLC7A11*$^{+/+}$ and *SLC7A11*$^{sut/sut}$ mice in the final quartile of the escalating dose protocol. While the median MMSS of the population of male and female (Fig. 4.4A), female (Fig. 4.4B), or male (Fig. 4.4C) *SLC7A11*$^{+/+}$ mice was at a seizure score = 8 in the fourth quartile, the median MMSS of the *SLC7A11*$^{sut/sut}$ mice was at a seizure score = 1 (Females and males, Fig. 4.4A, *p* < 0.0001; Females, Fig. 4.4B, *p* < 0.01; Males, Fig. 4.4C, *p* < 0.001; Kruskal-Wallis test).

Incidence of status epilepticus (SE) and fatality in escalated dosing paradigm.

The disparity in behavioral seizure activity induced by an escalating dose of KA was further exemplified by examining the incidence of status epilepticus in quartile four, which was three times greater in *SLC7A11*$^{+/+}$ [85.2% (23/27)] as compared to *SLC7A11*$^{sut/sut}$ mice [28% (7/25)] (Fig. 4.5A; p < 0.0001; Fisher's exact test). This effect was also sex-independent, with 81.3% of female and 91% of male *SLC7A11*$^{+/+}$ mice experiencing status epilepticus as compared to 33.3% of female and 23.1% of male *SLC7A11*$^{sut/sut}$ sex-matched littermate controls (Females, Fig. 4.5B, *p* = 0.0189; Males, Fig. 4.5C, *p* = 0.0013; Fisher's exact test).

In toto, 23% (12/53) of mice administered an escalating dose of KA died over the course of the four-hour paradigm, with all but one of the deaths occurring in the final hour after cessation of the 150 min dosing period (Fig. 4.6). Notably, the majority of

deaths occurred in *SLC7A11*^{+/+} mice, with just 64.3% (18/28) of *SLC7A11*^{+/+} as

compared to 92% (23/25) of *SLC7A11*[sut/sut] mice surviving the paradigm (Fig. 4.6A; *p* =

0.0137, Mantel-cox log-rank test). This effect was driven by a decreased incidence of

death in *SLC7A11*[sut/sut] male mice relative to *SLC7A11*^{+/+} sex-matched controls; 92.3%

(12/13) of *SLC7A11*[sut/sut] mice survived the paradigm as compared to 58.3% (7/12) of

SLC7A11^{+/+} mice (Fig. 4.6C; *p* = 0.0402; Mantel-cox log-rank test). A similar decrease

in KA-induced mortality, although statistically insignificant (Fig. 4.6B; *p* = 0.1374,

Mantel-cox log-rank test), was observed in *SLC7A11*[sut/sut] female mice.

KA-induced hippocampal neural degeneration occurs in different sub-regions in

SLC7A11*^{+/+} *and SLC7A11*[sut/sut] *mice.

A subset of *SLC7A11*^{+/+} and *SLC7A11*[sut/sut] mice dosed with 22.5 mg/kg KA (Fig.

4.3A) were sacrificed 72 hr post-seizure initiation and brains were processed for thionin

or Fluoro-Jade C staining. All of the tissue analyzed was derived from *SLC7A11*^{+/+} (Fig.

4.7A, 5 females, 3 males) or *SLC7A11*[sut/sut] (Fig. 4.7B, 4 females, 1 male) mice that

achieved behavioral seizure scores of 6 (generalized convulsion) or 7 (generalized

convulsion with loss of righting reflex and/or violent jumping) over the course of the

dosing paradigm. Despite their behavioral seizure similarities, the hippocampal neural

degeneration in *SLC7A11*^{+/+} and *SLC7A11*[sut/sut] mice occurred with striking sub-region

specificity. Though the incidence of neural degeneration occurred in a similar fraction of

SLC7A11^{+/+} [37.5% (3/8; 2 males, 1 female)] and *SLC7A11*[sut/sut] [60% (3/5; 1 male, 2

females)] mice (*p* = 0.5921; Fisher's exact test), degeneration in the *SLC7A11*^{+/+} mice
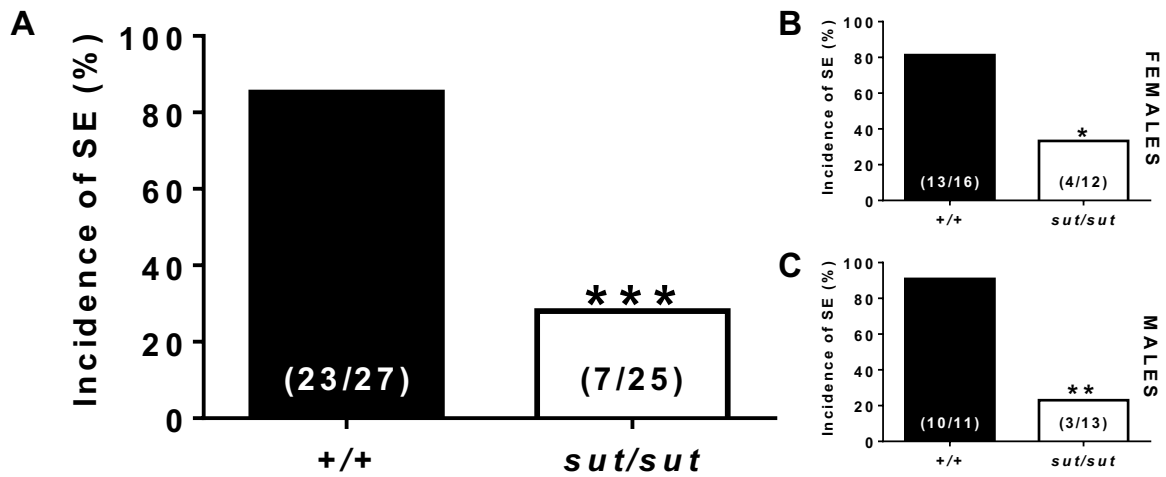
Figure 4.5 Effect of SLC7A11 disruption on incidence of status epilepticus SE in the escalating KA paradigm.

A-C) Bars represent the proportion (fraction within bars) of SLC7A11^{+/+} [+/+, n = 27 (11M, 16F)] and SLC7A11[sut/sut] [sut/sut, n = 25, (13M, 12F)] mice that experienced a seizure score = 8 (SE) in the final 60 min quartile of the four hour KA dosing paradigm. *Indicates significant between group difference (*p = 0.0189, **p = 0.0013, ***p < 0.0001; Fisher's exact test).
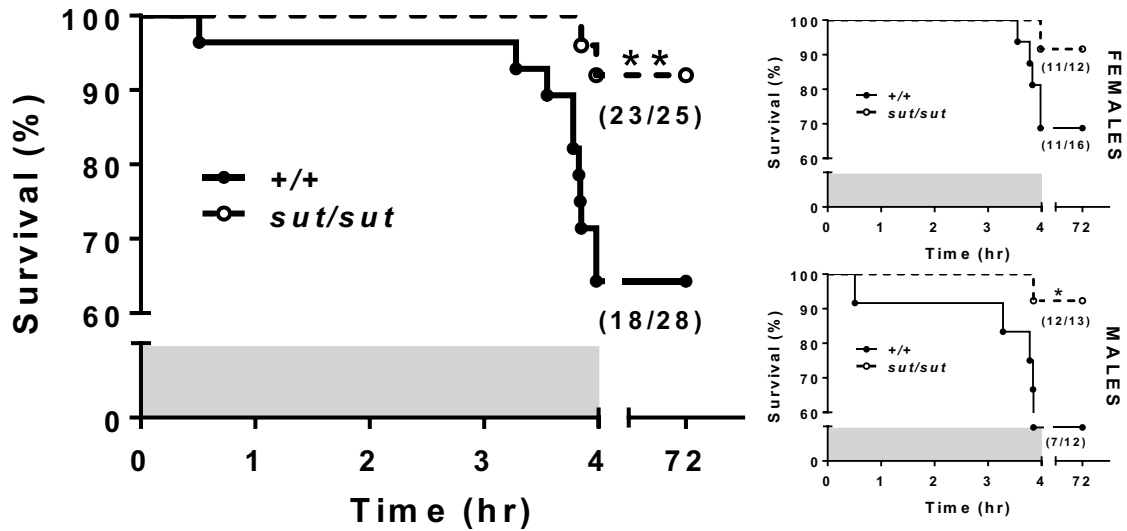
Figure 4.6 Effect of SLC7A11 disruption on mortality in the escalating KA paradigm.

A-C) Kaplan-Meier survival curves up to 72 hr following initial KA dose for *SLC7A11^{+/+}* [+/+, n = 28 (12M, 16F)] and *SLC7A11[sut/sut]* [*sut/sut*, n = 25, (13M, 12F)] (A) females and males combined, (B) females, or (C) males are graphed. Each data point represents the time at which individual mice died during the KA dosing protocol or over the following 72 hr. Fractions represent the proportion of mice that survived the 240 min KA paradigm (shaded region). *Indicates significant between group difference (*p = 0.0402, **p = 0.0137; Mantel-Cox log-rank test).
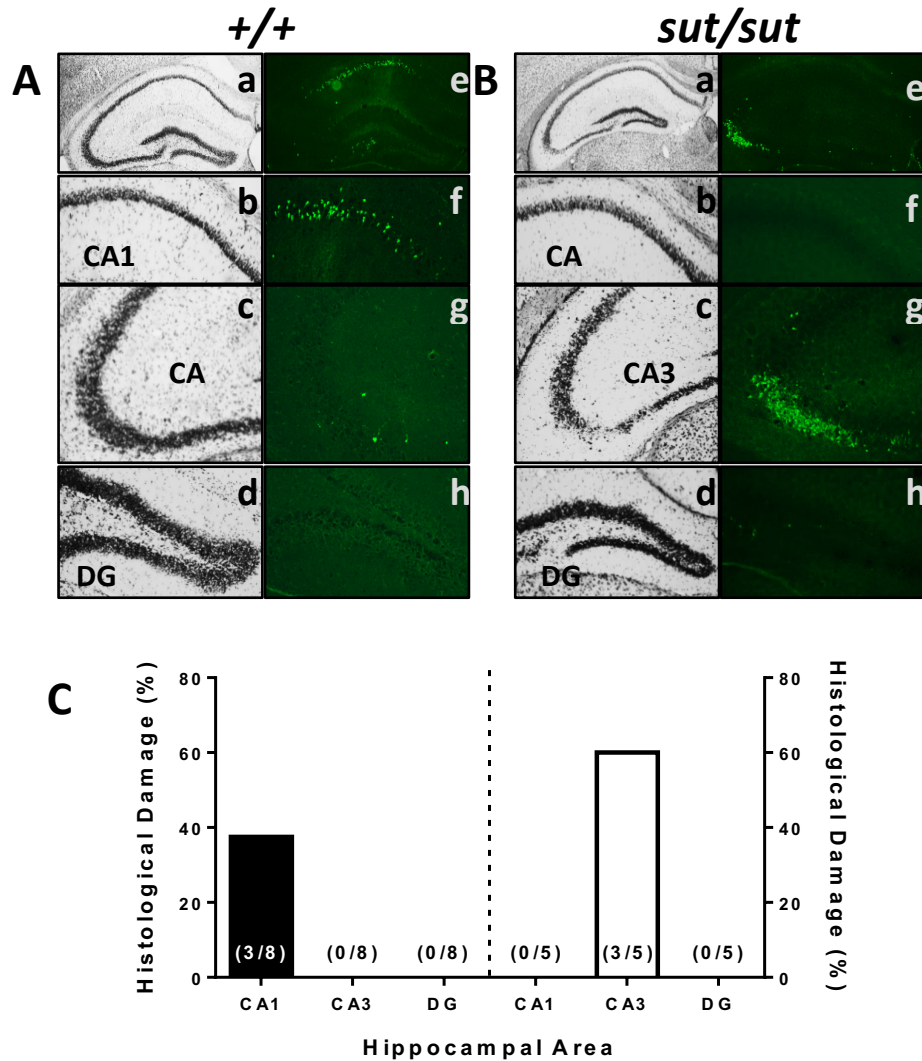
***Figure 4.7 Comparison of cellular degeneration in hippocampus of SLC7A11^{+/+}
and SLC7A11[sut/sut] mice exposed to the escalating KA dose paradigm***

A cohort of *SLC7A11^{+/+}* and *SLC7A11[sut/sut]* mice responding to the escalated KA dosing
paradigm with a seizure score ≥ 6 were sacrificed 72 hr later by transcardial perfusion
and fixation with 4% PFA. Brains were removed and coronal sections of 14 µm
thickness were taken at 28 µm intervals spanning the hippocampal formation.
A-B) Representative photomicrographs of (A) *SLC7A11^{+/+}* (+/+, n = 8) and (B)
SLC7A11[sut/sut] (*sut/sut*, n = 5) brain sections stained with (a-d) thionin or (e-h) Fluoro-
Jade C. Photomicrographs represent the hippocampal formation ≈ -1.2 to -1.9 anterior
to posterior from bregma (a, e; 4X); the CA1 (b, f; 10X); the CA3 (c, g; 10X); and the
dentate gyrus (DG) (d, h; 10X).
C) *Incidence of hippocampal histological damage*: Bars represent the proportion
(fraction within bars) of *SLC7A11^{+/+}* (+/+, black bar) and *SLC7A11[sut/sut]* (*sut/sut*, blue
bar) mice with degenerating cells in the hippocampal formation sub-regions (CA1, CA3,
or DG) as indicated by positive Fluoro-Jade C staining.

occurred primarily in the hippocampal CA1 sub-region whereas degeneration was limited to area CA3 in *SLC7A11^sut/sut^* mice (Fig. 4.7C). This was demonstrated by pyknosis or green fluorescence predominating in the CA1 (Fig. 4.7Ab and Fig. 4.7Af) or CA3 (Fig. 4.7Bc and Fig. 4.7Bg) of *SLC7A11^+/+^* or *SLC7A11^sut/sut^* mice, respectively.

Plasma membrane protein expression levels

Despite receiving 22.5 mg/kg KA over the course of the escalating dosing paradigm, the majority of *SLC7A11^sut/sut^* mice exhibited profound hypo-excitability (seizure score = 1) in the fourth quartile of the protocol, a behavioral state polar opposite to *SLC7A11^+/+^* littermate controls who entered into behavioral status epilepticus (seizure score = 8). Given that aberrations in plasma membrane levels of AMPA (GluA1, GluA2), NMDA (GluN1), or GABA (GABA$_A$Rα) receptor subunits are associated with abnormal neuronal synchronization (Kelley et al 2016, Mathern et al 1998, Raol et al 2006), we measured cortical plasma membrane expression levels of this suite of proteins to investigate whether alterations in such could underlie the behavioral hypo-excitability observed in the majority of *SLC7A11^sut/sut^* mice.

As such, comparisons were made between cortical plasma membrane proteins derived from naïve *SLC7A11^+/+^* and *SLC7A11^sut/sut^* mice as well as mice of each genotype that entered into a state of KA-induced hypomobility (MMSS = 1) or status epilepticus (MMSS = 8) in the final quartile of the escalating dose paradigm. Western blot analysis revealed no change in female and male *SLC7A11^+/+^* and *SLC7A11^sut/sut^* GluA1 (Fig. 4.8A), GluA2 (Fig. 4.8B), GluN1 (Fig. 4.8C), or GABA$_A$Rα (Fig. 4.8D) expression levels (two-way ANOVA with Tukey's multiple comparisons). Moreover,
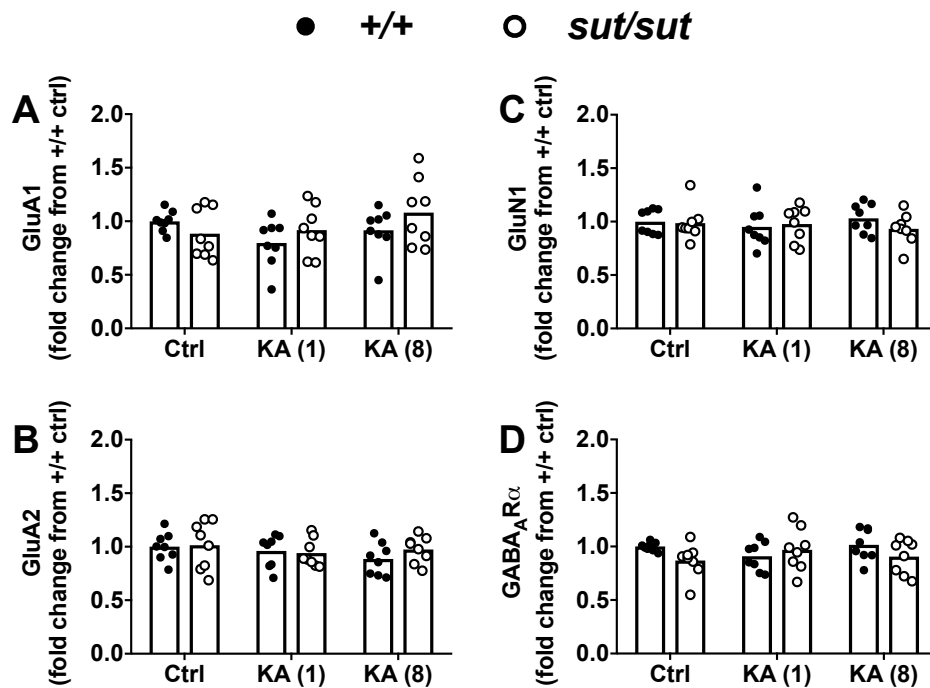
Figure 4.8 Comparison of plasma membrane protein expression in SLC7A11$^{+/+}$ and SLC7A11$^{sut/sut}$ mice

Plasma membrane protein levels in cortex derived from female and male *SLC7A11$^{+/+}$* (+/+) or *SLC7A11$^{sut/sut}$* (*sut/sut*) littermates naïve to any treatment (ctrl) or mice exhibiting hypo-mobility [KA (1)] or status epilepticus [KA (8)] in the final quartile of the four hour escalating dose paradigm were compared using Western blot analysis (see methods). Each data point [closed black circles (+/+; n = 8) or open circles (*sut/sut*; n = 8) represents the level of cortical (A) GluA1, (B) GluA2, (C) GluN1, or (D) GABA$_A$Rα protein following normalization to their respective loading control (i.e., Na$^+$/K$^+$ ATPase levels or total protein) and subsequent normalization to +/+ controls. Bars indicate the mean fold change from control (+/+), which was set to one. Cortical plasma membrane protein expression levels were compared using a two-way ANOVA on log-transformed data.
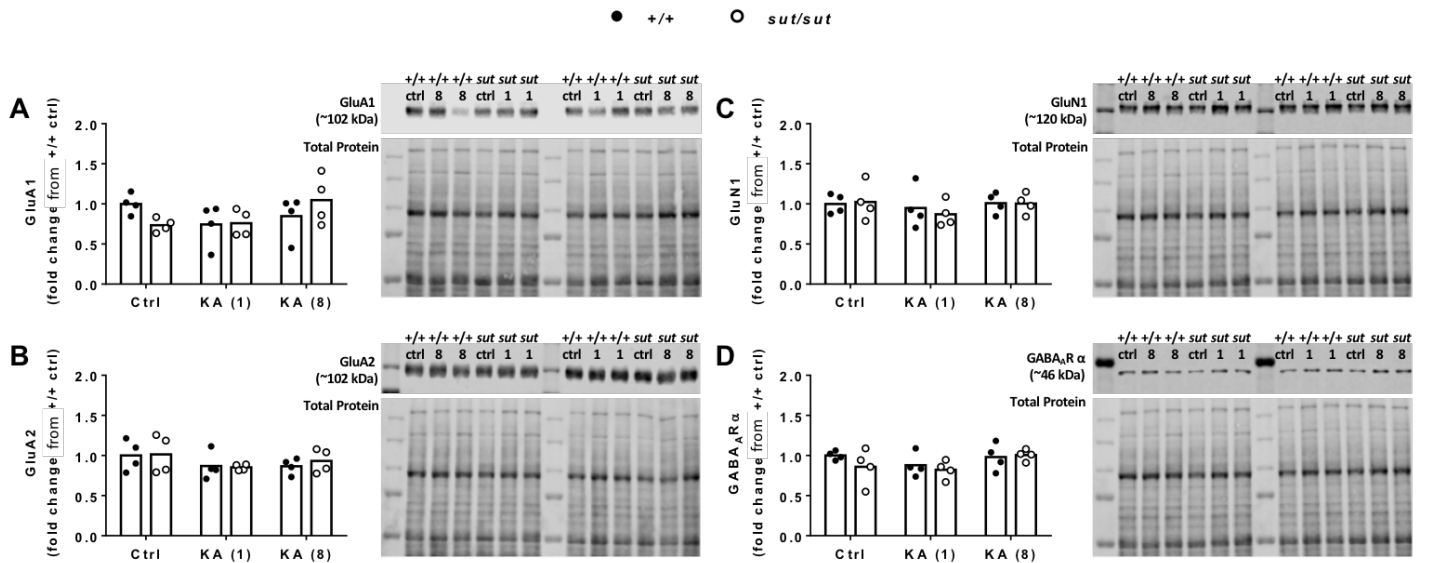
Figure 4.9 Comparison of plasma membrane protein expression in female SLC7A11$^{+/+}$ and SLC7A11$^{sut/sut}$ mice

Plasma membrane protein levels in cortex derived from female *SLC7A11*$^{+/+}$ (+/+) or *SLC7A11*$^{sut/sut}$ (*sut/sut*) littermates naïve to any treatment (ctrl) or mice exhibiting hypo-mobility [KA (1)] or status epilepticus [KA (8)] in the final quartile of the four hour escalating dose paradigm were compared using Western blot analysis (see methods). Each data point [closed black circles (+/+; n = 4) or open circles (*sut/sut*; n = 4) represents the level of cortical (A) GluA1, (B) GluA2, (C) GluN1, or (D) GABA$_A$Rα protein following normalization to their respective loading control (i.e. total protein levels) and subsequent normalization to +/+ controls. Bars indicate the mean fold change from control (+/+), which was set to one. Representative Western blots of +/+ and *sut/sut* cortical plasma membrane proteins are shown beside their respective graphs. Cortical plasma membrane protein expression levels were compared using a two-way ANOVA on log-transformed data.
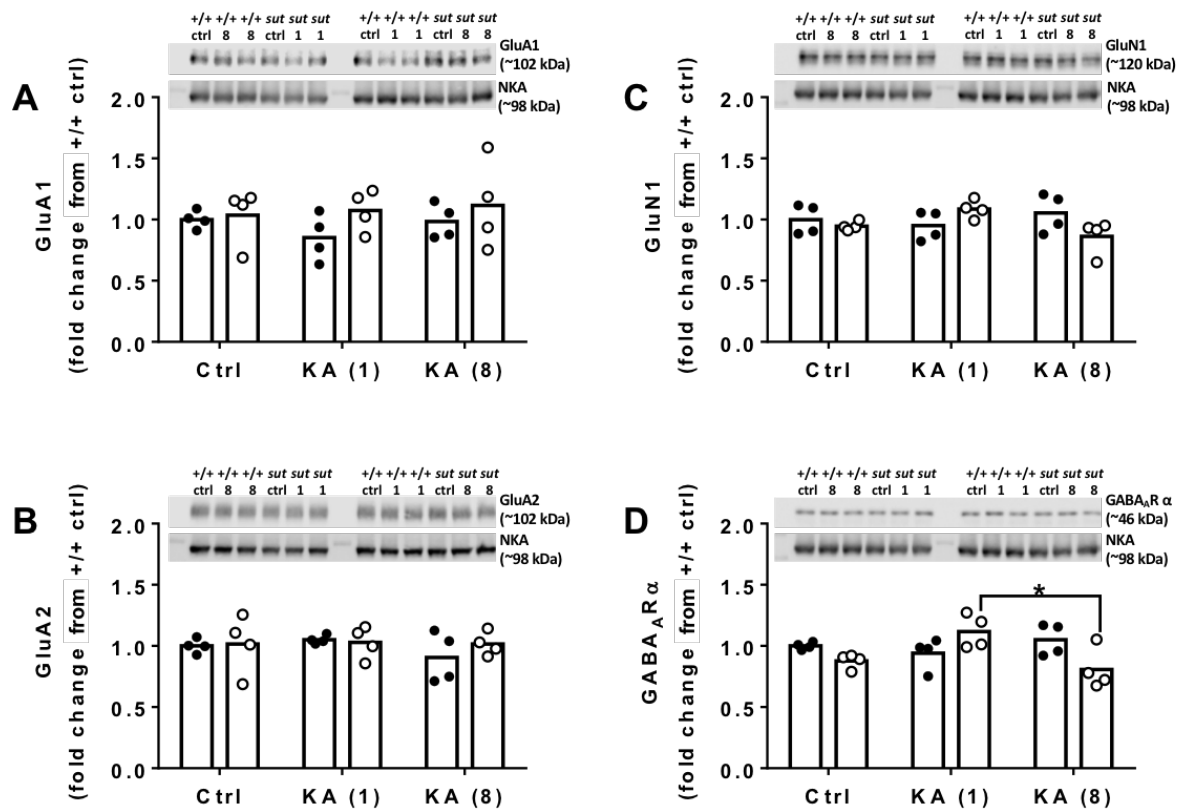
Figure 4.10 Comparison of plasma membrane protein expression in male SLC7A11⁺/⁺ and SLC7A11ˢᵘᵗ/ˢᵘᵗ mice

Plasma membrane protein levels in cortex derived from male *SLC7A11⁺/⁺* (+/+) or *SLC7A11ˢᵘᵗ/ˢᵘᵗ* (*sut/sut*) littermates naïve to any treatment (ctrl) or mice exhibiting hypo-mobility [KA (1)] or status epilepticus [KA (8)] in the final quartile of the four hour escalating dose paradigm were compared using Western blot analysis (see methods). Each data point [closed black circles (+/+; n = 4) or open circles (*sut/sut*; n = 4) represents the level of cortical (A) GluA1, (B) GluA2, (C) GluN1, or (D) GABA$_A$Rα protein following normalization to their respective loading control (i.e., Na⁺/K⁺ ATPase [NKA] levels) and subsequent normalization to +/+ controls. Bars indicate the mean fold change from control (+/+), which was set to one. Representative Western blots of +/+ and *sut/sut* cortical plasma membrane proteins are shown above their respective graphs. Cortical plasma membrane protein expression levels were compared using a two-way ANOVA on log-transformed data. An asterisk (*) represents a significant between group difference ($p < 0.05$).

stratification of this data by sex revealed a similar trend in female $SLC7A11^{+/+}$ as compared to $SLC7A11^{sut/sut}$ sex-matched littermates, who also demonstrated similar levels of GluA1, GluA2, GluN1, and GABA$_A$Rα protein levels (Fig. 4.9; two-way ANOVA with Tukey's multiple comparisons). Interestingly, while glutamate receptor subunits were similar between male $SLC7A11^{+/+}$ and $SLC7A11^{sut/sut}$ sex-matched littermates regardless of treatment (Fig. 4.10A-C), male $SLC7A11^{sut/sut}$ mice that became hypomobile by the end of the four-hour protocol demonstrated elevated GABA$_A$Rα expression levels as compared to male $SLC7A11^{sut/sut}$ mice that entered into status epilepticus (Fig. 4.10D, $p < 0.05$, two-way ANOVA with Tukey's multiple comparisons).

4.5   Discussion

Results presented in Chapter 2 demonstrated that $SLC7A11^{sut/sut}$ mice have a decreased seizure threshold upon administration of an acute dose of PTZ. Despite this, $SLC7A11^{sut/sut}$ mice were less susceptible to PTZ-kindling (Chapter 3), suggesting that Sx$_c^-$ contributes to E/I balance in a context-dependent manner. The present chapter extends these findings by demonstrating that alterations in excitability observed in $SLC7A11^{sut/sut}$ mice were generalizable to acute and elevated KA dosing seizure paradigms.

KA induces excitatory activity by binding to both AMPA receptors as well as its own cognate receptors (Vincent & Mulle 2009). In response to an acute systemic dose of KA, a significantly greater number of female and male $SLC7A11^{sut/sut}$ mice experienced a clonic or convulsive seizure as compared to $SLC7A11^{+/+}$ littermates, indicating that they have a decreased KA-induced seizure threshold. While these results support our initial studies using the GABA$_A$R antagonist PTZ (Chapter 2), they are in

contrast with results reported by De Bundel et al demonstrating that transgenic xCT null

(xCT$^{-/-}$) mice on a C57BL/6 background require a significantly greater dose of KA to

elicit behavioral clonus, and thus have an increased seizure threshold, as compared to

xCT$^{+/+}$ littermate controls (De Bundel et al 2011). Given that both the xCT$^{-/-}$ and

SLC7A11$^{sut/sut}$ mice are xCT null (Chintala et al 2005, De Bundel et al 2011, McCullagh

& Featherstone 2014), the reason for the discrepancy in findings is not immediately

clear. However, it may be accounted for by differences in experimental paradigms. In

De Bundel et al, continuous intravenous infusion of chemoconvulsant resulted in rapid

behavioral seizure onset such that clonic seizures were evoked in xCT$^{+/+}$ and xCT$^{-/-}$

mice by the time 58.1 or 75.6 mg/kg KA was infused, respectively (De Bundel et al

2011). However, it is difficult to attribute behavioral activity to a given dose when the

dose is continuously changing, and it is possible that 58 mg/kg KA could elicit clonus in

both xCT$^{+/+}$ and xCT$^{-/-}$ mice, but xCT$^{-/-}$ mice have an increase in clonic seizure latency.

While the clonic latencies were not calculated in De Bundel et al, keeping the weight of

an animal constant, the rapid infusion rate (150 μl/min) utilized in this protocol would

result in a dose of 58.1 mg/kg by $\approx$77 sec versus a dose of 75.6 mg/kg by $\approx$100

seconds, which were the doses that evoked clonic seizures in xCT$^{+/+}$ or xCT$^{-/-}$ mice,

respectively. Whether this change represents a significant difference in latency to

clonus (77 versus 100 sec) is uncertain. Despite the discrepancy between the De

Bundel et al study and our own, the present findings in this chapter parallel the results

seen using the GABA$_A$R antagonist PTZ (Chapter 2), and provide further evidence that

SLC7A11$^{sut/sut}$ mice have a decreased acute seizure threshold.

Interestingly, repeated administration of KA in the elevated dosing paradigm revealed the opposite behavioral results; regardless of sex, the majority of $SLC7A11^{sut/sut}$ mice became profoundly hypomobile as compared to $SLC7A11^{+/+}$ littermate controls in the final quartile of the dosing protocol. Given the acute hyper-excitability observed in the $SLC7A11^{sut/sut}$ mice, it is tempting to speculate that the hypomobility seen in the latter portion of the escalating dose paradigm is simply due to excessive excitation and a resultant comatose post-ictal state. However, this does not appear to be the case, as this type of hypo-activity is usually associated with death and the $SLC7A11^{sut/sut}$ mice exhibiting hypomobility in the final quartile fully recover – with diazepam administration ostensibly superfluous in some mice (S. Sears personal observations). In fact, $SLC7A11^{sut/sut}$ mice have significantly decreased mortality overall as compared to $SLC7A11^{+/+}$ littermate controls in this paradigm.

In the final quartile of the elevated dosing paradigm, $SLC7A11^{sut/sut}$ mice exhibited a significantly decreased incidence of status epilepticus as compared to $SLC7A11^{+/+}$ mice. KA-induced behavioral convulsions are typically associated with structural alterations, as excessive depolarization can result in cell death (Olney et al 1974), and cell populations in the CA3 sub-region of the hippocampal formation have been demonstrated to be particularly vulnerable to KA-induced degeneration (Nadler et al 1980). However, mouse strain differences with respect to KA-induced degeneration do exist (Schauwecker 2003). As such, a subset of mice that attained a seizure score $\geq$ 6 were examined for overt hippocampal cellular degeneration. Interestingly, degeneration was not pervasive in every mouse examined, though of the mice that did exhibit cell loss, the hippocampal sub-region affected was strikingly genotype specific

with the CA1 and CA3 region exhibiting neural degeneration in *SLC7A11*$^{+/+}$ and

SLC7A11$^{sut/sut}$ mice, respectively. Although xCT is expressed throughout the

hippocampal formation, Ottested-Hansen and colleagues recently demonstrated that

xCT protein levels are greatest in the *stratum lacunosum moleculare* (SLM) and the

molecular layer of the dentate gyrus (DG) (Ottestad-Hansen et al 2018). Interestingly,

afferent projections from the entorhinal cortex (EC) terminate in both of these layers

(Amaral et al 2007). This gives rise to the intriguing possibility that afferent EC

projections to the SLM, together with Sx$_c^-$ signaling, promotes neural degeneration in

the CA1 hippocampal sub-region, and that lack of Sx$_c^-$ thwarts this degeneration.

Although the DG molecular layer is relatively cell-free – containing granule cell dendrites

and inhibitory basket cells (Amaral et al 2007) – it is possible that afferent EC

projections, together with Sx$_c^-$ signaling, promotes basket cell-mediated inhibitory drive

onto granule cells, thus thwarting over-activation of their CA3 synaptic targets and

preventing KA-mediated CA3 cell death. Conversely, lack of Sx$_c^-$ signaling in the

molecular layer of *SLC7A11*$^{sut/sut}$ mice could render DG granule cells hyper-active, thus

underlying the enhanced neural degeneration of their CA3 synaptic partners.

Regardless of the underlying mechanism, the sub-region specific differences in

SLC7A11$^{+/+}$ and *SLC7A11*$^{sut/sut}$ mice neural degeneration elicited by an elevated dose

of KA suggest that Sx$_c^-$ signaling regulates hippocampal circuitry. Nevertheless,

hippocampal sub-region notwithstanding, the incidence of KA-induced cellular

degeneration was similar in either genotype. Taken together, although not completely

comparable to the chronic 21-day PTZ-kindling paradigm (Chapter 3), the behavioral

hypo-excitability observed in response to an elevated KA dosing protocol in the present

chapter is qualitatively similar, suggesting that loss of Sx_c^- increases seizure threshold in response to repeated/chronic chemoconvulsant administration.

The increased synaptic drive elicited by repeated chemoconvulsant administration could plausibly engage homeostatic synaptic scaling mechanisms to allow stabilization of neuronal firing rate (Christie & Jahr 2008, Turrigiano 2008, Turrigiano et al 1998). This process is largely accomplished through the addition and subtraction, respectively, of ionotropic AMPA (O'Brien et al 1998, Turrigiano et al 1998, Wierenga et al 2005), NMDA (Mu et al 2003, Rao & Craig 1997, Watt et al 2000) or $GABA_A$ (Kilman et al 2002, Stellwagen et al 2005) receptors at the postsynaptic membrane. As such, we compared glutamate and $GABA_A$ receptor levels in cortical plasma membrane of naïve or KA-treated *SLC7A11*^{+/+} and *SLC7A11*[sut/sut] mice. Out of all of the receptors investigated, the only difference observed was in $GABA_AR\alpha$ levels: male, but not female, *SLC7A11*[sut/sut] mice that attained a MMSS = 1 (hypomobility) in the final quartile of the escalated dosing paradigm had increased $GABA_AR\alpha$ levels as compared to sex-matched *SLC7A11*[sut/sut] mice that reached a MMSS = 8 (status epilepticus). However, neither KA-treated group significantly differed from naïve *SLC7A11*[sut/sut] mice nor from naïve or KA-treated *SLC7A11*^{+/+} sex-matched controls. These results give rise to the intriguing possibility that KA-administration resulting in a slight increase in $GABA_AR\alpha$ expression in the *SLC7A11*[sut/sut] mice confers diminished excitatory seizure activity – a behavioral state evident in the majority of *SLC7A11*[sut/sut] mice – whereas a slight decrease in $GABA_AR\alpha$ expression does the opposite. However, these findings do not rule out the possibility that the changes detected in plasma membrane are driven by alterations in extrasynaptic (Brickley & Mody 2012) versus

synaptic GABA$_A$Rs, and it will be important to determine whether GABA$_A$R-dependent inhibitory postsynaptic currents (IPSCs) are functionally enhanced in the KA-treated male *SLC7A11$^{sut/sut}$* mice with a fourth quartile MMSS = 1. Nevertheless, it is plausible that the fourth quartile hypo-excitability observed in *SLC7A11$^{sut/sut}$* male mice is driven by an increase in plasma membrane GABA$_A$Rα expression. The mechanism conferring behavioral hypo-excitability in female *SLC7A11$^{sut/sut}$* mice requires further investigation. Finally, the idea that this phenotype (behavioral hypo-excitability) is sex-independent yet could be driven by sex-dependent differences (altered GABA$_A$R expression in males versus unknown mechanism(s) in females) is perhaps unsurprising given results described in Chapter 2 of this dissertation, whereby a sex-independent hyperexcitable phenotype occurred in association with sex-dependent cellular morphological changes.

Taken together, our results demonstrate that *SLC7A11$^{sut/sut}$* mice have a decreased convulsive seizure threshold in response to acute KA administration whereas an elevated dosing paradigm using the same chemoconvulsant results in *SLC7A11$^{sut/sut}$* behavioral hypoactivity as compared to *SLC7A1$^{+/+}$* littermate controls. These results suggest that Sx$_c$$^-$ contributes to E/I balance in a context-dependent manner. Moreover, KA-induced behavioral hypo-excitability in male *SLC7A11$^{sut/sut}$* mice occurs in association with increased GABA$_A$Rα levels, suggesting that a change in GABAergic function could underlie this phenotype. Whether this alteration in GABA$_A$Rα protein levels confer a functional change in males, and the exact mechanism by which loss of Sx$_c$$^-$ signaling confers fourth quarter behavioral hypo-excitability in female mice, requires further experimentation.

Chapter 5: Discussion, conclusions, and future directions

5.1   Main findings

The goal of this dissertation was to elucidate whether and how System x_c^- (Sx_c^-)

signaling contributes to the excitatory/inhibitory (E/I) balance in brain. The main findings

of this dissertation are that (1) loss of Sx_c^- in *SLC7A11$^{sut/sut}$* mice renders them hyper-

excitable in response to acute administration of two pharmacologically distinct

chemoconvulsants, PTZ or KA. Furthermore, baseline hyper-excitability in

SLC7A11$^{sut/sut}$ mice occurs in association with morphological alterations at the gross,

cellular, and sub-cellular level, as well as with alterations in plasma membrane

glutamate receptor subunit expression and brain redox status, any or all of which could

underlie the behavioral responses elucidated. (2) Despite acute hyper-excitability in

response to either PTZ or KA, chronic/repeated dosing with these same

chemoconvulsants elicits a polar opposite response – behavioral hypo-excitability – in

SLC7A11$^{sut/sut}$ mice as compared to *SLC7A11$^{+/+}$* littermate controls.

5.2   Acute hyper-excitability in Sx_c^- null mice occurs in association with morphological, redox, and plasma membrane protein alterations

Findings presented in this dissertation demonstrate a sex-independent hyper-

excitability phenotype uncovered in *SLC7A11$^{sut/sut}$* mice via administration of two

pharmacologically distinct chemoconvulsants, PTZ or KA. *SLC7A11$^{sut/sut}$* mice are

viable, fertile, do not display spontaneous seizure activity, and, other than a subtle grey

coat color, particularly apparent in juvenile mice three to four weeks of age, are

indistinguishable from their C3H/HeSnJ *SLC7A11$^{+/+}$* littermates [personal observations

and (Chintala et al 2005, Lane 1988)]. Despite their overt similarities to *SLC7A11$^{+/+}$*

controls, the behavioral hyper-excitability in *SLC7A11^{sut/sut}* mice upon acute chemoconvulsant administration is indicative of a brain E/I imbalance.

Previous characterization of male xCT transgenic null mice on a C57BL/6 background revealed increased spontaneous and evoked miniature excitatory postsynaptic currents (mEPSCs) and synaptic AMPA receptor expression levels in hippocampal CA1 (Williams & Featherstone 2014). These findings, if true in the *SLC7A11^{sut/sut}* mice, could explain the increased susceptibility to chemoconvulsant-induced acute seizure activity (Croll et al 1999, Greenwood et al 2009). However, neither male (Chapter 3, Fig. 3.6) nor female (Supplementary Fig. S4) *SLC7A11^{sut/sut}* mice have increased levels of plasma membrane glutamate receptors. In fact, the AMPA receptor subunit GluA1 is *decreased* in cortical plasma membrane of male (Chapter 3, Fig. 3.6) and hippocampal plasma membrane of female (Supplementary Fig. S4) *SLC7A11^{sut/sut}* mice as compared to *SLC7A11^{+/+}* sex-matched littermate controls. However, our plasma membrane measurements capture receptors of both synaptic and extrasynaptic origin, as well as receptors in all hippocampal and cortical sub-regions. Thus, in order to determine if post-synaptic membranes are strengthened in *SLC7A11^{sut/sut}* mice, dendritic spine head width – which correlates with glutamate receptor abundance – was measured in cortical layer V pyramidal cells. In agreement with findings demonstrating increased synaptic strength in male xCT transgenic null mice (Williams & Featherstone 2014), spine head widths in male *SLC7A11^{sut/sut}* mice are increased as compared to *SLC7A11^{+/+}* sex-matched littermate controls (Chapter 2, Fig. 2.7). Thus, despite a reduction in total cortical plasma membrane GluA1 levels in *SLC7A11^{sut/sut}* male mice, synaptic strength – as measured by spine head width – was

enhanced, which could plausibly underlie the acute hyper-excitability in *SLC7A11*^{sut/sut}

males. Surprisingly, results in female mice demonstrated the opposite: spine head

widths of *SLC7A11*^{sut/sut} mice were significantly decreased as compared to *SLC7A11*^{+/+}

sex-matched littermate controls (Chapter 2, Fig. 2.7). However, these findings do not

rule out the possibility of changes to hippocampal synapses, which, unfortunately, were

precluded from our analysis due to the complexity and density of Golgi-Cox stained

neurons in the hippocampal formation. To further understand how these morphological

changes translate functionally – and to explore hippocampal synapses – an instructive

next step would be to record (miniature) excitatory postsynaptic potentials [(m)EPSPs])

from whole-cell patch-clamped neurons in order to precisely and quantitatively detect

changes in quantal content and/or postsynaptic glutamate receptors that could underlie

a shift in E/I balance towards excitation.

 To explore further mechanisms underlying hyper-excitability in *SLC7A11*^{sut/sut}

mice, two additional lines of inquiry, cellular morphology and redox balance, were

investigated in this dissertation. With respect to morphology, the work presented herein

uncovered that (1) sex-differences in cellular morphology exist in *SLC7A11*^{+/+} mice on

the C3H/HeSnJ background and (2) within-sex morphological alterations were

uncovered that could plausibly contribute to genotype-dependent differences in E/I

balance. With regards to the first finding, our results indicate that soma size is

significantly increased in female *SLC7A11*^{+/+} as compared to male *SLC7A11*^{+/+} mice on

the C3H/HeSnJ background (Chapter 2, Fig. 2.5). To our knowledge, this is the first

account of sex-differences in cortical layer V neuronal soma size reported in mouse.

Functionally, it is unclear why a sex-difference in soma size exists. However, loss of

Sx$_c^-$ lends credibility to one possibility: sex morphological differences exist to prevent functional differences (De Vries 2004). This idea seems plausible given that loss of Sx$_c^-$ in female *SLC7A11^sut/sut* mice leads to a reduction in soma area – which itself is associated with decreased inhibition (Hsu et al 2012, Ye et al 2015) – and occurs in association with increased behavioral excitability (decreased acute seizure threshold). As such, an increase in soma area in *SLC7A11^+/+* females as compared to *SLC7A11^+/+* males may be important in maintaining an elevated acute seizure threshold in female *SLC7A11^+/+* mice. Of note, a slight decrease in *SLC7A11^+/+* male versus female acute seizure threshold was uncovered in Chapter 2 (Fig. 2.10), and as such, male mice required a lower acute PTZ (or KA) dose to uncover an E/I imbalance in *SLC7A11^sut/sut* mice. Whether or not soma size is integrally linked to maintenance of E/I balance in females requires further investigation, including characterizing the abundance and strength of perisomatic inhibitory synapses using immunohistochemistry and electrophysiology, respectively.

If soma size correlates with E/I balance in female *SLC7A11^+/+* and *SLC7A11^sut/sut* mice, does the same hold true for males? Our results indicate that soma size is similar in male *SLC7A11^+/+* and *SLC7A11^sut/sut* sex-matched littermate controls. However, our results demonstrate that dendritic complexity is significantly decreased in *SLC7A11^+/+* male as compared to female mice on the C3H/HeSnJ background (Chapter 2, Fig. 2.3). Once again, to our knowledge, this is the first report of sex-differences in cortical layer V dendritic complexity in mouse. Furthermore, loss of Sx$_c^-$ in male mice increases dendritic complexity as compared to *SLC7A11^+/+* sex-matched littermates, such that their complexity is indistinguishable from female mice (Chapter 2, Fig. 2.3). Thus –

similar to soma size – these findings raise the intriguing possibility that morphological

sex-differences in dendritic complexity exist to maintain functional E/I balance. Given

that enhanced dendritic complexity is associated with increased excitability (Klenowski

et al 2016, Mainen & Sejnowski 1996), it is tempting to speculate that an increase in

cortical dendritic complexity underlies the decreased seizure threshold in $SLC7A11^{sut/sut}$

male mice. Whether this morphological change is associated with enhanced neuronal

excitability, such as increases in EPSC frequency or repetitive spikes, will require

electrophysiological confirmation.

Given that Sx_c^--mediated cystine import provides cells with the rate-limiting

substrate (cysteine) for synthesis of the thiol antioxidant GSH, we also explored whether

alterations in levels of reduced and oxidized glutathione (GSH and GSSG) or cysteine

(cysteine and cystine) could account for an E/I imbalance in $SLC7A11^{sut/sut}$ mice.

Interestingly, the brains of $SLC7A11^{sut/sut}$ females (Supplementary Fig. S2), but not

males (Chapter 3, Fig. 3.5), are under oxidative stress as demonstrated by elevated

cortical GSSG and hippocampal cystine levels compared to sex-matched $SLC7A11^{+/+}$

littermate controls. Given that increased levels of oxidants can decrease seizure

threshold (Liang & Patel 2004), the cysteine prodrug N-acetylcysteine (NAC) was

administered to female $SLC7A11^{sut/sut}$ mice and seizure threshold determined

(Supplementary Fig. S3). Our results indicate that NAC administration over eight days

does not increase $SLC7A11^{sut/sut}$ seizure threshold as compared to vehicle-administered

$SLC7A11^{sut/sut}$ littermate controls, suggesting that the decreased acute seizure threshold

in female $SLC7A11^{sut/sut}$ mice is not due to a redox imbalance. A potential caveat to this

study includes the length of NAC administration, which may not have been extensive

enough to restore brain redox status. However, oral supplementation of NAC for seven

days at the same dose used by our laboratory has been demonstrated to elevate brain

thiol content in the excitatory amino acid transporter 3 (EAAC1) null mouse (Berman et

al 2011). Conversely, in the case of the *SLC7A11^{sut/sut}* mice, a balanced redox status

may be required *throughout* development in order to properly establish E/I balance,

especially if redox state influences other downstream effectors that ultimately confer E/I

balance. One plausible example of redox status affecting E/I balance indirectly is

through soma size: during periods of decreased protein synthesis, net loss of cellular

protein results in somatic atrophy (Franklin & Johnson 1998). Interestingly, under

periods of oxidative stress, shunting of cysteine from its role as a macromolecular

building block to its incorporation into antioxidants, including GSH, is upregulated in

order to confer cellular protection (Ratan et al 1994). As such, it is conceivable that a

redox imbalance in female *SLC7A11^{sut/sut}* mice facilitates cysteine shunting from protein

synthesis to GSH synthesis, resulting in a reduction in soma size – and an associated

decrease in inhibitory tone – and ultimately leading to a decrease in seizure threshold. A

logical future direction is to administer NAC to female *SLC7A11^{sut/sut}* mice throughout

development, including *in utero* via dietary supplementation to the dam, to determine if

this rescues cell body size and/or seizure threshold to that of *SLC7A11^{+/+}* sex-matched

littermate controls.

5.3   Delayed hypo-excitability in Sx$_c^-$ null mice

Despite hyper-excitability elicited in response to an acute dose of

chemoconvulsant, *SLC7A11^{sut/sut}* mice show behavioral signs of hypoexcitability upon

chronic administration of PTZ (Chapter 3, Fig. 3.1) or repeated administration of KA (Chapter 4, Fig. 4.3). Specifically, repeated daily injections of an initially sub-convulsant dose of PTZ ultimately leads to a permanent decrease in the threshold of excitability in $SLC7A11^{+/+}$ mice (i.e., mice become kindled), whereas the percent $SLC7A11^{sut/sut}$ mice that kindle over the same 21 days is significantly lower (Chapter 3, Fig. 3.1). Similarly, $SLC7A11^{+/+}$ mice attain status epilepticus (seizure score = 8) after repeated dosing with KA, whereas $SLC7A11^{sut/sut}$ mice become hypomobile (seizure score = 1) (Chapter 4, Fig. 4.3). These data suggest that Sx_c^- activity modulates synaptic strength *in vivo* in a context-dependent manner.

In Chapter 3, PTZ-kindling was explored in male mice only, as the low seizure-threshold in $SLC7A11^{sut/sut}$ females precluded our ability to carry out a kindling protocol (data not shown). Post-kindling, our results indicate that mossy fiber sprouting and cellular degeneration are unlikely to contribute to the decreased incidence of PTZ-kindling in $SLC7A11^{sut/sut}$ mice, as neither reactive synaptogenesis nor cell loss were observed in mice of either genotype. Rather, it was postulated in Chapter 3 that decreased PTZ-kindling in $SLC7A11^{sut/sut}$ mice may be a result of hypo-glutamatergic signaling given that glutamate levels (McCullagh & Featherstone 2014) and basal plasma membrane expression levels of the glutamate receptor subunit GluA1 (Chapter 3, Fig. 3.6) are diminished in male $SLC7A11^{sut/sut}$ mice. However, morphological parameters presented in Chapter 2 indicate that, despite decreased plasma membrane GluA1 levels, cortical synapses may indeed be strengthened in male mice given their increased dendritic spine head widths (Chapter 2 Fig. 2.7). These contradictory results could be explained by the fact that plasma membrane protein expression levels are not

indicative of synaptic protein levels as they incorporate receptors expressed in both synaptic and extrasynaptic regions. As such, it will be necessary to perform *ex vivo* electrophysiological brain slice recordings to directly measure synaptic strength in *SLC7A11*^{sut/sut} mice.

Chronic excitation elicited by PTZ-kindling (Kapur et al 1989a, Kapur et al 1989b, Schröder et al 1993) or status epilepticus (Friedman et al 1994, Goodkin et al 2005, Grooms et al 2000, Naylor et al 2013) is associated with alterations in neurotransmitter receptor mRNA or protein expression levels, with increases in glutamate receptor subunits GluN1 and GluA1 (Naylor et al 2013, Schröder et al 1993) or decreases in GluA2 (Grooms et al 2000) and GABAergic receptors (Goodkin et al 2005, Kapur et al 1989a, Kapur et al 1989b) demonstrated. In order to determine whether alterations in repeated/chronic chemoconvulsant administration provoked changes in receptor expression levels, we assessed levels of glutamate (GluA1, GluA2, and GluN1) and GABA (GABA$_A$Rα) receptor subunits in plasma membrane following repeated KA administration, chosen because the paradigm is complete after 240 min and likely provides qualitatively the same data as the 21-day PTZ-kindling paradigm. While no changes in glutamate or GABA$_A$ receptor subunits between female or male *SLC7A11*^{+/+} or *SLC7A11*^{sut/sut} mice were detected, we did find that the behavioral response of male *SLC7A11*^{sut/sut} mice within the final quartile of the dosing paradigm correlated with GABA$_A$Rα expression levels: *SLC7A11*^{sut/sut} males that became hypomobile had significantly increased plasma membrane GABA$_A$Rα protein levels as compared to *SLC7A11*^{sut/sut} males that entered into status epilepticus (Chapter 4, Fig. 4.10). Whether increases or decreases in GABA$_A$Rα expression underlies male *SLC7A11*^{sut/sut}

behavioral hypomobility or status epilepticus, respectively, requires further experimentation. Moreover, this change was not detected in female *SLC7A11*[sut/sut] mice (Chapter 4, Fig. 4.9), and the mechanism underlying their behavioral hypo-excitability in the face of repeated KA administration remains unexplained.

The within-genotype change in GABA$_A$Rα expression in male *SLC7A11*[sut/sut] mice notwithstanding, receptor expression levels are overwhelmingly similar in *SLC7A11*^{+/+} and *SLC7A11*[sut/sut] mice following the repeated KA dosing paradigm. However, just as with basal plasma membrane protein expression levels discussed earlier, a caveat to this study is plasma membrane measurements do not exclusively measure synaptic receptors. Thus, measuring synaptic activity via electrophysiology or measuring synaptic protein expression via immunohistochemistry will be important next step(s) in determining whether alterations in synaptic protein levels account for *SLC7A11*[sut/sut] behavioral hypo-excitability in the repeated/chronic chemoconvulsant dosing paradigms.

5.4   Working model(s) to explain the dichotomy

Synaptic scaling: Neurons detect fluctuations in extracellular glutamate levels and/or in synaptic drive and autonomously adjust the strength of their synapses up or down to stabilize firing via a process known as homeostatic synaptic scaling (Christie & Jahr 2008, Turrigiano 2008, Turrigiano et al 1998). This is largely accomplished through the addition and subtraction, respectively, of ionotropic AMPA receptors at the postsynaptic membrane (Turrigiano et al 1998, Wierenga et al 2005), although this can only occur within a modifiable range (Rioult-Pedotti et al 2007, Rioult-Pedotti et al

2000). For example, scaling-up of AMPA receptors to a "ceiling" results in an occlusion

of processes dependent upon postsynaptic AMPA receptor membrane insertion, such

as long-term potentiation (LTP) (Li et al 2016). Interestingly, hippocampal LTP is

diminished in *SLC7A11*[sut/sut] mice and genetically engineered xCT nulls show deficits in

hippocampal-dependent spatial learning – a process dependent upon postsynaptic

AMPA receptor membrane insertion (De Bundel et al 2011, Li et al 2012). Moreover,

both kindling-induced plasticity (Cain 1989, Goddard & Douglas 1975) and status

epilepticus (Naylor et al 2013, Rice & DeLorenzo 1998, Rice et al 1998) share common

mechanisms with LTP, including the insertion of postsynaptic glutamate receptors

(Naylor et al 2013), a long-lasting increase in response to a constant stimulus (Cain

1989), and the dependency of this response on NMDAR activation (Rice & DeLorenzo

1998). Moreover, status epilepticus, and its subsequent epileptic sensitization, impaired

performance of rats in the Morris water maze, suggesting that status epilepticus-

induced neuronal sensitization and learning share common mechanisms (Rice et al

1998).

Given that enhanced expression of synaptic AMPA receptors has been

demonstrated in the hippocampus of transgenic xCT null mice (Williams & Featherstone

2014), and that *SLC7A11*[sut/sut] males (but not females) have increased dendritic spine

head widths as compared to *SLC7A11*^{+/+} littermate controls (Chapter 2, Fig. 2.7), it is

tempting to speculate that male mice null for Sx_c^- may have AMPA receptors scaled-up

to the apex of their modifiable range. This endogenous "scaling-up" in male

SLC7A11[sut/sut] mice, perhaps a result of diminished ambient extracellular glutamate

levels (De Bundel et al 2011, Massie et al 2011b, McCullagh & Featherstone 2014),

could explain their decreased acute seizure threshold. Conversely, repeated/chronic chemoconvulsant administration in a system already at the "ceiling" of its modifiable range could cause homeostatic scaling-down of glutamate receptors, explaining the reduced excitability of *SLC7A11*$^{sut/sut}$ mice in the PTZ-kindling and repeated KA-dosing paradigm. Given that enhanced dendritic spine head width was observed in cortical neurons derived from male – but not female – *SLC7A11*$^{sut/sut}$ mice, if the aforementioned mechanisms are driving the dichotomous excitability in *SLC7A11*$^{sut/sut}$ mice, they may be sex-dependent and present exclusively in males. In line with this, decreased ambient glutamate levels – that could plausibly evoke an endogenous "scaling-up" of glutamate receptors – have been reported in male (De Bundel et al 2011, Massie et al 2011b, McCullagh & Featherstone 2014) but not female (Borra et al 2014) Sx$_c^-$ null mice. However, it should be noted that glutamate measurements were carried out in the striatum in *SLC7A11*$^{sut/sut}$ female mice (Borra et al 2014), and our dendritic spine head measurements were limited to the cortex (Chapter 2, Fig. 2.7). As such, it remains plausible that reduced glutamate levels or increased spine head width exist in other brain regions in female Sx$_c^-$ null mice, especially given that Sx$_c^-$ appears to contribute to ambient extracellular glutamate levels in a brain-region dependent manner (McCullagh & Featherstone 2014).

Redox balance: Alternatively, the dichotomous changes in excitability evoked by acute or repeated chemoconvulsant stimulus could be a result of a redox imbalance in *SLC7A11*$^{sut/sut}$ mice. Glutamate transporters and the NMDA receptor possess redox-sensing properties that regulate their activity (Aizenman et al 1989, Köhr et al 1994, Sullivan et al 1994, Trotti et al 1997). Moreover, manganese superoxide dismutase

(SOD2$^{+/-}$) mice with chronic mitochondrial oxidative stress have a decreased KA-induced seizure threshold (Liang & Patel 2004). Given that female (but not male) *SLC7A11$^{sut/sut}$* brains have elevated levels of oxidized GSH and cysteine, it is tempting to speculate that their reduced acute seizure threshold is a result of a redox imbalance.

Furthermore, LTP is diminished in GSH-deficient rodents (Almaguer-Melian et al 2000, Robillard et al 2011), and normalizing GSH levels can restore LTP (Robillard et al 2011). These findings stress the importance of redox balance in the regulation of synaptic plasticity. Given the mechanistic similarities between LTP and the sustained excitation elicited by chemoconvulsants *in vivo* (Cain 1989, Goddard & Douglas 1975, Naylor et al 2013, Rice & DeLorenzo 1998, Rice et al 1998), it is plausible that a redox imbalance could thwart the progression of PTZ-kindling or KA-induced status epilepticus in *SLC7A11$^{sut/sut}$* mice, thus explaining their hypo-excitability in these models. As a redox imbalance was observed in female (Supplementary Fig. S2) – but not male (Chapter 3, Fig. 3.5) – *SLC7A11$^{sut/sut}$* mice, if the aforementioned mechanisms are driving the dichotomous excitability in *SLC7A11$^{sut/sut}$* mice, they may be sex-dependent and present exclusively in females.

5.5   Astrocytic maintenance of E/I balance

As discussed in Chapter 1, there is now indisputable evidence, stemming from both transcriptome and immunohistochemical analyses, that astrocytes are the primary cell types expressing Sx$_c^-$ in the mature brain *in vivo* (Ottestad-Hansen et al 2018, Pow 2001, Zhang et al 2014). As the most numerous glial subtype in the CNS, astrocytes perform a number of well-characterized homeostatic support functions, including

maintenance of perivascular homeostasis and blood brain barrier integrity (Alvarez et al 2013, Mathiisen et al 2010), K^+ buffering (Orkand et al 1966), supplying neurons with energy substrates (Pellerin et al 1998) and neurotransmitter precursors (Bak et al 2006), and glutamate uptake via EAATs [reviewed in (Danbolt 2001)]. With respect to the latter, astrocytic EAAT1 or EAAT2 knock-out mice demonstrate prolonged seizure duration in an amygdala kindling model (Watanabe et al 1999) or spontaneous electroencephalographic seizures (Tanaka et al 1997), respectively, highlighting the potent ways in which astrocytes regulate synaptic transmission. Additionally, more recent evidence implicates astrocytes in the positive and negative regulation of CNS synaptogenesis through their release of soluble factors such as thrombospondins (TSPs)-1 and -2 (Christopherson et al 2005), Hevin and SPARC (Kucukdereli et al 2011), and glypicans 4 and 6 (Allen et al 2012). While the aforementioned functions render astrocytes capable of modulating synaptic transmission indirectly, astrocytes also play an active role at the synapse by both responding to (Ding et al 2013, Murphy-Royal et al 2015) and releasing (Allen et al 2012, Guthrie et al 1999, Malarkey & Parpura 2008, Schell et al 1995, Schmitt et al 2012) neurotransmitters. Moreover, astrocytes are capable of modulating both Hebbian and homeostatic synaptic plasticity through their release of the NMDA receptor co-agonist, D-serine (Henneberger et al 2010) and the cytokine TNF-α (Stellwagen & Malenka 2006), respectively.

In light of the multitude of ways in which astrocytes participate in CNS activity, the findings presented in this dissertation support a growing theme for astrocytic transporters – including Sx$_c^-$ – in maintenance of E/I balance. Given that elevated KA dosing induced hippocampal neural degeneration in a sub-region dependent manner in

SLC7A11^{sut/sut} and *SLC7A11^{+/+}* littermate controls, our results also implicate Sx$_c$⁻ signaling in maintenance of hippocampal circuitry (Figure 4.7). Nevertheless, it is important to reiterate that the *SLC7A11^{sut/sut}* mice used in this study harbor a global natural null mutation in the *SLC7A11* gene. Given that Sx$_c$⁻ is predominantly astrocytic it is tempting to speculate that the results herein are a result of astrocytic Sx$_c$⁻ signaling. However, the cell type specificity of the observations reported in this dissertation will be necessary to confirm using an astrocyte conditional *SLC7A11* null mouse.

5.6   Future directions

While the results presented in this dissertation demonstrate that Sx$_c$⁻ signaling regulates E/I balance in a context dependent manner, several future directions remain. Clearly, the dichotomy that was uncovered – that *SLC7A11^{sut/sut}* mice are hyper-excitable or hypo-excitable depending on the chemoconvulsant dosing paradigm – is an interesting finding that warrants further investigation. Electrophysiological brain slice recordings from naïve mice, as well as from mice exposed to the repeated/chronic chemoconvulsant dosing paradigms described herein, should be made in order to understand physiological parameters – including both inhibitory and excitatory post-synaptic currents – driving neuronal activity that were potentially missed by our plasma membrane protein analysis. Electrophysiological slice recordings will also be informative to understand how the observed morphological alterations affect cell firing capacity. Furthermore, although our results indicate that NAC supplementation in female *SLC7A11^{sut/sut}* mice – whose brains are under oxidative stress – does not increase their acute PTZ seizure threshold, a future direction includes supplementation with NAC

throughout their lives in order to thwart changes that might occur early in development that confer an E/I imbalance. Additionally, developmental NAC supplementation, as well as its continued supplementation throughout the repeated/chronic dosing paradigms, would be an interesting study to pursue in both females and males in order to determine if hypo-excitability observed therein is a result of oxidative stress. Finally, as mentioned above, in order to confirm the cell type specificity of the findings presented in this dissertation, it would be necessary to confirm our findings using an astrocyte conditional *SLC7A11* null mouse.

5.7   Significance

The purpose of this dissertation research was to investigate whether and how Sx_c^- signaling contributes to E/I balance *in vivo*. This line of inquiry was of interest given that an E/I imbalance is implicated in numerous neurological disorders (Gao & Penzes 2015, Nelson & Valakh 2015) and disease states (Foerster et al 2013, Fritschy 2008, Lai et al 2014, Ren et al 2018, Snyder et al 2005). The findings presented herein that loss of Sx_c^- thwarts the progression of excitability upon repeated/chronic chemoconvulsant application, including in a model of epileptogenesis, suggests that inhibition of Sx_c^- signaling may be a therapeutic option in individuals suffering from an E/I imbalance, such as those prone to develop epilepsy as a result of traumatic brain injury or glioblastoma. However, these results should be interpreted with caution given that loss of Sx_c^- also results in acute hyper-excitability. Thus, whether the acute hyper-excitability phenotype uncovered in *SLC7A11$^{sut/sut}$* mice is a result of a developmental change or whether acute pharmacological inhibition of Sx_c^- elicits a similar acute hyper-

excitability needs to be determined prior to consideration of Sx_c^- targeting as a

therapeutic option for individuals suffering an E/I imbalance.

Appendix

Supplementary Figures
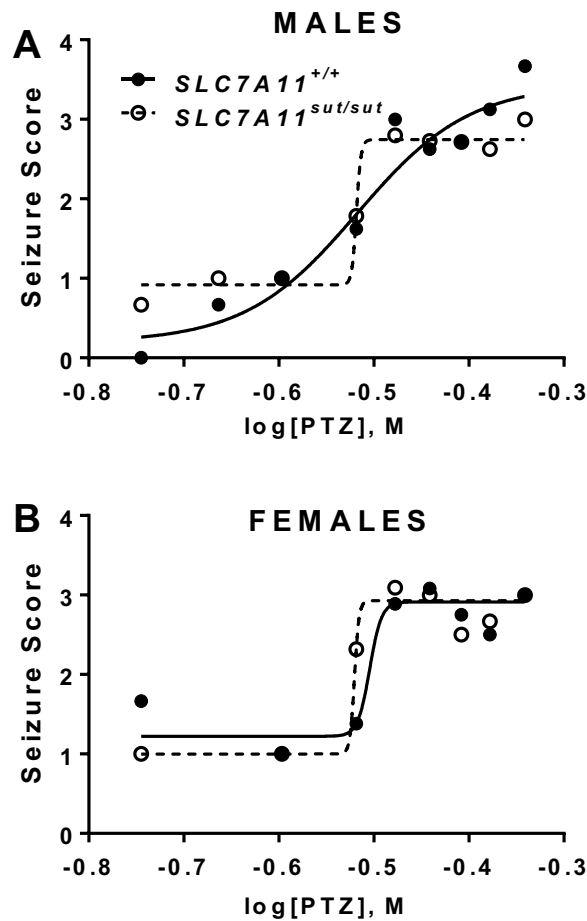
Supplemental Figure S1: Acute PTZ dose response curve in female and male SLC7A11⁺/⁺ and SLCA11^sut/sut mice

(A) Male *SLC7A11^{+/+}* (+/+; n = 3-29) and *SLC7A11^{sut/sut}* (*sut/sut;* n = 3-37) or **(B)** female *SLC7A11^{+/+}* (+/+; n = 3-21) and *SLC7A11^{sut/sut}* (*sut/sut;* n = 3-26) littermates were administered a single dose of PTZ (i.p.), after which behavior was monitored for 20-30 min. Seizure severity was scored using a 5-point scale as described in Chapter 2 materials and methods. Dose of PTZ (25-63 mg/kg) is expressed as log [PTZ], M. Symbols represent the mean maximal seizure score for +/+ (closed black circles) and *sut/sut* (open circles) mice during the 30 min observation period.

HIPPOCAMPUS   **CORTEX**
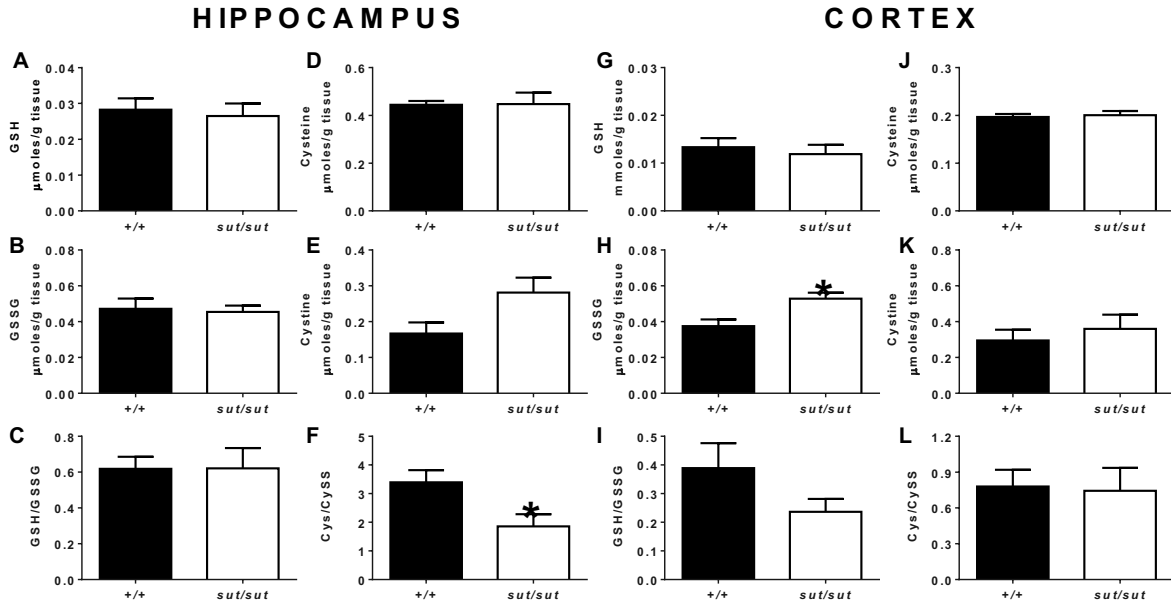
Supplemental Figure S2: Effect of SLC7A11 disruption on hippocampal and cortical reduced/oxidized glutathione and cysteine levels in female mice

Naïve female *SLC7A11*^{+/+} (+/+; n = 5) and *SLC7A11*[sut/sut] (*sut/sut*; n = 6) littermates were sacrificed by transcardial perfusion with ice-cold phosphate buffered saline and the left (A-F) hippocampus or (G-L) cortex rapidly dissected and snap-frozen in liquid nitrogen. The concentration of reduced and oxidized glutathione (GSH and GSSG) or cysteine (Cys and CySS) was determined by high performance liquid chromatography (HPLC) as described in Chapter 3 Materials and Methods. GSH, GSSG, Cys, and CySS levels were compared using an unpaired *t* test whereas GSH/GSSG or Cys/CySS ratios were compared using a Mann Whitney U test.

A-L) Bars [black bar (+/+) and open bar (*sut/sut*)] represent the mean µmoles/g tissue ± SEM of GSH (A and G), GSSG (B and H), Cys (D and J), CySS (E and K), or the ratio of GSH/GSSG (C and I) or Cys/CySS (F and L) in (A-F) hippocampus or (G-L) cortex. **Sut/sut* female mice have a decreased hippocampal Cys/CySS ratio (*p* = 0.03; Mann-Whitney U test) and elevated GSSG levels (*p* = 0.01; unpaired *t* test) as compared to +/+ littermate controls.
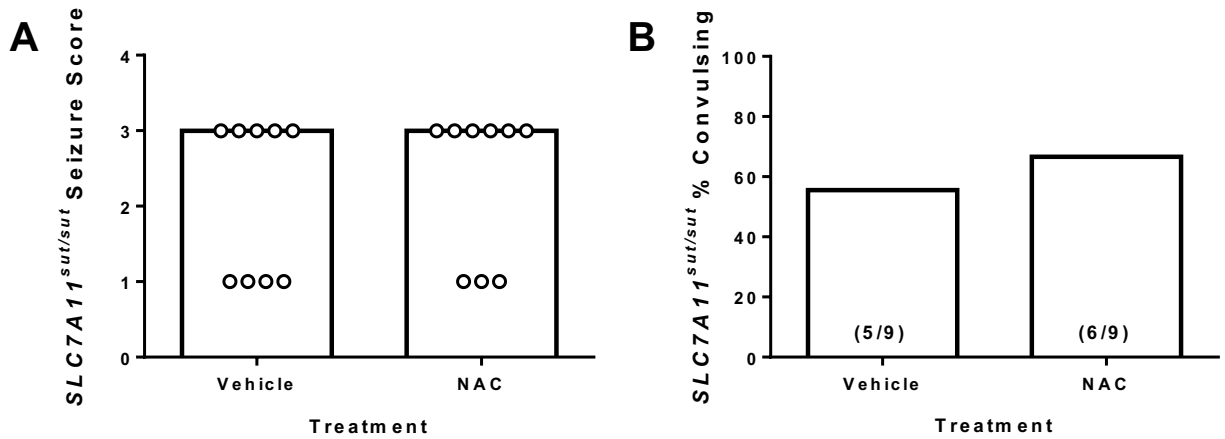
Supplemental Figure S3: Female SLC7A11$^{sut/sut}$ hyper-excitability is not rescued by administration of N-acetylcysteine

Naïve female *SLC7A11$^{sut/sut}$* (*sut/sut*) littermates were administered 2-3 mg/ml of the cysteine prodrug N-acetylcysteine (NAC) (n = 9) or vehicle (water) (n = 9) *ad libitum* for eight days. On days 4-8, animals were acclimated to handling by performing mock daily intraperitoneal (i.p.) injections which consisted of inverting the mouse and rubbing its abdomen. On day nine, mice received a single dose of 42 mg/kg PTZ (i.p.). Seizure behavior was scored using a 5-point scale as described in Chapter 2 Materials and Methods. Data were pooled from three independent experiments performed over three months.

A) *Seizure Scores:* Each data point represents the maximal seizure score obtained by an individual female mouse during a 30 min observation period. Horizontal lines represent the median seizure score for each treatment. Seizure severity was compared using the Mann-Whitney U test.

B) *Convulsive index:* Bars represent the proportion (fraction within bars) of mice that experienced a convulsive seizure (seizure score ≥ 3) in A expressed as a % of total mice exposed to PTZ. Convulsive incidence was compared using Fisher's Exact test.

Hippocampal protein expression

A — Plasma Membrane Protein (fold change over +/+)

● +/+
○ sut/sut

GluA1 · GluA2 · GluN1 · GABA_AR α1

Cortical protein expression

B — Plasma Membrane Protein (fold change over +/+)

GluA1 · GluA2 · GluN1 · GABA_AR α1 · GluN2A · GluN2B · ASCT1 · EAAT1 · EAAT2 · EAAT3 · KCC2
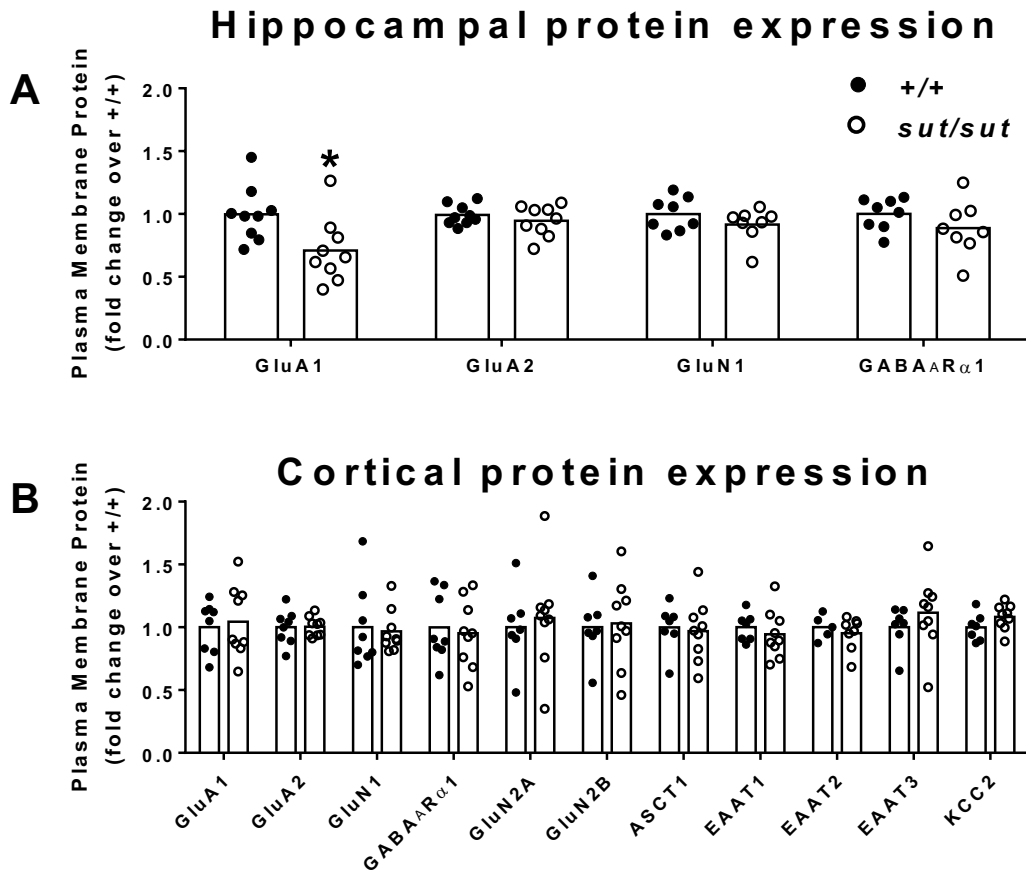
Supplementary Figure S4: Comparison of plasma membrane protein expression in female SLC7A11^{+/+} and SLC7A11[sut/sut] mice

Plasma membrane protein levels in hippocampus or cortex derived from female *SLC7A11^{+/+}* (+/+) or *SLC7A11[sut/sut]* (*sut/sut*) littermates were compared using Western blot analysis exactly as described for male mice in Chapter 3 Materials and Methods. Each data point [closed black circles (+/+; n = 7-9) or open circles (*sut/sut*; n = 5-9) represents the level of hippocampal (B) or cortical (C) protein following normalization to their respective loading control (i.e., Na^+/K^+ ATPase levels). Bars indicate the mean fold change over control (+/+), which was set to one. Hippocampal or cortical plasma membrane protein expression levels were compared using an unpaired *t* test on log-transformed data. An asterisk (*) represents a significant between group difference (p = 0.0160).

References

Aizenman E, Lipton SA, Loring RH. 1989. Selective modulation of NMDA responses by reduction and oxidation. *Neuron* 2: 1257-63

Akbarian S, Sucher N, Bradley D, Tafazzoli A, Trinh D, et al. 1996. Selective alterations in gene expression for NMDA receptor subunits in prefrontal cortex of schizophrenics. *J. Neurosci.* 16: 19-30

Albano R, Liu X, Lobner D. 2013. Regulation of system xc− in the SOD1-G93A mouse model of ALS. *Experimental neurology* 250: 69-73

Alexander AL, Lee JE, Lazar M, Boudos R, DuBray MB, et al. 2007. Diffusion tensor imaging of the corpus callosum in Autism. *Neuroimage* 34: 61-73

Allen NJ, Bennett ML, Foo LC, Wang GX, Chakraborty C, et al. 2012. Astrocyte glypicans 4 and 6 promote formation of excitatory synapses via GluA1 AMPA receptors. *Nature* 486: 410

Almaguer-Melian W, Cruz-Aguado R, Bergado JA. 2000. Synaptic plasticity is impaired in rats with a low glutathione content. *Synapse* 38: 369-74

Amaral DG, Scharfman HE, Lavenex P. 2007. The dentate gyrus: fundamental neuroanatomical organization (dentate gyrus for dummies). *Progress in Brain Research* 163: 3-790

Andrews P, Johnston G. 1979. GABA agonists and antagonists. *Biochemical Pharmacology* 28: 2697-702

Angulo MC, Kozlov AS, Charpak S, Audinat E. 2004. Glutamate released from glial cells synchronizes neuronal activity in the hippocampus. *J. Neurosci.* 24: 6920-27

Aoyama K, Suh SW, Hamby AM, Liu J, Chan WY, et al. 2006. Neuronal glutathione deficiency and age-dependent neurodegeneration in the EAAC1 deficient mouse. *Nat. Neurosci.* 9: 119

Araya R, Jiang J, Eisenthal KB, Yuste R. 2006. The spine neck filters membrane potentials. *Proceedings of the National Academy of Sciences* 103: 17961-66

Arfanakis K, Hermann BP, Rogers BP, Carew JD, Seidenberg M, Meyerand ME. 2002. Diffusion tensor MRI in temporal lobe epilepsy. *Magnetic resonance imaging* 20: 511-19

Arriza JL, Eliasof S, Kavanaugh MP, Amara SG. 1997. Excitatory amino acid transporter 5, a retinal glutamate transporter coupled to a chloride conductance. *Proceedings of the National Academy of Sciences* 94: 4155-60

Augustin H, Grosjean Y, Chen KY, Sheng Q, Featherstone DE. 2007. Nonvesicular release of glutamate by glial xCT transporters suppresses glutamate receptor clustering in vivo. *J. Neurosci.* 27: 111-23

Awapara J, Landua AJ, Fuerst R, Seale B. 1950. Free γ-aminobutyric acid in brain. *Journal of Biological Chemistry* 187: 35-39

Bak LK, Schousboe A, Waagepetersen HS. 2006. The glutamate/GABA-glutamine cycle: aspects of transport, neurotransmitter homeostasis and ammonia transfer. *Journal of neurochemistry* 98: 641-53

Baker DA, McFarland K, Lake RW, Shen H, Tang XC, et al. 2003. Neuroadaptations in cystine-glutamate exchange underlie cocaine relapse. *Nat Neurosci* 6: 743-9

Baker DA, Xi ZX, Shen H, Swanson CJ, Kalivas PW. 2002. The origin and neuronal function of in vivo nonsynaptic glutamate. *J. Neurosci.* 22: 9134-41

Banjac A, Perisic T, Sato H, Seiler A, Bannai S, et al. 2008. The cystine/cysteine cycle: a redox cycle regulating susceptibility versus resistance to cell death. *Oncogene* 27: 1618-28

Bannai S. 1986. Exchange of cystine and glutamate across plasma membrane of human fibroblasts. *Journal of Biological Chemistry* 261: 2256-63

Bannai S, Kitamura E. 1980. Transport interaction of L-cystine and L-glutamate in human diploid fibroblasts in culture. *Journal of Biological Chemistry* 255: 2372-76

Barbour B, Brew H, Attwell D. 1991. Electrogenic uptake of glutamate and aspartate into glial cells isolated from the salamander (Ambystoma) retina. *The Journal of physiology* 436: 169-93

Barger SW, Basile AS. 2001. Activation of microglia by secreted amyloid precursor protein evokes release of glutamate by cystine exchange and attenuates synaptic function. *Journal of Neurochemistry* 76: 846-54

Barnwell LF, Lugo JN, Lee WL, Willis SE, Gertz SJ, et al. 2009. Kv4.2 knockout mice demonstrate increased susceptibility to convulsant stimulation. *Epilepsia* 50: 1741-51

Barres BA. 2008. The mystery and magic of glia: a perspective on their roles in health and disease. *Neuron* 60: 430-40

Bassi M, Gasol E, Manzoni M, Pineda M, Riboni M, et al. 2001. Identification and characterisation of human xCT that co-expresses, with 4F2 heavy chain, the amino acid transport activity system x c. *Pflügers Archiv European Journal of Physiology* 442: 286-96

Beck H, Yaari Y. 2008. Plasticity of intrinsic neuronal properties in CNS disorders. *Nature Reviews Neuroscience* 9: 357

Ben-Ari Y. 2012. Kainate and Temporal Lobe Epilepsies. *Jasper's basic mechanisms of the epilepsies*: 432

Ben-Ari Y, Cossart R. 2000. Kainate, a double agent that generates seizures: two decades of progress. *Trends in neurosciences* 23: 580-87

Ben-Ari Y, Lagowska J. 1978. Epileptogenic action of intra-amygdaloid injection of kainic acid. *Comptes rendus hebdomadaires des seances de l'Academie des sciences. Serie D: Sciences naturelles* 287: 813-16

Bender A, Reichelt W, Norenberg M. 2000. Characterization of cystine uptake in cultured astrocytes. *Neurochem. Int.* 37: 269-76

Bentea E, Demuyser T, Van Liefferinge J, Albertini G, Deneyer L, et al. 2015a. Absence of system xc-in mice decreases anxiety and depressive-like behavior without affecting sensorimotor function or spatial vision. *Progress in Neuro-Psychopharmacology and Biological Psychiatry* 59: 49-58

Bentea E, Sconce MD, Churchill MJ, Van Liefferinge J, Sato H, et al. 2015b. MPTP-induced parkinsonism in mice alters striatal and nigral xCT expression but is unaffected by the genetic loss of xCT. *Neuroscience Letters* 593: 1-6

Benveniste H, Drejer J, Schousboe A, Diemer NH. 1984. Elevation of the extracellular concentrations of glutamate and aspartate in rat hippocampus during transient cerebral ischemia monitored by intracerebral microdialysis. *Journal of neurochemistry* 43: 1369-74

Bergles DE, Tzingounis AV, Jahr CE. 2002. Comparison of coupled and uncoupled currents during glutamate uptake by GLT-1 transporters. *J Neurosci* 22: 10153-62

Berman AE, Chan WY, Brennan AM, Reyes RC, Adler BL, et al. 2011. N-acetylcysteine prevents loss of dopaminergic neurons in the EAAC1−/− mouse. *Annals of neurology* 69: 509-20

Besag FM. 2018. Epilepsy in patients with autism: links, risks and treatment challenges. *Neuropsychiatric disease and treatment* 14: 1

Bezzi P, Carmignoto G, Pasti L, Vesce S, Rossi D, et al. 1998. Prostaglandins stimulate calcium-dependent glutamate release in astrocytes. *Nature* 391: 281

Bezzi P, Gundersen V, Galbete JL, Seifert G, Steinhäuser C, et al. 2004. Astrocytes contain a vesicular compartment that is competent for regulated exocytosis of glutamate. *Nat. Neurosci.* 7: 613

Bini L. 1938. Experimental researches on epileptic attacks induced by the electric current. *American Journal of Psychiatry* 94: 172-74

Bjørjås M, Gjesdal O, Erickson J, Torp R, Levy L, et al. 1996. Cloning and expression of a neuronal rat brain glutamate transporter. *Molecular brain research* 36: 163-68

Bloom JS, Hynd GW. 2005. The role of the corpus callosum in interhemispheric transfer of information: excitation or inhibition? *Neuropsychology review* 15: 59-71

Blundell J, Blaiss CA, Etherton MR, Espinosa F, Tabuchi K, et al. 2010. Neuroligin-1 deletion results in impaired spatial memory and increased repetitive behavior. *J. Neurosci.* 30: 2115-29

Bogen JE, Vogel PJ. 1962. Cerebral commissurotomy in man. Preliminary case report. *Bull Los Angeles Neuro Soc* 27: 169-72

Bonnert TP, McKernan RM, Farrar S, le Bourdellès B, Heavens RP, et al. 1999. θ, a novel γ-aminobutyric acid type A receptor subunit. *Proceedings of the National Academy of Sciences* 96: 9891-96

Bormann J. 2000. The 'ABC'of GABA receptors. *Trends in Pharmacological Sciences* 21: 16-19

Bormann J, Feigenspan A. 1995. GABAC receptors. *Trends in neurosciences* 18: 515-19

Borra S, McCullagh EA, Featherstone DE, Baker PM, Ragozzino ME, Shippy SA. 2014. Determining striatal extracellular glutamate levels in xCT mutant mice using LFPS CE-LIF. *Analytical Methods* 6: 2916-22

Bowery N, Doble A, Hill D, Hudson A, Shaw J, Turnbull M. 1979. Baclofen: a selective agonist for a novel type of GABA receptor] proceedings]. *British journal of pharmacology* 67: 444P

Bowie D. 2002. External anions and cations distinguish between AMPA and kainate receptor gating mechanisms. *The Journal of physiology* 539: 725-33

Bradford H. 1995. Glutamate, GABA and epilepsy. *Progress in neurobiology* 47: 477-511

Braitenberg V, Schüz A. 2013. *Cortex: statistics and geometry of neuronal connectivity*. Springer Science & Business Media.

Braunwald E, Hauser SL, Fauci AS, Longo DL, Kasper DL, Jameson JL, eds. 2001. *Harrison's Princliples of Internal Medicine*. New York: McGraw-Hill Medical Publishing Division. 15th ed.

Brickley SG, Mody I. 2012. Extrasynaptic GABAA receptors: their function in the CNS and implications for disease. *Neuron* 73: 23-34

Bridges R, Lutgen V, Lobner D, Baker DA. 2012a. Thinking Outside the Cleft to Understand Synaptic Activity: Contribution of the Cystine-Glutamate Antiporter (System x(c)(-)) to Normal and Pathological Glutamatergic Signaling. *Pharmacological Reviews* 64: 780-802

Bridges RJ, Natale NR, Patel SA. 2012b. System xc- cystine/glutamate antiporter: an update on molecular pharmacology and roles within the CNS. *British Journal of Pharmacology* 165: 20-34

Bron C, Rousseaux M, Spiazzi A, MacDonald H. 1986. Structural homology between the human 4F2 antigen and a murine cell surface glycoprotein associated with lymphocyte activation. *The Journal of Immunology* 137: 397-99

Bruzzone S, Guida L, Zocchi E, Franco L, De Flora A. 2001. Connexin 43 hemi channels mediate Ca2+-regulated transmembrane NAD+ fluxes in intact cells. *The FASEB Journal* 15: 10-12

Buckingham SC, Campbell SL, Haas BR, Montana V, Robel S, et al. 2011. Glutamate release by primary brain tumors induces epileptic activity. *Nature Medicine* 17: 1269

Buckmaster PS, Dudek FE. 1997. Neuron loss, granule cell axon reorganization, and functional changes in the dentate gyrus of epileptic kainate-treated rats. *Journal of Comparative Neurology* 385: 385-404

Buckmaster PS, Lew FH. 2011. Rapamycin suppresses mossy fiber sprouting but not seizure frequency in a mouse model of temporal lobe epilepsy. *J. Neurosci.* 31: 2337-47

Burdo J, Dargusch R, Schubert D. 2006. Distribution of the cystine/glutamate antiporter system x(c)(-) in the brain, kidney, and duodenum. *J. Histochem. Cytochem.* 54: 549-57

Burger PM, Mehl E, Cameron PL, Maycox PR, Baumert M, et al. 1989. Synaptic vesicles immunoisolated from rat cerebral cortex contain high levels of glutamate. *Neuron* 3: 715-20

Cahoy JD, Emery B, Kaushal A, Foo LC, Zamanian JL, et al. 2008. A transcriptome database for astrocytes, neurons, and oligodendrocytes: a new resource for understanding brain development and function. *J. Neurosci.* 28: 264-78

Cain DP. 1989. Long-term potentiation and kindling: how similar are the mechanisms? *Trends in neurosciences* 12: 6-10

Cannon WB. 1932. The wisdom of the body.

Castillo PE, Malenka RC, Nicoll RA. 1997. Kainate receptors mediate a slow postsynaptic current in hippocampal CA3 neurons. *Nature* 388: 182

Cavazos JE, Golarai G, Sutula TP. 1991. Mossy fiber synaptic reorganization induced by kindling: time course of development, progression, and permanence. *Journal of Neuroscience* 11: 2795-803

Cavazos JE, Sutula TP. 1990. Progressive neuronal loss induced by kindling: a possible mechanism for mossy fiber synaptic reorganization and hippocampal sclerosis. *Brain research* 527: 1-6

Cavelier P, Attwell D. 2005. Tonic release of glutamate by a DIDS-sensitive mechanism in rat hippocampal slices. *The Journal of physiology* 564: 397-410

Cavelier P, Hamann M, Rossi D, Mobbs P, Attwell D. 2005. Tonic excitation and inhibition of neurons: ambient transmitter sources and computational consequences. *Progress in Biophysics and Molecular Biology* 87: 3-16

Chance B, Sies H, Boveris A. 1979. Hydroperoxide metabolism in mammalian organs. *Physiological reviews* 59: 527-605

Chang Y, Weiss DS. 1999. Channel opening locks agonist onto the GABA C receptor. *Nat. Neurosci.* 2: 219

Chase LA, Smith D, Schiller N. *2013*. Federation of American Societies for Experimental Biology.

Chaudhry FA, Reimer RJ, Bellocchio EE, Danbolt NC, Osen KK, et al. 1998. The vesicular GABA transporter, VGAT, localizes to synaptic vesicles in sets of glycinergic as well as GABAergic neurons. *J. Neurosci.* 18: 9733-50

Chen C, Arai I, Satterfield R, Young Jr SM, Jonas P. 2017. Synaptotagmin 2 is the fast Ca2+ sensor at a central inhibitory synapse. *Cell reports* 18: 723-36

Chen W, Mahadomrongkul V, Berger UV, Bassan M, DeSilva T, et al. 2004. The glutamate transporter GLT1a is expressed in excitatory axon terminals of mature hippocampal neurons. *J. Neurosci.* 24: 1136-48

Chen Y, Swanson RA. 2003. The glutamate transporters EAAT2 and EAAT3 mediate cysteine uptake in cortical neuron cultures. *Journal of neurochemistry* 84: 1332-39

Chiara DC, Jayakar SS, Zhou X, Zhang X, Savechenkov PY, et al. 2013. Specificity of intersubunit general anesthetic binding sites in the transmembrane domain of the human α1β3γ2 GABAA receptor. *Journal of Biological Chemistry*: jbc. M113. 479725

Chintala S, Li W, Lamoreux ML, Ito S, Wakamatsu K, et al. 2005. Slc7a11 gene controls production of pheomelanin pigment and proliferation of cultured cells. *Proceedings of the National Academy of Sciences of the United States of America* 102: 10964-69

Chittajallu R, Vignes M, Dev KK, Barnes JM, Collingridge GL, Henley JM. 1996. Regulation of glutamate release by presynaptic kainate receptors in the hippocampus. *Nature* 379: 78

Chiu DN, Jahr CE. 2017. Extracellular glutamate in the nucleus accumbens is nanomolar in both synaptic and non-synaptic compartments. *Cell reports* 18: 2576-83

Cho Y, Bannai S. 1990. Uptake of glutamate and cystine in C-6 glioma cells and in cultured astrocytes. *Journal of neurochemistry* 55: 2091-97

Choi DW. 1992. Excitotoxic cell death. *Journal of neurobiology* 23: 1261-76

Chowdhury T, Allen M, Thorn T, He Y, Hewett S. 2018. Interleukin-1β protects neurons against oxidant-induced injury via the promotion of astrocyte glutathione production. *Antioxidants* 7: 100

Christie JM, Jahr CE. 2008. Dendritic NMDA receptors activate axonal calcium channels. *Neuron* 60: 298-307

Chung WJ, Lyons SA, Nelson GM, Hamza H, Gladson CL, et al. 2005. Inhibition of cystine uptake disrupts the growth of primary brain tumors. *The Journal of neuroscience* 25: 7101-10

Claycomb RJ, Hewett SJ, Hewett JA. 2011. Prophylactic, prandial rofecoxib treatment lacks efficacy against acute PTZ-induced seizure generation and kindling acquisition. *Epilepsia* 52: 273-83

Claycomb RJ, Hewett SJ, Hewett JA. 2012. Neuromodulatory role of endogenous interleukin-1β in acute seizures: possible contribution of cyclooxygenase-2. *Neurobiology of disease* 45: 234-42

Coghlan S, Horder J, Inkster B, Mendez MA, Murphy DG, Nutt DJ. 2012. GABA system dysfunction in autism and related disorders: from synapse to symptoms. *Neuroscience & Biobehavioral Reviews* 36: 2044-55

Colonnier M. 1968. Synaptic patterns on different cell types in the different laminae of the cat visual cortex. An electron microscope study. *Brain research* 9: 268-87

Conlon P, Trimble M. 1988. A study of the corpus callosum in epilepsy using magnetic resonance imaging. *Epilepsy research* 2: 122-26

Contreras JE, Sánchez HA, Eugenín EA, Speidel D, Theis M, et al. 2002. Metabolic inhibition induces opening of unapposed connexin 43 gap junction hemichannels and reduces gap junctional communication in cortical astrocytes in culture. *Proceedings of the National Academy of Sciences* 99: 495-500

Coulter DA, Eid T. 2012. Astrocytic regulation of glutamate homeostasis in epilepsy. *Glia* 60: 1215-26

Craig AM, Blackstone CD, Huganir RL, Banker G. 1993. The distribution of glutamate receptors in cultured rat hippocampal neurons: postsynaptic clustering of AMPA selective subunits. *Neuron* 10: 1055-68

Croll S, Suri C, Compton D, Simmons M, Yancopoulos G, et al. 1999. Brain-derived neurotrophic factor transgenic mice exhibit passive avoidance deficits, increased seizure severity and in vitro hyperexcitability in the hippocampus and entorhinal cortex. *Neuroscience* 93: 1491-506

Dalby NO, Mody I. 2003. Activation of NMDA receptors in rat dentate gyrus granule cells by spontaneous and evoked transmitter release. *Journal of Neurophysiology* 90: 786-97

Danbolt N, Furness D, Zhou Y. 2016. Neuronal vs glial glutamate uptake: resolving the conundrum. *Neurochem. Int.* 98: 29-45

Danbolt N, Storm-Mathisen J, Kanner B. 1992. An [Na++ K+] coupledl-glutamate transporter purified from rat brain is located in glial cell processes. *Neuroscience* 51: 295-310

Danbolt NC. 2001. Glutamate uptake. *Progress in Neurobiology* 65: 1-105

Danbolt NC, Pines G, Kanner BI. 1990. Purification and reconstitution of the sodium-and potassium-coupled glutamate transport glycoprotein from rat brain. *Biochemistry* 29: 6734-40

Dash MB, Douglas CL, Vyazovskiy VV, Cirelli C, Tononi G. 2009. Long-term homeostasis of extracellular glutamate in the rat cerebral cortex across sleep and waking states. *J. Neurosci.* 29: 620-29

Dave MH, Schulz N, Zecevic M, Wagner CA, Verrey F. 2004. Expression of heteromeric amino acid transporters along the murine intestine. *The Journal of physiology* 558: 597-610

De Bundel D, Schallier A, Loyens E, Fernando R, Miyashita H, et al. 2011. Loss of System x(c)(-) Does Not Induce Oxidative Stress But Decreases Extracellular Glutamate in Hippocampus and Influences Spatial Working Memory and Limbic Seizure Susceptibility. *J. Neurosci.* 31: 5792-803

De Pitta M, Brunel N, Volterra A. 2016. Astrocytes: Orchestrating synaptic plasticity? *Neuroscience* 323: 43-61

De Vries GJ. 2004. Minireview: sex differences in adult and developing brains: compensation, compensation, compensation. *Endocrinology* 145: 1063-68

Dennison Z, Teskey GC, Cain DP. 1995. Persistence of kindling: effect of partial kindling, retention interval, kindling site, and stimulation parameters. *Epilepsy research* 21: 171-82

Domercq M, Sánchez-Gómez MV, Sherwin C, Etxebarria E, Fern R, Matute C. 2007. System xc– and glutamate transporter inhibition mediates microglial toxicity to oligodendrocytes. *The Journal of Immunology* 178: 6549-56

Dringen R. 2000. Metabolism and functions of glutathione in brain. *Progress in neurobiology* 62: 649-71

Dringen R, Gutterer JM, Gros C, Hirrlinger J. 2001. Aminopeptidase N mediates the utilization of the GSH precursor CysGly by cultured neurons. *Journal of neuroscience research* 66: 1003-08

Dringen R, Gutterer JM, Hirrlinger J. 2000. Glutathione metabolism in brain: metabolic interaction between astrocytes and neurons in the defense against reactive oxygen species. *European Journal of Biochemistry* 267: 4912-16

Duan S, Anderson CM, Keung EC, Chen Y, Chen Y, Swanson RA. 2003. P2X7 receptor-mediated release of excitatory amino acids from astrocytes. *The Journal of neuroscience* 23: 1320-28

Duffney LJ, Wei J, Cheng J, Liu W, Smith KR, et al. 2013. Shank3 deficiency induces NMDA receptor hypofunction via an actin-dependent mechanism. *J. Neurosci.* 33: 15767-78

Dun Y, Mysona B, Van Ells T, Amarnath L, Ola MS, et al. 2006. Expression of the cystine-glutamate exchanger (x c−) in retinal ganglion cells and regulation by nitric oxide and oxidative stress. *Cell and tissue research* 324: 189-202

Egaas B, Courchesne E, Saitoh O. 1995. Reduced size of corpus callosum in autism. *Archives of neurology* 52: 794-801

Eid T, Lee TSW, Patrylo P, Zaveri HP. 2018. Astrocytes and Glutamine Synthetase in Epileptogenesis. *Journal of neuroscience research*

Elliott K. 1965. γ-Aminobutyric acid and other inhibitory substances. *British medical bulletin* 21: 70-75

Engert F, Bonhoeffer T. 1999. Dendritic spine changes associated with hippocampal long-term synaptic plasticity. *Nature* 399: 66-70

Erecińska M, Silver IA. 1990. Metabolism and role of glutamate in mammalian brain. *Progress in neurobiology* 35: 245-96

Errera M, Greenstein JP. 1949. Phosphate-activated glutaminase in kidney and other tissues. *Journal of Biological Chemistry* 178: 495-502

Estévez R, Camps M, Rojas AM, Testar X, Devés R, et al. 1998. The amino acid transport system y+ L/4F2hc is a heteromultimeric complex. *The FASEB Journal* 12: 1319-29

Eulenburg V, Gomeza J. 2010. Neurotransmitter transporters expressed in glial cells as regulators of synapse function. *Brain research reviews* 63: 103-12

Evonuk KS, Baker BJ, Doyle RE, Moseley CE, Sestero CM, et al. 2015. Inhibition of system xc− transporter attenuates autoimmune inflammatory demyelination. *The Journal of Immunology*: 1401108

Fairman W, Vandenberg R, Arriza J, Kavanaught M, Amara S. 1995. An excitatory amino-acid transporter with properties of a ligand-gated chloride channel. *Nature* 375: 599

Fame RM, MacDonald JL, Dunwoodie SL, Takahashi E, Macklis JD. 2016. Cited2 Regulates Neocortical Layer II/III Generation and Somatosensory Callosal Projection Neuron Development and Connectivity. *J Neurosci* 36: 6403-19

Fenczik CA, Sethi T, Ramos JW, Hughes PE, Ginsberg MH. 1997. Complementation of dominant suppression implicates CD98 in integrin activation. *Nature* 390: 81

Fernandez-Chacon R, Königstorfer A, Gerber SH, García J, Matos MF, et al. 2001. Synaptotagmin I functions as a calcium regulator of release probability. *Nature* 410: 41

Fernández E, Carrascal M, Rousaud F, Abián J, Zorzano A, et al. 2002. rBAT-b0,+ AT heterodimer is the main apical reabsorption system for cystine in the kidney. *American Journal of Physiology-Renal Physiology* 283: F540-F48

Fernández E, Torrents D, Zorzano A, Palacín M, Chillarón J. 2005. Identification and functional characterization of a novel low affinity aromatic-preferring amino acid transporter (arpAT) One of the few proteins silenced during primate evolution. *Journal of Biological Chemistry*

Ferraro TN, Golden GT, Smith GG, St Jean P, Schork NJ, et al. 1999. Mapping loci for pentylenetetrazol-induced seizure susceptibility in mice. *J Neurosci* 19: 6733-9

Fiacco TA, McCarthy KD. 2018. Multiple lines of evidence indicate that gliotransmission does not occur under physiological conditions. *J. Neurosci.* 38: 3-13

Fisher RS, Boas WvE, Blume W, Elger C, Genton P, et al. 2005. Epileptic seizures and epilepsy: definitions proposed by the International League Against Epilepsy (ILAE) and the International Bureau for Epilepsy (IBE). *Epilepsia* 46: 470-72

Foerster BR, Pomper MG, Callaghan BC, Petrou M, Edden RA, et al. 2013. An imbalance between excitatory and inhibitory neurotransmitters in amyotrophic lateral sclerosis revealed by use of 3-T proton magnetic resonance spectroscopy. *JAMA neurology* 70: 1009-16

Fogal B, Li J, Lobner D, McCullough LD, Hewett SJ. 2007. System xc− activity and astrocytes are necessary for interleukin-1β-mediated hypoxic neuronal injury. *J. Neurosci.* 27: 10094-105

Fonnum F. 1984. Glutamate: a neurotransmitter in mammalian brain. *Journal of neurochemistry* 42: 1-11

Fonnum F, Fyske E. 2000. Uptake and storage of GABA in synaptic vesicles. *GABA in the nervous system: the view at fifty years. Philadelphia: Lippincott Williams and Wilkins. p*: 51-64

Fotiadis D, Kanai Y, Palacín M. 2013. The SLC3 and SLC7 families of amino acid transporters. *Molecular aspects of medicine* 34: 139-58

Francke U, Foellmer B, Haynes B. 1983. Chromosome mapping of human cell surface molecules: monoclonal anti-human lymphocyte antibodies 4F2, A3D8, and A1G3 define antigens controlled by different regions of chromosome 11. *Somatic cell genetics* 9: 333-44

Franklin JL, Johnson EM. 1998. Control of Neuronal Size Homeostasis by Trophic Factor–mediated Coupling of Protein Degradation to Protein Synthesis. *The Journal of cell biology* 142: 1313-24

Frederick NM, Bertho J, Patel KK, Petr GT, Bakradze E, et al. 2014. Dysregulation of system xc− expression induced by mutant huntingtin in a striatal neuronal cell line and in R6/2 mice. *Neurochem. Int.* 76: 59-69

Frerking M, Malenka R, Nicoll R. 1998. Synaptic activation of kainate receptors on hippocampal interneurons. *Nat. Neurosci.* 1: 479

Frerking M, Schmitz D, Zhou Q, Johansen J, Nicoll RA. 2001. Kainate receptors depress excitatory synaptic transmission at CA3→ CA1 synapses in the hippocampus via a direct presynaptic action. *J. Neurosci.* 21: 2958-66

Friedman LK, Pellegrini-Giampietro DE, Sperber EF, Bennett M, Moshe SL, Zukin RS. 1994. Kainate-induced status epilepticus alters glutamate and GABAA receptor gene

expression in adult rat hippocampus: an in situ hybridization study. *J. Neurosci.* 14: 2697-707

Fritschy J-M. 2008. Epilepsy, E/I balance and GABAA receptor plasticity. *Frontiers in Molecular Neuroscience* 1: 5

Fukasawa Y, Segawa H, Kim JY, Chairoungdua A, Kim DK, et al. 2000. Identification and characterization of a Na+-independent neutral amino acid transporter that associates with the 4F2 heavy chain and exhibits substrate selectivity for small neutral D-and L-amino acids. *Journal of Biological Chemistry* 275: 9690-98

Furness D, Dehnes Y, Akhtar A, Rossi D, Hamann M, et al. 2008. A quantitative assessment of glutamate uptake into hippocampal synaptic terminals and astrocytes: new insights into a neuronal role for excitatory amino acid transporter 2 (EAAT2). *Neuroscience* 157: 80-94

Gao R, Penzes P. 2015. Common mechanisms of excitatory and inhibitory imbalance in schizophrenia and autism spectrum disorders. *Current Molecular Medicine* 15: 146-67

Gasol E, Jiménez-Vidal M, Chillarón J, Zorzano A, Palacín M. 2004. Membrane topology of system xc-light subunit reveals a re-entrant loop with substrate-restricted accessibility. *Journal of Biological Chemistry* 279: 31228-36

Ge S, Pradhan DA, Ming G-l, Song H. 2007. GABA sets the tempo for activity-dependent adult neurogenesis. *Trends in neurosciences* 30: 1-8

Gegg M, Clark J, Heales S. 2005. Co-culture of neurones with glutathione deficient astrocytes leads to increased neuronal susceptibility to nitric oxide and increased glutamate-cysteine ligase activity. *Brain research* 1036: 1-6

Geppert M, Goda Y, Hammer RE, Li C, Rosahl TW, et al. 1994. Synaptotagmin I: a major Ca2+ sensor for transmitter release at a central synapse. *Cell* 79: 717-27

Gochenauer GE, Robinson MB. 2001. Dibutyryl-cAMP (dbcAMP) up-regulates astrocytic chloride-dependent l-[3H] glutamate transport and expression of both system xc– subunits. *Journal of Neurochemistry* 78: 276-86

Goddard G, Douglas R. 1975. Does the engram of kindling model the engram of normal long term memory? *Canadian Journal of Neurological Sciences* 2: 385-94

Goddard GV. 1967. Development of epileptic seizures through brain stimulation at low intensity. *Nature* 214: 1020-21

Goddard GV, McIntyre DC, Leech CK. 1969. A permanent change in brain function resulting from daily electrical stimulation. *Experimental Neurology* 25: 295-330

Goodkin HP, Yeh J-L, Kapur J. 2005. Status epilepticus increases the intracellular accumulation of GABAA receptors. *J. Neurosci.* 25: 5511-20

Greenwood JS, Wang Y, Estrada RC, Ackerman L, Ohara PT, Baraban SC. 2009. Seizures, enhanced excitation, and increased vesicle number in Lis1 mutant mice. *Annals of Neurology: Official Journal of the American Neurological Association and the Child Neurology Society* 66: 644-53

Greger IH, Khatri L, Kong X, Ziff EB. 2003. AMPA receptor tetramerization is mediated by Q/R editing. *Neuron* 40: 763-74

Grooms SY, Opitz T, Bennett MV, Zukin RS. 2000. Status epilepticus decreases glutamate receptor 2 mRNA and protein expression in hippocampal pyramidal cells before neuronal death. *Proceedings of the National Academy of Sciences* 97: 3631-36

Gröppel G, Gallmetzer P, Prayer D, Serles W, Baumgartner C. 2009. Focal lesions in the splenium of the corpus callosum in patients with epilepsy. *Epilepsia* 50: 1354-60

Grosjean Y, Grillet M, Augustin H, Ferveur JF, Featherstone DE. 2008. A glial amino-acid transporter controls synapse strength and courtship in Drosophila. *Nat. Neurosci.* 11: 54-61

Gross DW, Concha L, Beaulieu C. 2006. Extratemporal white matter abnormalities in mesial temporal lobe epilepsy demonstrated with diffusion tensor imaging. *Epilepsia* 47: 1360-63

Guastella J, Nelson N, Nelson H, Czyzyk L, Keynan S, et al. 1990. Cloning and expression of a rat brain GABA transporter. *Science* 249: 1303-06

Hassel B, Dingledine R. 2012. Glutamate and glutamate receptors In *Basic Neurochemistry (Eighth Edition)*, pp. 342-66: Elsevier

Haugeto Ø, Ullensvang K, Levy LM, Chaudhry FA, Honoré T, et al. 1996. Brain glutamate transporter proteins form homomultimers. *Journal of Biological Chemistry* 271: 27715-22

Haury VG, and Gruber, C.M. . 1939. The action of pentamethylenetetrazole (Metrazol) on the circulatory system. *J. Pharmacol. Exp. Ther.* 65: 227-34

Hayashi T. 1952. A physiological study of epileptic seizures following cortical stimulation in animals and its application to human clinics. *The Japanese Journal of Physiology* 3: 46-64

Hayashi T. 1954. Effects of sodium glutamate on the nervous system. *The Keio Journal of Medicine* 3: 183-92

Heaney CF, Kinney JW. 2016. Role of GABAB receptors in learning and memory and neurological disorders. *Neuroscience & Biobehavioral Reviews* 63: 1-28

Hedblom E, Kirkness EF. 1997. A novel class of GABAA receptor subunit in tissues of the reproductive system. *Journal of Biological Chemistry* 272: 15346-50

Hediger MA, Clémençon B, Burrier RE, Bruford EA. 2013. The ABCs of membrane transporters in health and disease (SLC series): introduction. *Molecular aspects of medicine* 34: 95-107

Henderson ND. 1997. Spurious associations in unreplicated selected lines. *Behavior Genetics* 27: 145-54

Herman MA, Jahr CE. 2007. Extracellular glutamate concentration in hippocampal slice. *J Neurosci* 27: 9736-41

Hermann B, Hansen R, Seidenberg M, Magnotta V, O'leary D. 2003. Neurodevelopmental vulnerability of the corpus callosum to childhood onset localization-related epilepsy. *Neuroimage* 18: 284-92

Hertz L. 2013. The glutamate–glutamine (GABA) cycle: importance of late postnatal development and potential reciprocal interactions between biosynthesis and degradation. *Frontiers in Endocrinology* 4: 59

Hertz L, Murthy CR, Schousboe A. 1988. Metabolism of glutamate and related amino acids. *The Biochemical Pathology of Astrocytes* 395: 406

Hoffmann K, Lindner M, Gröticke I, Stangel M, Löscher W. 2008. Epileptic seizures and hippocampal damage after cuprizone-induced demyelination in C57BL/6 mice. *Experimental neurology* 210: 308-21

Holmseth S, Dehnes Y, Huang YH, Follin-Arbelet VV, Grutle NJ, et al. 2012. The density of EAAC1 (EAAT3) glutamate transporters expressed by neurons in the mammalian CNS. *J. Neurosci.* 32: 6000-13

Hosoya K-i, Tomi M, Ohtsuki S, Takanaga H, Saeki S, et al. 2002. Enhancement of L-cystine transport activity and its relation to xCT gene induction at the blood-brain barrier by diethyl maleate treatment. *J. Pharmacol. Exp. Ther.* 302: 225-31

Hsu R, Schofield CM, Cruz CGD, Jones-Davis DM, Blelloch R, Ullian EM. 2012. Loss of microRNAs in pyramidal neurons leads to specific changes in inhibitory synaptic transmission in the prefrontal cortex. *Molecular and Cellular Neuroscience* 50: 283-92

Hu WH, Walters WM, Xia XM, Karmally SA, Bethea JR. 2003. Neuronal glutamate transporter EAAT4 is expressed in astrocytes. *Glia* 44: 13-25

Huang R-Q, Bell-Horner CL, Dibas MI, Covey DF, Drewe JA, Dillon GH. 2001. Pentylenetetrazole-induced inhibition of recombinant γ-aminobutyric acid type A (GABAA) receptors: mechanism and site of action. *J. Pharmacol. Exp. Ther.* 298: 986-95

Hunt DL, Castillo PE. 2012. Synaptic plasticity of NMDA receptors: mechanisms and functional implications. *Current opinion in neurobiology* 22: 496-508

Hutchinson E, Pulsipher D, Dabbs K, y Gutierrez AM, Sheth R, et al. 2010. Children with new-onset epilepsy exhibit diffusion abnormalities in cerebral white matter in the absence of volumetric differences. *Epilepsy Research* 88: 208-14

Ito T, Hori M, Yoshida K, Shimizu M. 1977. Effect of anticonvulsants on seizures developing in the course of daily administration of pentetrazol to rats. *Eur J Pharmacol* 45: 165-72

Itoh M, Uchimura H. 1981. Regional differences in cofactor saturation of glutamate decarboxylase (GAD) in discrete brain nuclei of the rat. *Neurochemical Research* 6: 1283-89

Itoh M, Watanabe Y, Watanabe M, Tanaka K, Wada K, Takashima S. 1997. Expression of a glutamate transporter subtype, EAAT4, in the developing human cerebellum. *Brain research* 767: 265-71

Jabaudon D, Shimamoto K, Yasuda-Kamatani Y, Scanziani M, Gähwiler B, Gerber U. 1999. Inhibition of uptake unmasks rapid extracellular turnover of glutamate of nonvesicular origin. *Proceedings of the National Academy of Sciences* 96: 8733-38

Jackman NA, Uliasz TF, Hewett JA, Hewett SJ. 2010. Regulation of system x(c)(-)activity and expression in astrocytes by interleukin-1beta: implications for hypoxic neuronal injury. *Glia* 58: 1806-15

Jain A, Mårtensson J, Stole E, Auld P, Meister A. 1991. Glutathione deficiency leads to mitochondrial damage in brain. *Proceedings of the National Academy of Sciences* 88: 1913-17

Jensen FE. 2009. Introduction. Posttraumatic epilepsy: treatable epileptogenesis. *Epilepsia* 50 Suppl 2: 1-3

Jenstad M, Quazi AZ, Zilberter M, Haglerød C, Berghuis P, et al. 2008. System A transporter SAT2 mediates replenishment of dendritic glutamate pools controlling retrograde signaling by glutamate. *Cerebral Cortex* 19: 1092-106

Jiang D, Akopian G, Ho Y-S, Walsh JP, Andersen JK. 2000. Chronic brain oxidation in a glutathione peroxidase knockout mouse model results in increased resistance to induced epileptic seizures. *Experimental Neurology* 164: 257-68

Jiménez-Vidal M, Gasol E, Zorzano A, Nunes V, Palacín M, Chillarón J. 2004. Thiol modification of cysteine 327 in the eighth transmembrane domain of the light subunit xCT of the heteromeric cystine/glutamate antiporter suggests close proximity to the substrate binding site/permeation pathway. *Journal of Biological Chemistry* 279: 11214-21

John SA, Kondo R, Wang S-Y, Goldhaber JI, Weiss JN. 1999. Connexin-43 hemichannels opened by metabolic inhibition. *Journal of Biological Chemistry* 274: 236-40

Jones EV, Bernardinelli Y, Tse YC, Chierzi S, Wong TP, Murai KK. 2011. Astrocytes control glutamate receptor levels at developing synapses through SPARC–β-integrin interactions. *J. Neurosci.* 31: 4154-65

Jones MV, Westbrook GL. 1996. The impact of receptor desensitization on fast synaptic transmission. *Trends in neurosciences* 19: 96-101

Just MA, Cherkassky VL, Keller TA, Kana RK, Minshew NJ. 2006. Functional and anatomical cortical underconnectivity in autism: evidence from an FMRI study of an executive function task and corpus callosum morphometry. *Cerebral cortex* 17: 951-61

Kabashima N, Shibuya I, Ibrahim N, Ueta Y, Yamashita H. 1997. Inhibition of spontaneous EPSCs and IPSCs by presynaptic GABAB receptors on rat supraoptic magnocellular neurons. *The Journal of physiology* 504: 113-26

Kamermans M, Fahrenfort I, Schultz K, Janssen-Bienhold U, Sjoerdsma T, Weiler R. 2001. Hemichannel-mediated inhibition in the outer retina. *Science* 292: 1178-80

Kanai Y, Hediger MA. 1992. Primary structure and functional characterization of a high-affinity glutamate transporter. *Nature* 360: 467

Kanai Y, Segawa H, Miyamoto K-i, Uchino H, Takeda E, Endou H. 1998. Expression cloning and characterization of a transporter for large neutral amino acids activated by the heavy chain of 4F2 antigen (CD98). *Journal of Biological Chemistry* 273: 23629-32

Kanner BI, Schuldiner S. 1987. Mechanism of transport and storage of neurotransmitter. *Critical Reviews in Biochemistry* 22: 1-38

Kapur J, Bennett Jr JP, Wooten GF, Lothman EW. 1989a. Evidence for a chronic loss of inhibition in the hippocampus after kindling: biochemical studies. *Epilepsy Research* 4: 100-08

Kapur J, Michelson HB, Buterbaugh GG, Lothman EW. 1989b. Evidence for a chronic loss of inhibition in the hippocampus after kindling: electrophysiological studies. *Epilepsy Research* 4: 90-99

Karim N, Wellendorph P, Absalom N, Johnston GA, Hanrahan JR, Chebib M. 2013. Potency of GABA at human recombinant GABA A receptors expressed in Xenopus oocytes: a mini review. *Amino acids* 44: 1139-49

Kasai H, Matsuzaki M, Noguchi J, Yasumatsu N, Nakahara H. 2003. Structure–stability–function relationships of dendritic spines. *Trends in neurosciences* 26: 360-68

Kato S, Negishi K, Mawatari K, Kuo C-H. 1992. A mechanism for glutamate toxicity in the C6 glioma cells involving inhibition of cystine uptake leading to glutathione depletion. *Neuroscience* 48: 903-14

Kelley MR, Deeb TZ, Brandon NJ, Dunlop J, Davies PA, Moss SJ. 2016. Compromising KCC2 transporter activity enhances the development of continuous seizure activity. *Neuropharmacology* 108: 103-10

Kew JN, Koester A, Moreau J-L, Jenck F, Ouagazzal A-M, et al. 2000. Functional consequences of reduction in NMDA receptor glycine affinity in mice carrying targeted point mutations in the glycine binding site. *J. Neurosci.* 20: 4037-49

Kilman V, Van Rossum MC, Turrigiano GG. 2002. Activity deprivation reduces miniature IPSC amplitude by decreasing the number of postsynaptic GABAA receptors clustered at neocortical synapses. *J. Neurosci.* 22: 1328-37

Kim J-A, Chung JI, Yoon PH, Kim DI, Chung T-S, et al. 2001. Transient MR signal changes in patients with generalized tonicoclonic seizure or status epilepticus: periictal diffusion-weighted imaging. *American Journal of Neuroradiology* 22: 1149-60

Kimelberg H, Goderie S, Higman S, Pang S, Waniewski R. 1990. Swelling-induced release of glutamate, aspartate, and taurine from astrocyte cultures. *J. Neurosci.* 10: 1583-91

Klatt P, Lamas S. 2000. Regulation of protein function by S-glutathiolation in response to oxidative and nitrosative stress. *European Journal of Biochemistry* 267: 4928-44

Klenowski PM, Fogarty MJ, Shariff M, Belmer A, Bellingham MC, Bartlett SE. 2016. Increased synaptic excitation and abnormal dendritic structure of prefrontal cortex layer V pyramidal neurons following prolonged binge-like consumption of ethanol. *eNeuro*: 0248-16.2016

Knackstedt LA, Melendez RI, Kalivas PW. 2010. Ceftriaxone restores glutamate homeostasis and prevents relapse to cocaine seeking. *Biological Psychiatry* 67: 81-84

Kodama M, Yamada N, Sato K, Kitamura Y, Koyama F, et al. 1999. Effects of YM90K, a selective AMPA receptor antagonist, on amygdala-kindling and long-term hippocampal potentiation in the rat. *European Journal of Pharmacology* 374: 11-19

Köhler M, Burnashev N, Sakmann B, Seeburg PH. 1993. Determinants of Ca^{2+} permeability in both TM1 and TM2 of high affinity kainate receptor channels: diversity by RNA editing. *Neuron* 10: 491-500

Köhr G, Eckardt S, Lüddens H, Monyer H, Seeburg PH. 1994. NMDA receptor channels: subunit-specific potentiation by reducing agents. *Neuron* 12: 1031-40

Kosobud AE, Cross SJ, Crabbe JC. 1992. Neural sensitivity to pentylenetetrazol convulsions in inbred and selectively bred mice. *Brain research* 592: 122-28

Krebs HA. 1935. Metabolism of amino-acids: The synthesis of glutamine from glutamic acid and ammonia, and the enzymic hydrolysis of glutamine in animal tissues. *Biochemical Journal* 29: 1951

Krnjević K, Phillis J. 1963. Iontophoretic studies of neurones in the mammalian cerebral cortex. *The Journal of physiology* 165: 274-304

Krnjević K, Whittaker V. 1965. Excitation and depression of cortical neurones by brain fractions released from micropipettes. *The Journal of physiology* 179: 298-322

Kugler P, Schleyer V. 2004. Developmental expression of glutamate transporters and glutamate dehydrogenase in astrocytes of the postnatal rat hippocampus. *Hippocampus* 14: 975-85

La Bella V, Valentino F, Piccoli T, Piccoli F. 2007. Expression and developmental regulation of the cystine/glutamate exchanger (x c−) in the rat. *Neurochemical Research* 32: 1081-90

Laake J, Takumi Y, Eidet J, Torgner IA, Roberg B, et al. 1999. Postembedding immunogold labelling reveals subcellular localization and pathway-specific enrichment of phosphate activated glutaminase in rat cerebellum. *Neuroscience* 88: 1137-51

Lai TW, Zhang S, Wang YT. 2014. Excitotoxicity and stroke: identifying novel targets for neuroprotection. *Progress in Neurobiology* 115: 157-88

Lamigeon C, Bellier J, Sacchettoni S, Rujano M, Jacquemont B. 2001. Enhanced neuronal protection from oxidative stress by coculture with glutamic acid decarboxylase-expressing astrocytes. *Journal of Neurochemistry* 77: 598-606

Lane P. 1988. Subtle gray (sut); small with kinky tail (skt). *Mouse News Lett* 80: 165

Laube B, Hirai H, Sturgess M, Betz H, Kuhse J. 1997. Molecular determinants of agonist discrimination by NMDA receptor subunits: analysis of the glutamate binding site on the NR2B subunit. *Neuron* 18: 493-503

Lehre KP, Levy LM, Ottersen OP, Storm-Mathisen J, Danbolt NC. 1995. Differential expression of two glial glutamate transporters in the rat brain: quantitative and immunocytochemical observations. *The Journal of Neuroscience* 15: 1835-53

Levy LM, Warr O, Attwell D. 1998. Stoichiometry of the glial glutamate transporter GLT-1 expressed inducibly in a Chinese hamster ovary cell line selected for low endogenous Na+-dependent glutamate uptake. *J. Neurosci.* 18: 9620-28

Lewerenz J, Baxter P, Kassubek R, Albrecht P, Van Liefferinge J, et al. 2014. Phosphoinositide 3-kinases upregulate system xc(-) via eukaryotic initiation factor 2alpha and activating transcription factor 4 - a pathway active in glioblastomas and epilepsy. *Antioxid Redox Signal* 20: 2907-22

Lewerenz J, Letz J, Methner A. 2003. Activation of stimulatory heterotrimeric G proteins increases glutathione and protects neuronal cells against oxidative stress. *Journal of Neurochemistry* 87: 522-31

Li D, Hérault K, Silm K, Evrard A, Wojcik S, et al. 2013. Lack of evidence for vesicular glutamate transporter expression in mouse astrocytes. *J. Neurosci.* 33: 4434-55

Li W, Xu X, Pozzo-Miller L. 2016. Excitatory synapses are stronger in the hippocampus of Rett syndrome mice due to altered synaptic trafficking of AMPA-type glutamate receptors. *Proceedings of the National Academy of Sciences* 113: E1575-E84

Li Y, Tan Z, Li Z, Sun Z, Duan S, Li W. 2012. Impaired long-term potentiation and long-term memory deficits in xCT-deficient sut mice. *Bioscience reports* 32: 315-21

Li Z-q, Yamamoto Y, Morimoto T, Ono J, Okada S, Yamatodani A. 2000. The effect of pentylenetetrazole-kindling on the extracellular glutamate and taurine levels in the frontal cortex of rats. *Neuroscience Letters* 282: 117-19

Liang L-P, Patel M. 2004. Mitochondrial oxidative stress and increased seizure susceptibility in Sod2−/+ mice. *Free Radical Biology and Medicine* 36: 542-54

Liu Q-R, Lopez-Corcuera B, Mandiyan S, Nelson H, Nelson N. 1993. Molecular characterization of four pharmacologically distinct gamma-aminobutyric acid transporters in mouse brain [corrected]. *Journal of Biological Chemistry* 268: 2106-12

Liu Q-R, Mandiyan S, Nelson H, Nelson N. 1992. A family of genes encoding neurotransmitter transporters. *Proceedings of the National Academy of Sciences* 89: 6639-43

Lomeli H, Sprengel R, Laurie DJ, Köhr G, Herb A, et al. 1993. The rat delta-1 and delta-2 subunits extend the excitatory amino acid receptor family. *FEBS Letters* 315: 318-22

Longo BM, Mello LE. 1997. Blockade of pilocarpine-or kainate-induced mossy fiber sprouting by cycloheximide does not prevent subsequent epileptogenesis in rats. *Neuroscience Letters* 226: 163-66

Longuemare M, Swanson RA. 1995. Excitatory amino acid release from astrocytes during energy failure by reversal of sodium-dependent uptake. *Journal of neuroscience research* 40: 379-86

Lopez-Corcuera B, Liu Q-R, Mandiyan S, Nelson H, Nelson N. 1992. Expression of a mouse brain cDNA encoding novel gamma-aminobutyric acid transporter. *Journal of Biological Chemistry* 267: 17491-93

LoTurco JJ, Blanton M, Kriegstein AR. 1991. Initial expression and endogenous activation of NMDA channels in early neocortical development. *J. Neurosci.* 11: 792-99

LoTurco JJ, Owens DF, Heath MJ, Davis MB, Kriegstein AR. 1995. GABA and glutamate depolarize cortical progenitor cells and inhibit DNA synthesis. *Neuron* 15: 1287-98

Lu SC. 2009. Regulation of glutathione synthesis. *Molecular aspects of medicine* 30: 42-59

Lumadue JA, Glick AB, Ruddle FH. 1987. Cloning, sequence analysis, and expression of the large subunit of the human lymphocyte activation antigen 4F2. *Proceedings of the National Academy of Sciences* 84: 9204-08

Luscher B, Fuchs T. 2015. GABAergic control of depression-related brain states In *Advances in Pharmacology*, pp. 97-144: Elsevier

Lüscher C, Xia H, Beattie EC, Carroll RC, von Zastrow M, et al. 1999. Role of AMPA receptor cycling in synaptic transmission and plasticity. *Neuron* 24: 649-58

Macdonald RL, Barker JL. 1978. Specific antagonism of GABA-mediated postsynaptic inhibition in cultured mammalian spinal cord neurons A common mode of convulsant action. *Neurology* 28: 325-25

Macdonald RL, Olsen RW. 1994. GABAA receptor channels. *Annual Review of Neuroscience* 17: 569-602

MacGregor D, Higgins M, Jones P, Maxwell W, Watson M, et al. 1996. Ascorbate attenuates the systemic kainate-induced neurotoxicity in the rat hippocampus. *Brain research* 727: 133-44

Mackenzie B, Erickson JD. 2004. Sodium-coupled neutral amino acid (System N/A) transporters of the SLC38 gene family. *Pflügers Archiv* 447: 784-95

Mainen ZF, Sejnowski TJ. 1996. Influence of dendritic structure on firing pattern in model neocortical neurons. *Nature* 382: 363-66

Maletic-Savatic M, Malinow R, Svoboda K. 1999. Rapid dendritic morphogenesis in CA1 hippocampal dendrites induced by synaptic activity. *Science* 283: 1923-27

Maliszewska-Cyna E, Bawa D, Eubanks J. 2010. Diminished prevalence but preserved synaptic distribution of N-methyl-D-aspartate receptor subunits in the methyl CpG binding protein 2 (MeCP2)-null mouse brain. *Neuroscience* 168: 624-32

Manent J-B, Demarque M, Jorquera I, Pellegrino C, Ben-Ari Y, et al. 2005. A noncanonical release of GABA and glutamate modulates neuronal migration. *J. Neurosci.* 25: 4755-65

Martin DL, Rimvall K. 1993. Regulation of γ-aminobutyric acid synthesis in the brain. *Journal of Neurochemistry* 60: 395-407

Masel J. 2011. Genetic drift. *Current Biology* 21: R837-R38

Mason CR, Cooper RM. 1972. A permanent change in convulsive threshold in normal and brain-damaged rats with repeated small doses of pentylenetetrazol. *Epilepsia* 13: 663-74

Massie A, A. S, D. DB, SW. K, R. F, et al. 2011a. System xc- deficient mice show decreased susceptibility for limbic seizures as well as for 6-OHDA induced neurodegeneration. *Glia* 59: S77-S8

Massie A, Schallier A, Kim SW, Fernando R, Kobayashi S, et al. 2011b. Dopaminergic neurons of system xc–-deficient mice are highly protected against 6-hydroxydopamine-induced toxicity. *The FASEB Journal* 25: 1359-69

Massie A, Schallier A, Mertens B, Vermoesen K, Bannai S, et al. 2008. Time-dependent changes in striatal xCT protein expression in hemi-Parkinson rats. *Neuroreport* 19: 1589-92

Mastroberardino L, Spindler B, Pfeiffer R, Skelly PJ, Loffing J, et al. 1998. Amino-acid transport by heterodimers of 4F2hc/CD98 and members of a permease family. *Nature* 395: 288

Mathern GW, Pretorius JK, Mendoza D, Lozada A, Leite JP, et al. 1998. Increased hippocampal AMPA and NMDA receptor subunit immunoreactivity in temporal lobe epilepsy patients. *Journal of Neuropathology & Experimental Neurology* 57: 615-34

Matsuda K, Kamiya Y, Matsuda S, Yuzaki M. 2002. Cloning and characterization of a novel NMDA receptor subunit NR3B: a dominant subunit that reduces calcium permeability. *Molecular Brain Research* 100: 43-52

Matsuzaki M, Ellis-Davies GC, Nemoto T, Miyashita Y, Iino M, Kasai H. 2001. Dendritic spine geometry is critical for AMPA receptor expression in hippocampal CA1 pyramidal neurons. *Nat. Neurosci.* 4: 1086-92

Mayer ML, Westbrook GL, Guthrie PB. 1984. Voltage-dependent block by Mg2+ of NMDA responses in spinal cord neurones. *Nature* 309: 261

McBean GJ. 2012. The transsulfuration pathway: a source of cysteine for glutathione in astrocytes. *Amino acids* 42: 199-205

McCullagh EA, Featherstone DE. 2014. Behavioral characterization of system xc-mutant mice. *Behav. Brain Res.* 265: 1-11

McGeer PL, Eccles JC, McGeer EG. 1978. Putative excitatory neurons: glutamate and aspartate In *Molecular Neurobiology of the Mammalian Brain*, pp. 183-98: Springer

McIntire SL, Reimer RJ, Schuske K, Edwards RH, Jorgensen EM. 1997. Identification and characterization of the vesicular GABA transporter. *Nature* 389: 870

McKhann II G, Wenzel H, Robbins C, Sosunov A, Schwartzkroin P. 2003. Mouse strain differences in kainic acid sensitivity, seizure behavior, mortality, and hippocampal pathology. *Neuroscience* 122: 551-61

McLeod F, Ganley R, Williams L, Selfridge J, Bird A, Cobb S. 2013. Reduced seizure threshold and altered network oscillatory properties in a mouse model of Rett syndrome. *Neuroscience* 231: 195-205

McNamara J. 1986. Kindling model of epilepsy. *Advances in Neurology* 44: 303-18

Meduna L. 1932. Clinical and anatomical contributions to the question of genuine epilepsy. *Journal of Neurology* 129: 17-42

Meduna LJ. 1935. Attempts to Influence the Cause of Schizophrenia by Biological Means: Camphor and Cardiazol. *Zeitschrift fur die Gesamte Neurologie und Psychiatrie* 152: 235-62

Megıas M, Emri Z, Freund T, Gulyas A. 2001. Total number and distribution of inhibitory and excitatory synapses on hippocampal CA1 pyramidal cells. *Neuroscience* 102: 527-40

Meister A. 1974. Glutathione Synthesis In *The enzymes*, pp. 671-97: Elsevier

Meister A. 1979. Biochemistry of glutamate: glutamine and glutathione. *Glutamic Acid: Advances in Biochemistry and Physiology*: 69-84

Meldrum BS. 1994. The role of glutamate in epilepsy and other CNS disorders. *Neurology*

Melendez RI, Vuthiganon J, Kalivas PW. 2005. Regulation of extracellular glutamate in the prefrontal cortex: Focus on the cystine glutamate exchanger and group I metabotropic glutamate receptors. *J. Pharmacol. Exp. Ther.* 314: 139-47

Meng L, Xiang J, Kotecha R, Rose D, Zhao H, et al. 2010. White matter abnormalities in children and adolescents with temporal lobe epilepsy. *Magnetic Resonance Imaging* 28: 1290-98

Mesci P, Zaïdi S, Lobsiger CS, Millecamps S, Escartin C, et al. 2014. System x C− is a mediator of microglial function and its deletion slows symptoms in amyotrophic lateral sclerosis mice. *Brain* 138: 53-68

Meur KL, Galante M, Angulo MC, Audinat E. 2007. Tonic activation of NMDA receptors by ambient glutamate of non-synaptic origin in the rat hippocampus. *The Journal of physiology* 580: 373-83

Miles R, Wong RK. 1983. Single neurones can initiate synchronized population discharge in the hippocampus. *Nature* 306: 371-3

Miller LP, Walters JR, Eng N, Martin DL. 1980. Glutamate holodecarboxylase levels and the regulation of GABA synthesis. *Brain Research Bulletin* 5: 89-94

Minelli A, Brecha N, Karschin C, DeBiasi S, Conti F. 1995. GAT-1, a high-affinity GABA plasma membrane transporter, is localized to neurons and astroglia in the cerebral cortex. *J. Neurosci.* 15: 7734-46

Minelli A, DeBiasi S, Brecha NC, Zuccarello LV, Conti F. 1996. GAT-3, a high-affinity GABA plasma membrane transporter, is localized to astrocytic processes, and it is not confined to the vicinity of GABAergic synapses in the cerebral cortex. *J. Neurosci.* 16: 6255-64

Minich T, Riemer J, Schulz JB, Wielinga P, Wijnholds J, Dringen R. 2006. The multidrug resistance protein 1 (Mrp1), but not Mrp5, mediates export of glutathione and glutathione disulfide from brain astrocytes. *Journal of Neurochemistry* 97: 373-84

Moghaddam B, Javitt D. 2012. From revolution to evolution: the glutamate hypothesis of schizophrenia and its implication for treatment. *Neuropsychopharmacology* 37: 4

Mohapel P, Armitage LL, Gilbert TH, Hannesson DK, Teskey GC, Corcoran ME. 2000. Mossy fiber sprouting is dissociated from kindling of generalized seizures in the guinea-pig. *Neuroreport* 11: 2897-901

Mongin AA, Orlov SN. 2001. Mechanisms of cell volume regulation and possible nature of the cell volume sensor. *Pathophysiology* 8: 77-88

Moran MM, McFarland K, Melendez RI, Kalivas PW, Seamans JK. 2005. Cystine/glutamate exchange regulates metabotropic glutamate receptor presynaptic inhibition of excitatory transmission and vulnerability to cocaine seeking. *The Journal of Neuroscience* 25: 6389-93

Morrell F. 1985. Secondary epileptogenesis in man. *Archives of Neurology* 42: 318-35

Morris BJ, Cochran SM, Pratt JA. 2005. PCP: from pharmacology to modelling schizophrenia. *Current Opinion in Pharmacology* 5: 101-06

Moussawi K, Riegel A, Nair S, Kalivas PW. 2011. Extracellular glutamate: functional compartments operate in different concentration ranges. *Frontiers in Systems Neuroscience* 5: 94

Mu Y, Otsuka T, Horton AC, Scott DB, Ehlers MD. 2003. Activity-dependent mRNA splicing controls ER export and synaptic delivery of NMDA receptors. *Neuron* 40: 581-94

Mulholland PJ, Carpenter-Hyland EP, Hearing MC, Becker HC, Woodward JJ, Chandler LJ. 2008. Glutamate transporters regulate extrasynaptic NMDA receptor modulation of Kv2. 1 potassium channels. *Journal of Neuroscience* 28: 8801-09

Murakami S, Takemoto T, Shimizu Z. 1953. Studies on the effective principles of Digenea-simplex aq. 1. separation of the effective fraction by liquid chromatography. *Yakugaku Zasshi-Journal of the Pharmaceutical Society of Japan* 73: 1026-28

Murakoshi H, Trimmer JS. 1999. Identification of the Kv2. 1 K+ channel as a major component of the delayed rectifier K+ current in rat hippocampal neurons. *Journal of Neuroscience* 19: 1728-35

Murphy T, Schnaar R, Coyle J. 1990. Immature cortical neurons are uniquely sensitive to glutamate toxicity by inhibition of cystine uptake. *The FASEB Journal* 4: 1624-33

Nabeyama A, Kurita A, Asano K, Miyake Y, Yasuda T, et al. 2010. xCT deficiency accelerates chemically induced tumorigenesis. *Proceedings of the National Academy of Sciences* 107: 6436-41

Nadler JV, Perry BW, Cotman CW. 1978. Intraventricular kainic acid preferentially destroys hippocampal pyramidal cells. *Nature*: 676-77

Nadler JV, Perry BW, Gentry C, Cotman CW. 1980. Degeneration of hippocampal CA3 pyramidal cells induced by intraventricular kainic acid. *Journal of Comparative Neurology* 192: 333-59

Nagamori S, Wiriyasermkul P, Guarch ME, Okuyama H, Nakagomi S, et al. 2016. Novel cystine transporter in renal proximal tubule identified as a missing partner of cystinuria-related plasma membrane protein rBAT/SLC3A1. *Proceedings of the National Academy of Sciences* 113: 775-80

Naito S, Ueda T. 1985. Characterization of glutamate uptake into synaptic vesicles. *Journal of Neurochemistry* 44: 99-109

Nakamura E, Sato M, Yang H, Miyagawa F, Harasaki M, et al. 1999. 4F2 (CD98) heavy chain is associated covalently with an amino acid transporter and controls intracellular trafficking and membrane topology of 4F2 heterodimer. *Journal of Biological Chemistry* 274: 3009-16

Namba T, Morimoto K, Sato K, Yamada N, Kuroda S. 1994. Antiepileptogenic and anticonvulsant effects of NBQX, a selective AMPA receptor antagonist, in the rat kindling model of epilepsy. *Brain research* 638: 36-44

Naur P, Hansen KB, Kristensen AS, Dravid SM, Pickering DS, et al. 2007. Ionotropic glutamate-like receptor δ2 binds D-serine and glycine. *Proceedings of the National Academy of Sciences* 104: 14116-21

Naylor DE, Liu H, Niquet J, Wasterlain CG. 2013. Rapid surface accumulation of NMDA receptors increases glutamatergic excitation during status epilepticus. *Neurobiology of disease* 54: 225-38

Nelson SB, Valakh V. 2015. Excitatory/inhibitory balance and circuit homeostasis in autism spectrum disorders. *Neuron* 87: 684-98

Nguyen HTT, Dalmasso G, Yan Y, Obertone TS, Sitaraman SV, Merlin D. 2008. Ecto-phosphorylation of CD98 regulates cell-cell interactions. *PloS one* 3: e3895

Nguyen L, Rigo J-M, Rocher V, Belachew S, Malgrange B, et al. 2001. Neurotransmitters as early signals for central nervous system development. *Cell and Tissue Research* 305: 187-202

Nicholls D, Attwell D. 1990. The release and uptake of excitatory amino acids. *Trends in Pharmacological Sciences* 11: 462-68

Nishi M, Hinds H, Lu H-P, Kawata M, Hayashi Y. 2001. Motoneuron-specific expression of NR3B, a novel NMDA-type glutamate receptor subunit that works in a dominant-negative manner. *J. Neurosci.* 21: RC185-RC85

Niswender CM, Conn PJ. 2010. Metabotropic glutamate receptors: physiology, pharmacology, and disease. *Annual Review of Pharmacology and Toxicology* 50: 295-322

Noguchi J, Matsuzaki M, Ellis-Davies GC, Kasai H. 2005. Spine-neck geometry determines NMDA receptor-dependent Ca2+ signaling in dendrites. *Neuron* 46: 609-22

O'Brien RJ, Kamboj S, Ehlers MD, Rosen KR, Fischbach GD, Huganir RL. 1998. Activity-dependent modulation of synaptic AMPA receptor accumulation. *Neuron* 21: 1067-78

Okamoto S. 1951. Epileptogenic action of glutamate directly applied into the brains of animals and inhibitory effects of protein and tissue emulsions on its action. *J. Physiol. Soc. Jpn* 13: 555-62

Olney JW. 1969. Brain lesions, obesity, and other disturbances in mice treated with monosodium glutamate. *Science* 164: 719-21

Olney JW, Rhee V, Ho OL. 1974. Kainic acid: a powerful neurotoxic analogue of glutamate. *Brain research* 77: 507-12

Olsen RW, Avoli M. 1997. GABA and epileptogenesis. *Epilepsia* 38: 399-407

Omote H, Miyaji T, Juge N, Moriyama Y. 2011. Vesicular neurotransmitter transporter: bioenergetics and regulation of glutamate transport. *Biochemistry* 50: 5558-65

Osawa M, Uemura S, Kimura H, Sato M. 2001. Amygdala kindling develops without mossy fiber sprouting and hippocampal neuronal degeneration in rats. *Psychiatry and Clinical Neurosciences* 55: 549-57

Otis TS, Kavanaugh MP. 2000. Isolation of current components and partial reaction cycles in the glial glutamate transporter EAAT2. *J. Neurosci.* 20: 2749-57

Ottersen OP, Storm-Mathisen J. 1984. Glutamate-and GABA-containing neurons in the mouse and rat brain, as demonstrated with a new immunocytochemical technique. *Journal of Comparative Neurology* 229: 374-92

Ottestad-Hansen S, Hu QX, Follin-Arbelet VV, Bentea E, Sato H, et al. 2018. The cystine-glutamate exchanger (xCT, Slc7a11) is expressed in significant concentrations in a subpopulation of astrocytes in the mouse brain. *Glia* 66: 951-70

Padgett CL, Slesinger PA. 2010. GABAB receptor coupling to G-proteins and ion channels In *Advances in Pharmacology*, pp. 123-47: Elsevier

Palacín M, Nunes V, Font-Llitjós M, Jiménez-Vidal M, Fort J, et al. 2005. The genetics of heteromeric amino acid transporters. *Physiology* 20: 112-24

Pampliega O, Domercq M, Soria FN, Villoslada P, Rodríguez-Antigüedad A, Matute C. 2011. Increased expression of cystine/glutamate antiporter in multiple sclerosis. *Journal of Neuroinflammation* 8: 63

Parmacek MS, Karpinski BA, Gottesdiener KM, Thompson CB, Leiden JM. 1989. Structure, expression and regulation of the murine 4F2 heavy chain. *Nucleic acids research* 17: 1915-31

Parpura V, Basarsky TA, Liu F, Jeftinija K, Jeftinija S, Haydon PG. 1994. Glutamate-mediated astrocyte–neuron signalling. *Nature* 369: 744

Parpura V, Fang Y, Basarsky T, Jahn R, Haydon PG. 1995. Expression of synaptobrevin II, cellubrevin and syntaxin but not SNAP-25 in cultured astrocytes. *FEBS Letters* 377: 489-92

Paternain AV, Cohen A, Stern-Bach Y, Lerma J. 2003. A role for extracellular Na+ in the channel gating of native and recombinant kainate receptors. *J. Neurosci.* 23: 8641-48

Peng L, Hertz L, Huang R, Sonnewald U, Petersen SB, et al. 1993. Utilization of glutamine and of TCA cycle constituents as precursors for transmitter glutamate and GABA. *Developmental Neuroscience* 15: 367-77

Pérez-Garci E, Gassmann M, Bettler B, Larkum ME. 2006. The GABA B1b isoform mediates long-lasting inhibition of dendritic Ca 2+ spikes in layer 5 somatosensory pyramidal neurons. *Neuron* 50: 603-16

Pérez-Otaño I, Ehlers MD. 2005. Homeostatic plasticity and NMDA receptor trafficking. *Trends in neurosciences* 28: 229-38

Petr GT, Sun Y, Frederick NM, Zhou Y, Dhamne SC, et al. 2015. Conditional deletion of the glutamate transporter GLT-1 reveals that astrocytic GLT-1 protects against fatal epilepsy while neuronal GLT-1 contributes significantly to glutamate uptake into synaptosomes. *J. Neurosci.* 35: 5187-201

Pfeiffer R, Rossier G, Spindler B, Meier C, Kühn L, Verrey F. 1999. Amino acid transport of y+ L-type by heterodimers of 4F2hc/CD98 and members of the glycoprotein-associated amino acid transporter family. *The EMBO journal* 18: 49-57

Piani D, Fontana A. 1994. Involvement of the cystine transport system xc-in the macrophage-induced glutamate-dependent cytotoxicity to neurons. *The Journal of Immunology* 152: 3578-85

Pick JR, Little JM. 1965. Effect of Type of Bedding Material on Thresholds of Pentylenetetrazol Convulsions in Mice. *Lab Anim Care* 15: 29-33

Pin J-P, Acher F. 2002. The metabotropic glutamate receptors: structure, activation mechanism and pharmacology. *Current Drug Targets-CNS & Neurological Disorders* 1: 297-317

Pineda M, Fernández E, Torrents D, Estévez R, López C, et al. 1999. Identification of a membrane protein, LAT-2, that co-expresses with 4F2 heavy chain, an L-type amino acid transport activity with broad specificity for small and large zwitterionic amino acids. *Journal of Biological Chemistry* 274: 19738-44

Pitkanen A, ed. 2006. *Models of Seizures and Epilepsy*. Boston, MA: Elsevier Academic Press.

Piyankarage SC, Augustin H, Grosjean Y, Featherstone DE, Shippy SA. 2008. Hemolymph amino acid analysis of individual Drosophila larvae. *Analytical Chemistry* 80: 1201-07

Plant K, Pelkey KA, Bortolotto ZA, Morita D, Terashima A, et al. 2006. Transient incorporation of native GluR2-lacking AMPA receptors during hippocampal long-term potentiation. *Nat. Neurosci.* 9: 602

Platel J-C, Stamboulian S, Nguyen I, Bordey A. 2010. Neurotransmitter signaling in postnatal neurogenesis: The first leg. *Brain Research Reviews* 63: 60-71

Plotkin L, Bellido T. 2001. Bisphosphonate-induced, hemichannel-mediated, anti-apoptosis through the Src/ERK pathway: a gap junction-independent action of connexin43. *Cell Communication & Adhesion* 8: 377-82

Poduri A, Lowenstein D. 2011. Epilepsy genetics—past, present, and future. *Current Opinion in Genetics & Development* 21: 325-32

Poot M, Teubert H, Rabinovitch PS, Kavanagh TJ. 1995. De novo synthesis of glutathione is required for both entry into and progression through the cell cycle. *J. Cell. Physiol.* 163: 555-60

Porter RH, Eastwood SL, Harrison PJ. 1997. Distribution of kainate receptor subunit mRNAs in human hippocampus, neocortex and cerebellum, and bilateral reduction of hippocampal GluR6 and KA2 transcripts in schizophrenia. *Brain research* 751: 217-31

Pow DV. 2001. Visualising the activity of the cystine-glutamate antiporter in glial cells using antibodies to aminoadipic acid, a selectively transported substrate. *Glia* 34: 27-38

Pratt KG, Aizenman CD. 2007. Homeostatic regulation of intrinsic excitability and synaptic transmission in a developing visual circuit. *J. Neurosci.* 27: 8268-77

Pritchett DB, Luddens H, Seeburg PH. 1989. Type I and type II GABAA-benzodiazepine receptors produced in transfected cells. *Science* 245: 1389-92

Qin S, Colin C, Hinners I, Gervais A, Cheret C, Mallat M. 2006. System xc− and apolipoprotein E expressed by microglia have opposite effects on the neurotoxicity of amyloid-β peptide 1–40. *J. Neurosci.* 26: 3345-56

Quackenbush E, Clabby M, Gottesdiener KM, Barbosa J, Jones NH, et al. 1987. Molecular cloning of complementary DNAs encoding the heavy chain of the human 4F2 cell-surface antigen: a type II membrane glycoprotein involved in normal and neoplastic cell growth. *Proceedings of the National Academy of Sciences* 84: 6526-30

Quist AP, Rhee SK, Lin H, Lal R. 2000. Physiological role of gap-junctional hemichannels: extracellular calcium-dependent isosmotic volume regulation. *The Journal of Cell Biology* 148: 1063-74

Racine RJ. 1972. Modification of seizure activity by electrical stimulation. II. Motor seizure. *Electroencephalogr Clin Neurophysiol* 32: 281-94

Radian R, Bendahan A, Kanner B. 1986. Purification and identification of the functional sodium- and chloride-coupled gamma-aminobutyric acid transport glycoprotein from rat brain. *Journal of Biological Chemistry* 261: 15437-41

Ramanjaneyulu R, Ticku MK. 1984. Interactions of pentamethylenetetrazole and tetrazole analogues with the picrotoxinin site of the benzodiazepine-GABA receptor-ionophore complex. *European Journal of Pharmacology* 98: 337-45

Rao A, Craig AM. 1997. Activity regulates the synaptic localization of the NMDA receptor in hippocampal neurons. *Neuron* 19: 801-12

Raol YH, Lund IV, Bandyopadhyay S, Zhang G, Roberts DS, et al. 2006. Enhancing GABAA receptor α1 subunit levels in hippocampal dentate gyrus inhibits epilepsy development in an animal model of temporal lobe epilepsy. *Journal of Neuroscience* 26: 11342-46

Ratan RR, Murphy TH, Baraban JM. 1994. Macromolecular synthesis inhibitors prevent oxidative stress-induced apoptosis in embryonic cortical neurons by shunting cysteine from protein synthesis to glutathione. *J. Neurosci.* 14: 4385-92

Redmond L, Kashani AH, Ghosh A. 2002. Calcium regulation of dendritic growth via CaM kinase IV and CREB-mediated transcription. *Neuron* 34: 999-1010

Ren S-Q, Yao W, Yan J-Z, Jin C, Yin J-J, et al. 2018. Amyloid β causes excitation/inhibition imbalance through dopamine receptor 1-dependent disruption of fast-spiking GABAergic input in anterior cingulate cortex. *Scientific Reports* 8: 302

Rice AC, DeLorenzo RJ. 1998. NMDA receptor activation during status epilepticus is required for the development of epilepsy. *Brain research* 782: 240-47

Rice AC, Floyd CL, Lyeth BG, Hamm RJ, DeLorenzo RJ. 1998. Status epilepticus causes long-term NMDA receptor-dependent behavioral changes and cognitive deficits. *Epilepsia* 39: 1148-57

Richman P, Meister A. 1975. Regulation of gamma-glutamyl-cysteine synthetase by nonallosteric feedback inhibition by glutathione. *Journal of Biological Chemistry* 250: 1422-26

Rioult-Pedotti M-S, Donoghue JP, Dunaevsky A. 2007. Plasticity of the synaptic modification range. *Journal of Neurophysiology* 98: 3688-95

Rioult-Pedotti M-S, Friedman D, Donoghue JP. 2000. Learning-induced LTP in neocortex. *Science* 290: 533-36

Risher WC, Ustunkaya T, Alvarado JS, Eroglu C. 2014. Rapid Golgi analysis method for efficient and unbiased classification of dendritic spines. *PloS one* 9: e107591

Rivera C, Voipio J, Payne JA, Ruusuvuori E, Lahtinen H, et al. 1999. The K+/Cl− co-transporter KCC2 renders GABA hyperpolarizing during neuronal maturation. *Nature* 397: 251

Riveros N, Fiedler J, Lagos N, Mun C, Orrego F. 1986. Glutamate in rat brain cortex synaptic vesicles: influence of the vesicle isolation procedure. *Brain research* 386: 405-08

Robert SM, Buckingham SC, Campbell SL, Robel S, Holt KT, et al. 2015. SLC7A11 expression is associated with seizures and predicts poor survival in patients with malignant glioma. *Science Translational Medicine* 7: 289ra86

Roberts E, Frankel S. 1950. γ-Aminobutyric acid in brain: its formation from glutamic acid. *Journal of Biological Chemistry* 187: 55-63

Robillard JM, Gordon GR, Choi HB, Christie BR, MacVicar BA. 2011. Glutathione restores the mechanism of synaptic plasticity in aged mice to that of the adult. *PloS one* 6: e20676

Robinson JH, Deadwyler SA. 1981. Kainic acid produces depolarization of CA3 pyramidal cells in the vitro hippocampal slice. *Brain Res* 221: 117-27

Rodríguez-Moreno A, Herreras O, Lerma J. 1997. Kainate receptors presynaptically downregulate GABAergic inhibition in the rat hippocampus. *Neuron* 19: 893-901

Rodríguez-Moreno A, Lerma J. 1998. Kainate receptor modulation of GABA release involves a metabotropic function. *Neuron* 20: 1211-18

Rong Y, Doctrow SR, Tocco G, Baudry M. 1999. EUK-134, a synthetic superoxide dismutase and catalase mimetic, prevents oxidative stress and attenuates kainate-induced neuropathology. *Proceedings of the National Academy of Sciences* 96: 9897-902

Rosell A, Meury M, Álvarez-Marimon E, Costa M, Pérez-Cano L, et al. 2014. Structural bases for the interaction and stabilization of the human amino acid transporter LAT2 with its ancillary protein 4F2hc. *Proceedings of the National Academy of Sciences* 111: 2966-71

Rossier G, Meier C, Bauch C, Summa V, Sordat B, et al. 1999. LAT2, a new basolateral 4F2hc/CD98-associated amino acid transporter of kidney and intestine. *Journal of Biological Chemistry* 274: 34948-54

Rothstein JD, Martin L, Levey AI, Dykes-Hoberg M, Jin L, et al. 1994. Localization of neuronal and glial glutamate transporters. *Neuron* 13: 713-25

Saez GT, Bannister WH, Bannister J, V. 1990. Free radicals and thiol compounds - the role of glutathione against free radical toxicity. *Glutathione: Metabolism and Physiological Functions* In: Vina, J. (Ed.): CRC Press, Boca Raton, FL, USA, pp. 237-54

Sagara Ji, Makino N, Bannai S. 1996. Glutathione efflux from cultured astrocytes. *Journal of Neurochemistry* 66: 1876-81

Sah P, Hestrin S, Nicoll R. 1989. Tonic activation of NMDA receptors by ambient glutamate enhances excitability of neurons. *Science* 246: 815-18

Sakaba T, Neher E. 2003. Direct modulation of synaptic vesicle priming by GABA B receptor activation at a glutamatergic synapse. *Nature* 424: 775

Sanz-Clemente A, Nicoll RA, Roche KW. 2013. Diversity in NMDA receptor composition: many regulators, many consequences. *The Neuroscientist* 19: 62-75

Sasaki H, Sato H, Kuriyama-Matsumura K, Sato K, Maebara K, et al. 2002. Electrophile response element-mediated induction of the cystine/glutamate exchange transporter gene expression. *Journal of Biological Chemistry* 277: 44765-71

Sato H, Kuriyama-Matsumura K, Siow R, Ishii T, Bannai S, Mann GE. 1998. Induction of cystine transport via system xc− and maintenance of intracellular glutathione levels in pancreatic acinar and islet cell lines. *Biochimica et Biophysica Acta (BBA)-Biomembranes* 1414: 85-94

Sato H, Shiiya A, Kimata M, Maebara K, Tamba M, et al. 2005. Redox imbalance in cystine/glutamate transporter-deficient mice. *Journal of Biological Chemistry* 280: 37423-29

Sato H, Tamba M, Ishii T, Bannai S. 1999. Cloning and expression of a plasma membrane cystine/glutamate exchange transporter composed of two distinct proteins. *Journal of Biological Chemistry* 274: 11455-58

Sato H, Tamba M, Okuno S, Sato K, Keino-Masu K, et al. 2002. Distribution of cystine/glutamate exchange transporter, system x(c)(-), in the mouse brain. *J. Neurosci.* 22: 8028-33

Savtchouk I, Volterra A. 2018. Gliotransmission: beyond black-and-white. *J. Neurosci.* 38: 14-25

Scanlon C, Mueller SG, Cheong I, Hartig M, Weiner MW, Laxer KD. 2013. Grey and white matter abnormalities in temporal lobe epilepsy with and without mesial temporal sclerosis. *Journal of neurology* 260: 2320-29

Scharfman HE, Sollas AL, Berger RE, Goodman JH. 2003. Electrophysiological evidence of monosynaptic excitatory transmission between granule cells after seizure-induced mossy fiber sprouting. *Journal of Neurophysiology* 90: 2536-47

Schauwecker PE. 2003. Genetic basis of kainate-induced excitotoxicity in mice: phenotypic modulation of seizure-induced cell death. *Epilepsy research* 55: 201-10

Schiller J, Schiller Y. 2001. NMDA receptor-mediated dendritic spikes and coincident signal amplification. *Current opinion in neurobiology* 11: 343-48

Schmitz D, Frerking M, Nicoll RA. 2000. Synaptic activation of presynaptic kainate receptors on hippocampal mossy fiber synapses. *Neuron* 27: 327-38

Schröder H, Becker A, Lössner B. 1993. Glutamate Binding to Brain Membranes Is Increased in Pentylenetetrazole-Kindled Rats. *Journal of Neurochemistry* 60: 1007-11

Schwarz Y, Zhao N, Kirchhoff F, Bruns D. 2017. Astrocytes control synaptic strength by two distinct v-SNARE-dependent release pathways. *Nat. Neurosci.* 20: 1529

Segawa H, Fukasawa Y, Miyamoto K-i, Takeda E, Endou H, Kanai Y. 1999. Identification and functional characterization of a Na+-independent neutral amino acid transporter with broad substrate selectivity. *Journal of Biological Chemistry* 274: 19745-51

Shaffer PL, Goehring A, Shankaranarayanan A, Gouaux E. 2009. Structure and mechanism of a Na+-independent amino acid transporter. *Science (New York, N.Y.)* 325: 1010-14

Shih AY, Erb H, Sun X, Toda S, Kalivas PW, Murphy TH. 2006. Cystine/glutamate exchange modulates glutathione supply for neuroprotection from oxidative stress and cell proliferation. *The Journal of Neuroscience* 26: 10514-23

Shinozaki H. 1978. Discovery of novel actions of kainic acid and related compounds In *Kainic Acid as a Tool in Neurobiology*, pp. 17-35: Raven Press New York

Shinozaki H, Konishi S. 1970. Actions of several anthelmintics and insecticides on rat cortical neurones. *Brain Research* 24: 368-71

Sholl D. 1953. Dendritic organization in the neurons of the visual and motor cortices of the cat. *Journal of Anatomy* 87: 387

Sin WC, Haas K, Ruthazer ES, Cline HT. 2002. Dendrite growth increased by visual activity requires NMDA receptor and Rho GTPases. *Nature* 419: 475

Sloviter R, Damiano B. 1981. On the relationship between kainic acid-induced epileptiform activity and hippocampal neuronal damage. *Neuropharmacology* 20: 1003-11

Sloviter RS, Zappone CA, Harvey BD, Frotscher M. 2006. Kainic acid-induced recurrent mossy fiber innervation of dentate gyrus inhibitory interneurons: Possible anatomical substrate of granule cell hyperinhibition in chronically epileptic rats. *Journal of Comparative Neurology* 494: 944-60

Snyder EM, Nong Y, Almeida CG, Paul S, Moran T, et al. 2005. Regulation of NMDA receptor trafficking by amyloid-β. *Nat. Neurosci.* 8: 1051

Solbu TT, Bjørkmo M, Berghuis P, Harkany T, Chaudhry FA. 2010. SAT1, a glutamine transporter, is preferentially expressed in GABAergic neurons. *Frontiers in Neuroanatomy* 3: 1

Sommer B, Köhler M, Sprengel R, Seeburg PH. 1991. RNA editing in brain controls a determinant of ion flow in glutamate-gated channels. *Cell* 67: 11-19

Soria FN, Pérez-Samartín A, Martin A, Gona KB, Llop J, et al. 2014. Extrasynaptic glutamate release through cystine/glutamate antiporter contributes to ischemic damage. *The Journal of Clinical Investigation* 124: 3645-55

Squires RF, Saederup E, Crawley JN, Skolnick P, Paul SM. 1984. Convulsant potencies of tetrazoles are highly correlated with actions on GABA/benzodiazepine/picrotoxin receptor complexes in brain. *Life Sciences* 35: 1439-44

Stamler JS, Hausladen A. 1998. Oxidative modifications in nitrosative stress. 5: 247-49

Stellwagen D, Beattie EC, Seo JY, Malenka RC. 2005. Differential regulation of AMPA receptor and GABA receptor trafficking by tumor necrosis factor-α. *J. Neurosci.* 25: 3219-28

Stellwagen D, Malenka RC. 2006. Synaptic scaling mediated by glial TNF-α. *Nature* 440: 1054-59

Steppuhn KG, Turski L. 1993. Modulation of the seizure threshold for excitatory amino acids in mice by antiepileptic drugs and chemoconvulsants. *J. Pharmacol. Exp. Ther.* 265: 1063-70

Storck T, Schulte S, Hofmann K, Stoffel W. 1992. Structure, expression, and functional analysis of a Na (+)-dependent glutamate/aspartate transporter from rat brain. *Proceedings of the National Academy of Sciences* 89: 10955-59

Sullivan JM, Traynelis SF, Chen H-SV, Escobar W, Heinemann SF, Lipton SA. 1994. Identification of two cysteine residues that are required for redox modulation of the NMDA subtype of glutamate receptor. *Neuron* 13: 929-36

Sun W, McConnell E, Pare J-F, Xu Q, Chen M, et al. 2013. Glutamate-dependent neuroglial calcium signaling differs between young and adult brain. *Science* 339: 197-200

Sun W, Shchepakin D, Kalachev LV, Kavanaugh MP. 2014. Glutamate transporter control of ambient glutamate levels. *Neurochem. Int.* 73: 146-51

Swinyard EA. 1949. Laboratory assay of clinically effective antiepileptic drugs. *Journal of the American Pharmaceutical Association* 38: 201-04

Szatkowski M, Barbour B, Attwell D. 1990. Non-vesicular release of glutamate from glial cells by reversed electrogenic glutamate uptake. *Nature* 348: 443-46

Taguchi K, Tamba M, Bannai S, Sato H. 2007. Induction of cystine/glutamate transporter in bacterial lipopolysaccharide induced endotoxemia in mice. *Journal of Inflammation* 4: 20

Takaki M, Ueda Y, Doi T, Nagatomo K, Murashima YL, Kannan H. 2008. Molecular regulation of antioxidant ability in the hippocampus of EL mice. *Brain Research* 1228: 1-5

Takeuchi S, Wada K, Toyooka T, Shinomiya N, Shimazaki H, et al. 2012. Increased xCT expression correlates with tumor invasion and outcome in patients with glioblastomas. *Neurosurgery* 72: 33-41

Tan Dx, Manchester LC, Reiter RJ, Qi W, Kim SJ, El-Sokkary GH. 1998. Melatonin protects hippocampal neurons in vivo against kainic acid-induced damage in mice. *Journal of neuroscience research* 54: 382-89

Tanaka K. 1993. Cloning and expression of a glutamate transporter from mouse brain. *Neuroscience letters* 159: 183-86

Tanaka K, Watase K, Manabe T, Yamada K, Watanabe M, et al. 1997. Epilepsy and exacerbation of brain injury in mice lacking the glutamate transporter GLT-1. *Science* 276: 1699-702

Tani H, Dulla CG, Farzampour Z, Taylor-Weiner A, Huguenard JR, Reimer RJ. 2014. A local glutamate-glutamine cycle sustains synaptic excitatory transmitter release. *Neuron* 81: 888-900

Taniguchi N, Ikeda Y. 1998. c-Glutamyl transpeptidase: catalytic mechanism and gene expression. *Adv Enzymol Relat Areas Mol Biol* 72: 239-78

Taylor M, David A. 1998. Agenesis of the corpus callosum: a United Kingdom series of 56 cases. *Journal of Neurology, Neurosurgery & Psychiatry* 64: 131-34

Thorn TL, He Y, Jackman NA, Lobner D, Hewett JA, Hewett SJ. 2015. A Cytotoxic, Co-operative Interaction Between Energy Deprivation and Glutamate Release From System xc– Mediates Aglycemic Neuronal Cell Death. *ASN neuro* 7: 1-14

Torrents D, Estévez R, Pineda M, Fernández E, Lloberas J, et al. 1998. Identification and characterization of a membrane protein (y+ L amino acid transporter-1) that associates with 4F2hc to encode the amino acid transport activity y+ LA candidate gene for lysinuric protein intolerance. *Journal of Biological Chemistry* 273: 32437-45

Traynelis SF, Wollmuth LP, McBain CJ, Menniti FS, Vance KM, et al. 2010. Glutamate receptor ion channels: structure, regulation, and function. *Pharmacological reviews* 62: 405-96

Trotti D, Rizzini BL, Rossi D, Haugeto O, Racagni G, et al. 1997. Neuronal and glial glutamate transporters possess an SH-based redox regulatory mechanism. *European Journal of Neuroscience* 9: 1236-43

Turrigiano GG. 2008. The self-tuning neuron: synaptic scaling of excitatory synapses. *Cell* 135: 422-35

Turrigiano GG, Leslie KR, Desai NS, Rutherford LC, Nelson SB. 1998. Activity-dependent scaling of quantal amplitude in neocortical neurons. *Nature* 391: 892-96

Turrigiano GG, Nelson SB. 2004. Homeostatic plasticity in the developing nervous system. *Nature Reviews Neuroscience* 5: 97

Van Liefferinge J, Bentea E, Demuyser T, Albertini G, Follin-Arbelet V, et al. 2016. Comparative analysis of antibodies to xCT (Slc7a11): forewarned is forearmed. *Journal of Comparative Neurology* 524: 1015-32

Van Wagenen WP, Herren RY. 1940. Surgical division of commissural pathways in the corpus callosum: relation to spread of an epileptic attack. *Archives of Neurology & Psychiatry* 44: 740-59

Varma N, Carlson GC, Ledent C, Alger BE. 2001. Metabotropic glutamate receptors drive the endocannabinoid system in hippocampus. *J. Neurosci.* 21: RC188-RC88

Verrey F, Closs EI, Wagner CA, Palacin M, Endou H, Kanai Y. 2004. CATs and HATs: the SLC7 family of amino acid transporters. *Pflugers Arch.* 447: 532-42

Victor M, Ropper AH, eds. 2002. *Adams and Victor's Manual of Neurology*. New York: McGraw-Hill Medical Publishing Division. 7th ed.

Vincent P, Mulle C. 2009. Kainate receptors in epilepsy and excitotoxicity. *Neuroscience* 158: 309-23

Waagepetersen H, Bakken I, Larsson O, Sonnewald U, Schousboe A. 1998. Comparison of lactate and glucose metabolism in cultured neocortical neurons and astrocytes using 13C-NMR spectroscopy. *Developmental neuroscience* 20: 310-20

Waagepetersen HS, Sonnewald U, Schousboe A. 1999. The GABA paradox: multiple roles as metabolite, neurotransmitter, and neurodifferentiative agent. *Journal of neurochemistry* 73: 1335-42

Wada JA, Sato M, Corcoran ME. 1974. Persistent seizure susceptibility and recurrent spontaneous seizures in kindled cats. *Epilepsia* 15: 465-78

Wadiche JI, Arriza JL, Amara SG, Kavanaugh MP. 1995. Kinetics of a human glutamate transporter. *Neuron* 14: 1019-27

Wagner CA, Bröer A, Albers A, Gamper N, Lang F, Bröer S. 2000. The heterodimeric amino acid transporter 4F2hc/LAT1 is associated in Xenopus oocytes with a non-selective cation channel that is regulated by the serine/threonine kinase sgk-1. *The Journal of physiology* 526: 35-46

Wang H, Tamba M, Kimata M, Sakamoto K, Bannai S, Sato H. 2003. Expression of the activity of cystine/glutamate exchange transporter, system x c−, by xCT and rBAT. *Biochem. Biophys. Res. Commun.* 305: 611-18

Warr O, Takahashi M, Attwell D. 1999. Modulation of extracellular glutamate concentration in rat brain slices by cystine-glutamate exchange. *J. Physiol.-London* 514: 783-93

Watanabe T, Morimoto K, Hirao T, Suwaki H, Watase K, Tanaka K. 1999. Amygdala-kindled and pentylenetetrazole-induced seizures in glutamate transporter GLAST-deficient mice. *Brain research* 845: 92-96

Watkins J, Evans R. 1981. Excitatory amino acid transmitters. *Annual review of pharmacology and toxicology* 21: 165-204

Watt AJ, van Rossum MC, MacLeod KM, Nelson SB, Turrigiano GG. 2000. Activity coregulates quantal AMPA and NMDA currents at neocortical synapses. *Neuron* 26: 659-70

Watts SD, Torres-Salazar D, Divito CB, Amara SG. 2014. Cysteine transport through excitatory amino acid transporter 3 (EAAT3). *PloS one* 9: e109245

Weber B, Luders E, Faber J, Richter S, Quesada CM, et al. 2007. Distinct regional atrophy in the corpus callosum of patients with temporal lobe epilepsy. *Brain* 130: 3149-54

Weil-Malherbe H. 1950. Significance of glutamic acid for the metabolism of nervous tissue. *Physiological reviews* 30: 549-68

Westbrook GL, Lothman EW. 1983. Cellular and synaptic basis of kainic acid-induced hippocampal epileptiform activity. *Brain Res* 273: 97-109

Westergaard N, Sonnewald U, Petersen SB, Schousboe A. 1995. Glutamate and glutamine metabolism in cultured GABAergic neurons studied by 13C NMR spectroscopy may indicate compartmentation and mitochondrial heterogeneity. *Neuroscience letters* 185: 24-28

Wierenga CJ, Ibata K, Turrigiano GG. 2005. Postsynaptic expression of homeostatic plasticity at neocortical synapses. *The Journal of neuroscience* 25: 2895-905

Williams LE, Featherstone DE. 2014. Regulation of Hippocampal Synaptic Strength by Glial xCT. *The Journal of Neuroscience* 34: 16093-102

Winterbourn CC, Metodiewa D. 1994. The reaction of superoxide with reduced glutathione. *Archives of biochemistry and biophysics* 314: 284-90

Wojcik SM, Katsurabayashi S, Guillemin I, Friauf E, Rosenmund C, et al. 2006. A shared vesicular carrier allows synaptic corelease of GABA and glycine. *Neuron* 50: 575-87

Wotring VE, Chang Y, Weiss DS. 1999. Permeability and single channel conductance of human homomeric ρ1 GABAC receptors. *The Journal of physiology* 521: 327-36

Wu G, Fang Y-Z, Yang S, Lupton JR, Turner ND. 2004. Glutathione metabolism and its implications for health. *The Journal of nutrition* 134: 489-92

Yamauchi A, Uchida S, Kwon HM, Preston A, Robey RB, et al. 1992. Cloning of a Na (+)-and Cl (-)-dependent betaine transporter that is regulated by hypertonicity. *Journal of Biological Chemistry* 267: 649-52

Yamazaki M, Araki K, Shibata A, Mishina M. 1992. Molecular cloning of a cDNA encoding a novel member of the mouse glutamate receptor channel family. *Biochem. Biophys. Res. Commun.* 183: 886-92

Yang Y, Wang X-b, Zhou Q. 2010. Perisynaptic GluR2-lacking AMPA receptors control the reversibility of synaptic and spines modifications. *Proceedings of the National Academy of Sciences* 107: 11999-2004

Ye Z-C, Rothstein JD, Sontheimer H. 1999. Compromised glutamate transport in human glioma cells: reduction–mislocalization of sodium-dependent glutamate transporters and enhanced activity of cystine–glutamate exchange. *J. Neurosci.* 19: 10767-77

Ye Z-C, Sontheimer H. 1999. Glioma cells release excitotoxic concentrations of glutamate. *Cancer research* 59: 4383-91

Ye Z-C, Wyeth MS, Baltan-Tekkok S, Ransom BR. 2003. Functional hemichannels in astrocytes: a novel mechanism of glutamate release. *Journal of Neuroscience* 23: 3588-96

Ye Z, Mostajo-Radji MA, Brown JR, Rouaux C, Tomassy GS, et al. 2015. Instructing perisomatic inhibition by direct lineage reprogramming of neocortical projection neurons. *Neuron* 88: 475-83

Yu X, Malenka RC. 2003. β-catenin is critical for dendritic morphogenesis. *Nat. Neurosci.* 6: 1169

Yuen TI, Morokoff AP, Bjorksten A, D'abaco G, Paradiso L, et al. 2012. Glutamate is associated with a higher risk of seizures in patients with gliomas. *Neurology* 79: 883-89

Zaeri S, and Emamghoreishi, Masoumeh. 2015. Acute and Chronic Effects of N-acetylcysteine on Pentylenetetrazole-induced Seizure and Neuromuscular Coordination in Mice. pp. 118. *Iranian journal of medical sciences*

Zaia KA, Reimer RJ. 2009. Synaptic vesicle protein NTT4/XT1 (SLC6A17) catalyzes Na+-coupled neutral amino acid transport. *Journal of Biological Chemistry* 284: 8439-48

Zerangue N, Kavanaugh MP. 1996. Flux coupling in a neuronal glutamate transporter. *Nature* 383: 634

Zhang D, Jin B, Ondrejcak T, Rowan MJ. 2016a. Opposite in vivo effects of agents that stimulate or inhibit the glutamate/cysteine exchanger system on the inhibition of hippocampal LTP by Aß. *Hippocampus* 26: 1655-65

Zhang D, Pan Z-H, Awobuluyi M, Lipton SA. 2001. Structure and function of GABAC receptors: a comparison of native versus recombinant receptors. *Trends in Pharmacological Sciences* 22: 121-32

Zhang Y, Chen K, Sloan SA, Bennett ML, Scholze AR, et al. 2014. An RNA-sequencing transcriptome and splicing database of glia, neurons, and vascular cells of the cerebral cortex. *J. Neurosci.* 34: 11929-47

Zhang Y, Sloan SA, Clarke LE, Caneda C, Plaza CA, et al. 2016b. Purification and characterization of progenitor and mature human astrocytes reveals transcriptional and functional differences with mouse. *Neuron* 89: 37-53

Zhao W-J, Ma Y-H, Fei J, Mei Z-T, Guo L-H. 2003. Increase in drug-induced seizure susceptibility of transgenic mice overexpressing GABA transporter-1. *Acta Pharmacologica Sinica* 24: 991-95

Zhou S, Yu Y. 2018. Synaptic EI Balance Underlies Efficient Neural Coding. *Frontiers in Neuroscience* 12: 46

Zhou Y, Hassel B, Eid T, Danbolt NC. 2018. Axon-terminals expressing EAAT2 (GLT-1; Slc1a2) are common in the forebrain and not limited to the hippocampus. *Neurochem. Int.*

Zhou Y, Holmseth S, Guo C, Hassel B, Höfner G, et al. 2012. Deletion of the γ-aminobutyric acid transporter 2 (GAT2 and SLC6A13) gene in mice leads to changes in liver and brain taurine contents. *Journal of Biological Chemistry* 287: 35733-46

Zhou Y, Holmseth S, Hua R, Lehre AC, Olofsson AM, et al. 2011. The betaine-GABA transporter (BGT1, slc6a12) is predominantly expressed in the liver and at lower levels in the kidneys and at the brain surface. *American Journal of Physiology-Renal Physiology* 302: F316-F28

Zito K, Scheuss V, Knott G, Hill T, Svoboda K. 2009. Rapid functional maturation of nascent dendritic spines. *Neuron* 61: 247-58

Zorumski C, Mennerick S, Que J. 1996. Modulation of excitatory synaptic transmission by low concentrations of glutamate in cultured rat hippocampal neurons. *Journal of Physiology* 494: 465-77

<div align="center">

Curriculum Vitae

Sheila Shahidzadeh

107 College Place, Rm 110, Syracuse University • Syracuse, NY 13244
Cell Phone: 925-949-6887 • Work Phone: 315-443-2743
Email: smshahid@syr.edu

</div>

Education

Ph.D. in Biology (neuroscience concentration), Syracuse University, Syracuse, NY	**2018**
B.S. in Biopsychology (French minor), University of California, Santa Barbara.	**2012**

Research Experience

PhD Student, Syracuse University, NY.   **2013– Present**
Principal Investigator: Dr. Sandra J. Hewett
Project: Understanding the role of system x_c^- in maintenance of the excitatory/inhibitory balance *in vivo*.

Undergraduate Research Assistant, University of California, Santa Barbara.   **2011 – 2012**
Principal Investigator: Dr. Steven Fisher
Project: Investigating astrocyte morphological changes in response to a mouse model of retinal degeneration.

Undergraduate Research Assistant, University of California, Santa Barbara.   **2010 – 2011**
Principal Investigator: Dr. James Roney
Project: Investigating the hormonal correlates of mate attractiveness.

Honors and Awards

Outstanding Teaching Assistant Award , awarded to recognize teaching assistants who have made distinguished contributions to Syracuse University by demonstrating excellence in significant instructional capacities, The Graduate School, Syracuse University   **April 2018**

Certificate in University Teaching, awarded by The Graduate School Future Professoriate Program at Syracuse University   **April 2018**

Best Graduate Student Poster Presentation, Life Sciences Annual Symposium, Syracuse University Biology Department   **April 2018**

Travel fellowship recipient ($900), awarded by the Syracuse University Graduate Student Organization ($400) and Neuroscience Program ($500) to attend the 49th Annual Meeting of the American Society for Neurochemistry in Riverside, CA.   **March 2018**

Marilyn Kerr Scholarship ($31,750), awarded full stipend support by the Biology Department at Syracuse University   **8/2017 - 8/2018**

Travel fellowship recipient ($1400), awarded to attend the 26th Biennial International Society for Neurochemistry meeting in Paris, France from the International Society of Neurochemistry.

August 2017

Travel fellowship recipient ($850), awarded by the Syracuse University Biology Department ($350) and Graduate Student Organization ($500) to attend the 46th Annual Society for Neuroscience meeting in San Diego, CA

October 2016

Fellowship awarded to attend the ISN-JNC Flagship School ($900 + full-board accommodation) in Alpbach, Austria by the International Society of Neurochemistry-Journal of Neurochemistry (ISN-JNC).

September 2016

Best Graduate Student Poster Presentation, Neuroscience Research Day, Syracuse University

April 2016

Travel fellowship recipient ($1100), awarded by the Syracuse University Graduate Student Organization ($600) and Neuroscience Program ($500) to attend the 47th Annual American Society for Neurochemistry meeting in Denver, CO.

March 2016

Travel fellowship recipient ($350), awarded to attend the 45th Annual Society for Neuroscience meeting in Chicago, IL by the Biology Department, Syracuse University.

October 2015

Admitted into the Women in Science and Engineering Future Professionals Program (WiSE-FPP), Syracuse University

8/2015 - 8/2017

Attendee of "Workshop in Surgical Techniques in the Laboratory Mouse," held by the Jackson Laboratories in Paris, France.

6/24–6/27/2014

Dean's List, University of California, Santa Barbara.

2008/2012

Publications

Schaefer N, Rotermund C, Blumrich E, Lourenco M, Joshi P, Hegemann R, Jamwal S, Ali N, Garcia Romero Ezra, Sharma S, Ghosh S, Sinha J, Loke H, Jain V, Lepeta K, Salamian A, Sharma M, Golpich M, Nawrotek K, Kumar P, **Shahidzadeh S.M.**, Piermartiri T, Amini E, Pastor V, Wilson Y, Adeniyi P, Datusalia A, Vafadari B, Saini V, Suarez-Pozos Edna, Kushwah N, Fontanet P, Turner A. (2017). The malleable brain: plasticity of neural circuits and behavior – A review from students to students. Journal of Neurochemistry. 142 (6): 790-811.

Shahidzadeh, S.M., Hewett, JA, and Hewett, SJ. Decreased epileptogenesis in mice lacking the System x_c^- transporter occurs in association with a reduction in AMPA receptor subunit GluA1. *Submitted*.

Shahidzadeh, S.M., Hewett, JA, and Hewett, SJ. Sex differences in redox environment and neuronal morphology occur in association with enhancement of excitability in system x_c^- null mice. *In prep*.

Presentations

Invited talks

"Altered brain excitability in system x_c^- null mice", Mclaughlin Research Institute, Great Falls, Montana | **March 2018**

"Altered CNS excitability in system x_c^- null mice uncovered using the kainic acid model of status epilepticus", Astrocyte-neuron regulation of excitatory signaling workshop at the American Society for Neurochemistry meeting in Denver, Colorado. | **March 2016**

Posters

Shahidzadeh S.M., Hewett J.A., Hewett S.J. Sex differences in redox environment and neuronal morphology occur in association with enhancement of excitability in system x_c^- null mice. Presented at the American Society for Neurochemistry Meeting in Riverside, CA. March 2018.

Shahidzadeh S.M., Hewett J.A., Hewett S.J. Altered neuronal excitability in system x_c^- null mice in vivo uncovered by chemoconvulsant challenge. Presented at the International Society for Neurochemistry Biennial Meeting in Paris, France. August 2017.

Shahidzadeh S.M., Hewett J.A, Hewett S.J. System x_c^- null mice are resistant to pentylenetetrazole kindling. Presented at the Society for Neuroscience Meeting in San Diego, CA. November 2016.

Shahidzadeh S.M., Hewett J.A, Hewett S.J. Altered CNS excitability in system x_c^- null mice uncovered using the kainic acid model of status epilepticus. Presented at the American Society for Neurochemistry Meeting in Denver, CO. March 2016.

Shahidzadeh S.M., Hewett J.A, Hewett S.J. Role of system x_c^- in the pentylenetetrazole model of temporal lobe epilepsy. Presented at the Society for Neuroscience Meeting in Chicago, IL. October 2015.

Teaching Experience

Lecturer, Biology Department, Syracuse University, Syracuse, NY
> "**Synaptic Plasticity**" Advanced Neuroscience course. Syracuse University. (2017-2018, yearly).
> "**The Blood Brain Barrier**" Advanced Neuroscience course. Syracuse University. (2015-2017, yearly).

Teaching Assistant, Biology Department, Syracuse University, Syracuse, NY
> **Introduction to Biology** (BIO 121); two semesters. (Fall 2013/2014).
> **Anatomy and Physiology I and II** (BIO 216); two semesters. (Spring 2014/fall 2015).
> **Biology of Adaptive Behavior** (BIO 414); one semester. (Spring 2015).
> **Developmental Biology** (BIO 504); two semesters. (Spring 2016/17).
> **Cell Biology** (BIO 327); one semester. (Fall 2016).
> **Advanced Neuroscience** (BIO 407/607); three semesters. (Spring 2015/16/17).

University Service

Ad hoc Reviewer, Brain Research, (May 2017 – Present).

Ad hoc Reviewer, Neurochemistry International, (February 2018 – Present).

Graduate Representative, Graduate Recruitment Committee, Biology Department at Syracuse University (May 2016 – May 2017).

Graduate Scientific Member, Institutional Animal Care and Use Committee (IACUC) at Syracuse University (June 2016 – September 2018).

Vice President, Biology Graduate Student Organization (BGSO), Syracuse University (2014 – 2016).

Vice President, National Society of Collegiate Scholars, UCSB Chapter (2010-2012).

Professional Training

Postdoctoral Tenure-Track Boot Camp, sponsored by Women in Science and Engineering at Syracuse University. June 2018.

Future Professoriate Program (FPP) Workshop, sponsored by Syracuse University FPP, White Eagle Conference Center, New York. May 2017.

Astrocyte-Neuron Regulation of Excitatory Signaling Workshop, the 47th ASN meeting, Denver. March 2016.

Neurobiology of Disease Workshop, the 44th SfN meeting, Washington, DC. November 2014.

Workshop on Surgical Techniques in the Laboratory Mouse, The Jackson Laboratory, Paris, Fr. June 2014.

Professional Associations

Member, American Society for Neurochemistry, 2016 - Present

Member, International Society for Neurochemistry, 2016 - Present

Member, Institutional Animal Care and Use Committee, 2016 - Present

Member, Women in Science and Engineering Future Professionals Program, 2015 - Present

Member, Society for Neuroscience, 2014 - Present

Member, Biology Graduate Student Organization, 2013 - Present

National Society of Collegiate Scholars, UCSB Chapter, 2010 – 2012

Psi Chi National Honor Society in Psychology, UCSB Chapter, 2010 – 2012

Technical Skills

Animal behavioral studies including the kainic acid model of status epilepticus, pentylenetetrazole kindling model of epileptogenesis, and chemoconvulsant induced acute seizures.

Transcardial perfusion of rodents and tissue (brain) sectioning.

Histochemical staining and stereological analysis; Golgi-Cox stain, Timm stain, Nissl stain, and Fluorojade-C stain.

Primary cell culture (purified neurons and astrocytes).

q-PCR, Western blot, and immunohistochemistry

Skilled in major professional software (Word, PowerPoint, Excel, EndNote, Photoshop) as well as GraphPad Prism, Adobe Illustrator, and ImageJ (NIH).